Facultad de Ciencias
Departamento de Biología Molecular

Polycationic multivalency: Protein recognition and cell uptake *via* oligoguanidinium scaffolds

Director:

Javier de Mendoza Sans

Memoria que presenta:

Vera Martos Riaño

Para optar al grado de Doctora en Biología Molecular

Madrid, febrero 2009

Agradecimientos

Muchas son las personas que me han acompañado a lo largo de esta tesis…fue mi profesor de "complementos de química orgánica" y futuro director de tésis Javier de Mendoza el que despertó en mí el gusanillo por la química orgánica; por lo tanto si alguien es el "culpable" de todo esto, es sin duda él. Sin embargo nada de esto hubiese sido posible sin la ayuda de la Pr. Jorgina Satrústegui que apostó por un proyecto fuera de lo común. Posteriormente, tuve la enorme suerte de ser iniciada en la teoría y en la práctica de la química orgánica por la Pr. Pilar Prados, que con sus dotes pedagógicas y generosidad, acabó por embelesarme.

Recuerdo con especial cariño a mis primeras tutoras en el laboratorio Ruth y Margot, así como a mis compañeros de la UAM: Hitos, Curra, José y Juanjo (el erasmus de Tomás) por sus buenos consejos y su chispa madrileña.

A mis compañeros "tarraconins" de poyata –es decir de penas y alegrías- Fred y Julián, agradezco el ambiente musical, las conversaciones científicas, la calidez humana y tantas risas. A Enrique su humanidad e inmejorables consejos calixarénicos y a Aritz su gran ayuda y labor técnica. A Eric el recordarnos la importancia de los incisos en nuestra labor intelectual diaria. A Pascal y Jesús el haberme amenizado largas cromatografías con conversaciones cinéfilas apasionadas. A Elisa su don de gentes y a Caterina su encanto y serena complicidad. A Gerald el ser nuestro modelo de científico ideal, and last but not least a Alla y Augustín el representar tan bien la nueva generación de "rompe y rasga".

Especial mención merece mi amiga y compañera Pilar, a la que agradezco haberme regalado a lo largo de estos años con su ternura, alegría y tenacidad científica.

A mis dos colaboradoras inmejorables Eva y Susana, querría agradecer la paciencia con la que en ocasiones se enfrentaron a mis dudas, preguntas y peticiones y también recalcar la calidad de su trabajo. El colaborar con ellas ha sido sin duda una de las mejores experiencias de esta tesis.

Del Parc Científic de Barcelona, agradezco a los profesores Fernando Albericio y Ernest Giralt el haberse enrolado con tanto optimismo en nuestros proyectos.

Las enseñanzas de Angelita y la disponibilidad de Sonia, Marc y Annabel en el departamento de química combinatoria fueron de gran ayuda en mi introducción al mundo de la síntesis en fase sólida. Pero sobretodo las ideas y los ánimos de Miriam Royo fueron esenciales para superar momentos de inseguridad y crisis de inspiración.

Dall' Università di Parma, in brevissimo stage, devo assolutamente ringraziare tanto il Professore Enrico Dalcanale, quanto l'inestimabile aiuto e amicizia di Elisa e Roger.

From the University of California in Berkeley, I would like to thank first of all Professor Dirk Trauner for making my stage come true. My enthusiastic coach and TEVC-teacher Sarah, made it possible to obtain results in a very short time and thanks to her fruitful work and the contributions of Professor Ehud Isacoff, Francesco and Matt, we finally made it to a great collaboration.

Naturalmente, también agradezco "la buena onda" del grupo de "los

Salen salen" encabezado por Arjan y la inestimable ayuda de Margot, Joanne y Mada en las arduas tareas burocráticas.

Por último doy gracias muy sentidas a mi familia y amigos por su cariño y compresión.

List of abbreviations

Amino acids:

Ala (A): alanine	Leu (L): leucine
Arg (R): arginine	Lys (K): lysine
Asn (N): asparagine	Met (M): methionine
Asp (D): aspartate	Phe (F): phenylalanine
Cys (C): cysteine	Pro (P): proline
Glu (E): glutamate	Ser (S): serine
Gln (Q): glutamine	Thr (T): threonine
Gly (G): glycine	Trp (W): tryptophan
His (H): hystidine	Tyr (Y): tyrosine
Ile (I): isoleucine	Val (V): valine

DNA-bases:

Purines (Pu)	Pyrimidines (Py)
G: Guanine	C: Cytosine
A: Adenine	T: Thymine

ACC: Adrenal carcinoma

AgTx: agitoxin

Alloc: alloxycarbonyl

Ar: aromatic

ATP: adenosine triphosphate

ax: axial

Bal: 5-(4-formyl-3,5-dimethoxyphenoxy) butyric acid

BB: building block

Bn: benzyl

Boc: *tert*-butoxycarbonyl

^{t}Bu: *tert*-butyl

cAMP: cyclic adenosine monophosphate

CF: carboxyfluorescein

CT: cholera toxin

CPP: cell penetrating peptide

Cyt C: Cytochrome C

DCC: *N*,*N'*-dicyclohexylcarbodiimide

dec: decomposition

DIPCDI: *N*,*N'*-diisopropylcarbodiimide

D*i*PEA: diisopropylethylamine

DMF: *N*,*N'*-dimethylformamide

DMAP: dimethylaminepyridine

DMSO: dimethylsulfoxide

DNA: deoxyribonucleic acid

Ds: 5-(dimethylamino)naphthalene-1-sulfonyl or dansyl

DTT: dithiothreitol

E: electrophile

Et_2O: diethylether

Et_3N: triethylamine

EtOAc: ethyl acetate

eq: equatorial

Fmoc: fluorenylmethyloxycarbonyl

Guan: guanidine

GRT: guanidinium rich transporter

HATU: 2-(1H-7-Azabenzotriazol- 1-yl)--1,1,3,3-tetramethyl uronium hexafluorophosphate

HEPES: *N*-(2-hydroxyethyl)-piperazine-*N'*-2-ethanesulfonic acid

HMTA: hexamethylenediamine

HOBt: hydroxybenzotriazole

Hex: hexane

IPr: propyl iodide

K_v1: K_v1 family of voltage dependent K^+ channels

MALDI: matrix-assisted laser desorption/ionization sprectrometry

MBHA: methylbenzhydrylamine polystyrene

Ms: methanesulfonyl or mesyl

Me: methyl

Mmt: 4-methoxytrityl

MTT: [1-(4,5-dimethylthiazol-2-yl)-3,5-diphenylformazan]

NBS: *N*-bromosuccinimide

NMM: *N*-methylmorpholine

NMP: *N*-methylpyrrolidinone

Pbf: 2,2,4,6,7-pentamethyldihydrobenzofuran-5-sufonyl

n-$P(Bu)_3$: tri-n-butylphosphine

$P(Ph)_3$ or TPP: triphenylphosphine

pdb: Protein Data Bank

PG: protecting group

PDGF: platelet derived growth factor

Ph: phenyl

PNA: peptide nucleic acid

PyBOP: benzotriazol-1-yloxy)tripyrrolidinophosphonium hexafluorophosphate

p53DBD: p53 DNA-binding domain

p53TD: tetramerization domain of p53

p53R337H: p53 mutant R337H

^{15}N-p53TD: p53TD labeled wtih ^{15}N

quant: quantitative

RE: recognition element

RGD: arginine-glycine-aspartate motif

RNA: ribonucleic acid

mRNA: messenger RNA

SPS: solid phase synthesis

SPPS: solid phase peptide synthesis

S_N: nucleophilic substitution reaction

S1-S6: K^+ channel pore domains 1 to 6
rt: room temperature
TBAF: *tert*-butylammonium fluoride
TBDMS: *tert*-butyldimethylsilyl
TBDPS: *tert*-butyldiphenylsilyl
TEA: triethylammonium cation
TEVC: two electrode voltage clamp
TFA: trifluoroacetic acid
Tf_2O: trifluoromethanesulfonic acid anhydride or triflic anhydride
THF: tetrahydrofurane
TIS: triisopropylsilane
TM: transmembrane domain
MS-TOF: time of flight spectrometry
Trt: trityl
Ts: *p*-toluenesulfonyl or tosyl
wt: wild type

Parameters
ppm: part per million
K_a: equilibrium association constant
K_d: equilibrium dissociation constant
h: Hill coefficient
IC_{50}: inhibitor concentration necessary to half-inhibit the protease activity
m: slop of sigmoidal curve
Mp: melting point
SEM: standard error of the mean
T_M: melting temperature
$T_{0.5}$: temperature corresponding to the half of T_M
$V_{0.5}$: voltage corresponding to the half of the voltage maximum

Techniques & apparatus

CD: circular dichroism

DSC: differential scanning calorimetry

ELSD: evaporative light scattering detectors

ESI-MS: electrospray ionization mass spectrometry

[^{1}H,^{15}N]-HSQC: heteronuclear single quantum correlation

HPLC: high pressure liquid chromatography

LC-MS: liquid chromatography-mass spectroscopy

ITC: isothermal calorimetry

MD: molecular dynamics

MW or μW: microwave reactor

NMR: nuclear magnetic resonance

RMSD: root main square deviation

RP: reverse phase

STD: Saturation transfer difference spectroscopy

TLC: thin layer chromatography

UV: ultraviolet detection

Chapter 1

General introduction

Chapter 2

Guanidilated calix[4]arene ligands for p53 tetramerization domain (p53TD)

Chapter 3

Conical calix[4]arenes as reversible blockers of voltage-dependent potassium channels

Chapter 4

Solid phase synthesis of chiral bicyclic guanidinium oligomers for

cellular uptake

Chapter 1

General introduction

1.1 Biomolecular surface recognition by multivalent abiotic ligands.

Reversible interactions, based on recognition between biological macromolecules are essential for the regulation of biochemical processes: Inside the cells, proteins rarely act alone, but interact instead with each other, assembled in complexes either homo-oligomeric or formed by several different components (1). Outside the cell, processes like cell recognition, endocytosis or drug internalization are mediated by surface recognition on the cell membrane. Therefore studying the principles of biomolecular surface interactions allow for both prediction and mimicry of molecular recognition and represent an important class of targets for human therapeutics (2).

From a physico-chemical point of view biomolecular interactions rely on the complementary association between functional groups through noncovalent interactions of hydrophobic or electrostatic nature, as well as on hydrogen bonds. Based on the site of association two types of recognition may be distinguished: one which takes place at the cavity of a biological macromolecule, such as the one between an enzyme and its substrate, and another which takes place at its surface, like the recognition of an antigen by its antibody. The difference between them lies in the fact that a substrate -generally highly functionalized- is recognized in a reduced

cavity free from solvent molecules, while interactions at protein or membrane surfaces have a divergent character and compete against the solvent (3).

Nevertheless, the recognition of protein surfaces by designed ligands is nowadays a current pursuit in drug discovery (4), and a formidable challenge as well, since the lack of characteristic features, the large extension, the planarity or the discontinuity of protein surfaces and protein-protein interfaces, coupled with their conformational flexibility and dynamic behavior (5), make it difficult to establish general rules for the selective attachment of suitable ligands to the target biomolecules. Still, there are a number of strategies that address the rational design of molecules capable of recognizing surfaces or disrupting interfaces of proteins (6), many of them supported by computational methods (7).

Generally, chemists seek for an optimized matching of non covalent interactions between the ligand and the biological target for efficient drug design (8). However, a general problem in supramolecular chemistry is that molecular recognition is based on noncovalent interactions which in contrast to covalent bonds are highly dependent on external parameters such as solvent composition, polarity or even temperature. In this context water as a solvent is the most challenging parameter. On the one hand, electrostatic interactions (H-bonds or ion pairs), which are quite well understood and have been extensively used in supramolecular systems, are rather weak in this solvent (9). On the other hand, hydrophobic or aromatic interactions, which can be rather strong in aqueous solvents, are much more difficult to predict by design and to use in artificial receptors (10).

Recently, a new concept, multivalency, has gained importance to overcome the intrinsic limitations of small noncovalent abiotic surface ligands. Multivalency which is the ability of a particle (or molecule) to bind another one *via* multiple simultaneous noncovalent interactions. In this case, the valency refers to the number of functional groups of the same type that are bound to the same scaffold and participate simultaneously in the binding event (Fig. 1.1) (11).

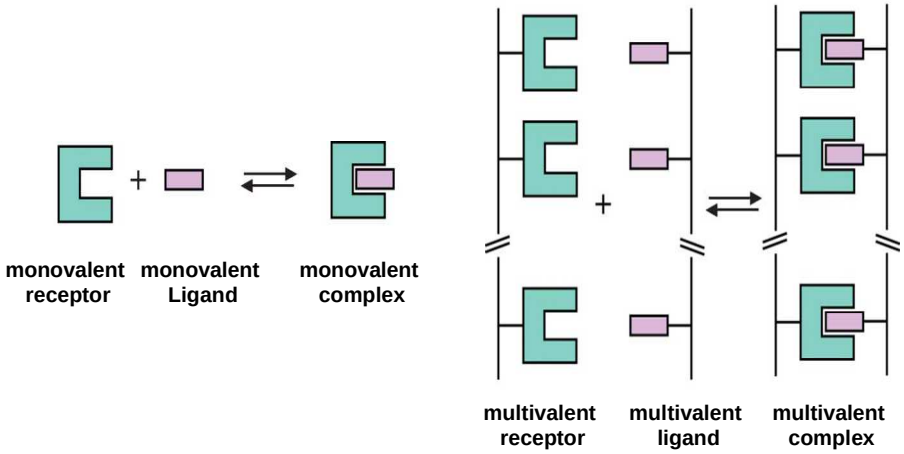

Fig. 1.1: Monovalent *vs* multivalent complex formation, reproduced from ref. 8.

In fact, multivalency is widely represented in nature, where relatively weak interactions (e.g. carbohydrate-protein) are converted into strong and specific recognition events, which control essential biological processes such as the adhesion of cells, viruses/bacteria or antibodies/macrophages to the cell surface (12). Moreover, multivalency has several and attractive features in common to the supramolecular concepts of self-assembly, reversibility, complementarity, molecular recognition, effective molarity,

and effective concentration (13). Actually, in biomimetic approaches to drug design, application of multivalency has already allowed the development of therapeutic agents able to neutralize bacterial toxins or to prevent viral or bacterial infections (14). Scaffolds of diverse structure, flexibility, and valency have been proposed as artificial multivalent ligands for these interfaces (Fig. 1.2) (15).

Relevant examples of low valency multivalent scaffolds range from small C_2 and C_4 symmetric porphyrin ligands (16) and calix[4]arenes (see chapters 2 and 3) to similar aromatic scaffolds such as anthracenes (17), DNA-quadruplex (18), and cyclophanes (19), Fig. 1.2a.

a)

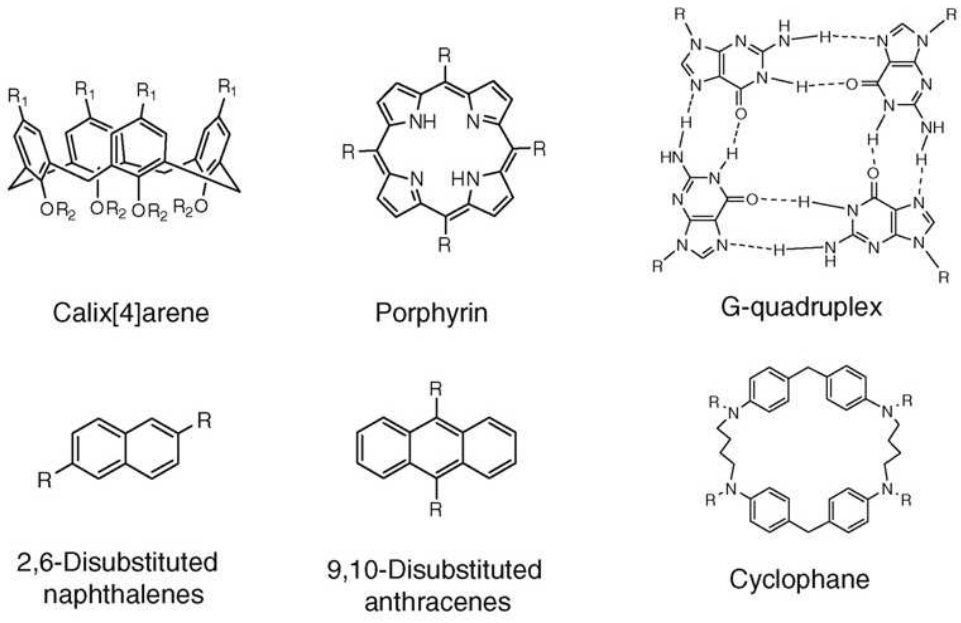

b)

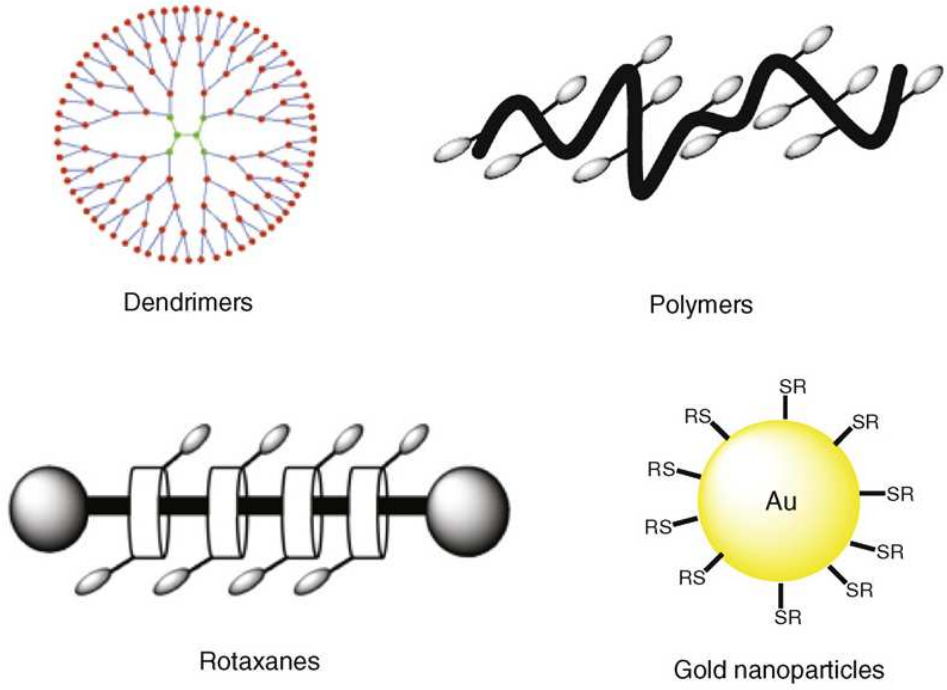

Fig. 1.2: Examples of multivalent scaffolds of low (a) and high valency (b) designed to allow biological interactions through multivalent contacts, from reference 14.

Among the high valency multivalent scaffolds are dendrimers that provide promising adherence-inhibition for toxins and other relevant lectins (20). In addition, highly flexible supramolecular platforms like rotaxanes (21) and polymers (22) have been proposed as challenging alternatives to more rigid designs. Finally, even nanoparticles are being exploited for this aim as they present important advantages from the biological and synthetic points of view (Fig. 1.2b) (23).

Multivalent guanidinium scaffolds

Besides the topology of the scaffold and the flexibility of the linkers, the strength of the noncovalent forces involved and the number of binding elements -also called recognition elements (REs)- are key aspects of the synergistic recognition event.

1.2 The guanidinium group: An efficient recognition element for surface association.

Each protein or membrane surface has a unique exterior composed of charged, hydrophobic and hydrophilic elements, but all association processes are determined by the thermodynamic aspects of the ligand-surface association and the relative importance of enthalpy, entropy and heat capacity effects in stabilizing complex formation (24). Though it is accepted that hydrophobic interactions generally provide the key driving force for complex formation on water-solvated surfaces, electrostatic associations also play an important role, as they often confer specificity to the binding process (5a).

Certain amino acid residues, particularly tryptophan (21%), arginine (13%), and tyrosine (12%) appear more frequently in hot spots of protein surfaces. The enrichment of these surfaces on cationic and aromatic amino acid residues is a result of their contribution to the binding energy through hydrophobic effects and electrostatic interactions, without a substantial entropic penalty, as they have fewer rotable bonds.

In particular, the guanidine functional group is widely spread as mediator of specific molecular recognition events in nature (25), some of which are shown herein:

Guanidine appears as a carboxylate binding element in the active site of enzymes such as carboxypeptidase A (Fig. 1.3) (26), creatine kinase (27), fumarate reductase (28), and malate dehydrogenase (29).

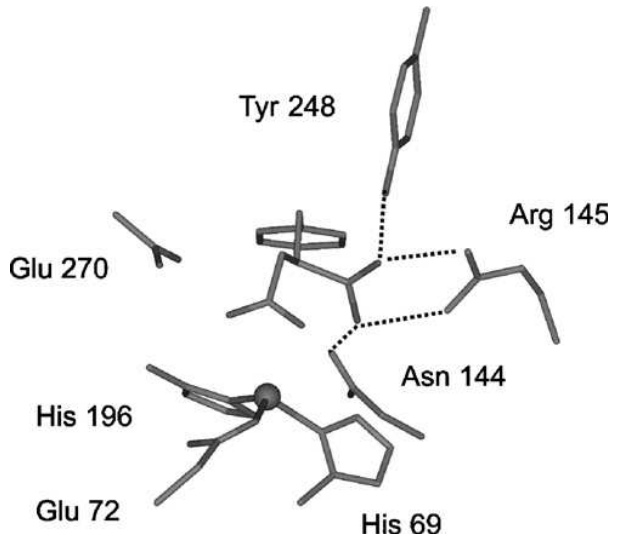

Fig. 1.3 Binding of an inhibitor (benzyl glutamic acid) within the active site of carboxypeptidase A. The carboxylate forms an ion pair with the Arg145 guanidinium cation. Two additional H-bonds from Asn144 and Tyr248 further stabilize the complex (reproduced from ref. 25b).

Furthermore, it has a major role in the condensation of DNA through arginine-rich histones. Part of these arginines stabilize histone-histone interactions essential for nucleosome formation, while another part directly associates with the phosphodiester groups of DNA, both interactions being essential for nucleosome formation (30). Moreover, methylation of arginines in the histone core leads to conformational changes which ultimately regulate gene expression (31).

Binding of phosphorylated serines *via* guanidine at arginine side chains, further mediates protein-protein heterodimerization processes between receptors at the cell membrane (32). A related case is the involvement of

the guanidinium group in the cell-cell and cell-matrix adhesion via the RGD (arginine-glycine-aspartate) motif, identified in a variety of biological processes such as bone mineralization or cancer metastasis (33). Finally, the guanidine functional group also constitutes an essential base pairing element in nucleic acids, taking into account that guanine is formally an acylated guanidine (Fig. 1.4b).

The properties of the guanidinium functional group that, besides the alkyl chain, do account for arginines' importance, rely on high basicity (pK_a: ~13), causing the group to stay protonated throughout a wide pH range. Its positive charge is stabilized by delocalization over the three nitrogen atoms and four out of the five hydrogen bond donors present in the guanidinium group of arginine can complement bidentate oxoanion acceptors, along the two available edges (Fig. 1.4a). Thus, both ion-pairing and hydrogen bonding account for its high oxoanion binding ability.

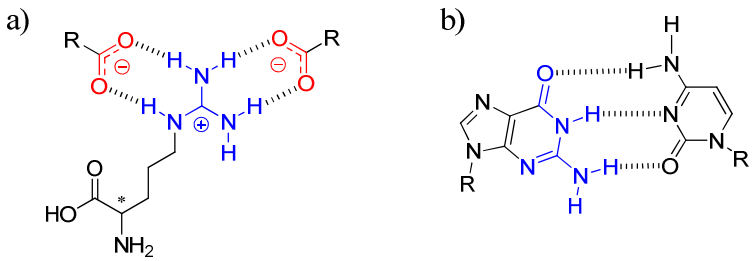

Fig. 1.4: (a) The guanidnium group of arginine and its two possible binding modes. (b) G-C base pairing with highlighted acylated guanidinium integrated in guanine structure.

However, as already mentioned, a guanidinium-oxoanion pair is only stable in solvents of low polarity while highly unstable in aqueous media,

unless shielded with an hydrophobic pocket. For example, the lactate-guanidinium ion pair has a stability of only $K_a \leq 6\ M^{-1}$ in water (34).

Nevertheless, inspired in nature's use of arginine, a number of abiotic supramolecular host systems based on guanidines have been designed in the last decades (35). Examples of receptors for phosphate (36), carboxylates (37), and sulfates (38), have paved the way for bioorganic receptors able to associate to citrate (Fig. 1.5a) (39), amino acids (Fig. 1.5b) (40), dipeptides (41) and even oligopeptides (Fig. 1.5c) (42) in aqueous media.

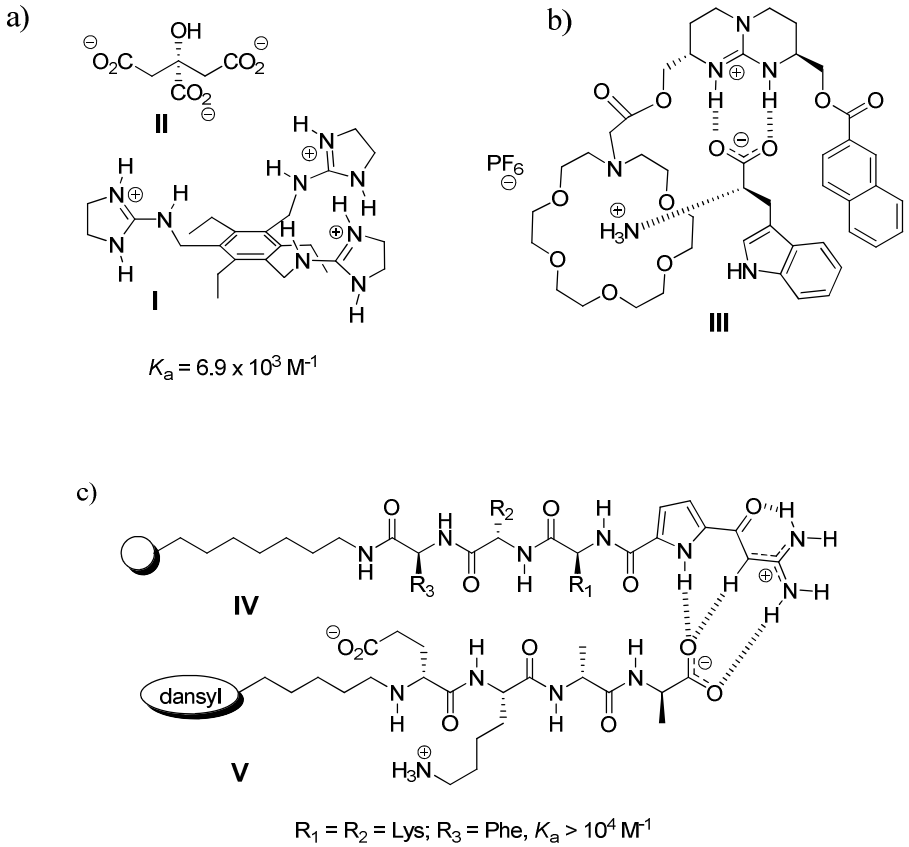

Fig. 1.5: (a) Anslyn's guanidinium receptor **I** forms stable complexes with citrate **II** in water, due to the triple ion-pair formation. (b) de Mendoza's bicyclic guanidinium receptor **III** for D-tryptophan. (c) Schmuck's lead compound **IV,** from a tripeptide based library of cationic guanidiniocarbonyl pyrrole receptors, binds the *C*-terminus tetrapeptide of Aβ (**V)**.

In these examples the substantial decrease of binding in water is overcome by increasing the number of recognition elements (multivalency), combining different noncovalent interactions (Gulliver effect) or by designing more sophisticated ligands with restricted solvent access (43).

Multivalent guanidinium scaffolds

Initial efforts from supramolecular chemists in the area of surface protein recognition concentrated on the design of small molecules able to associate to functional side chains located at positions typical of secondary structures such as α-helices. Compound **VI** (Fig. 1.6), represents a concave scaffold that orients two guanidinium subunits to interact with two aspartates of model peptide **VII** in *i*(*i* + 3) positions (K_a = 2200 M^{-1} in 10% water-methanol, NMR titrations) (44). Analogous peptides with aspartates in *i*(*i* + 4) and *i*(*i* + 11) positions, gave weaker complexes (K_a = 770 and 390 M^{-1}, respectively).

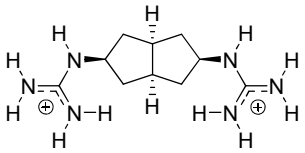

VI

VII : Ac-Ala-Ala-Gln-**Asp**-Ala-Ala-**Asp**-Ala-Ala-Ala-Ala-Ala-Gln-Ala-Ala-Tyr-NH_2

Fig. 1.6: Compound **VI** and model peptide **VII**.

Peptide **VII** was designed to possess a significant α-helical character, a necessary condition to establish ion-pairs with **VI**, because in this conformation the carboxylates are spaced 4-5 Å in an approximate parallel arrangement, so they can interact with the guanidinium groups of the receptor (Fig. 1.7) (45).

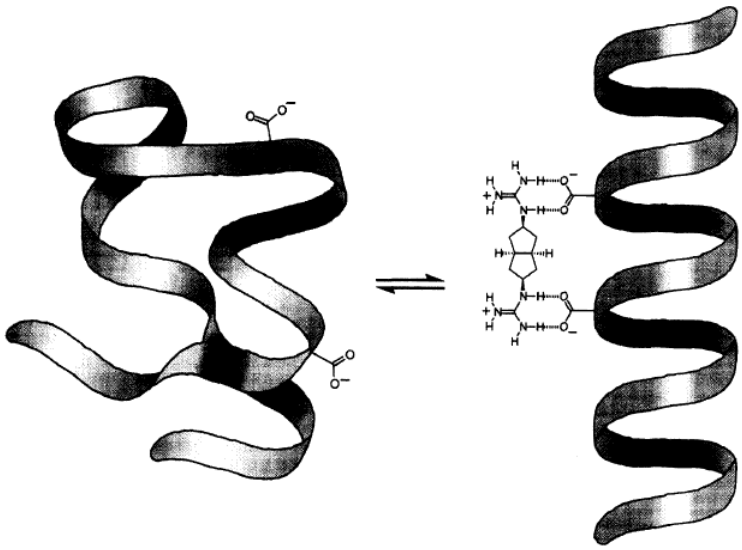

Fig. 1.7: Schematic representation of rigid receptor **VI** binding to an α-helical representation of peptide **VII** (from ref. 45).

Further oligoguanidinium based protein surface ligands synthesized and evaluated by the group of de Mendoza and coll. are described in section 2.3. Moreover, due to the high density of oxoanions on the cell membrane, oligo- and polyguanidiniums constitute a versatile source of cell permeabilizing and transfection agents (46). The nature of the scaffold, the number and spacing between the guanidine moeities, as well as the flexibility and topology of the overall polycationic molecules, are some of the parameters that influence cell uptake and are further explained in section 4.1.

1.3 Objectives of the thesis

The aims of these thesis are rational design of protein surface ligands combining guanidine recognition elements with the preassembled supramolecular calix[4]arene scaffold, and the methodological proposal of a solid-phase synthetic strategy for bicyclic guanidinium oligomers.

1.3.1 Guanidiniocalix[4]arenes for designed protein surface interactions

In chapters 2 and 3 we describe the design, synthesis, computational modelling, and biophysical evaluation of guanidiniocalix[4]arene ligands for two different protein surfaces.

1.3.1.1 Stabilizing ligands for p53TD

Conical ligands **1a** and **1b,** designed to associate and stabilize the tetrameric structure of p53 as well as its mutant p53R337H with deffective association properties will be presented in Chapter 2, besides controls **2a** and **2b** (Fig. 1.8).

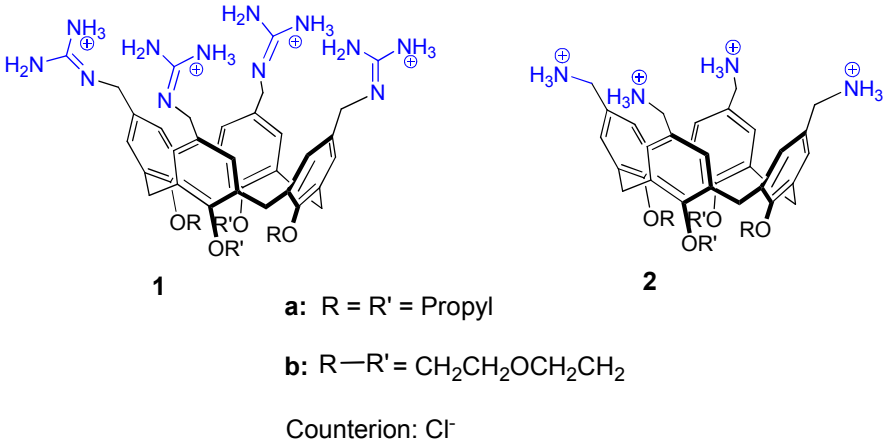

Fig. 1.8: Ligands for p53TD surface described in Chapter 2.

1.3.1.2 Conical molecular blockers of voltage-dependent K^+ channels

With the aim to identify reversible inhibitors of the voltage dependent K^+ channel family K_v1, we synthesized the small series of ligands **3-14**, with cationic, neutral and negatively charged ligands (Fig. 1.9). Their synthesis and blocker activity are described in Chapter 3.

Multivalent guanidinium scaffolds

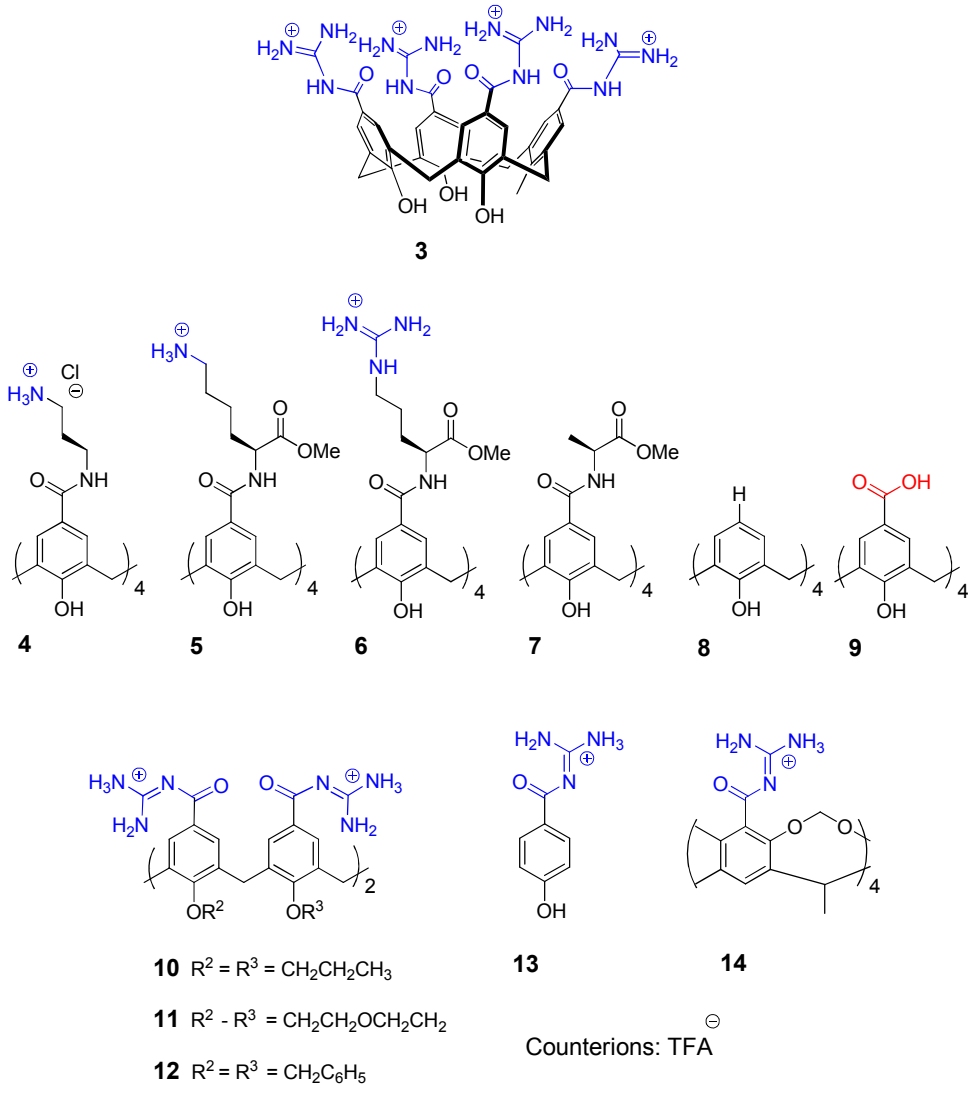

Fig. 1.9: Small series of potential K_v1 blockers presented in Chapter 3.

1.3.2 Solid phase synthesis of bicyclic guanidinium oligomers

In Chapter 4 we describe the development of a solid phase strategy to obtain a series of cell vectors based on bicyclic oligoguanidinium scaffolds. Several bicyclic guanidinium building blocks (**15**-**20**, Fig. 1.10a) as well as different resins were employed for this purpose (Fig. 1.10b).

a)

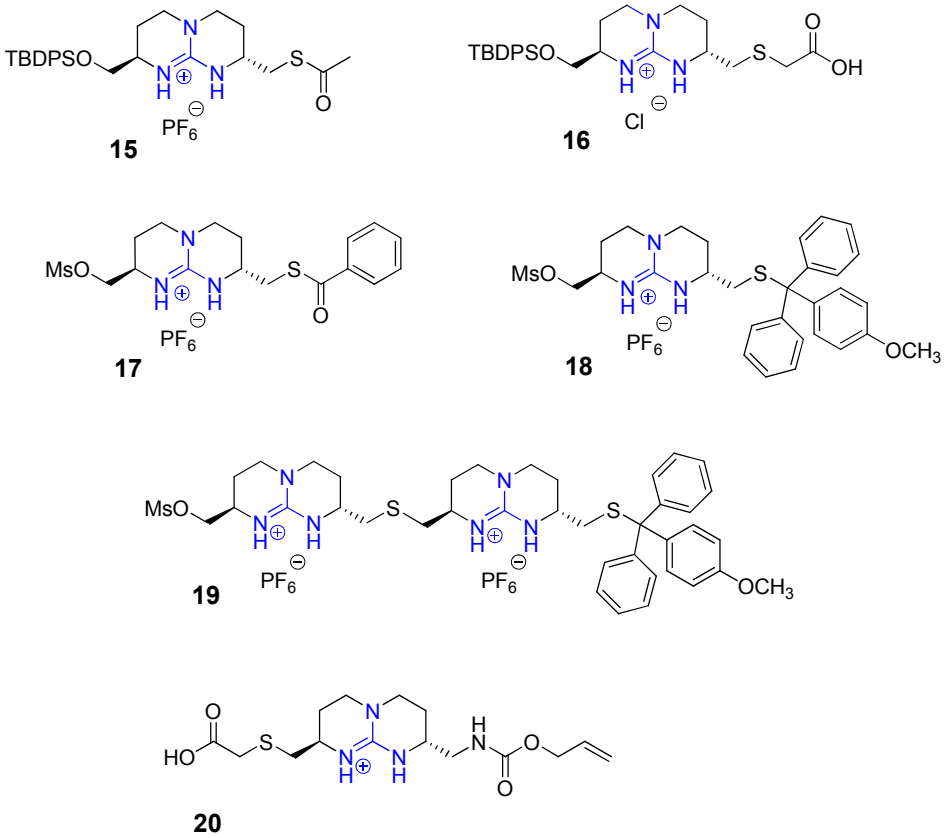

b)

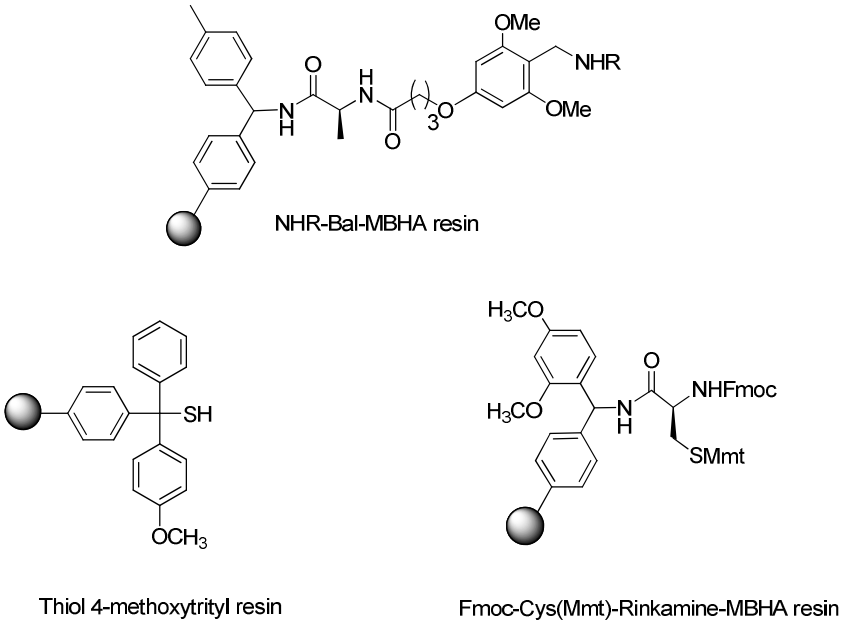

Fig. 1.10: Bicyclic building blocks (a) and resins (b) described in Chapter 4.

1.4 References

1. (a) Ali MH, Imperiali B (2005) Protein oligomerization: how and why. *Bioorg Med Chem* 13:5013-5020.
   (b) Dunker AK, Cortese MS, Romero P, Iakoucheva LM, Uversky VN (2005) The roles of intrinsic disorder in protein interaction networks. *FEBS J* 272:5129-5148.

2. Arkin MR, Wells JA (2004) Small-molecule inhibitors of protein–protein interactions: progressing towards the dream. *Nature Rev* 3:301-317.

3. Barratt E, Bingham RJ, Warner DJ, Laughton CA, Phillips SEV, Homans SW (2005) Van der Waals interactions dominate ligand-protein association in a protein binding site occluded from solvent water. *J Am Chem Soc* 127:11827-11834.

4. (a) Arkin MR (2005) Protein–protein interactions and cancer: small molecules going in for the kill. *Curr Op Chem Biol* 9:317-324.
   (b) Chène P (2006) Drugs targeting protein-protein interactions. *Chem Med Chem* 1:400-411.

5. (a) Stites WE (1997) Protein interactions: Interface structure, binding thermodynamics, and mutational analysis. *Chem Rev* 97:1233-1250.
   (b) LoConte L, Chothia C, Janin J (1999) The atomic structure of protein-protein recognition sites. *J Mol Biol* 285:2177-2198.
   (c) Trakselis MA, Alley SC, Ishmael FT (2005) Identification and mapping of protein-protein interactions by a combination of cross-linking, cleavage, and proteomics. *Bioconj Chem* 16:741-750.

6. (a) Berg T (2003) Modulation of protein-protein interactions with small organic molecules. *Angew Chem Int Ed* 42:2462-2481.
   (b) Fry DC (2006) Protein-protein interactions as targets for small molecule drug discovery. *Biopolymers* 84:535-552.

7. (a) González-Ruiz D, Gohlke H (2006) Targeting protein-protein interactions with small molecules: challenges and perspectives for computational binding epitope detection and ligand finding. *Curr Med Chem* 13:2607-2625.
   (b) Che Y, Brooks BR, Marshall GR (2006) Development of small molecules designed to modulate protein–protein interactions. *J Comput Aided Mol Des* 20:109-130.
   (c) Ivanov AS, Gnedenko OV, Molnar AA, Mezentsev YV, Lisitsa AV, Archakov AI (2007) Protein-protein interactions as new targets for drug design: virtual and experimental approaches. *J Bioinform Comput Biol* 5:579-592.

8. Baldini L, Casnati C, Sansone F, Ungaro R (2007) Calixarene-based multivalent ligands. *Chem Soc Rev* 36:254-266.

9. (a) Prins LJ, Reinhoudt DN, Timmermann P (2001) Noncovalent synthesis using hydrogen bonding. *Angew Chem Int Ed* 40:2383-2426.
   (b) Jeffrey GA (1997) An introduction to Hydrogen Bonding, Oxford University Press

(New York).

10. (a) Hunter CA, Lawson KR, Perkins J, Urch CJ (2001) Aromatic interactions. *J Chem Soc Perkin Trans* 2:651-669.
(b) Pratt LR, Pohorille A (2002) Hydrophobic effects and modeling of biophysical aqueous Solution interfaces. *Chem Rev* 102:2671-2692.
(c) Waters ML (2002) Aromatic interactions in model systems. *Curr Op Chem Biol* 6:736-741.
(d) Chung DM, Dou Y, Baldi P, Nowick JS (2005) The absence of favorable aromatic interactions between β-sheet peptides. *J Am Chem Soc* 127:9998-9999.

11. Kiessling LL, Gestwicki JE, Strong LE (2006) Synthetic multivalent ligands as probes of signal transduction. *Angew Chem Int Ed* 45:2348-2368.

12. Krishnamurthy VM, Semetey V, Paul JB, Shen N, Whitesides GB (2007) Polyvalent interactions in biological systems: implications for design and use of multivalent ligands and inhibitors. *J Am Chem Soc* 129:1312-1320.

13. Badjic JD, Nelson A, Cantrill SJ, Turnbull WB, Stoddart JF (2005) Multivalency and cooperativity in supramolecular chemistry. *Acc Chem Res* 38:723-732.

14. Martos V, Castreño P, Valero J, de Mendoza J (2008) Binding to protein surfaces by supramolecular multivalent scaffolds. *Curr Op Chem Biol* 12:698-706.

15. (a) Hershberger SJ, Lee SG, Chmielewski J (2007) Scaffolds for blocking of protein-protein interactions. *Curr Top Med Chem* 7:928-942.
(b) Choi S-K (2004) Synthetic Multivalent Molecules, John Wiley & Sons (Hoboken, New Jersey).

16. Zhou H, Baldini L, Hong J, Wilson AJ, Hamilton AD (2006) Pattern recognition of proteins based on an array of functionalized porphyrins. *J Am Chem Soc* 128:2421-2425.

17. Wilson AJ, Hong J, Fletcher S, Hamilton AD (2007) Recognition of solvent exposed protein surfaces using anthracene derived receptors. *Org Biomol Chem* 5:276-285.

18. Tagore DM, Sprinz KI, Fletcher S, Jayawickramarajah J, Hamilton AD (2007) Protein recognition and denaturation by self-assembling fragments on a DNA quadruplex scaffold. *Angew Chem Int Ed* 46:223-225.

19. Hayashida O, Takaokac Y, Hamachida I (2005) Synthesis and guest-binding study of polytopic multi(cyclophane) hosts. *Tetrahedron Lett* 46:6589-6592.

20. (a) Kitov PI, Sadowska JM, Mulvey G, Arnstrong GD, Ling H, Pannu NS, Read RJ, Bundle DR (2000) Shiga-like toxins are neutralized by tailored multivalent carbohydrate ligands. *Nature* 403:669-672.
(b) Shane L, Cloninger MJ (2006) Binding of monomeric and dimeric concavalin A to mannose-funtionalized dendrimers. *Org Biomol Chem* 4:2458-2465.

(c) Branderhorst HM, Liskamp RM J, Visser GM, Pieters RJ (2007) Strong inhibition of cholera toxin by multivalent GM1 derivatives. *Chem Commun* 5043-5045.

21. (a) Nelson A, Belitsky JM, Vidal S, Joiner CS, Baum LG, Stoddart JF (2004) A self-assembled multivalent pseudopolyrotaxane for binding Galectin-1. *J Am Chem Soc* 126:914-11922.
(b) Yui N, Ooya T (2006) Molecular mobility of interlocked structures exploiting new functions of advanced biomaterials. *Chem Eur J* 12:6730-6737.

22. Puffer EB, Pontrello JK, Hollenbeck JJ, Kink JA, Kiessling LL (2007) Activating B cell signaling with defined multivalent ligands. *Chem Biol* 2:252-262.

23. (a) You CC, Agasti SS, Rotello VM (2008). Isomeric control of protein recognition with amino acid- and dipeptide-functionalized gold nanoparticles. *Chem Eur J* 14:143-150.
(b) Bowman MC, Ballard TE, Ackerson CJ, Feldheim DL, Margolis DM, Melander C (2008) Inhibition of HIV fusion with multivalent gold nanoparticles. *J Am Chem Soc* 130:6896-6897.

24. Yin H, Hamilton AD, (2005) Strategies for targeting protein-protein interactions with synthetic agents. *Angew Chem Int Ed* 44:4130-4163.

25. (a) Padlan EA (1990) On the nature of antibody combining sites: unusual structural features that may confer on these sites an enhanced capacity for binding ligands. *Proteins Struct Funct Genet* 7:112-124.
(b) Schmuck C (2006) How to improve guanidinium cations for oxoanion binding in aqueous solution? The design of artificial peptide receptors. *Coord Chem Rev* 250:3053-3067.

26. Kim DH, Park J (1996) 2-Benzyl-3,4-iminobutanoic acid as inhibitor of carboxypeptidase A. *Bioorg Med Chem Lett* 6:2967-2970.

27. Wang P F, McLeish MM, Kneen G, Lee G, Kenyon GL (2001) An unusually low pKa for Cys282 in the active site of human muscle creatine kinase. *Biochemistry* 40:11698-11705.

28. Mowat CG, Moysey R Miles CS, Leys D, Doherty MK, Taylor P, Walkinshaw M D, Reid GA, Chapman SK (2001) Kinetic and crystallographic analysis of the key active site acid/base arginine in a soluble fumarate reductase. *Biochemistry* 40:12292-12298.

29. Bell JK, Yennawar HP, Wright SK, Thompson JR, Viola RE, Banaszak LJ (2001) Structural analyses of a malate dehydrogenase with a malate dehydrogenase with a variable active site. *J Biol Chem* 276:31156-31162.

30. García-Pérez M, Pinto M, Subirana JA (2003) Non sequence-specific arginine interactions in the nucleosome core particle. *Biopolymers* 69:432-439.

31. Zhang Y, Reinberg D (2001) Transcription regulation by histone methylation: interplay

between different covalent modifications of the core histone tails. *Genes Dev* 15:2343-2360.

32. Woods AS, Ferre SJ (2005) Amazing stability of the arginine-phosphate electrostatic interaction. *Proteome Res* 4:1397-1402.

33. (a) Ruoslahti E (1996) RGD and other related sequences for integrins. *Annu Rev CelDev Biol* 12: 697-715.
(b) Christensen B, Nielsen MS, Haselmann KF, Petersen TE, Sorensen S (2005) Posttranslationally modified residues of native human osteopontin are located in clusters. Identification of thirty-six phosphorylation sites and five O-glycosylation sites and their biological implications. *Biochem J* 390:285-292.

34. Horvath P, Gergely B, Noszal B (1996) Characterization of lactate-guanidinium and lactate-lactate interactions in aqueous solution by spectropolarimetry. *J Chem Soc, Perkin Trans 2* 1419-1422.

35. (a) Schug KA, Lindner W (2005) Noncovalent binding between guanidinium and anionic groups: Focus on biological -and synthetic- based arginine/guanidinium interactions with phosph[on]ate and sulf[on]ate residues. *Chem Rev* 105:67-113.
(b) Best MD, Tobey SL, Anslyn EV (2003) Abiotic guanidinium containing. receptors for anionic species. *Coord Chem Rev* 240:3-15.

36. (a) Dixon RP, Geib SJ, Hamilton AD (1992) Molecular recognition: bis-acylguanidiniums provide a simple family of receptors for phosphodiesters. *J Am Chem Soc* 114:365-366.
(b) Niikura K, Metzger A, Anslyn EV (1998) Chemosensor ensemble with selectivity for inositol-trisphosphate. *J Am Chem Soc* 120:8533-8534.
(c) Tobey SL, Anslyn EV (2003) Energetics of phosphate binding to ammonium and guanidinium containing metallo-receptors in water. *J Am Chem Soc* 125:14807-14815.

37. (a) Berger M, Schmidtchen FP (1999) Boronic acid and guanidinium based synthetic receptors: new applications in differential sensing. *J Am Chem Soc* 121:9986-9993.
(b) Linton B R, Goodman MS, Fan E, Van Arman SA, Hamilton AD (2001) Dicarboxylate recognition by simple artificial receptors. Thermodynamic aspects. *J Org Chem* 66:7313-7319.

38. (a) Sánchez-Quesada J, Seel C, Prados P, de Mendoza J (1996) Anion helicates: double strand helical self-assembly of chiral bicyclic guanidinium dimers and tetramers around sulfate templates. *J Am Chem Soc* 118:277-278.
(b) Berger M, Schmidtchen FP (1998) The binding of sulfate anions by guanidinium receptors is entropy-driven *Angew Chem Int Ed* 37:2694-2696.
(c) Grossel M C, Merckel DAS, Hutchings MG (2003) The effect of preorganisation on the solid state behaviour of simple aromatic-cored bis(guanidinium) sulfates *Cryst Eng Comm* 5:77-81.

39. (a) Metzger A, Lynch VM, Anslyn EV (1997) A synthetic receptor selective for citrate

Angew Chem Int Ed Engl 36:862-865.
(b) Schmuck C, Schwegmann M (2005) A molecular flytrap for the selective binding of citrate and other tris-carboxylates in water. *J Am Chem Soc* 127:3373-3379.

40. (a) Lawless LJ, Blackburn AG, Ayling AJ, Perez-Payan MN, Davis AP (2001) *J Chem Soc, Perkins Trans 1* 11:1329-1341.
(b) Breccia P, Van Gool M, Pérez-Fernández R, Martín-Santamaría S, Gago F, Prados P, de Mendoza J (2003) Guanidinium receptors as enantioselective amino acid membrane carriers. *J Am Chem Soc* 125:8270-8274.
(c) Schmuck C, Geiger L (2005) Efficient complexation of N-acetyl-amino acid carboxylates in water by an artificial receptor: unexpected cooperativity in the binding of glutamate but not aspartate. *J Am Chem Soc* 127:10486-10487.

41 Schmuck C, Geiger L (2004) Dipeptide binding in water by a de-novo designed guanidiniocarbonylpyrrole receptor. *J Am Chem Soc* 126:8898-8899.

42. (a) Schmuck C, Wich P (2006) Sequence-dependent stereoselectivity in the binding of tetrapeptides in water by a flexible artificial receptor. *Angew Chem Int Ed* 45:4277-4281.
(b) Schmuck C, Heil M (2006) One-armed artificial receptors for the binding of polar tetrapeptides in water: probing the substrate selectivity of a combinatorial receptor library. *Chem-Eur J* 12:1339-1348.

43. Schneider H-J, Yatsimirsky AK (2008) Selectivity in supramolecular host-guest complexes *Chem Soc Rev* 37:263-277.

44. Albert JS, Goodman MS, Hamilton AD (1995) Molecular recognition of proteins: sequence-selective binding of aspartate pairs in helical peptides. *Angew Chem Int Ed Engl* 117:1143-1144.

45. Albert JS, Peczuh M, Hamilton AD (1997) Design, synthesis and evaluation of synthetic receptors for the recognition of aspartate pairs in an alpha-helical conformation. *Bioorg Med Chem* 5:1455-1467.

46. Wender PA, Galliher WC, Goun EA, Jones LR, Pillow TH (2008) The design of guanidinium-rich transporters and their internalization mechanisms. *Adv Drug Del Rev* 60:452-472.

Chapter 2

Guanidilated calix[4]arene ligands for p53 tetramerization domain (p53TD)

2.1 Multivalent ligands based on calix[4]arenes

Calix[4]arenes have become one of the most popular scaffolds employed in the design of ligands for biomolecular recognition and bionanotechnology. Calix[n]arenes are synthetic macrocycles derived from the condensation of phenol and formaldehyde (1). Its chemistry is well established; depending on the experimental conditions, they can be formed by four to eight aromatic units arranged cyclically and linked by methylene bridges. In their conical conformation, they display basket-like structures with wider and narrower edges (upper and lower rims) as shown in Fig. 2.1.

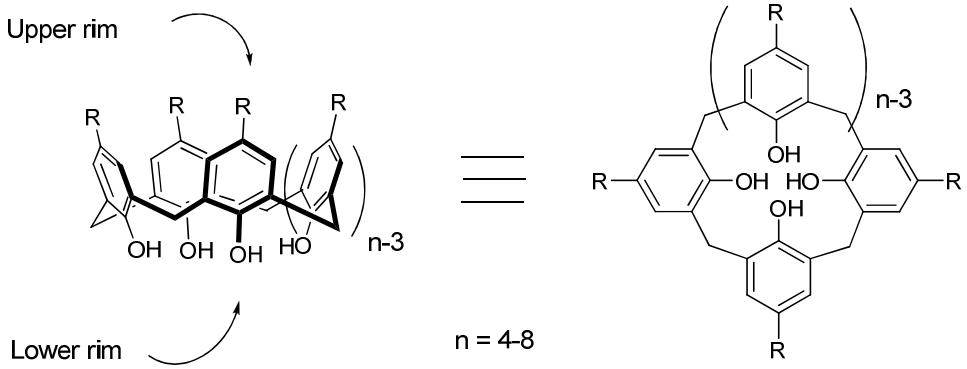

Fig. 2.1: Calix[n]arenes. The cone conformation is represented at the left.

Depending on the reaction conditions and the bulkiness of the *O*-substituents at the lower rim, the macrocycles can be freezed in one of their conformations, exemplified on calix[4]arenes in Fig. 2.2 (2).

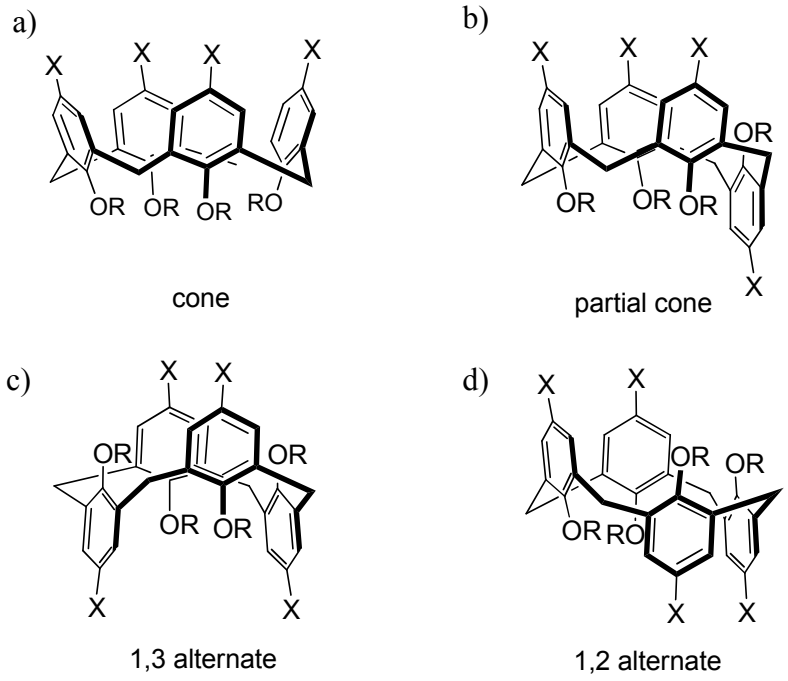

Fig. 2.2: Chemical representation of (a) cone, (b) partial cone, (c) 1,3 alternate and (d) 1,2 alternate conformation of calix[4]arenes.

Traditionally, calix[n]arenes, like cyclodextrins and crown ethers, have played a central role in supramolecular chemistry, as hosts or model receptors for ions and neutral molecules, or guests (3). Thereafter, they have found applications in the construction of electrodes, selective membranes, and sensors for analytical applications (4). Moreover, they have been applied recently for the solubilization of molecules of

biopharmaceutical interest (5), as well as in medical diagnosis (6), and even in nuclear waste decontamination (7).

Furthermore, calix[4]arenes have been exploited as multivalent ligands, with the upper rim of the conical platform as the main scaffold to bear several covalent connections to the peripheral ligating units, also called recognition elements (REs). These classical supramolecular molecules present several advantages in the multivalent approach towards drug design: First, they constitute a scaffold with multiple reactive positions that can be functionalized selectively. Second, flexibility of the macrocycle and stereochemical orientation of the ligating arms can be tuned by selecting the proper calix[n]arene (n = 4-8) and shaping the macrocycle in one of its possible conformations (Figs. 2.1 and 2.2). Third, efficient procedures are nowadays available to easily functionalize both the lower and the upper rim with most of the functional groups usually employed for conjugation of RE's (-NH_2, -CHO, -CO_2H, -NCS, -C≡C) (8).

In fact, multifunctional calix[4]arenes have already been successfully employed as biomimetic receptors for drug encapsulation (9), as building blocks for nanostructures or protein inmobilization on microarrays (10), as DNA transfection agents (11), and as modulators of several biological processes (protein inhibitors and protein surface binders), as summarized in Fig. 2.3 (12).

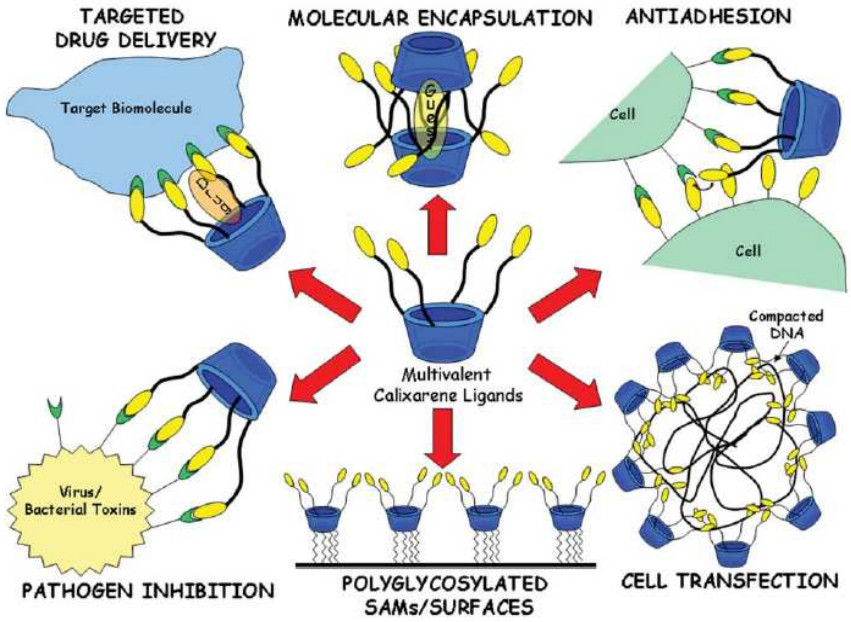

Fig. 2.3: Multivalent calixarene ligands in drug design and bionanotechnology (ref. 12).

In the context of protein surface recognition (see Chapter 1), extensive work has been reported by Hamilton and co-workers. In their search for specific ligands for positively charged protein surfaces, they developed calix[4]arene ligands for cytochrome C (Cyt C) (13), chymotrypsin (14), and platelet derived growth factor (PDGF) (15). They identified a powerful pharmacological agent, from a second generation library of multivalent calix[4]arene derivatives, which blocks the function of PDGF and VEGF (vascular endothelial growth factor), simultaneously inhibiting initiation and maintenance of blood vessels around a tumor (16). This conical ligand, GFB204, endowed with polar and non polar cyclopeptides, was further optimized by replacing its peptidic loops by isophthalate groups with similar polarity: GFB111 (Fig. 2.4) (17). Finally, systematic modifications

of the number of upper rim elements, the linker to the calixarene scaffold and the *O*-substituents in the narrower edge led to a simplified ligand endowed with three isophthalate groups and OH-free phenols (Fig. 2.4) (18).

a)

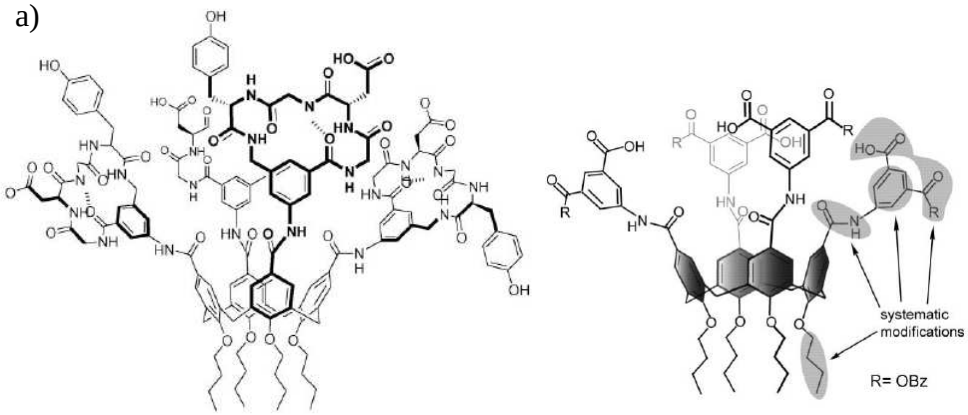

GFB111 GFB204

b)

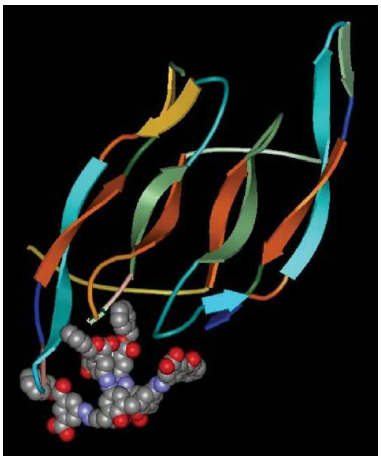

Fig. 2.4: a) **GFB111** structure and systematic modifications on **GFB204** scaffold. b) Docking between a **GFB204**-derived ligand with diazo linkers, three isophthalate arms and four free OH groups, carried out using GOLD (Goldscore fitness function). Graph was generated using WebLab Viewer Pro (from ref. 18).

Guanidilated calix[4]arene ligands for p53 tetramerization domain (p53TD)

A series of conical peptidocalix[4]arene regioisomers were conceived by Neri *et al.* to target the surface of transglutaminase, a crucial enzyme in Huntington disease (19). Competition assays suggested that inhibitors bind to a hot spot of the proteins' surface, rather than to the active site, thus exerting their inhibitory effects either by causing a conformational change in the protein or by hindering the approach of the enzyme's substrate.

Conical and 1,3-alternate calix[n]arenes functionalized with sugars have been exploited by the group of Ungaro *et al.* as scaffolds to target lectins (20). These are proteins able to recognize carbohydrates on glycoproteins present on the cell surface and responsible for recognition and entry of pathogens into cells. Recently, these authors prepared an array of calix[n]arenes presenting spacered galactose and lactose moieties and analyzed their reactivity towards a plant toxin and several human galectins (Fig. 2.5). Interestingly, bioassays revealed difference in selectivity for the different galectins and dependence of inhibition on the conformational properties of the calix[n]arene scaffold, as well as on the shape and valency of the glycoclusters (21).

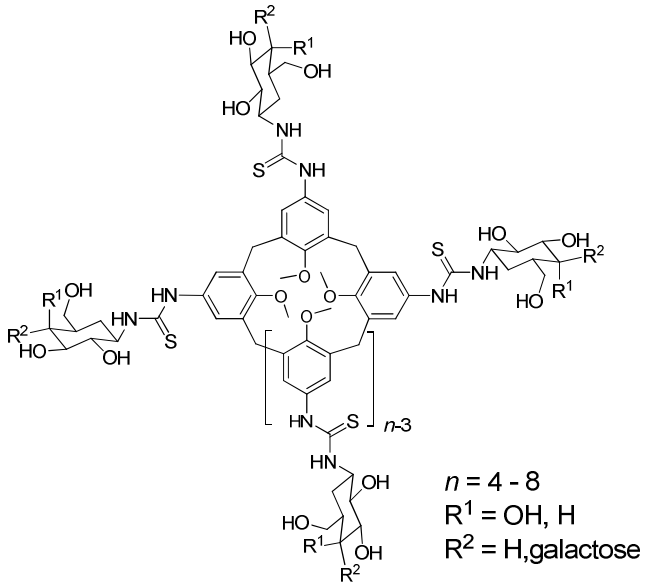

Fig. 2.5: Scheme of one of the series of sugar bound-calix[4]rene ligands developed for galectin recognition.

Furthermore, in collaboration with Bernardi's research group, they designed a conical calix[4]arene ligand for cholera toxin (CT), the pathogenic lectin causing the cholera disease (22). Efficient inhibition through adherence (IC_{50} of 0.048 µM) was obtained through a divalent ligand **I** with two opposite subunits of a mimic of the natural pentasaccharide *o*-GM1 (pseudo *o*-GM1) recognized by CT and linked to the scaffold through a flexible polyethyleneglycol spacer (Fig. 2.6).

Guanidilated calix[4]arene ligands for p53 tetramerization domain (p53TD)

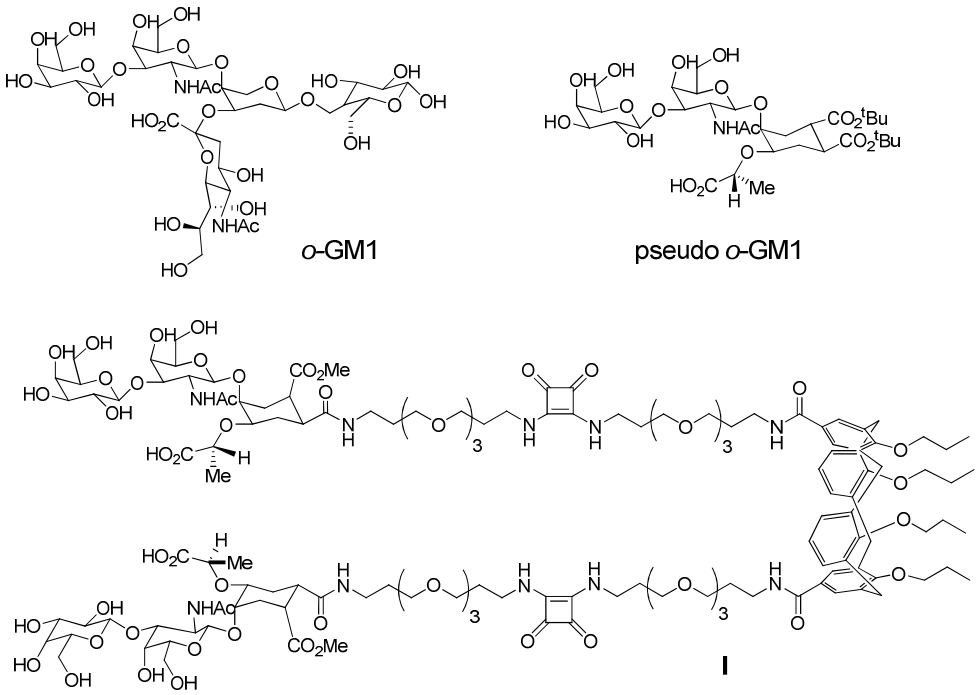

Fig. 2.6: CT ligand **I** based on a pseudo *o*-GM1-attachment to a conical calix[4]arene.

In an effort to bind tryptase -a key enzyme involved in allergic and inflammatory responses- Cunsolo and co-workers synthesized positively charged competitive inhibitors of the tetrameric protein. These flexible macrocycles based on peptidocalix[8]arenes have shown to bind to aspartic residues near the active site (23).

Ligands for heparin, based on the same multivalent scaffold, were also developed. Initial lead compounds effectively disrupted the heparin-protein binding event underpinning blood coagulation cascade (24). Similar macrocycles called calix[n]resorcarenes or resorcinarenes were exploited

by the group of Aoyama to target cell specific adhesion and transfection through proteoglycan mimicry (25). Calix[4]resorcarenes (cyclic oligomers obtained by reacting resorcinol with aldehydes), functionalized with one to four chondroitin sulfate polysaccharides on their upper rim, inhibit cell adhesion with nanomolar affinity. In addition, lactose functionalized macrocycles form glycoclusters of viral size (4-5 nm) and show specific targeting of hepatocytes *via* multiple saccharide-receptor interactions and transfection of reporter DNA (luciferase) (26).

Enhanced valency-ligands may be achieved by binding calix[n]arenes or resorcinarenes to further multivalent scaffolds. One example of this are cyclophane-based resorcinarene oligomers reported by Uchiyama *et al.*. Carboxylic resorcinarenes bound to tetraaza[6,1,6,1]paracyclophane skeletons, afforded ligands of pentameric and dodecameric resorcinarene-valency (Fig. 2.7) (27). In addition to histone binding, these receptors carried fluorescent molecules from the bulk aqueous phase to the histone surface, allowing a visual discrimination between post-translationally modified and non modified histones (28).

Guanidilated calix[4]arene ligands for p53 tetramerization domain (p53TD)

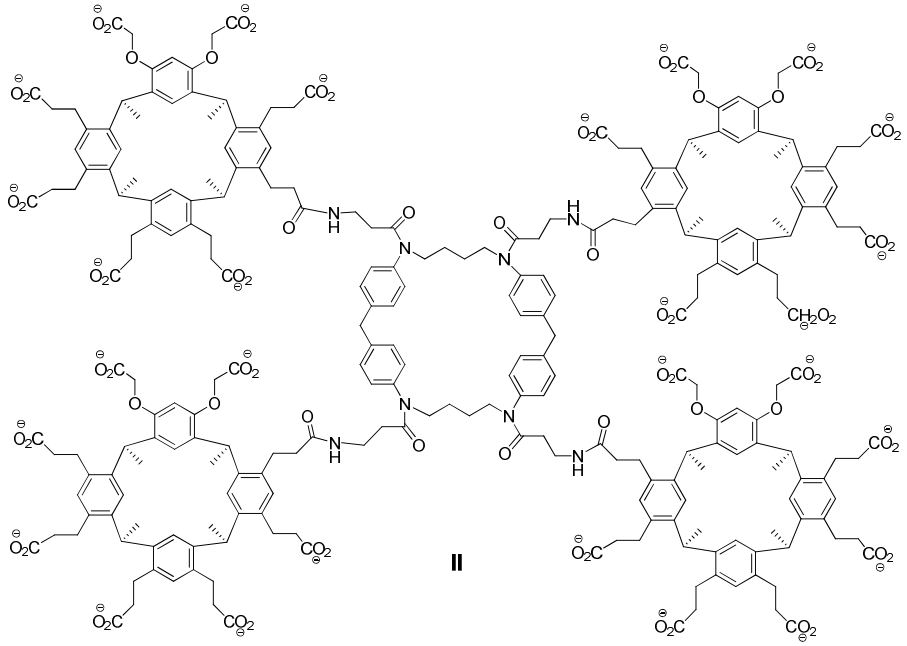

II

Fig. 2.7: Cyclophane-based tetra(resorcinarene) **II**, with tetrameric resorcinarene valency as ligands for histones.

In all the above examples, either electrostatic or sugar mediated complementarity was searched for, but none of them reports a rational designed ligand with spatial, electrostatic and symmetry complementarity to a defined protein surface.

Herein we will describe the design, synthesis and evaluation of two different series of calix[4]arene ligands which complement and specifically bind two defined protein surface targets, namely the tetramerization domain of p53 (p53TD) and the voltage dependent potassium channel subfamily K_v1 (see Chapter 3).

2.2 Introduction to target protein p53TD

The Genome guardian: P53

P53 is a transcription factor crucial for cell cycle and genomic integrity. It is an oligomeric protein able to trigger cell arrest when DNA damage in the cell is detected and activate the expression of DNA repair machinery. However, once DNA damage or cell senescence is irreversible, p53 induces apoptosis (29). Moreover it is a key target for anticancer research due to the high frequency of p53 mutations (50%) found in human cancers (30).

The main part of p53 activity comes from its ability to stimulate the transcription of various genes which contain a p53-binding element in their promoter (palindromic sequence: 5'-PuPuPuCA/TT/AGPyPyPy-3') (31). The transcriptional activity of p53 is tightly controlled by a complex feedback-regulated network *via* the negative-regulator MDM2 in concert with its homolog MDM4 (32). It is further regulated through post-translational modifications (such as phosphorylation, acetylation, methylation, etc.), interaction with a variety of signaling proteins and by degradation through ubiquitination (Fig. 2.8) (33).

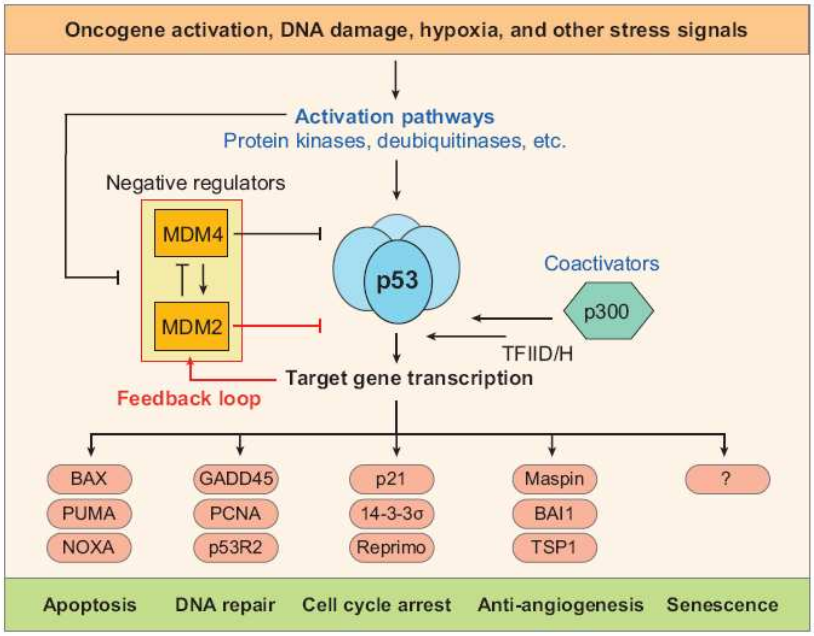

Fig. 2.8: Simplified scheme of the core regulatory network of the p53 pathway (from ref. 30).

From the structural point of view, p53 is a multidomain protein, active as a homotetramer, with four identical chains of 393 residues. A transactivation (p53TAD) and a proline-rich domain or SH_3-binding site (residues 1 to 42 and 61 to 94, respectively) are present at the *N*-terminus and are intrinsically disordered. The DNA-binding domain (p53DBD) is located in the middle of the protein (residues 102 to 292) and is responsible for sequence-specific DNA binding. This domain is connected, *via* a flexible linker to a short tetramerization domain (p53TD) that regulates the oligomerization state of p53 (residues 326-357). Finally, the regulatory domain (residues 360-393), an unfolded region rich in basic amino acids with non specific binding to DNA, is located at the *C*-terminus (Fig. 2.9) (34).

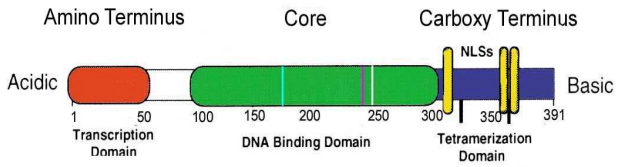

Fig. 2.9: Domains represented on the primary sequence of p53 (reproduced from ref. 34).

The quaternary structure of p53 consists basically of a folded core and the tetramerization domain, linked and flanked by intrinsically disordered segments that prevent or difficult structure analysis by x-ray crystallography or NMR. However, Fersht *et al.* recently solved the quaternary structure of human p53 in solution, by a combination of small-angle x-ray scattering (SAXS), which defined the shape, and NMR, which identified the core domain interfaces (35). They showed that the folded domains had the same structure in the intact protein than when solved separately. Thereafter, they combined solution data with 3D electron microscopy images of the closed and open forms of the oligomer and suggested the structure represented in Fig. 2.10.

a)

b)

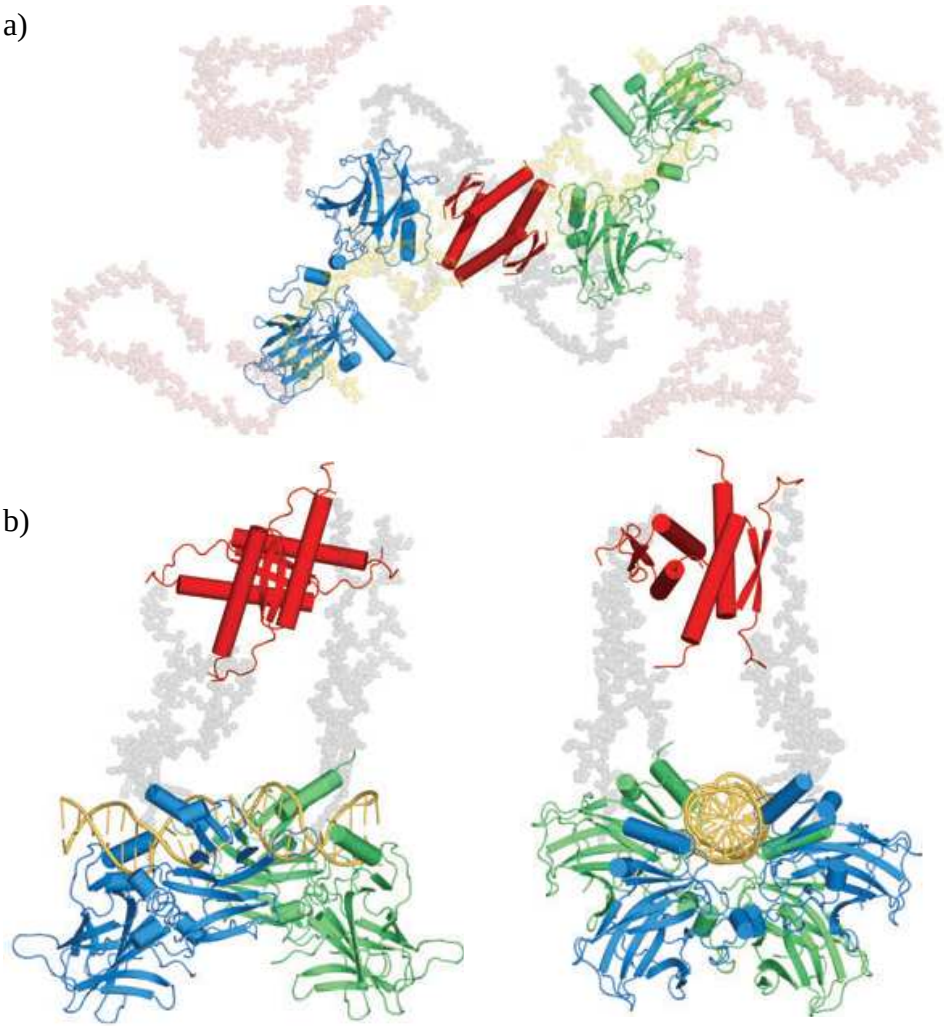

Fig. 2.10: Rigid body models of (a) free and (b) DNA-bound p53 in solution from small-angle x-ray scattering data. The second model is represented in 2 different orientations. The core (*green* and *blue*) and tetramerization domains (*red*) are shown as cartoon representations. Flexible connecting linkers (*grey*), *N*-termini (*pink*), and *C*-termini (*yellow*) are shown as semitransparent space-fill models. Models of *N*- and *C*-termini in the free protein are approximations to illustrate the space occupied by these flexible regions, rather than representing defined conformations. (reproduced from refs. 30 and 35).

The fine balance of the p53 pathway can be altered by many factors (Fig. 2.8). The most common impairment is the direct mutation of *p53* gene, which in more than 95% of the cases affects the prominent DNA binding region (36). Single missense mutations can compromise the structure of the protein or modify key residues either directly involved in the interaction with other biomolecules or required for post-translational modifications. Besides loss-of-function, mutations can also result in a protein with undesired oncogenic activity by promoting the transcription of oncogenes (gain-of-function) (37).

Mutations and specific post-translational modifications in the *C*-terminal domain affect p53 transcriptional activity by means of its dimer-tetramer equilibrium (38). Also p53 degradation mediated by ubiquitination is subject to control through this conformational equilibrium. Thus, the tetramerization domain (p53TD) plays a pivotal role in p53's activation state (39).

The tetramerization domain: p53TD

Since it was discovered, p53TD has been the matter of thorough structural and biophysical studies. Its structure, as revealed by x-ray crystallography (40) and in solution by NMR (41), is best described as a dimer of primary dimers. The monomer of the tetramerization domain is formed by a β-strand and an α-helix linked by a sharp turn (Gly334). Two monomers form a primary dimer, which is stabilized *via* an antiparallel intermolecular β-sheet and antiparallel helix packing (42). Residues Leu330, Ile332 and Phe341

make contact with each other at the interface between monomers in each primary dimer, and are the most critical residues for overall stability (Fig. 2.11).

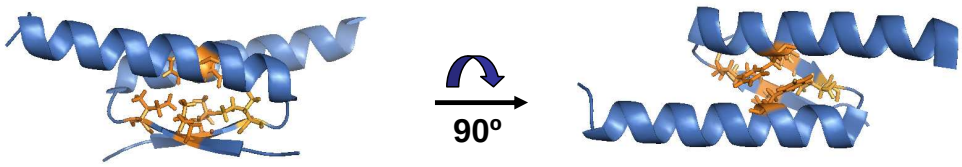

Fig. 2.11: Primary dimers stabilized by α-helix packing (Leu330, Ile332, Phe341) shown in two different orientations (ribbon representation, residues 326-356, pdb: 2JOZ).

Moreover, the side chains of Phe328, Phe338, Met340 and the aliphatic portion of Arg337 surround the minicore formed by the three critical residues and are partially buried. In addition, ionic interactions, such as Arg337-Asp352 -described later in more detail- contribute to the stability of the primary dimers (43). Two such dimers associate through their helices to form a four-helix bundle tetramer of C_2 symmetry. The driving force is mainly the formation of a hydrophobic core (44). Thermodynamic studies on p53TD stability have shown that nine hydrophobic residues per monomer, highlighted in Fig. 2.12, constitute critical determinants for its stability and oligomerization status: Leu330, Ile332, Phe341, Leu344 and Leu348 and, to a lesser extent, Phe328, Arg337, Phe338 and Met340 (45).

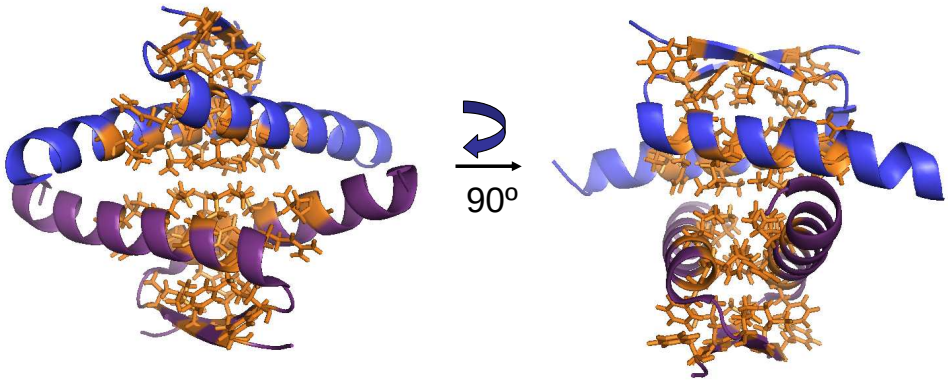

Fig. 2.12: Wild type p53TD with highlighted residues in sphere representation: Leu330, Ile332, Phe341, Leu344, Leu348, Phe328, Arg337, Phe338, Met340, Asp352 in two different orientations.

The topology of the tetramerization domain is reflected by its folding pathway, which proceeds *via* a dimeric intermediate (46). Moreover, a study of *in vitro* p53 biogenesis found that dimer formation occurs co-translationally on the polysome, whereas tetramers are formed post-translationally by dimerization of dimers in solution (47).

Germline mutation p53-R337H

It has been shown that mutations compromising the ability to form the tetrameric functional structure in the tumor suppressor protein p53, may end in cancer development (48). For instance, p53-R337H, the most frequent germline mutation of p53 gene (Arg337 is replaced by a histidine) (49), is associated to the high rate of adrenocortical carcinoma (ACC) cases in an infant population of southern Brazil. The tetramerization domain of mutant R337H can adopt a native-like structure, but is less stable than the

wild-type domain. The tetrameric stability is highly sensitive to pH in the physiological range (pH 6.5 to 8.0) (50), and this sensitivity can be correlated with the protonation state of His337.

In the wild-type sequence, the guanidinium group of Arg337 side-chain forms a hydrogen bonded salt bridge and with the carboxylate group of the Asp352 side-chain (51). This ionic pair, together with the hydrophobic interactions established between the methylene groups of the arginine and other residues (*i.e.* Ile332, Met340, Phe341 and Phe348), markedly contribute to the stability of the whole tetrameric structure (Figs. 2.12 and 2.13).

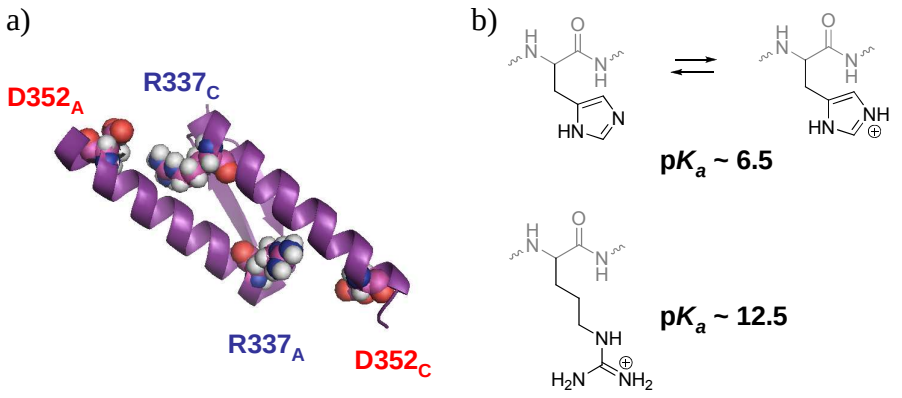

Fig. 2.13: Dimer with highlighted Arg337-Asp352 residues naming as A and C the two monomers forming one primary dimer (a) and pK_a's of histidine *vs* arginine (b).

When His337 is protonated, the mutant protein can form a stable tetramer, and roughly functions like the wild-type p53 (wt p53). However, the neutralization of the His337-Asp352 salt bridge at the high end of the physiological pH range results in an unstable tetramerization domain that is hardly folded under physiological conditions. As such, intracellular pH

modulates the function of mutant R337H (Fig. 2.14) (52). Therefore, the tissue specificity observed in ACC disease may be associated with the high pH of adrenal cells (~7.9).

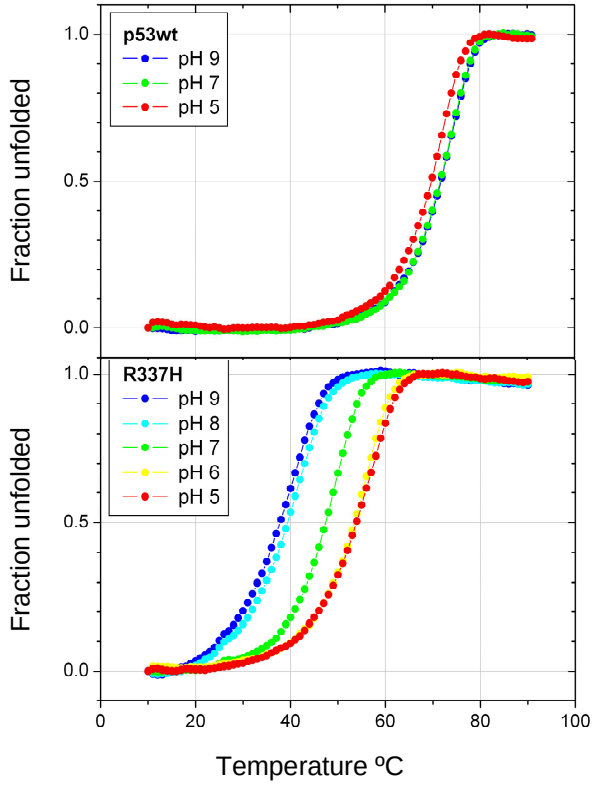

Fig. 2.14: CD melting curves of 8 µM wt p53 and 10 µM p53-R337H (monomer) at several pH's. Experiments reproduced by Dr. S. Gordo from ref. 52.

In conclusion, under certain situations, p53-R337H can not efficiently assemble the active tetramer and consequently leads to an organism prone to tumor set up (53).

2.3 Designed ligands to interact with p53TD

In the design of ligands with the capacity to modulate protein-protein surface interactions most of the effort has concentrated so far on molecules able to disrupt specific protein interactions (15) or to inhibit unspecific aggregation (54). However, little precedents refer to molecules which could induce oligomerization (55), or allow the stabilization or recovery of proteins which have lost their ability to oligomerize (56).

Previous work on bicyclic guanidinium ligands

A decade ago, the research group of Javier de Mendoza, in collaboration with those of Andrew D. Hamilton (Yale, USA), who first designed guanidinium based molecules for α-helical anionic peptides (57), and Ernest Giralt (PCB, Barcelona) showed that bicyclic guanidinium compounds, such as ligand **III**, bind helical tetraanionic patches on the surface of peptides in alcoholic media, *via* charge and shape complementarity (Fig. 2.15) (58).

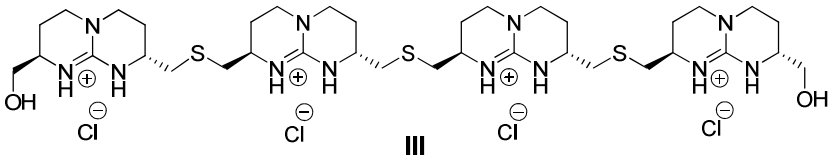

III

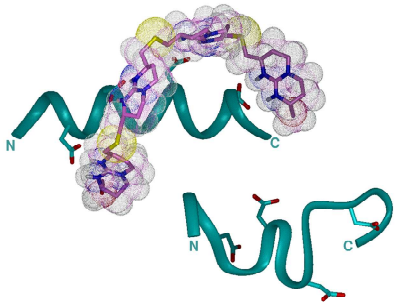

Fig. 2.15: Ligand **III** and interaction of **III** with a tetranionic peptide: Molecular dynamics simulation at 300 K and 500 ps on a peptide with an D *i*(*i*+3) motif, in the presence (a) and in the absence (b) of ligand **III** (from ref. 58a).

Two overlapping helical tetraanionic patches on the surface of p53TD were identified, one formed by residues Glu336, Glu339, Glu343 and Glu346 and the other by Glu343, Glu346, Glu349 and Asp352 (Fig. 2.16).

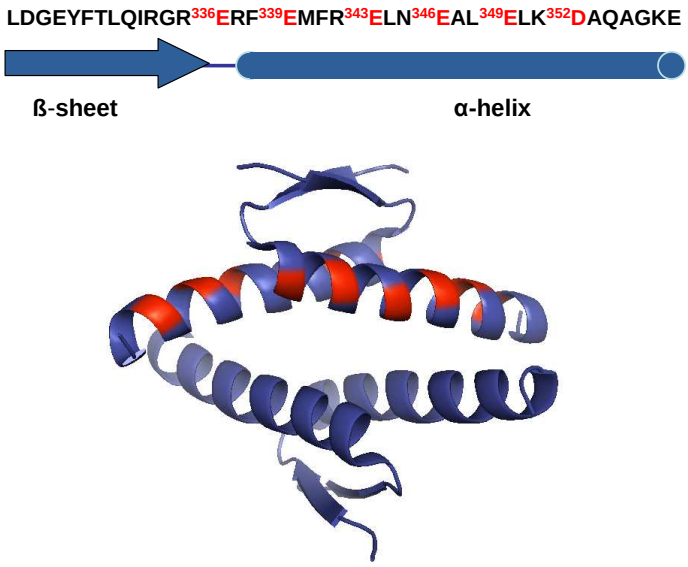

Fig. 2.16: P53TD primary sequence with highlighted acid residues belonging to two overlapping tetranionic patches on the α-helix (top). Highlighted hexanionic patch on p53TD (bottom, ribbon repr.: PyMol).

Binding of **III** was studied against p53TD by NMR-techniques ([^{1}H,^{15}N]-HSQC[i] and STD[ii]) in 10% aqueous methanol and an approximate K_d = 50 µM was observed (59). A preferred interaction was predicted for residues Glu343, Glu346, Glu 349 and Asp352. However, computational studies, carried out by Eva Santos and Carles Bo at the Institute of Chemical Research in Catalonia (ICIQ), showed that **III** shifts from one binding site to the other (non published data) so the synthesis of new hexacationic bicyclic guanidinium ligands was envisaged.

[i] Heteronuclear Single Quantum Correlation

[ii] Saturation Transfer Difference Spectroscopy

Recently, Giralt *et al.* designed a polyguanidilated peptide to interact with the surface of p53TD by employing a combination of molecular mechanics and molecular dynamics simulations. Peptide **IV** (Fig. 2.17) was obtained after four iterations of design, based on an extended conformation in which four arginine residues are arranged in an *i*/*i*+2/*i*+4/*i*+6 distribution, thus mimicking the interguanidinium distances of tetraguanidinium **III**.

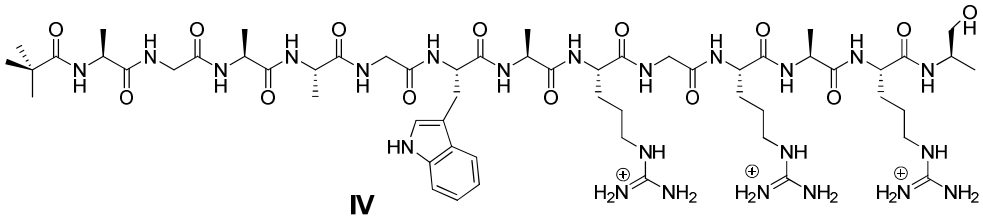

IV

Fig. 2.17: Ligand **IV**.

The interaction with p53TD was evaluated by several techniques ([^{1}H, ^{15}N]-HSQC and ITC[iii]), and a K_d of 8 μM was calculated. This value represents almost an order of magnitude of improvement in binding affinity compared to tetraguanidinium ligand **III** (Fig. 2.15) (60).

P53TD ligands based on calix[4]arenes

Compounds **III** and **IV** interact on a patch buried in the hydrophobic core of the globular domain p53TD. Hence, this recognition event may disrupt the tetramer rather than stabilize it.

Thus, taking advantage of the spatial arrangement of E336 and E339

[iii] Isothermal Calorimetry

residues in strands of two different monomers, whose free carboxylate side chains form an almost perfect square just above the hydrophobic pocket located within the strands, we reasoned that a hydrophobic, conically shaped molecule, such as **1**, endowed with four cationic residues at suitable distances to the above mentioned anionic residues, would efficiently complement the shape of the protein tetramer, thus stabilizing the whole ensemble (Fig. 2.18).

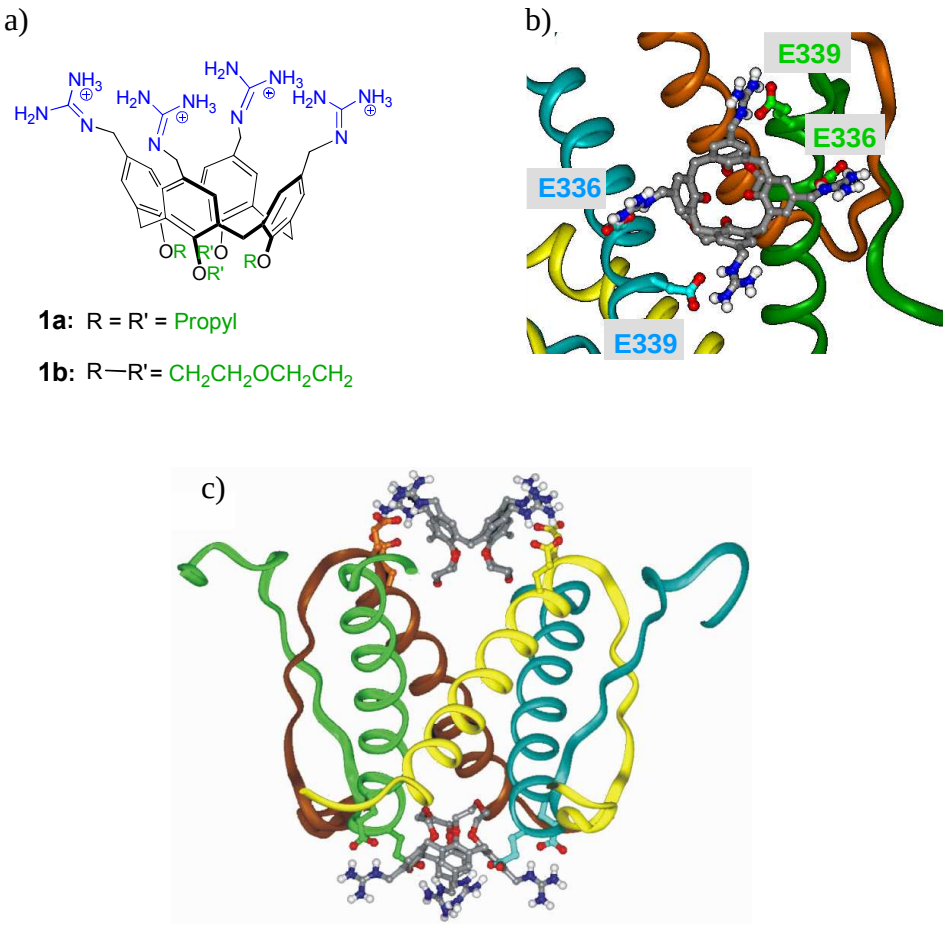

Fig. 2.18: (a) Chemical formula of ligands **1a** and **1b**. (b) Top view showing one of the ligands interacting with Glu336 and Glu339 of two different chains/monomers. (c) Tetramerization domain with two molecules of ligand **1b** (side view). Molecular mechanics optimization (Insight-II/Discover).

This is the case for conical calix[4]arene compounds **1a** and **1b** bearing: i) four guanidiniomethyl residues at the upper rim to interact with Glu336 and Glu339 of two different monomers *via* ion-pairing and hydrogen bonding and ii) an hydrophobic surface (the calixarene and the lower rim *O*-

substituents) to fit into the hydrophobic pocket located within the strands.

Each guanidine motif is linked to the calixarene platform by means of a methylene spacer, to enable the correct alignment of the group for an optimal chelation with a minimal distortion of the side chains of the protein. Moreover, ligand **1a** presents propyl chains, whereas **1b** is functionalized with diethyleneglycol loops in its lower rim. Hence, macrocycles **1a** and **1b** are both fixed in a conical conformations but their overall flexibility differs. This should be mirrored in their respective binding behavior (61).

The narrower edge of calixarene **1a** contains four conformationally-free propyl chains, long enough to prevent internal rotation of the calix[4]arene (cone inversion), but allowing the cone to oscillate between two distorted, pinched structures (Fig. 2.19).

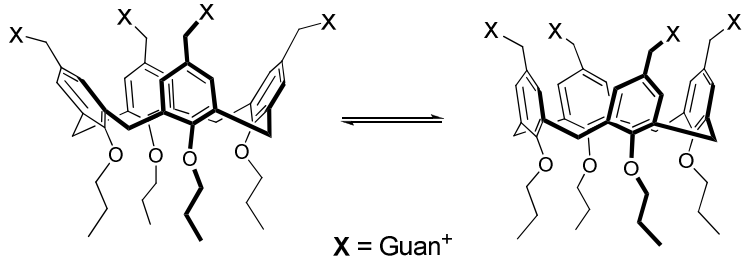

Fig. 2.19: Oscillation between two distorted pinched conformations in the conical *O*-propyl ligand **1a**.

On the contrary, macrocycle **1b** is endowed with an enhanced conical rigidity preventing its collapse into these pinched-cone conformations (64). A priori, we expected these latter property to reduce the entropic penalty of complexation of **1b** with p53TD compared to **1a**, and thus favoring

association.

As the therapeutic target we selected the naturally mutated p53-R337H tetramer, whose overall destabilization has already been described (Section 2.2). Hence, the system constituted by protein p53TD and its less stable mutant p53-R337H with defective association properties, represents an optimum model for the evaluation of our *de novo* designed calix[4]arene ligands, slightly differing in their overall flexibility.

2.4 Synthesis of p53TD ligands

The initial steps of the synthesis of compounds **1a** and **1b** (up to compound **2**), were described by Ungaro *et al*. (62): dealkylation of *tert*-butylcalix[4]arene, to yield calix[4]arene **8**, was followed by *O*-alkylation with either propyl groups for **21a** (63), or CH_2OCH_2 bridges in the case of **21b** (2, 64) Next, *para* positions were treated with *N*-bromosuccinimide (NBS) in DMF, to generate *p*-bromocalix[4]arenes **22a** and **22b**. Bromine atoms were replaced by cyano groups with CuCN in *N*-methyl pyrrolidinone (NMP) to yield the *O*-alkylated-*p*-cyanocalix[4]arenes **23a** and **23b**. Use of a microwave oven at 200 ºC shortened the reaction times from the reported 24 h (62) to 15 min. Subsequently, the cyano groups were reduced to amines with borane in THF (1M BH_3-THF) in a screw-capped tube, in order to incorporate bis-*Boc*-protected guanidinium groups on the free bases of **2a** and **2b**. The guanidilation reagent used was *N,N'*-bis-(*tert*-butoxycarbonyl)guanidine *N''*-triflate (**25**), described by Feichtinger *et al.* (65).

After deprotection of the Boc groups from precursors **24a** and **24b** under standard acid conditions, pure **1a** was obtained after sonication, wherease **1b** required additional semi-preparative HPLC purification (Fig. 2.20).

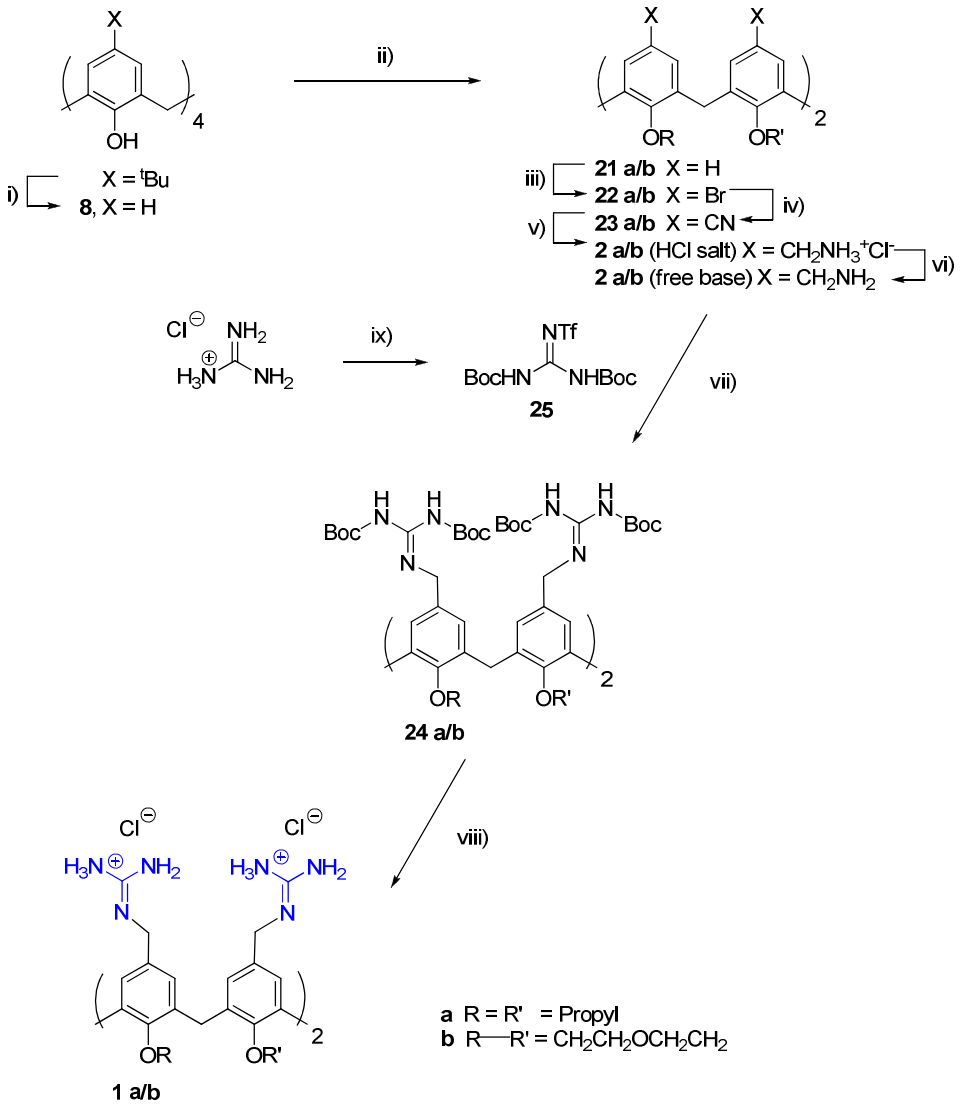

i) $AlCl_3$, phenol, toluene, 24 ºC, 24 h (84%). ii) a: IPr, NaH, DMF, 105 ºC, 7 days (74%); b: $(TsOCH_2CH_2)_2O$, NaH, DMF, 24 ºC, 4 h (41%). iii) NBS, DMF, 24 ºC, 24 h (a: 90%; b: 95%). iv) CuCN, NMP, 200 ºC, MW, 15 min (a: 62%; b: 48%). v) 1M BH_3-THF, sealed tube, reflux, 24 h (a: 79%; b: 80%). vi) extraction of **2a/b** in CH_2Cl_2 from 1N NaOH solution to obtain free base **2** (quant.). vii) **25**, Et_3N, CH_2Cl_2, 4 ºC, 24 h (a: 40%; b: 48%). viii) 4M HCl in 1,4 dioxane, 24 ºC, 24 h, (a: 84%; b: 50%). ix) a) NaOH, $(Boc)_2O$, 1,4-dioxane, 0-24 ºC, 24 h. b) Tf_2O, Et_3N, -78-24 ºC, 5 h (52%).

Fig. 2.20: Synthesis of ligands **1a** and **1b**.

In addition, the chloride salts of **2a** and **2b** were isolated and employed as negative controls for the need to assess the importance of guanidinium-groups at the upper rim. Compared to ammonium, the guanidinium group is more basic and forms concomitantly multiple hydrogen bonds, hence binding strength should be significantly higher.

Since p53TD is rich in positively charged amino acids (Arg333, Arg335, Arg337, Arg342 and Lys351), the tetracarboxylate ligand **27** was also employed as a control to rule out non-specific ionic binding of the designed ligands (Fig. 2.21).

Compounds **27a/b** were obtained by oxidation of the corresponding tetraformyl precursors **26a/b** as described by Ungaro *et al*. (66).

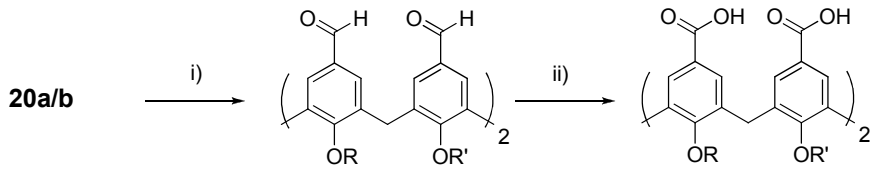

26a/b **27a/b**

a R = R' = Propyl
b R—R' = $CH_2CH_2OCH_2CH_2$

i) HMTA, TFA, 100 ºC, 18h, HCl 1h at rt (**a**: 87%; **b**: 60%). ii) H_2NSO_3H, $NaClO_2$, Acetone/H_2O/$CHCl_3$, (**a**: 73%; **b**: 70%).

Fig. 2.21: Synthesis of compound **27**.

Tetra-*p*-guanidine-tetrapropylcalix[4]arene tetrahydrochloride (**V**) (11a), an analogue to compound **1a,** was kindly provided by F. Sansone and R. Ungaro. The guanidinium moieties of **V** are directly bound to the aromatic

rings (Fig. 2.22) hence missing the methylene bridges which in our design should facilitate H-bond orientation towards carboxylates of residues Glu336 and Glu339.

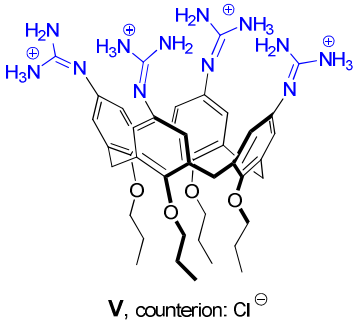

Fig. 2.22: Chemical structure of **V**.

Ligands **1a** and **1b** were evaluated as stabilizing ligands of wild type p53TD (wt p53TD) and mutated tetramer p53-R337H by i) molecular dynamics (67), and ii) a full complement of biophysical methods (68).

Interaction, binding mode and relevance of lower *vs* upper rim functionalization for **1a/1b**, were investigated by both approaches. In addition, biophysical studies highlighted the different interaction affinities relying on the distinct lower rim functionalization of **1a** *vs* **1b** (69).

2.5 Results from computational studies performed at ICIQ (Drs. C. Bo, E. Santos)

To validate the above described design, protein and protein-ligand stabilities were assessed by analyzing the trajectories obtained over 10 ns molecular dynamics simulations in a box of water at 300 and also at 400 K (aimed at simulating thermal denaturating conditions). Amber94 force field parameters were applied on wt p53TD (pdb: 1aie) (40b) and molecular dynamics simulations were performed using the Gromacs simulation package (70).

Although a recent 15 ns trajectory study reports on the changes caused by the R337H mutation in the hydrogen bonding network at different pH values (71), we wished to have a deeper insight into the contribution of both the hydrogen bonds and the hydrophobic contacts along the trajectory. As a measure of the structural changes of the protein backbone over time, hence of structural stability, we studied the root mean square deviation (RMSD) of the backbone referred to the x-ray structure, Fig. 2.23.

In the absence of ligands the structure of wt p53TD was highly stable at either 300 or 400 K over the whole dynamics and remained undisturbed in the presence of calix[4]arene ligands at both temperatures (Figs. 2.23a and b). On the contrary, the RMSD of mutant p53-R337H was moderate but grew gradually at 300 K, never recovering its initial value. Interestingly, at thermal denaturing conditions (400 K), the differences between wild type and mutated proteins were evident from the very early steps of the trajectory (Fig. 2.23c and d). These results nicely agreed with the circular

dichroism studies reported by DiGiammarino and reproduced by us (52).

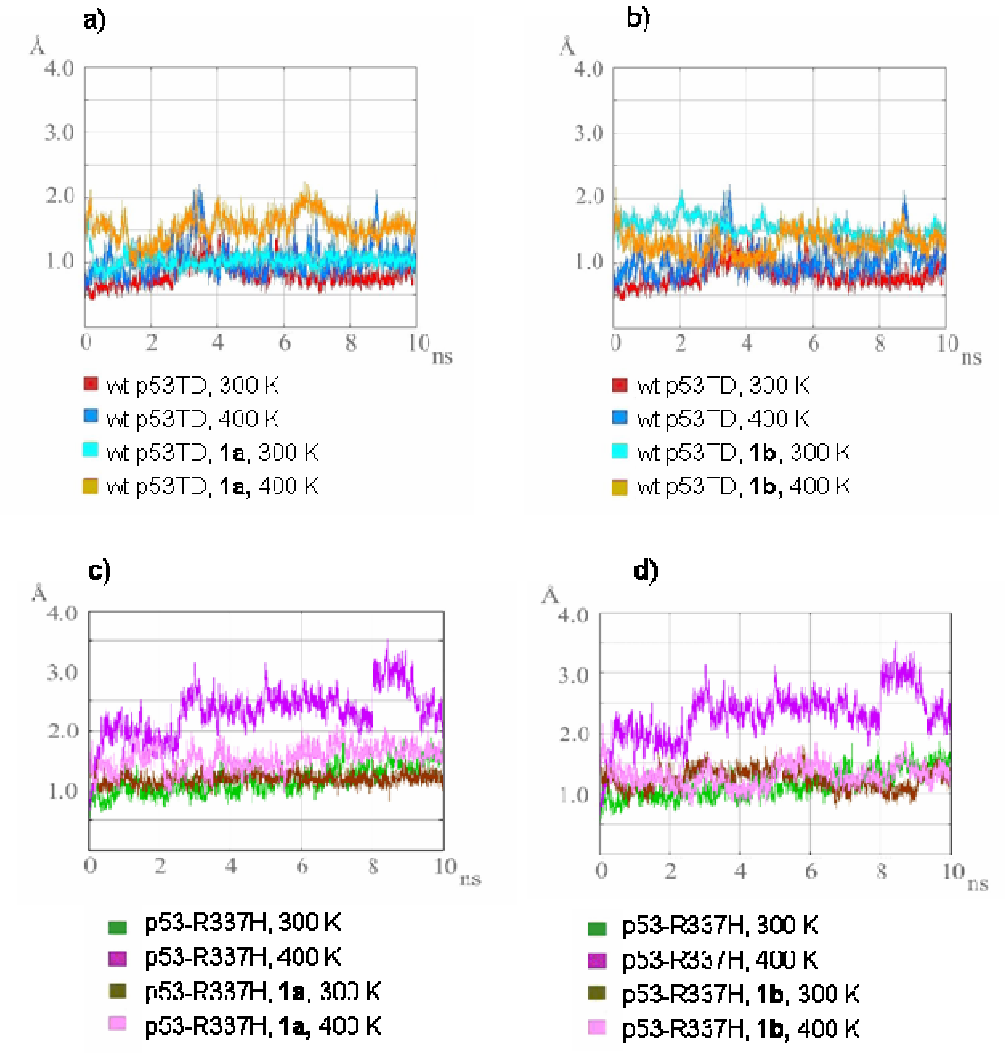

Fig. 2.23: Comparison of RMSD backbone at 300 K and 400 K. (a) wt p53TD + **1a**. (b) wt p53TD + **1b**. (c) p53-R337H + **1a**. (d) p53-R337H + **1b** (reproduced from ref. 67).

Docked ligands **1a** and **1b** remained stable at the same site they were initially positioned, interacting with the protein through hydrogen bonds

and hydrophobic interactions. Most remarkably, they strongly stabilized mutant p53-R337H, as clearly show the decrease in the RMSD value and the attenuation of fluctuations (Fig. 2.23c and d). This fully agrees with the design principles stated above. Moreover, in the presence of the bridged ligand **1b**, p53-R337H structure resembles more the native tetramer than the one promoted by ligand **1a**.

Time-evolution analysis of the secondary structure of wt p53TD and p53-R337H allowed to zoom into the site where the mutated protein in denaturing conditions experiments the largest changes. Analysis of the dimer-to-dimer interactions revealed that hydrogen bond distances for the Arg337-Glu349 ion-pair were quite constant and short in wt p53TD, whereas the corresponding His337-Glu349 pair was never hydrogen bonded along the trajectory. Other analyzed distances, such as Arg333-Asp352, or Arg/His337-Asp345, fully supported a weaker dimer-to-dimer hydrogen bonding network in the mutated protein.

On the other hand, relevant hydrophobic contacts which were essential for tetramer integrity (44), were strongly affected by the mutation. For instance (naming as A and C the two monomers forming one primary dimer, and B and D those forming the other one), $His337_A$-$Phe341_A$, $Ile332_A$-$Phe341_A$, $Met340_A$-$Met340_C$ and $Ile332_A$-$His337_A$, were notably weakened, whereas $Leu330_D$-$Phe341_A$ turned shorter. Therefore, the replacement of Arg337 by His in the mutated protein caused not only missing three hydrogen bonding contacts (with Glu349, Asp352 and Asn345) but also deeply disturbed the hydrophobic surface responsible of the stability of the structure. However, all hydrophobic distances remained at their wild-type values in the presence

of ligands **1a** and **1b,** while no improvement in the distances between pairs involved in hydrogen bonding was observed.

Hence, addition of both ligands **1a** or **1b** to the mutated protein does not produce significant shortening in the hydrogen bonding distances. However, the structure keeps fairly fixed along the whole trajectory, as in wild-type protein, due to hydrophobic contacts with the lower rim of the calixarenes, which prevent from the very beginning the cascade of events leading to disassembly.

In conclusion, MD simulations predict the stabilizing effect of ligands **1a** and **1b** on mutated p53TD, by major stabilization of the hydrophobic core (69). However, these studies do not shed light on the different association modes of **1a** and **1b,** revealed by the several binding studies described below (68).

2.6 Binding studies performed at PCB (Drs. E. Giralt, S. Gordo)

2.6.1 Binding results for 1a

Stability effects

The tetramerization domains of both wt p53TD and mutant R337H experienced a significant increase in their thermal stability in the presence of **1a,** as observed by differential scanning calorimetry (DSC, Fig. 2.24).

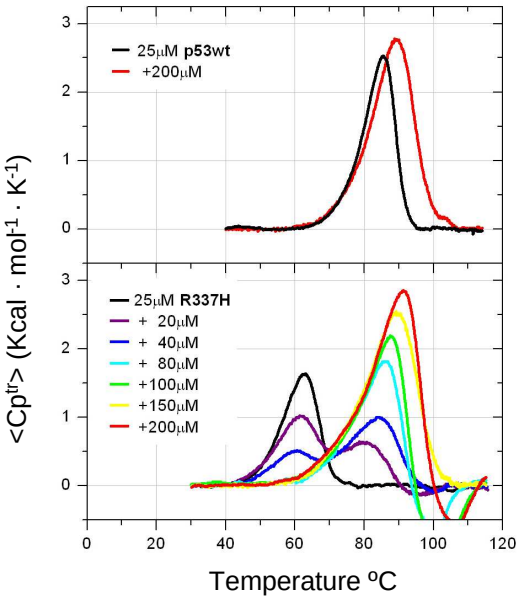

Fig. 2.24: DSC thermograms for **1a** with wt p53TD (top) and for **1a** with p53-R337H (bottom) (reproduced from ref. 68).

The shift in the transition peak for the stable wild-type tetramer was moderate with a slight increase in the unfolding enthalpy (72). However, the changes were substantially larger for the tetramerization-defective mutant p53-R337H: The shift observed in the maximum of the DSC

endotherm was of nearly 30 ºC, raising the melting temperature (T_M) from 62 ºC for the free protein, to nearly 89 ºC.

Similar results were revealed by circular dichroism: CD changes induced by **1a** on p53-R337H were more evident compared to wt p53TD, in both the secondary structure and in the CD unfolding curves. In accordance with DSC, CD unfolding curves were largely shifted towards higher temperatures (ΔT_{05} ~ 25 ºC). Interestingly, the unfolding profiles for p53-R337H and wt p53TD in the presence of 8 eq. of ligand were very similar, just as observed by DSC.

Structural and thermodynamic characterization by NMR

Once the interaction through thermal stabilization was confirmed, we addressed further structural issues by NMR. Titration of ^{15}N-labelled protein with **1a,** followed by ^{1}H-^{15}N-HSQC spectra (Fig. 2.25), revealed that the ligand binds the protein in a slow chemical exchange (in the NMR time scale). Hence, the interaction should occur with high binding affinity, and the thermodynamic dissociation constants might be in the very low micromolar range. Changes for p53-R337H take place more easily than for the wild-type protein which, in agreement with the aforementioned DSC results, suggest a higher affinity of **1a** towards the mutant (70).

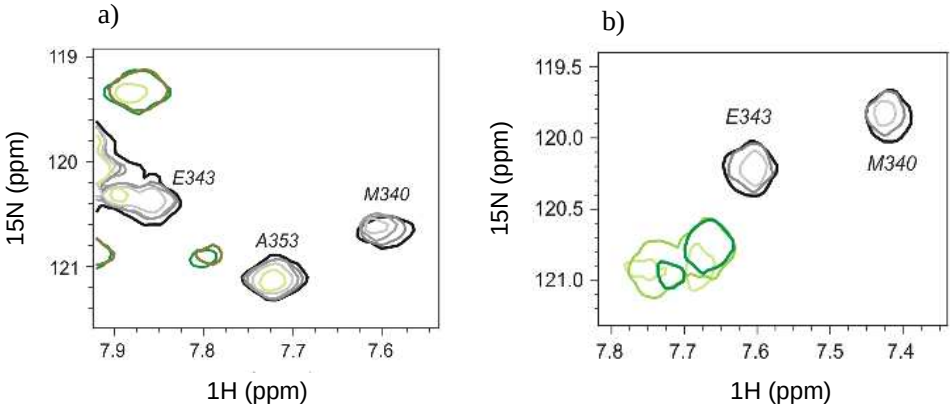

Fig. 2.25: Evolution for the ^{1}H-^{15}N-HSQC resonances of 100 µM tetrameric protein during the titration with the calix[4]arene **1a**, in water (pH 7.0, 298 K). (a) Wild-type p53TD and (b) p53-R337H titrated with ligand **1a** (reproduced from ref. 68).

The fact that almost every resonance was affected by the presence of **1a**, together with the slow exchange regime and the lost trace of the former resonances, strongly suggested that the proteins underwent some structural rearrangements upon ligand binding.

No single-bound (hence, asymmetric) intermediate was detected by NMR. This indicated that the interaction of the two ligand molecules was sequential and highly cooperative (73). However, the slow exchange regime, the significant structural rearrangements and the loss of track in the resonances did not enable to map the protein binding site. Therefore, we tested the lower affinity tetrapropylcalix[4]arene ligand **2a** where the four guanidinium groups in the upper rim have been replaced by primary amines. Titration of the proteins with this calix[4]arene was also monitored by HSQC and confirmed the lower affinity of the ligand. Moreover, mapping the chemical shifts for the first binding event on the wild-type

p53TD structure (Fig. 2.26), revealed that the parts of the protein most sensitive to the presence of ligand were those defining the hydrophobic pocket and the hydrophobic core. Such a map indicates that **2a** is bound to the protein hydrophobic pocket. Thus, the interaction seems to take place mainly with the highly stable hydrophobic core.

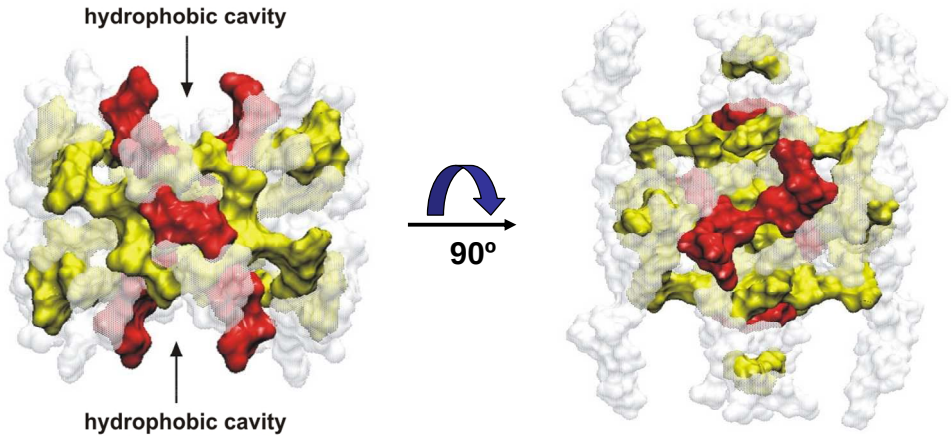

Fig. 2.26: wt p53TD mapping with **2a**. In red, residues with changes above 0.1 ppm, in yellow, those changing above 0.053 ppm. The terminal tails are removed to better appreciate the hydrophobic cavity; side view (left), top view (right, reproduced from ref. 68).

The final spectra for both proteins after titration with **1a** and **2a**, although similar, were not identical. The differences could account for looser interaction of the amino groups from the ligand with the protein carboxylates. In conjunction with the lower affinity displayed by the amino-ligand, this highlights the relevance of the guanidinium-carboxylate chelation for ligand binding (74). The effects of **V** on the protein structures were also evaluated by ^{1}H-^{15}N-HSQC. Interestingly, the changes promoted by **V** were identical to those described for the tetraamino-ligand **2a**. The

newly emerged set of resonances presented only some minor differences with the ones corresponding to **2a**, and the ligand concentrations required to promote the changes (i. e. shifts and peak disappearance) in the spectra were almost the same.

These results reveal the importance of upper rim functionalization: Comparing the three cationic ligands tested (**1a**, **2a**, **V**) it seems obvious that the length, the flexibility as well as the basicity and H-bond formation ability influence the interaction. The higher affinity results obtained for **1a** may be explained by optimal distance and orientation for carboxylate chelation, provided by methylguanidinium groups, as suggested in Fig. 2.27.

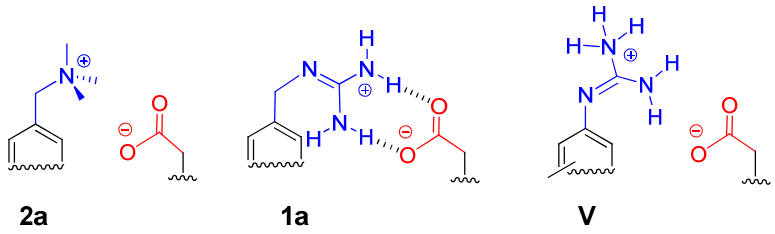

Fig. 2.27: Comparative representation of interaction of upper rim cations with carboxylates on the protein.

Furthermore compound **27a**, the tetracarboxylic calix[4]arene with propyl groups at the lower rim, was employed as a negative control. Considering the large number of positive residues on the protein surface, the carboxylates from the calix[4]arene might establish interactions with them. However, this was not the case, as calix[4]arene **27a** behaved primarily as a detergent, generating foam when the sample was mixed and causing denaturation and precipitation of the protein (68).

Non covalent complex formation

The stoichiometry of the complex with **1a** for both the wild-type and the mutant was confirmed by mass spectrometry using soft electrospray ionization (ESI-MS) (Fig. 2.28). ESI-MS experiments not only detected the non-covalent tetramer of wt p53TD, but also the non-covalent complexes with one and two calix[4]arene-bound molecules and were even better detected for mutant p53-R337H. However, the intensity of the observed species in the gas phase cannot be directly related to the affinity in solution, given that ESI-MS has a bias for electrostatic interactions, whereas it weakens the hydrophobic ones (75).

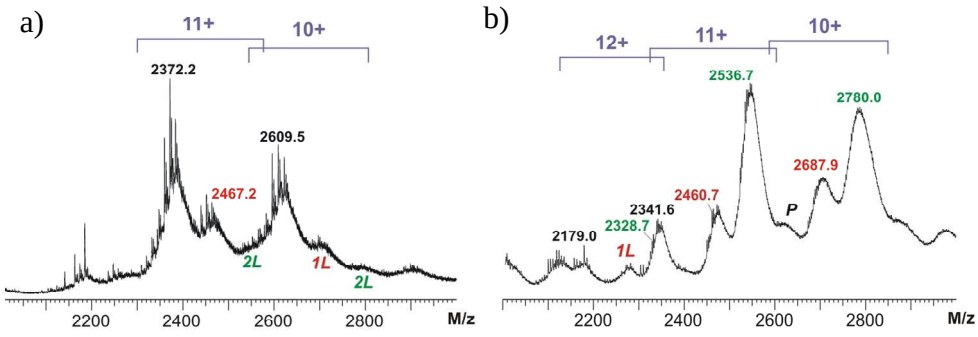

Fig. 2.28: Samples with ligand **1a** (125 μM) and (a) wt p53TD (12.5 μM) or (b) p53-R337H (12.5 μM). Masses labeled in black correspond to the free protein; in green, to the single-bound complex; and in red, to the double-bound complex. The charge state of the respective tetramer is indicated above the peaks (10 mM NH_4Cl, pH 7.0, reproduced from ref. 68).

In conclusion, **1a** promoted large thermal stabilization, especially on protein p53-R337H. The large shift in T_M as well as the enthalpic increase in the unfolding of the ligand-bound protein, suggested a tight and energetic

interaction of sequential and cooperative nature. Moreover the changes experienced by the protein resonances strongly pointed towards important structural changes not only for p53-R337H but also for wt p53TD. Finally, mass spectrometry confirmed the tight binding of two molecules of **1a**.

As predicted in the model, hydrophobic interactions (Fig. 2.18) play a major role in the interaction of ligands **1a**, **2a** and **V**. However, a better carboxylate chelation and thus higher affinity was achieved by ligand **1a** through methylguanidinium moieties.

2.6.2 Binding results for 1b

Stability effects

Experimentally, the thermal effects caused by ligand **1b** on the stability of both, wild-type and mutated proteins, were also evaluated by DSC (Fig. 2.29) and CD, showing very similar behaviors compared to **1a**. Calixarene ligand **1b** displayed rather low affinity for the stable wild type protein, while it induced an outstanding thermal stabilization in mutant p53-R337H (Fig. 4B), shifting T_M 20 ºC, a little less than **1a** (27 ºC). Hence, as for **1a**, thermal changes pointed not only to a tight protein-ligand interaction but also suggested that the tetramer was the actual stabilized structure, because T_M for ligand-bound p53-R337H (~82 ºC) rose close to that for wt p53TD (85.5 ºC).

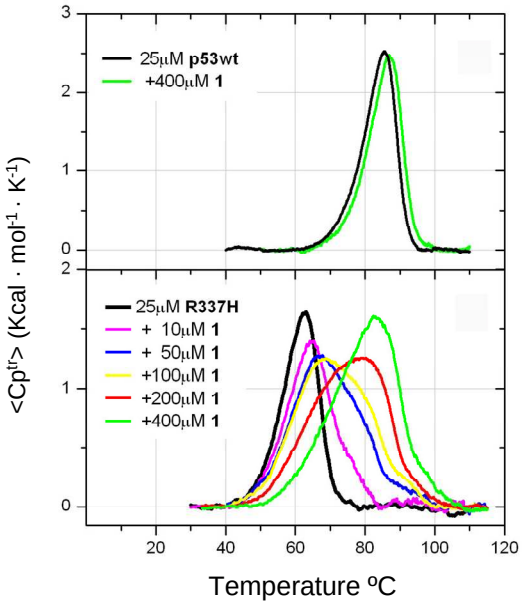

Fig. 2.29: DSC thermograms of **1b** with (a) wild-type p53TD and (b) p53-R337H (reproduced from ref. 69a).

Structural and thermodynamic characterization by NMR

Structural aspects were examined by NMR on both the ligand and the protein. These experiments not only determined that wt p53TD and ligand **1b** interacted specifically, but also mapped the interacting molecules.

^{1}H-Saturation Transfer Difference (^{1}H-STD) experiments were employed to resolve the ligand binding mode (76). Normalized values for the different protons are directly labeled on formula **1b** (Fig. 2.30), 100% meaning the highest saturation, *i.e.* the proton closest to the protein.

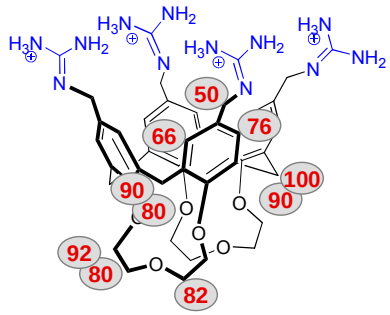

Fig. 2.30: STD epitope mapping: Saturation normalized percentages for the protons of ligand **1b**. 100% corresponds to the ^{1}H with the highest saturation degree, thus, the one closer to the protein.

STD results completely agreed with the design rationale for ligand **1b** (Fig. 2.18), with the hydrophobic lower rim of the calixarene "inserted" like a cork into the protein cleft (hence experiencing higher saturation), while the upper rim remained outside (lower saturation).

Regarding the protein, a thorough titration of ^{15}N-p53TD with ligand **1b**, followed by ^{1}H-^{15}N-HSQC proved which parts of the protein structure were directly involved in the interaction. Representation of the most strongly shifted residues at the end of the titration led to the mapping of the protein binding site (Fig. 2.31), which was in perfect agreement with the designed model, since all the solvent exposed residues constituting the protein cleft were sensitive to the presence of ligand **1b**.

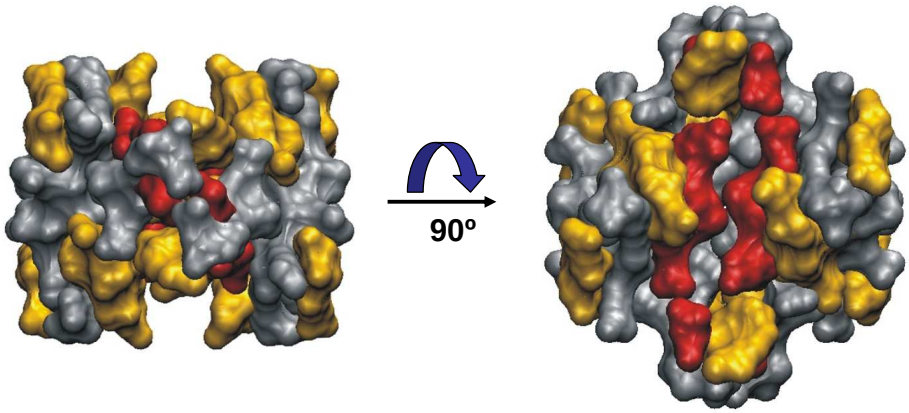

Fig. 2.31: wt p53TD mapping with **1b**: In red, residues shifted > 0.075 ppm; in orange, those shifted > 0.04 ppm (the mean shift, reproduced from ref. 69a).

When a similar titration was carried out for mutant p53-R337H, a totally different evolution for the HSQC spectra occurred, indicating that interaction of ligand **1b** with p53-R337H took place through a different and more complex mechanism. Likely, the histidine mutated residue, as a part of the hydrophobic pocket, causes significant distortions and conformational changes with respect to the wild type protein.

Further understanding about the binding mechanism and its thermodynamics was achieved by analyzing changes in NMR line shape, shift and intensity upon titration of the protein with the ligand (77). The interaction between the wild-type p53TD and the calixarene underwent a fast chemical exchange (in the NMR time scale), and unidirectional shift in the 2D spectrum movement was only feasible assuming both sites on the protein equivalent and independent. Adjustment of the clear chemical shifts for Met340 signal (Fig. 2.32a) to a 1:2 protein-ligand binding model (Fig.

2.32b), resulted in an apparent dissociation constant of ~280 ± 40 μM.

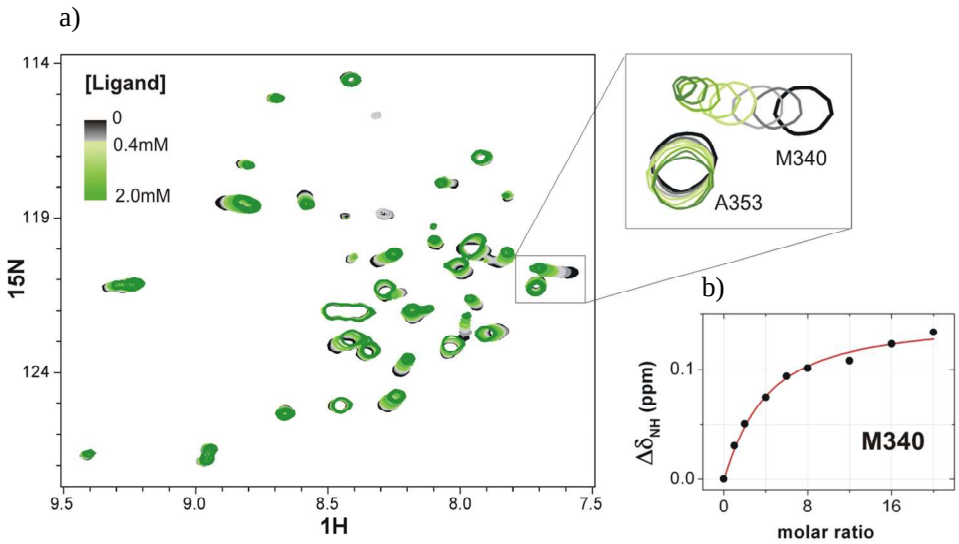

Fig. 2.32: (*a*) ^{1}H-^{15}N-HSQC overlaid spectra for the titration of p53TD with **1b**. Only central region shown. Color code: black: free protein (125 μM tetramer); grey scale: up to 500 μM of ligand (*i.e.* < 4 eq); green scale: from 500 μM to 2.5 μM of **1b** (*b*) Perturbation of Met340 resonance adjusted to a simplified 1:1 binding model (reproduced from ref. 69a).

The contribution of the guanidinium groups to the binding was assessed by comparison with the ammonium derivative **2b**: Though **2b** also bound to the protein, it displayed considerably lower affinity, in analogy to **2a**.

For mutant p53-R337H, the interaction with calixarene **1b** took place by a more complex mechanism, that could be interpreted considering two sequential events, as suggested for **1a**, each of them probably corresponding to the binding of a molecule of calixarene ligand to the tetramer. No clear intermediate was detected suggesting again, as for **1a**, that the second binding event is of larger affinity than the first one. Indeed, the dissociation

constants for both binding events were estimated to be K_{d1} = 70 ± 6 μM and K_{d2} = 8 ± 5 μM, clearly lower than that for the wt p53TD.

Additional evidence for robustness of the final assembly came from electrospray mass spectrometry (ESI-MS) measurements, in which the tetrameric protein, non covalently bound to two synthetic ligands, was detected.

In conclusion, the experimental results here presented, fully validate the rational design for **1b** binding to p53TD: Thermal stability induced by on p53-R337H mutant was observed. Moreover, characterization by NMR enabled to assess first the structural binding model on either p53TD proteins and ligand **1b**, as well as their thermodynamic behaviour: On the stable and well-packed wt p53TD, the two binding sites for **1b** were likely equivalent and independent, while for the mutated protein the binding of the two ligand molecules was cooperative and implied some major structural rearrangements. Finally, the predicted stoichiometry was confirmed by ESI-MS.

2.7 Conclusions and outlook

Associations between either calixarenes **1a** and **1b** and tetramers wt p53TD and mutant p53-R337H were correctly predicted by molecular dynamics (MD) and characterized by a variety of biophysical methods. Both approaches, the theoretical and the empirical one, show that hydrophobic forces play the major role, while optimized ionic and hydrogen bond interactions further contribute to strengthen the complexes.

Stabilization and tighter binding to mutant p53-R337H *vs* wt p53TD were observed with both ligands **1a** and **1b**. This outstanding observation may be explained by a greater plasticity of the mutant tetramer, which enables better adaptation to the protein-ligand complex.

Furthermore, **1a** interacts stronger with both tetramers, as assessed by the approximated K_d's of both ligands. Again this may have its origin in the greater flexibility of **1a** over **1b**. Remarkably, our results show that **1a** binds more tightly to both proteins, thereby supporting the hypothesis that higher flexibility helps the ligand (and the protein) to adopt the optimal conformations for the best fit. Moreover, through this tight binding, **1a** also promotes some structural perturbation on the proteins, which could not be predicted in advance, but results in more stable species. These findings underscore the crucial role of flexibility in recognition processes, not only for the ligand, but also for the biomolecular surface.

In this respect, it would be interesting to evaluate novel ligands with different *O*-substituents, such as methylene, ethylene or even using OH-free

p-methylguanidinium calix[4]arenes, in order to better assess or even quantify the importance of conical prearrangement and hydrophobic surface in binding.

Finally, we wanted to verify if ligands **1a** and **1b** could still efficiently bind to p53TD, as part of the whole p53 protein, since the *in vitro* affinity of these ligands for p53TD (μM range) might be not enough to interact with p53 or their multivalency might lead to nonspecific interactions with other biomolecules (*e.g.* DNA, RNA and lipids). However, though experiments using entire p53 were originally envisioned, we were unable to carry them out, as both ligands precipitated in buffered solutions.

Nevertheless, our study paves the way for new strategies in drug discovery and provides a proof of principle for the feasibility of approaches using designed complex chemical ligands to recover the supramolecular integrity of damaged protein assemblies, through surface recognition.

2.8 Experimental part

General procedures.

Synthesis. All reactions were carried out under argon with dry solvents unless otherwise noted. All commercially available reagents were used without further purification. The solvents were dried and distilled as described in the literature (78).

Chromatography. Reactions were monitored by thin layer chromatography (TLC) performed on DC-Fertigplatten SIL G-25 UV_{254} (MACHEREY-NAGEL GmbH) or by analytical high performance liquid chromatography (HPLC) with a RP-C_{18} column Symmetry300^{TM} C18 5 µm 4.6 x 150 mm, $UV_{210-220}$, 5 µl inj., 1 ml/min flux, on a high performance liquid chromatograph (HPLC: Agilent Technologies Series 1200 with UV-detection). Semipreparative-HPLC purification was performed on Waters HPLC 600 equipment with a quaternary pump (0.01-20 mL/min). Standard column chromatography was done on silica gel by SDS (chromagel 60 ACC, 40-60 mm) following the procedure described by W. C. Still (79).

Analysis. Yields refer to chromatographically pure compounds. ^{1}H NMR and ^{13}C NMR spectra were recorded on Bruker Avance 400 UltraShield spectrometer (^{1}H: 400 MHz, ^{13}C: 100 MHz) and are reported in parts per million (ppm) relative to the residual solvent peak. Data for ^{1}H are reported as follows: chemical shift (δ ppm), multiplicity (s = singlet, bs = broad singlet, d = doublet, tr = triplet, q = quartet, sex = sextet, m = multiplet), coupling constant in Hz, and integration. Exact masses were measured on a Waters LCT Premier liquid chromatograph coupled time-of-flight mass

spectrometer (HPLC/MS-TOF) with electrospray ionization (ESI). Melting points (Mp) were measured with a Büchi B-540 apparatus.

25,26,27,28-Tetrahydroxycalix[4]arene (8).

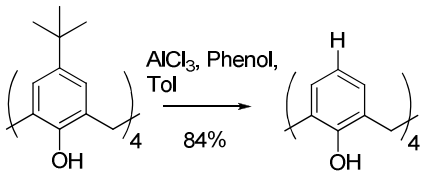

8

To a suspension of *p-tert*-butylcalix[4]arene (3 g, 4.6 mmol) in toluene (45 mL), phenol (0.46 g, 4.9 mmol) and $AlCl_3$ (3 g, 23 mmol) were added sequentially. The mixture was stirred at rt for 18 h. Thereafter, the reaction was quenched with 1M HCl (25 mL) and stirred at rt for an additional hour. Next, CH_2Cl_2 (100 mL) was added to the mixture and the aqueous layer was extracted several times with CH_2Cl_2 (3 x 30 mL). The combined extracts were washed with H_2O (30 mL) and brine (30 mL). After drying the organic layer over $MgSO_4$ and filtering, the solvents were eliminated *in vacuo*. The final residue was triturated in cold Et_2O and a colorless precipitate was obtained which was filtered and dried under reduced pressure. Compound **8** was obtained in a 84% yield. Product **8** may be further recrystallized in $CHCl_3/CH_3OH$ (80). Mp: 315-318 ºC. ^{1}H NMR ($CDCl_3$): δ 10.19 (s, 4H, OH), 7.22-6.64 (m, 12H, ArH), 3.63-3.48 (bs, 8H, CH_2). ^{13}C NMR ($CDCl_3$): δ 148.4, 129.0 (CAr), 128.2, 122.2 (CHAr), 31.7 (CH_2). ESI(-): *m/z*: $[M - H]^-$: 423.2 uma.

25,26,27,28-Tetrapropoxy-calix[4]arene (21a).

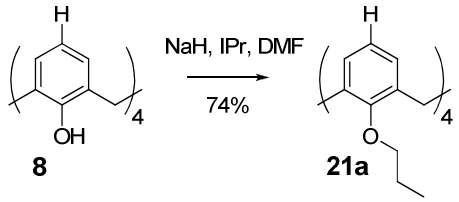

A mixture of calix[4]arene **8** (2.00 g. 4.7 mmol), NaH (2.26 g, 47.1 mmol of a 50% dispersion in oil), propyl iodide (4.6 mL, 47.1 mmol), and DMF (30 mL) was stirred overnight at rt, and then slowly poured into aqueous 1M HCI (100 mL) to precipitate crude compound **21a.** The solid was recovered by filtration, dried and triturated with CH_3OH to give pure **21a** as a colorless solid in a 74% yield: Mp: 197-199 ºC.^{1}H NMR: δ 6.61-6.55 (m, 12H, ArH), 4.44 (d. J = 13.3 Hz, 8H, ArCHH*ax*Ar), 3.84 (tr, 8H, J = 7.4 Hz, OCH_2CH$_2$CH$_3$), 3.14 (d, J = 13.3 Hz, 8H, ArCHH*eq*Ar), 1.91 (sex, J = 7.4 Hz, CH$_2$CH_2CH$_3$), 0.98 (tr, J = 7.4 Hz, 12H, CH$_3$). ^{13}C NMR: δ 156.6, 135.1 (CAr), 128.1, 121.9 (CHAr), 76.7 (O*C*H$_2$CH$_2$CH$_3$), 31.0 (ArCH$_2$Ar), 23.2 (CH$_2$*C*H$_2$CH$_3$), 10.3 (CH$_3$). ESI(+) *m/z*: [M + Na]$^+$: 615.3 uma.

25,26-27,28-Biscrown-3-calix[4]arene (21b).

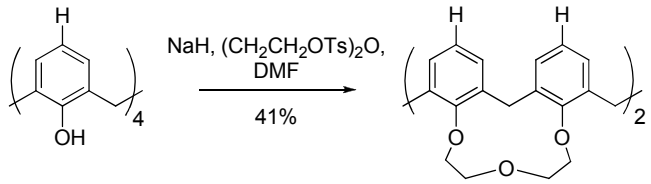

8 **21b**

NaH (1.7 g, 38.0 mmol of a 50% dispersion in oil) was added to a solution containing calix[4]arene **8** (2.00 g, 4.7 mmol) dissolved in DMF (500 mL) and the mixture was heated to 80 ºC. Thereafter, diethylene glycol ditosylate (4.9 g, 11.8 mmol) dissolved in 5 mL of DMF was added. The reaction was stirred for 4 h at rt and evaporated to dryness.The residue was taken up with 10% HCl (100 mL, caution!) and extracted with EtOAc. The organic layer was dried over anhydrous Na_2S0_4 and purified by column chromatography on silica gel (eluent: Hex/EtOAc, 5:1→3:1. Finally compound **20b** was obtained as a colorless solid in a 41% yield. Mp 265-268 ºC. ^{1}H NMR ($CDCl_3$): δ 7.01-6.98 (m, 8H, ArH), 6.73 (tr, J = 7.5 Hz, 4H, ArH), 5.05 (d**,** J = 12.1 Hz, 2H, ArCH*Hax*Ar) 4.49 (d**,** J = 12.1 Hz, 2H, ArCH*Hax*Ar), 4.31-3.84 (m, 16H, CH_2O), 3.26 (d**,** J = 12.1 Hz, 2H, ArCH*Heq*Ar), 3.21 (d, J = 12.1 Hz, 2H, ArCH*Heq*Ar). ^{13}C NMR ($CDCl_3$): δ 135.6, 135.5 (CAr), 129.0, 128.1, 123.7 (CHAr), 76.3, 74.8 (CH_2O), 30.7, 29.8 ($ArCH_2Ar$). ESI(+) *m/z*: $[M + H]^+$: 565.25 uma.

General procedure for the synthesis of *p*-bromo-calix[4]arenes 22a and 22b

To a stirring solution of 1.7 mmol of precursors **21a** or **21b** in 30 mL of

DMF, NBS (8.4 mmol for **21a** and 14 mmol for **21b**) was added. After 24 h at rt, the reaction mixture was quenched by addition of 50 mL of a 1M HCl solution. The resulting solid was filtered on a Buchner funnel and recrystallized from CH_3OH.

5,11,17,23-Tetrabromo-25,26,27,28-tetra-*n*-propoxycalix[4]arene (22a).

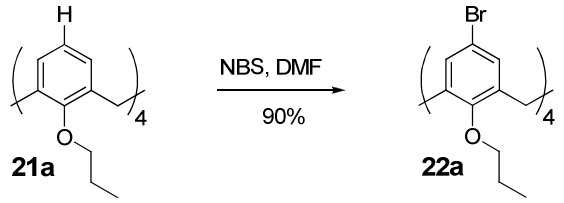

Compound **22a** was obtained as a colorless solid in a 90% yield. Mp: 277-280 °C. ^{1}H NMR ($CDCl_3$): δ 6.78 (s, 8H, ArH), 4.33 (d, J = 13.5 Hz, 4H, ArCH*H*axAr), 3.78 (tr, J = 7.5 Hz, 8H, OCH_2CH$_2$CH$_3$), 3.07 (d, J = 13.5 Hz, 4H, ArCH*H*eqAr), 1.85 (m, J = 7.5 Hz, 8H, OCH$_2$CH_2CH$_3$), 0.94 (tr, J = 7.5 Hz, 12H, CH_3). ^{13}C NMR ($CDCl_3$): δ 155.6, 136.6 (CAr), 131.3 (CHAr), 115.4 (CAr), 77.3 (O*C*H$_2$CH$_2$CH$_3$), 31.0 (ArCH$_2$Ar), 23.3 (OCH$_2$*C*H$_2$CH$_3$), 10.4 (CH_3). ESI(+) *m/z*: $[M + Na]^+$: 927.0 uma.

5,11,17,23-Tetrabromo-25,26-27,28-biscrown-3-calix[4]arene (22b).

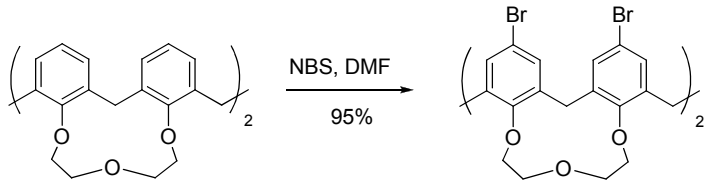

Compound **22b** was obtained as a colorless solid in a 95% yield. Mp: > 350 °C. ^{1}H NMR ($CDCl_3$): δ 7.15 (d, J = 2.4 Hz, 4H, ArH), 7.13 (d, J = 2.4 Hz, 4H, ArH), 4.96 (d, J = 12.1 Hz, 2H, ArCH*H*axAr), 4.37 (d, J = 12 Hz,

2H, ArCH*H*axAr), 4.33 (tr, *J* = 11.6 Hz, 4H, CH_2O), 4.21, 4.08 (m, 8H, CH_2O), 3.82 (tr, *J* = 11.6 Hz, 4H, CH_2O), 3.33 (d, *J* = 12.2 Hz, 2H, ArCH*H*eqAr), 3.28 (d, *J* = 12.1 Hz, 2H, ArCH*H*eqAr).^{13}C NMR ($CDCl_3$): δ 154.7, 137.2, 137.0 (CAr), 132.3, 131.3 (CHAr), 116.6 (CAr), 75.9, 74.7 (CH_2O), 30.5, 29.7 ($ArCH_2Ar$). ESI(+) *m/z*: $[M + Na]^+$: 898.9 uma.

General procedure for the synthesis of *p*-cyanocalixarenes 23a and 23b.

To a microwave tube with tetrabromo-calix[4]arenes **22a** or **22b** (0.3 mmol)**,** CuCN (224 mg, 2.15 mmol) and NMP (1,5 mL) were added. The reaction was stirred and heated in a microwave reactor at 200 °C for 15 min (200 Watt and 100 PSI). After cooling the reaction mixture to 50 ºC, a solution of $FeCl_3$ (0.54 g, 3.4 mmol) in 10 mL HCl 1N was added and the mixture was stirred additionally for 30 min. The resulting solid was filtered on a Buchner funnel and compounds **18a** and **18b** were purified by silica gel flash chromatography.

5,11,17,23-Tetracyano 25,26,27,28-tetra-*n*-propoxycalix[4]arene (23a).

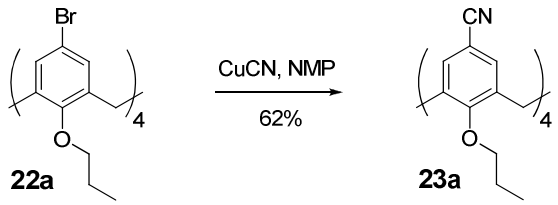

Eluent: CH_2Cl_2/EtOAc, 80:20. Subsequently, **23a** was triturated in hexane and obtained as a grey solid in a 62% yield. Mp: > 350 °C. ^{1}H NMR ($CDCl_3$): δ 6.99 (s, 8H, ArH), 4.44 (d, *J* = 11.5 Hz, 4H, ArCH*H*axAr), 3.90 (tr, *J* = 6.2 Hz, 8H, $OCH_2CH_2CH_3$), 3.25 (d, *J* = 11.5 Hz, 4H,

ArCH*H*eqAr), 1.88 (sex, *J* = 6.2 Hz, $OCH_2CH_2CH_3$, 8H), 0.99 (tr, *J* = 6.2 Hz, 12H, CH_3). ^{13}C NMR ($CDCl_3$): δ 154.8, 135.8 (CAr), 132.7 (CHAr), 116.2 (CN), 107.3 (CAr), 77.6 ($OCH_2CH_2CH_3$), 30.6 ($ArCH_2Ar$), 23.4 ($OCH_2CH_2CH_3$), 10.3 (CH_3). IR (KBr): 2224 cm^{-1} (ν, C≡N). ESI(+) *m/z*: $[M + Na]^+$: 715.4 uma.

5,11,17,23-Tetracyano-25,26-27,28-biscrown-3-calix[4]arene (23b).

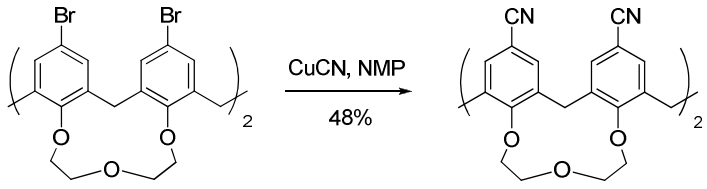

22b **23b**

Eluent: CH_2Cl_2/EtOAc, 95:5→80:20. Compound **23b** was obtained as a cream coloured solid in a 48% yield. Mp: > 350 °C. ^1H NMR ($CDCl_3$): δ 7.82 (d, *J* = 1.8 Hz, 4H, ArH), 7.77 (d, *J* = 1.8 Hz, 4H, ArH), 5.02 (d, *J* = 12.1 Hz, 2H, ArCH*H*axAr), 4.38 (d, *J* = 12.2 Hz, 2H, ArCH*H*axAr), 4.33 (tr, *J* = 9.8 Hz, 4H, OCH_2), 4.21-4.08 (m, 8H, OCH_2), 3.82 (tr, *J* = 9.8 Hz, 4H, OCH_2), 3.33 (d, *J* = 12.2 Hz, 2H, ArCH*H*eqAr), 3.28 (d, *J* = 12.1 Hz, 2H, ArCH*H*eqAr). ^{13}C NMR ($CDCl_3$): δ 158.3, 136.0, 135.8 (CAr), 134.4, 133.2 (CHAr), 119.0 (CN), 108.0 (CAr), 76.8, 74.7 (CH_2O), 29.3, 28.6 ($ArCH_2Ar$). ESI(+) *m/z*: $[M + Na]^+$: 687.2 uma.

General procedure for the synthesis of *p*-amino-calixarenes 2a and 2b.

Tetracyano-calixarenes **23a** or **23b** (0.15 mmol) were introduced into a screw-capped tube and a solution of 1M BH_3-THF (4.5 mL, 4.5 mmol) was added at 0 ºC. The solution was heated at 80 ºC for 24 h. Then CH_3OH (1

mL) and 1N HCl (3 mL) were added dropwise to the solution and the reaction mixture was heated at 50 °C for additional 30 min. THF and CH_3OH were removed under reduced pressure and the tetramino derivatives were isolated as follows.

5,11,17,23-Tetraminomethyl-25,26,27,28-tetra-*n*-propoxycalix[4]arene tetrahydrochloride (2a).

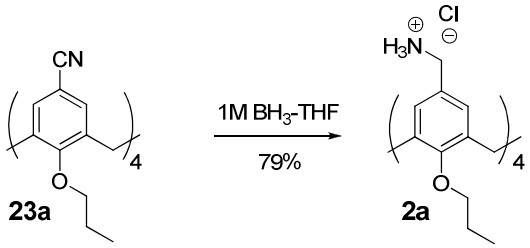

To the resulting residue CH_2Cl_2 was added and the colorless solid was filtered and washed repeatedly. The chloride salt of compound **2a** was obtained in a 79% yield. Mp: 290-293 °C (dec.). ^{1}H NMR (CD_3OD): δ 6.87 (s, 8H, ArH), 4.49 (d, *J* = 13.2 Hz, 4H, ArCH*H*axAr), 3.88 (tr, *J* = 5.3 Hz, 8H, OCH_2), 3.82 (bs, 8H, NH_2), 3.30 (bs, 8H, CH_2N); 3.26 (d, *J* = 13.2 Hz, 4H, ArCH*Heq*Ar), 1.94 (m, *J* = 7.4 Hz, 8H, $OCH_2CH_2CH_3$), 1.02 (t, *J* = 7.4 Hz, 12H, CH_3). ^{13}C NMR (CD_3OD): δ 158.4, 136.7 (CAr), 130.5 (CHAr), 128.3 (CAr), 78.1 ($OCH_2CH_2CH_3$), 44.0 (CH_2N), 31.7 ($ArCH_2Ar$), 24.4 ($OCH_2CH_2CH_3$), 10.7 (CH_3). ESI(+) *m/z*: $[M - 4HCl + H]^+$: 709.5 uma.

Compound **2a**, in its non-protonated form, can be obtained by extraction in CH_2Cl_2 from 1N NaOH aqueous solution.

5,11,17,23-Tetraminomethyl-25,26-27,28-biscrown-3-calix[4]arene tetrahydrochloride (2b).

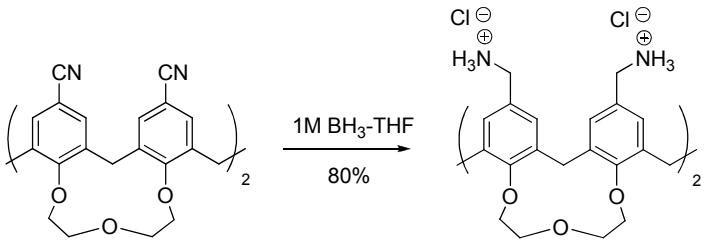

23b **2b**

After removal of the aqueous solvent under reduced pressure, the remaining residue was triturated in EtOAc and filtered. **2b** was obtained as a pure colorless compound in a 80% yield. Mp: > 350 °C. ^{1}H NMR (CD_3OD): δ 6.93 (s, 8H, ArH), 4.92 (d, J = 12.8 Hz, 2H, ArCH*H*axAr), 4.40 (d, J = 12.7 Hz, 2H, ArCH*H*axAr), 4.23-4.14 (m, 8H, OCH_2), 3.80-3.73 (m, 8H, OCH_2), 3.56 (s, 8H, CH_2N), 3.21 (d, J = 12.7 Hz, 2H, ArCH*H*eqAr), 3.15 (d, J = 12.8 Hz 2H, ArCH*H*eqAr), 2.85 (bs, 8H, NH_2). ^{13}C NMR (CD_3OD): δ 155.4, 136.7, 135.4 (CAr), 129.7, 128.8 (CHAr), 77.4 (CH_2O), 75.7 (CH_2O), 55.4 (CH_2N), 30.5 (Ar*C*H_2Ar). ESI(+) *m/z*: $[M - 3HCl + H]^+$: 717.3 uma.

Compound **2b**, in its non-protonated form, can be obtained by extraction in CH_2Cl_2 from 1N NaOH aqueous solution.

General procedure for the synthesis of *p*-bis-*tert*-butoxycarbonyl)guanidinemethyl-calix[4]arenes 24a and 24b.

To a solution of the basic forms of *p*-aminomethylcalix[4]arenes **2a** or **2b** (0.16 mmol) in CH_2Cl_2 (1.5 mL), were added Et_3N (0.088 mL, 0.63 mmol) and *N,N'*-bis-(*tert*-butoxycarbonyl)guanidine *N''*-triflate (**25**) (0.249 g, 0.63 mmol), previously dissolved in CH_2Cl_2 (1.5 mL). The reaction was stirred

at rt, 4 h for **2a** and 36 h for **2b**. Quenching was performed by washing with HCl 1N (2 x 2 mL), water (1 x 2 mL) and brine (1 x 2 mL). After drying the organic solvent over anhydrous Na_2CO_3 and filtering it, it was removed under reduced pressure and pure compounds were purified by silica gel flash chromatography as follows.

5,11,17,23-Tetradibocguanidinemethyl-25,26-27,28-tetrapropoxycalix[4]arene (24a).

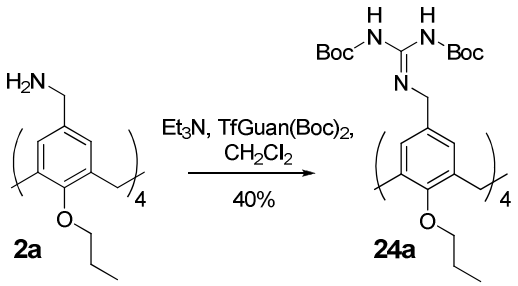

Eluent: 100% CH_2Cl_2→Hex/Et_2O, 4:1. Compound **24a** was obtained pure as a colorless compound in a 40% yield. Mp: > 350 ºC.^{1}H NMR ($CDCl_3$): δ 8.27 (s, 4H, NH), 6.60 (s, 8H, ArH), 4.40 (d, *J* = 13.2 Hz, 4H, ArCH*Hax*Ar), 4.28 (d, *J* = 5.7 Hz, 8H, CH_2N), 3.83 (t, *J* = 7.4 Hz, 8H, OC*H*$_2$CH$_2$CH$_3$), 3.12 (d, *J* = 13.2, 4H, ArCH*Heq*Ar), 1.93 (m, 8H, OCH$_2$C*H*$_2$CH$_3$), 1.48 (d, *J* = 5.7 Hz, 72H, C(CH$_3$)$_3$), 0.98 (t, *J* = 7.4 Hz, 12H, CH_3). ^{13}C NMR ($CDCl_3$): δ 163.6 (CO), 156.0, 155.6 (CGuan), 153.1, 134.9, 130.5 (CAr), 127.8 (CHAr), 82.8 (*C*(CH$_3$)$_3$), 78.9 (OC*H*$_2$CH$_2$CH$_3$), 44.9 (CH_2N), 31.0 (ArCH$_2$Ar), 28.4, 28.1 (C(*C*H$_3$)$_3$), 23.2 (OCH$_2$*C*H$_2$CH$_3$), 10.3 (CH_3). Exact Mass (ESI): *m/z* [M + H]$^+$: calc. 1678.9793 uma, found: 1678.9995 uma.

5,11,17,23-Tetrakis(*N,N'*-bis-*tert*-butoxycarbonyl)guanidinemethyl-25,26-27,28-biscrown-3-calix[4]arene (24b).

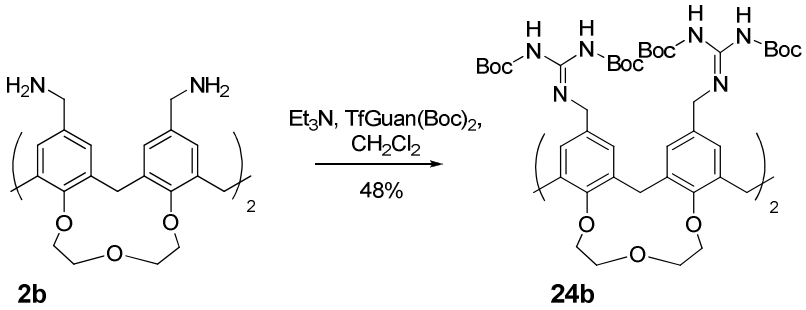

Eluent: Hex/Et_2O, 4:1. Compound **24b** was obtained as a colorless solid in a 48% yield. Mp: > 350 °C. ^{1}H NMR ($CDCl_3$): δ 8.38 (s, 4H, NH), 6.88 (d, J = 5.0 Hz, 8H, ArH), 4.90 (d, J = 12.3 Hz, 2H, ArCH*H*axAr), 4.39-4.27 (m, 10H, ArCH*H*axAr, CH_2O), 4.19-4.13 (m, 12H, CH_2O, CH_2N, ArCH*H*axAr), 3.79-3.73 (m, 4H, CH_2O), 3.16 (d, J = 11.7 Hz, 2H, ArCH*H*eqAr), 3.11 (d, J = 12.3 Hz, 2H, ArCH*H*eqAr), 1.41 (d, J = 10.5 Hz, 72H, $C(CH_3)_3$). ^{13}C NMR ($CDCl_3$): δ 163.6 (CO), 155.7, 154.79 (CGuan), 153.1, 135.7, 135.5, 132.1 (CAr), 128.6, 127.6 (CHAr), 83.0 ($C(CH_3)_3$), 79.1 (CH_2O), 74.8 (CH_2O), 45.0 (CH_2N), 30.8, 30.0 ($ArCH_2Ar$), 28.3, 28.1 ($C(CH_3)_3$). Exact Mass (ESI): *m/z* $[M + H]^+$: calc.: 1649.8713, found: 1649.8678.

General procedure for the synthesis of *p*-guanidinemethyl-calix[4]arenes 1a and 1b.

To a solution of bis-Boc guanidine derivatives **24a** or **24b** (0.03 mmol) in 1,4 dioxane (3 mL), concentrated HCl (1 mmol per Boc group) was added dropwise. The solution was stirred for 24 h at rt. Solvents were removed under reduced pressure and the products were obtained as follows.

5,11,17,23-Tetraguanidinemethyl-25,26-27,28-tetra-*n*-propoxycalix[4]arene tetrahydrochloride (1a).

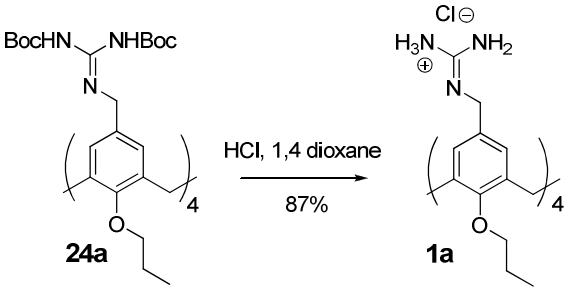

After elimination of the solvent, the product was recrystallized by dissolving it in CH_3OH (0.5 mL) and adding dropwise cold EtOAc. The suspension was left standing for 24 h at rt, giving rise to a colorless solid in a 87% yield. Mp: > 350 ºC. ^{1}H-NMR (MeOD): δ 6.27 (s, 8H, ArH), 4.51 (d, J = 13.2 Hz, 4H, ArCH*Hax*Ar), 4.12 (s, 8H, CH_2Guan), 3.83 (t, J = 7.4 Hz, 8H, OCH_2 CH_2CH_3), 3.22 (d, J = 13.2 Hz, 8H, ArCH*Heq*Ar), 1.93 (m, 8H, $OCH_2CH_2CH_3$), 1.04 (t, J = 7.4 Hz, 9H, CH_3). ^{13}C NMR (CD_3OD): δ 158.41 (CGuan), 157.67, 136.63, 130.82 (CAr), 129.04 (CHAr), 78.15 ($OCH_2CH_2CH_3$), 46.06 (CH_2Guan), 31.94 ($ArCH_2Ar$), 24.45 ($OCH_2CH_2CH_3$), 10.82 (CH_3). Exact Mass (ESI+): *m/z* of $[M - HCl + H]^+$: calc.: 987.4836 uma, found: 987.4896 uma. Elemental Analysis: $C_{48}H_{72}Cl_4N_{12}O_4$+3$H_2O$, calc.:C (53.53%), H (7.3%), N (15.61%), found: C (53.80%), H (6.96%), N (15.47%).

5,11,17,23-Tetraguanidinemethyl-25,26-27,28-biscrown-3-calix[4]arene tetrahydrochloride (1b).

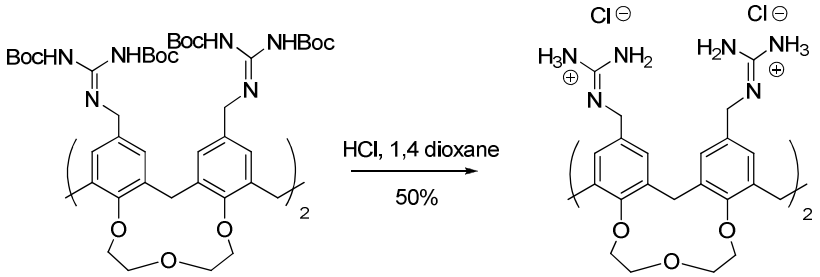

24b **1b**

After evaporation of the solvent, the residue was triturated in EtOAc. The resulting solid was purified by semi-preparative HPLC (conc.: 37.5 mg/mL, elution: 5→35% CH_3CN in H_2O + 0.05% TFA along 20 min, inj.: 100 µL, flux: 4.7 mL/min, UV_{220}). The final compound was obtained in a 50% yield. Anion exchange to chloride yielded the tetrahydrochloride salt **1b**. Mp: > 350 °C. ^{1}H NMR (CD_3CN): δ 7.08 (s, 8H, ArH), 5.03 (d, J = 12.1 Hz, 2H, ArCH*Hax*Ar), 4.48 (d, J = 12.1 Hz, 2H, ArCH*Hax*Ar), 4.28-4.23 (m, 12H, CH_2O), 4.13 (d, J = 6.2 Hz, 8H, CH_2Guan), 3.74-3.69 (m, 4H, CH_2O), 3.28 (d, J = 12.3 Hz, 2H, ArCH*Heq*Ar), 3.21 (d, J = 12.3 Hz, 2H, ArCH*Heq*Ar). ^{13}C NMR (CD_3CN): δ 157.3 (CAr), 154.8 (CGuan), 135.9, 132.0 (CAr), 129.9, 128.1 (CHAr), 76.7, 74.4 (CH_2O), 43.3 (CH_2Guan), 29.7 ($ArCH_2Ar$), 29.0 ($ArCH_2Ar$). Exact Mass (ESI+): *m/z* of $[M - HCl + H]^+$: calc.: 957.3867 uma, found: 987.3824 uma.

***N,N'*-Di-Boc-*N''*-trifluoromethanesulfonylguanidine (25).**

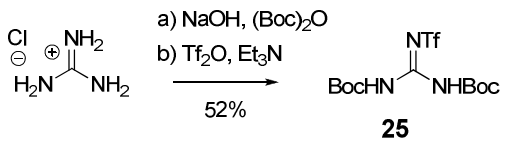

25

1,4-Dioxane (7 mL) was added to a solution of guanidine hydrochloride (0.32 g, 3.38 mmol) and NaOH (0.5 g, 13.5 mmol) in H_2O (3 mL). Di-*tert*-butyl dicarbonate (1.6 g, 7.4 mmol) was added in one portion, and the reaction mixture was allowed to warm to rt within 2 h. After stirring for 20 h, the mixture was concentrated *in vacuo* to 1/3 of its original volume. The resulting suspension was diluted with H_2O (7 mL) and extracted with EtOAc (3 x 7 mL). The combined extracts were washed with 10% citric acid (7 mL) , H_2O (7 mL), and brine (7 mL) and dried over $MgSO_4$. After filtration and removal of the solvent under reduced pressure, the crude product was purified by flash chromatography on silica gel (eluent: 100% $CH_2Cl_2 \rightarrow CH_2Cl_2/CH_3OH$, 97:3). Then, the resulting colorless powder (0.52 g, 2.0 mmol) was dissolved in anhydrous CH_2Cl_2 (10 mL). Et_3N (0.29 mL, 2.1 mmol) was added and the solution was cooled to -78 ºC. Triflic anhydride (0.35 mL, 2.1 mmol) was added dropwise at a rate such as that the reaction temperature did not exceed -65 ºC. After the addition, the mixture was allowed to warm to rt within 4h. The solution was washed with 2M $NaHSO_4$ (7 mL) and H_2O (7 mL), and dried over anhydrous Na_2SO_4. After filtration and removal of the solvent *in vacuo,* the crude was purified by flash column chromatography on silica gel (eluent: 100% CH_2Cl_2). Compound **25** was obtained as a colorless powder in a 52% yield. Mp: 114-116 ºC. ^{1}H NMR (DMSO-d_6): δ 11.45 (bs, 2H), 1.45 (s, 18H). ESI(+) *m/z*: $[M + H]^+$: 392.1 uma.

General procedure for the synthesis of *p*-formylcalixarenes 26a and 26b.

A mixture of calixarenes **21a** or **21b** (0.96 mmol), hexamethylenetetramine (HMTA, 4.04 g. 28.8 mmol), and trifluoroacetic

acid (20 mL) was stirred at 125 ºC tube for 5 h in a screw-capped tube for precursor **21a**, or at reflux for 24 h in the case of **21b**. Thereafter the reactions were cooled to rt and treated with aqueous solutions as follows.

5,11,27,23-Tetraformyl-25,26,27,28-tetrapropoxycalix[4]arene (26a).

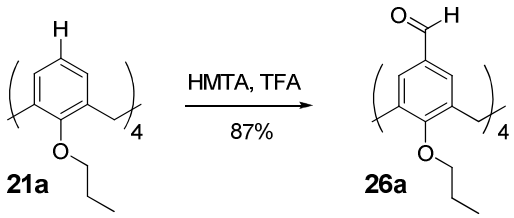

The mixture was diluted with 1M HCl (50 mL) and CH_2Cl_2 (50 mL), and vigorously stirred at rt for additional 3 h. The organic layer was separated, and the aqueous layer was extracted with CH_2Cl_2 (50 mL). The combined organic layers were washed with sat. Na_2CO_3 (50 mL), dried over anhydrous Na_2SO_4 and evaporated to dryness. Trituration of the residue with CH_3OH afforded **26a** as a colorless solid in a 87% yield. Mp: 289-290 ºC. ^{1}H NMR ($CDCl_3$): δ 9.58 (s, 4H, CHO), 7.15 (s, 8H, ArH), 4.51 (d, J = 13.8 Hz; 4H, ArCH*Hax*Ar), 3.94 (tr, J = 7.4 Hz, 8H, OCH_2CH$_2$CH$_3$), 3.35 (d, J =13.8 Hz, 4H, ArCH*Heq*Ar), 1.90 (sex, J = 7.4 Hz, 8H, CH$_2$CH_2CH$_3$), 1.01 (tr, J = 7.5 Hz, 12H, CH_3). ^{13}C NMR ($CDCl_3$): δ 191.1 (CHO), 161.7, 135.4, 131.3 (CAr), 130.1 (CHAr), 76.4 (O*C*H$_2$CH$_2$CH$_3$), 30.8 (ArCH$_2$Ar), 23.2 (OCH$_2$*C*H$_2$CH$_3$), 10.1 (CH_3). ESI(+) *m/z*: $[M + Na]^+$: 727.3 uma.

5,11,17,23-Tetraformylcalix[4]arene-25,26:27,28-biscrown (26b).

21b **26b**

The mixture was poured into ice/water (50 mL), neutralized with Na_2CO_3 and extracted with EtOAc. The organic phase was washed with H_2O (2 x 30 mL), dried over anhydrous Na_2CO_3 and evaporated to dryness. Purification by column chromatography in silica gel (eluent: Hex/EtOAc, 4:1) led to pure **26b** in a 60% yield. Mp: 303 °C (dec.).^{1}H NMR ($CDCl_3$): δ 9.76 (s, 4H, CHO), 7.61 (d, *J* = 2.4 Hz, 8H, ArH), 7.57 (d, *J* = 2.4 Hz, 8H, ArH), 4.57 (d, *J* = 12.4 Hz, 4H, ArCH*H*axAr), 5.21 (d, *J* = 12.4 Hz, 4H, ArCH*Hax*Ar), 3.9-4.4 (m, 16H, H_20), 3.41 (d, *J* = 12.4 Hz, 4H, ArCH*Heq*Ar), 3.46 (d, *J* = 12.4 Hz, 4H, ArCH*Heq*Ar). ^{13}C NMR ($CDCl_3$): δ 161.11 (CHO), 136.50, 133.10, 131.66 (CAr), 130.62 (CHAr), 76.67, 74.37 (CH_2O), 30.00, 30.05 ($ArCH_2Ar$). ESI(+) *m/z*: $[M + Na]^+$: 699.2 uma.

General procedure for the synthesis of *p*-carboxycalix[4]arenes 27a and 27b.

p-Tetraformylcalix[4]arenes **26a** and **26b** (0.5 mmol) were dissolved in $CHCl_3$/acetone (1:1, v/v, 15 mL) and the solution cooled to 0 ºC. An aqueous solution (1.5 mL) of sulfamic acid (0.58 g, 6 mmol) and sodium chlorite (0.45 g, 5 mmol) was rapidly added and the mixture was vigorously stirred at rt for 18 h. The reaction was quenched by removal of the organic solvents and addition of 2N HCl (2 mL). The resulting precipitate was

filtered and purified by trituration in CH_3OH.

25,26,27,28-Tetra-n-propoxycalix[4]arene-5,11,17,23-tetracarboxylic acid (27a).

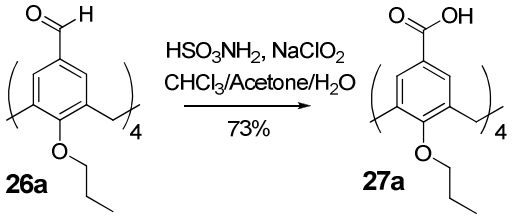

Compound **27a** was obtained as a colorless solid in a 73% yield. Mp > 350 °C. ^{1}H NMR (CD_3OD): δ 7.37 (s, 8H, ArH), 4.51 (d, J = 13.5 Hz, 4H, ArCH*H*axAr), 3.95 (tr, J = 7.3 Hz, 8H, $OCH_2CH_2CH_3$), 3.31 (d, J = 13.5 Hz, 4H, ArCH*H*eqAr), 1.97-1.87 (m, 8H, $OCH_2CH_2CH_3$), 1.03 (tr, J = 7.4 Hz, 12H, CH_3).^{13}C NMR ($CDCl_3/CD_3OD$ 9/1): δ 169.5 (CO), 161.7, 135.7, 131.3 (CAr), 125.2 (CHAr), 77.9 ($OCH_2CH_2CH_3$), 31.8 ($ArCH_2Ar$), 24.2 ($OCH_2CH_2CH_3$), 10.9 (CH_3). ESI(-) *m/z*: $[M - H]^-$: 767.3 uma.

5,11,17,23-Tetracarboxycalix[4]arene-25,26:27,28-biscrown (27b).

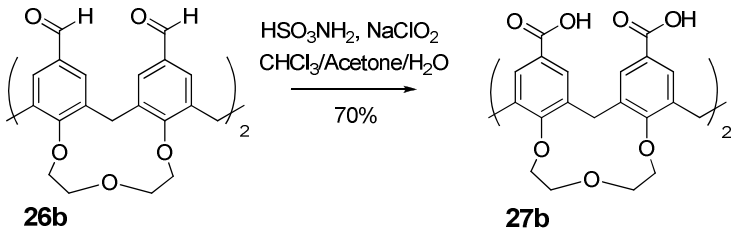

Compound **27b** was obtained as a colorless solid in a 70% yield. Mp: > 350 ºC. ^{1}H NMR (DMSO-d_6): δ 7.72 (s, 8H; ArH), 5.00 (d, J = 12.0 Hz, 2H; ArCH*H*axAr), 4.45 (d, J = 12.3 Hz, 2H, ArCH*Hax*Ar), 4.41-4.20 (m, 8H, CH_2O), 3.75-3.65 (m, 8H, CH_2O), 3.51 (d, J = 12.3 Hz, 2H;

ArCH*Heq*Ar), 3.43 (d, 2H, *J* = 12.0 Hz, 2H, ArCH*Heq*Ar). ^{13}C NMR (DMSO-d_6): δ 166.7 (CO), 159.2, 135.5 (CAr), 130.5, 129.7 (CHAr), 126.2 (CAr), 76.6, 73.8 (CH_2O), 29.5, 28.9 ($ArCH_2Ar$). ESI(-) *m/z* $[M - H]^-$ 739.2 uma.

2.9 References

1. Gutsche CD, Dhawan B, No KH, Muthukrishnan R (1981) The synthesis, characterization, and properties of the calixarenes from p-tert-butylphenol. *J Am Chem Soc* 103:3782-3792.

2. (a) Gutsche CD (1989) Calixarenes, Royal Society of Chemistry (Cambridge, UK).
(b) Gutsche C.D (1998) Calixarenes Revisited, Royal Society of Chemistry (Cambridge, UK).
(c) Iwamoto K, Araki K, Shinkai S (1991) Conformations and structures of tetra-0-alkyl-p-tert-butylcalix[4]arenes. How is the conformation of calix[4]arenes immobilized? *J Org Chem* 56:4955-4962.
(d) Shinkai S, Nagasaki T, Iwamoto K, Ikeda A, He G-X, Matsuda T, Iwamoto M (1991) New syntheses and physical properties of p-alkylcalix[n]arenes. *Bull Chem Soc Jap* 64:381-386.
(e) Galán H, de Mendoza J, Prados P (2005) Conformational control of calix[6]arenes through multiple bridges. *Eur J Org Chem* 19:4093-4097.

3. Böhmer V (1995) Calixarenes, macrocycles with (almost) unlimited possibilities. *Angew Chem Int Ed Engl* 34:713-745.

4. Jose P, Menon S (2007) Lower-rim substituted calixarenes and their applications. *Bioinorg Chem App* 2007:16 pages.

5. Perret F, Lazar AN, Coleman AW (2006) Biochemistry of the para-sulfonato-calix[4]arenes. *Chem Commun* 2425-2438.

6. Bünzli JC (2006) Benefiting from the unique properties of lanthanide ions. *Acc Chem Res* 39:53-61.

7. Leydier A, Lecerclé D, Pellet-Rostaing S, Favre-Réguillon A, Taran F, Lemaire M, (2008) Sequestering agent for uranyl chelation: New calixarene ligands. *Tetrahedron* 64:11319-11324.

8. Casnati A, Sansone F, Ungaro R (2003) Peptido-and glycocalixarenes: Playing with hydrogen bonds around hydrophobic cavities. *Acc Chem Res* 36:246-254.

9. Agrawal YK, Bhatt H (2004) Calixarenes and their biomimetic applications. *Bioinorg Chem Appl* 237-274.

10. (a) Wang W, Gong S, Chen Y, Ma J (2005) Fibriform one-dimensional hydrogen-bonded network composed of 1,2-alt calix[4]arene tetra acetic acid. *New J Chem* 11:1390-1392.
(b) Oh SW, Moon JD, Lim HJ, Park SY, Kim T, Park JB, Han MH, Snyder M, Choi EY (2005) Calixarene derivative as a tool for highly sensitive detection and oriented immobilization of proteins in a microarray format through noncovalent molecular

interaction. *FASEB J* 19:1335-1337.

11. (a) Sansone F, Dudic M, Donofrio G, Rivetti C, Baldini L, Casnati A, Callai S, Ungaro R (2006) DNA condensation and cell transfection properties of guanidinium calixarenes: Dependence on macrocycle lipophilicity, size, and conformation. *J Am Chem Soc* 126:14528-14536.
(b) Bagnacani V, Sansone F, Donofrio G, Baldini L, Casnati A, Ungaro R (2008) Macrocyclic nonviral vectors: High cell transfection efficiency and low toxicity in a lower rim guanidinium calix[4]arene. *Org Lett* 10:3953-3956.

12. Baldini L, Casnati C, Sansone F, Ungaro R (2007) Calixarene-based multivalent ligands. *Chem Soc Rev* 36:254-266.

13. Wei Y, McLendon G L, Hamilton A D, Case M A, Purring CB, Lin Q, Park HS, Lee CS, Yu T (2001) Disruption of protein–protein interactions: Design of a synthetic receptor that blocks the binding of cytochrome c to cytochrome c peroxidase. *Chem Commun* 1580-1581.

14. (a) Park HS, Lin Q, Hamilton AD (1999) Protein surface recognition by synthetic receptors: A route to novel submicromolar inhibitors for R-chymotrypsin. *J Am Chem Soc* 121:8-13.
(b) Park HS, Lin Q, Hamilton AD (2002) Modulation of protein–protein interactions by synthetic receptors: Design of molecules that disrupt serine protease–proteinaceous inhibitor interaction. *Proc Natl Acad Sci USA* 99:5105-5109.

15. Yin H, Hamilton AD, (2005) Strategies for targeting protein-protein interactions with synthetic agents. *Angew Chem Int Ed* 44:4130-4163.

16. Blaskovich MA, Lin Q, Delarue FL, Sun J; Park HS, Coppola D, Hamilton AD, Sebti SM (2000) Inhibiting angiogenesis and tumorigenesis by a synthetic molecule that blocks binding of both VEGF and PDGF to their receptors. *Nat Biotech* 18:1065-1070.

17. Fletcher S, Hamilton AD (2006) Targeting protein–protein interactions by rational design: mimicry of protein surfaces. *J R Soc Interface* 3:215-233.

18. Zhou H, Wang D, Baldini L, Ennis E, Jain R, Carie A, Sebti SM, Hamilton AD (2006) Structure–activity studies on a library of potent calix[4]arene-based PDGF antagonists that inhibit PDGF-stimulated PDGFR tyrosine phosphorylation. *Org Biomol Chem* 4:2376-2386.

19. Francese S, Cozzolino A, Caputo L, Esposito C, Martino M, Gaeta C, Troisi F, Neri P (2005) Transglutaminase surface recognition by peptidocalix[4]arene diversomers. *Tetrahedron Lett* 46:1611-1615.

20. (a) Sansone F, Chierici E, Casnati A, Ungaro R (2003) Thiourea-linked upper rim calix[4]arene neoglycoconjugates: synthesis, conformations and binding properties. *Org Biomol Chem* 1:1802-1809.

(b) Consoli GML, Cunsolo C, Geraci C, Sgarlata V (2004) Synthesis and lectin binding ability of glycosamino acid-calixarenes exposing GlcNAc clusters. *Org Lett* 6:4163-4166.

21. André S, Sansone F, Kaltner H, Casnati A, Kopitz J, Gabius HJ, Ungaro R (2008) Calix[n]arene-based glycoclusters: bioactivity of thiourea-linked galactose/lactose moieties as inhibitors of binding of medically relevant lectins to a glycoprotein and cell surface glycoconjugates and selectivity among human adhesion/growth-regulatory galectins. *ChemBioChem* 9:1649-1661.

22. Arosio D, Fontanella M, Baldini L, Mauri L, Bernardi A, Casnati A, Sansone F, Ungaro R (2005) A synthetic divalent Cholera toxin glycocalix[4]arene ligand having higher affinity than natural GM1 oligosaccharide. *J Am Chem Soc* 127:3660-3661.

23. Mecca T, Consoli GML, Geraci C, Cunsolo F (2004) A synthetic divalent cholera toxin glycocalix[4]arene ligand having higher affinity than natural GM1 oligosaccharide. *Bioorg Med Chem* 12:5057-5062.

24. Mecca T, Consoli GML, Geraci C, La Spina R, Cunsolo F (2006) Designed calix[8]arene-based ligands for selective tryptase surface recognition. *Org Biomol Chem* 4:3763-3768.

25. Tomiteta N, Sando S, Sera T, Aoyama Y (2004) Macrocyclic proteoglycan mimics. Potent inhibition of cell adhesion by a bundle of chondroitin sulfate chains assembled on the calix[4]resorcarene platform. *Bioorg Med Chem Lett* 14:2087-2090.

26. Horiuchi S, Aoyama Y (2006) Systematic lactose-functionalization of amphiphilic octaamine macrocycle as a gene carrier. Optimization of the charge, size, toxicity, and receptor factors for hepatocyte targeting. *J Contr Rel* 116*:*107-114.

27. Hayashida O, Uchiyama M (2007) Multivalent macrocyclic hosts: histone surface recognition, guest binding, and delivery by cyclophane-based resorcinarene oligomers. *J Org Chem* 72:610-616.

28. Hayashida O, Ogawa N, Uchiyama N (2007) Surface recognition and fluorescence sensing of histone by dansyl-appended cyclophane-based resorcinarene trimer. *J Am Chem Soc* 129:13698-13705.

29. (a) Levine AJ (1997) Surfing the p53 network. *Cell* 88:323-331.
(b) Bates S, Vousden KH (1999) Mechanisms of p53-mediated apoptosis. *Cell Mol Life Sci* 55:28-37.
(c) Prives C, Hall P A (1999) The p53 pathway. *J Pathol* 187:112-116.

30. Joerger AC, Fersht AL (2008) Structural Biology of the tumor suppressor p53. *Annu Rev Biochem* 77:557-582.

31. Selinova G, Wiman KG (1995) P53: A cell cycle regulator activated by DNA damage.

Adv Cancer Res 66:143-180.

32. (a) Brooks CL, Gu W (2006) P53 ubiquitination: Mdm2 and beyond. *Mol. Cell* 21:307-315.

33. (a) Lavin MF, Gueven N (2006) The complexity of p53 stabilization and activation. Cell death & differentiation. *Cell Death Differ* 13:941-950.
(b) Braithwaite AW, Del Sal G, Lu X (2006) Some p53-binding proteins that can function as arbiters of life and death. *Cell Death Differ* 13:984-993.

34. Wang P, Reed M, Wang Y, Mayr G, Stenger JE, Anderson ME, Schwedes JF, Tegtmeyer P (1994) P53 domains: Structure, oligomerization, and transformation. *Mol Cell Biol* 14:5182-5191.

35. Tidow H, Melero R, Mylonas E, Freund SMV, Grossmann JG, Carazo JM, Svergun DI, Valle M, Fersht AL (2007) Quaternary structures of tumor suppressor p53 and a specific p53-DNA complex *Proc Natl Acad Sci USA* 104:12324-12329.

36. (a) Greenblatt MS, Bennet WP, Hollstein M, Harris CC (1994) Mutations in the p53 tumor supressor gene: Clues to cancer etiology and molecular pathogenesis. *Cancer Res* 35:429-434.
(b) Sigal A, Rotter V (2000) Oncogenic mutations of the p53 tumor suppressor: The demons of the guardian of the genome. *Cancer Res* 60:6788-6793.
(c) Olivier M, Petijean A, Marcel V, Pétré A, Mounawar M, Plymoth A, Fromentel CC, Hainaut P (2008) Recent advances in p53 research: An interdisciplinary perspective. *Cancer Gene Ther* 16:1-12.

37. Bullock AN, Fersht AR (2001) Rescue of mutants of the tumor suppressor p53 in cancer cells by a designed peptide. *Nature* 1:68-76.

38. Rajagopalan S, Jaulent AM, Wells M, Veprintsev DB, Fersht AR (2008) 14-3-3 activation of DNA binding of p53 by enhancing its association into tetramers. *Nucl Acids Res* 36:5983-5991.

39. Chène P (2001) The role of tetramerization in p53 function. *Oncogene* 20: 2611-2617.

40. (a) Jeffrey PD, Gorina S, Pavletich NP (1995) Crystal structure of the tetramerization domain of the p53 tumor suppressor at 1.7 angstroms. *Science* 267:1498-1502.
(b) Mittl P R, Chène P, Grütter MG (1998) Crystallization and structure solution of p53 (residues 326-356) by molecular replacement using an NMR model as template. *Acta Crystallog* 54:86-89.

41. (a) Clore GM, Ernst J, Clubb R, Omichinski JG, Kennedy WM, Sakaguchi K, Appella E, Gronenborn AM (1995) Refined solution structure of the oligomerization domain of the tumour suppressor p53. *Nat Struct Biol* 2:321-333.
(b) Sot B, Freund SM, Fersht AR (2007) Comparative biophysical characterization of p53 with the pro-apoptotic BAK and the anti-apoptotic BCL-xL. *J Biol Chem* 282:29193-29200.

42. Mateu MG, Fersht AR (1999) Mutually compensatory mutations during evolution of the tetramerization domain of tumor suppressor p53 lead to impaired hetero-oligomerization. *Proc Natl Acad Sci USA* 96:3595-3599.

43. Brokx RD, Bolewska-Pedyczak E, Gariépy J (2003) A stable human p53 heterotetramer based on constructive charge interactions within the tetramerization domain. *J Biol Chem* 278:2327-2332.

44. (a) Waterman JL, Shenk JL, Halazonetis TD (1995) The dihedral symmetry of the p53 tetramerization domain mandates a conformational switch upon DNA binding. *EMBO J* 14:512-519.
(b) Mateu MG, Fersh, A. (1998) Nine hydrophobic side chains are key determinants of the thermodynamic stability and oligomerization status of tumour suppressor p53 tetramerization domain. *EMBO J* 273:873-881.

45. Mora P, Carbajo RJ, Pineda-Lucena A, Sánchez del Pino MM, Pérez-Payá E (2008) Solvent-exposed residues located in the beta-sheet modulate the stability of the tetramerization domain of p53--a structural and combinatorial approach. *Proteins* 71:1670-1685.

46. Mateu MG, Sánchez del Pino MM, Fersht AR (1999) Mechanism of folding and assembly of a small tetrameric protein domain from tumor suppressor p53. *Nat Struct Biol* 6:191-198.

47. Nicholls CD, McLure KG, Shields MA, Lee PW (2002) Biogenesis of p53 involves cotranslational dimerization of monomers and posttranslational dimerization of dimers *J Biol Chem* 277:12937-12945.

48. Petitjean A, Mathe E, Kato S, Ishioka C, Tavtigian SV, Hainaut P, Olivier M (2007) Impact of mutant p53 functional properties on TP53 mutation patterns and tumor phenotype: Lessons from recent developments in the IARC TP53 database. *Hum Mutat* 28:622-629.

49. Nichols KE, Malkin D, Garber JE, Fraumeni JF Jr, Li FP (2001) Germ-line p53 mutations predispose to a wide spectrum of early-onset cancers. *Cancer Epidemiol Biomarkers prev* 10:83-87.

50. Mathews CK, van Holde KE, Ahern KG (2000) Biochemistry, 3rd ed, The Benjamin/Cummings Publishing Co. (San Francisco).

51. Bosshard HR, Marti DN, Jelesarov I (2004) Protein stabilization by salt bridges: Concepts, experimental approaches and clarification of some misunderstandings *J Mol Recognit* 17:1-16.

52. Di Giammarino EL, Lee AS, Cadwell C, Zhang W, Bothner B, Ribeiro RC, Zambetti G, Kriwacki RW (2002) A novel mechanism of tumorigenesis involving involving pH-dependent destabilization of a mutant p53 tetramer. *Nat Struct Biol* 9:12-16.

53. Figuereido BC, Sandrini R, Zambetti GP, Pereira RM, Cheng C, Liu W, Lacerda L, Pianovski MA, Michalkiewicz E, Jenkins J, Rodriguez-Galindo C, Mastellaro MJ, Vianna S, Watanabe F, Sandrini F, Arram SBI, Boffetta P, Ribeiro RC (2006) *J Med Gene* 43:91-96.

54. Cohen FE, Kelly JW (2003) Therapeutic approaches to protein-misfolding diseases. *Nature* 426:905-909.

55. Gestwicki JE, Cairo CW, Strong LE, Oetjen KA, Kiessling, LL (2002) Influencing receptor-ligand binding mechanisms with multivalent ligand architecture. *J Am Chem Soc* 124:14922-14933.

56. (a) Boeckler FM, Joerger AC, Jaggi G, Rutherford TJ, Veprintsev DB, Fersht AR (2008) Targeted rescue of a destabilized mutant of p53 by an in silico screened drug. *Proc Natl Acad Sci USA* 105:10360-10365.
(b) Block P, Weskamp N, Wolf A, Klebe G (2007) Strategies to search and design stabilizers of protein-protein interactions: A feasibility study. *Proteins* 68:170-186.

57. Albert JS, Goodman MS, Hamilton AD (1995) Molecular recognition of proteins: sequence-selective binding of aspartate pairs in helical peptides. *Angew Chem Int Ed Engl* 117:1143-1144.

58. (a) Peczuh MW, Hamilton AD, Sánchez-Quesada J, de Mendoza J, Haack T, Giralt E (1997) Recognition and stabilization of an α-helical peptide by a synthetic receptor. *J Am Chem Soc* 119:9327-9328.
(b) Haack T, Peczuh MW, Salvatella X, Sánchez-Quesada J, de Mendoza J, Hamilton A, D Giralt E (1999) Surface recognition and helix stabilization of a tetraaspartate peptide by shape and electrostatic complementarity of an artificial receptor *J Am Chem Soc* 121:1813-11820.
(c) Orner PB, Salvatella X, Sánchez-Quesada J, de Mendoza J, Giralt E, Hamilton AD (2002) De novo protein surface design: Use of cation-π interactions to enhance binding between an α-helical peptide and a cationic molecule in 50% aqueous solution. *Angew Chem Int Ed* 41:117-119.

59. Salvatella X, Martinell M, Gairi M, Mateu MG, Feliz M, Hamilton AD, de Mendoza J (2004) A tetraguanidinium ligand binds to the surface of the tetramerization domain of protein p53. *Angew Chem Int Ed* 43:196-198.

60. Martinell M, Salvatella X, Fernández-Carneado J, Gordo S, Felix M, Menéndez M, Giralt E (2006) Synthetic ligands able to interact with the p53 tetramerization domain. towards understanding a protein surface recognition event. *ChemBioChem* 7:1105-1113.

61. Sansone F, Barboso S, Casnati A, Sciotto D, Ungaro R (1999) A new chiral rigid cone water soluble peptidocalix[4]arene and its inclusion complexes with a-amino acids and aromatic ammonium cations. *Tetrahedron Lett* 40:4741-4744.

62. Casnati A, Pirondini L, Pelizzi N, Ungaro R (2000) New tetrafunctionalized cone calix[4]arenes as neutral hosts for anion recognition. *Supramol Chem* 12:53-65.

63. Dondoni A, Marra A, Scherrmann M-C, Casnati, A, Sansone F, Ungaro R (1997) Synthesis and properties of 0-Glycosyl calix[4]arenes (calixsugars). *Chem Eur J* 3:1774-1782.

64. (a) Arduini A, Fabbi M, Mantovani M, Mirone L, Pochini A, Secchi A, Ungaro R (1995) Calix[4]arenes blocked in a rigid cone conformation by selective functionalization at the lower rim. *J Org Chem* 60:1454-1457.
(b) Arduini A, McGregor WM, Paganuzzi D, Pochini A, Secchi A, Ugozzoli F, Ungaro R (1996) Rigid cone calix[4]arenes as donor systems: Complexation of organic molecules and ammonium ions in organic media. *J Chem Soc, Perkin Trans 2* 839-846.

65. Feichtinger K, Heather LS, Baker TJ, Matthews K, Goodman M (1998) Triurethane-protected guanidines and triflyldiurethane-protected guanidines: New reagents for guanidinylation reactions. *J Org Chem* 63:8432-8439.

66. Sansone F, Barboso S, Casnati A, Fabbi M, Pochini A, Ugozzoli F, Ungaro R (1998) synthesis and structure of chiral cone calix[4]arenes functionalized at the upper rim with L-alanine units. *Eur J Org Chem* 897-905.

67. Santos E (July 2008) Computational studies on supramolecular hydrogen-bonded structures: from nanocapsules to proteins. PhD Thesis, Universitat Rovira i Virgili (URV).

68. Gordo S (June 2008) Use of calix[4]arenes to recover the self-assembly ability of mutated p53 tetramerization domains. PhD Thesis, Universitat de Barcelona (UB).

69. (a) Gordo S, Martos V, Santos E, Menéndez M, Bo C, Giralt E, de Mendoza J (2008) Stability and structural recovery of the tetramerization domain of p53-R337H mutant induced by a designed templating ligand.*Proc Natl Acad Sci USA* 105:16426-16431.
(b) Gordo S, Martos V, Vilaseca M, Menéndez M, de Mendoza J, Giralt E (2008) On the role of flexibility in protein-ligand interactions: The example of p53 tetramerization domain. *J Am Chem Soc*, submitted.

70. Van der Spoel D, Lindahl E, Hess B, Groenhof G, Mark AE, Berendsen HG (2005) GROMACS: fast, flexible, and free. *J Comp Chem* 26:1701-1718.

71. Lwin TZ, Durant JJ, Bashford D (2007) A fluid salt-bridging cluster and the stabilization of p53. *J Mol Biol* 373:1334-1347.

72. Johnson CR, Morin PE, Arrowsmith CH, Freire E (1995) Thermodynamic analysis of the structural stability of the tetrameric oligomerization domain of p53 tumor suppressor. *Biochemistry* 34: 5309-5316.

73. Stevens SY, Sanker S, Kent C, Zuiderweg ER (2001) Delineation of the allosteric

mechanism of a cytidylyltransferase exhibiting negative cooperativity *Nat Struct Biol* 8:947-952.

74. Ohara K (2007) Amine-guanidine switch: a promising approach to improve DNA binding and antiproliferative activities *J Med Chem* 50:6465-6475.

75. Robinson CV, Chung EW, Kragelund BB, Knudsen J, Aplin RT, Poulsen FM, Dobson CM (1996) Probing the nature of noncovalent interactions by mass spectrometry. A study of protein−CoA ligand binding and assembly. *J Am Chem Soc* 118:8646-8653.

76. Mayer M, Meyer B (2001) Group epitope mapping by saturation transfer difference NMR to identify segments of a ligand in direct contact with a protein receptor. *J Am Chem Soc* 123:6108-6117.

77. Nageswara Rao BD (1989) Nuclear magnetic resonance line-shape analysis and determination of exchange rates. *Methods Enzymol* 176:279-311.

78. Perrin DD, Perrin DR, Amarego WLF (1980) Purification Of Laboratory Chemicals, 2nd ed, Pergamon Press Ltd (Oxford)**.**

79. Still WC, Kahn M, Mitra AJ (1978) Rapid chromatographic technique for preparative separations with moderate resolution *J Org Chem* 43:2923-2925.

80. Gutsche CD, Levine JA (1982) Calixarenes. 6. Synthesis of a functionalizable calix[4]arene in a conformationally rigid cone conformation. *J Am Chem Soc* 104:2652-2653.

Chapter 3

Conical calix[4]arenes as reversible blockers of voltage-dependent potassium channels

3.1 Potassium channels: Function, structure and K_v-family

K^+ conduction: at the basis of cell functionality

Potassium channels are the most common type of ion channels occuring in virtually every eukaryotic and prokaryotic cell (1). They conduct K^+ ions across the cell membrane through potassium-selective pores that span membranes and are key elements for cell function, as they underpin excitability, proliferation, secretion and volume regulation.

There are over 80 mammalian genes that encode potassium channel subunits (2). The diversity among members of the K^+ channel family is related to the various stimuli they respond to: cations like Ca^{2+} (e.g.: BK, SK, MthK), voltage (e.g.: Shaker, K_v family) or ligands such as ATP (K_{ir}), cAMP (KcsA) and phosphoinositol derivatives (3).

From a structural point of view they are formed by four subunits which have a distinctive pore-loop structure that lines the top of the pore and is responsible for K^+ selectivity. Depending on the number of membrane-spanning helices and the number of pores they contain, the following classes are distinguished: the two-transmembrane class (2TM) which

includes the inward rectifier channels (K_{ir}) and the bacterial channels KcsA and MthK, and the six-transmembrane class (6TM) which contains the family of voltage gated potassium channels (Shaker, K_vAP, K_v channels and others), as well as the KCNQ and the eag-like channels. However, channels of the 6TM family are an extended version of the 2TM family, as will be described later (1).

The most important subunit (α-subunit) of K^+ channels of the 2TM and 6TM category, assembles as either homomeric or heteromeric tetramers to form the K^+-selective pore (4). Furthermore bacterial, archael and eukaryotic K^+ channels belong to a single protein family because they contain a highly conserved segment called the K^+ channel signature sequence (5).

Structure-function correlation in K^+ channels

Since 1998, several x-ray structures of bacterial and mammalian potassium channels have been solved by MacKinnon *et al.*: KcsA (bacterial, cAMP-gated channel) (6), MthK (bacterial, Ca^{2+}-gated) (7), K_vAP (archaebacterial, voltage-gated channel) (8), $K_v1.2{\cdot}\beta2$ (mammalian *Shaker* like channel, voltage-gated) (9), and the $K_v1.2$-$K_v2.1$ (paddle chimaera, voltage gated) (10). In all crystal structures, four identical subunits assemble as a tetramer with a central C_4 axis of symmetry.

A single K^+-subunit, from KcsA crystal structure, represented in Fig. 3.1, shows the characteristic sections: 1st the S5 and S6 helices (*grey*), 2nd the turret loop (*grey*), 3rd the pore helix (*red*), and 4th the selectivity filter

(*yellow*).

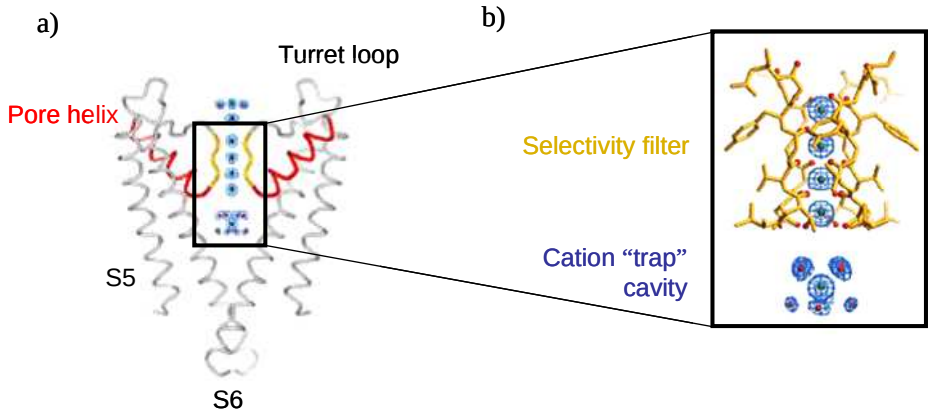

Fig. 3.1: (a) Two of the four subunits from the KcsA pore are shown with the extracellular part on the top. (b) Detail of pore domain: blue mesh shows electron density for K^+ and water along the pore.

The S5 helix spans the membrane. Once the polypeptide chain reaches the extracellular surface, it unwinds to form an approximately *s*-shaped turret loop, connecting S5 to the so-called pore helix (P-helix). The turret is a region of hypervariability specific to every K^+ channel. The main chain then turns back into the membrane, crossing it halfway as the P-helix. At this point the backbone bends back again, towards the extracellular side and forms the selectivity filter (Fig. 3.1a).

The pore itself is formed by the highly conserved sequence (XGYG), whose backbone carbonyl groups provide the selectivity filter and underpin the ability of the channel to prevent the passage of Na^+ (11). The selectivity filter contains multiple binding sites that mimic specifically a hydrated K^+ ion's hydration shell. Four evenly spaced layers of carbonyl oxygen atoms and a single layer of threonines hydroxyl oxygen atoms create four K^+ ion

binding sites, as shown in Fig. 3.1b. The ability of these proteins to conduct K^+ ions at levels near the limit of diffusion is traditionally described in terms of concerted mechanisms in which ion-channel attraction and ion-ion repulsion have compensating effects, as several ions are moving simultaneously in single file through the narrow pore.

Across the four positions of the selectivity filter there are, on average, two K^+ ions present at a given time and they reside predominantly in two configurations: 1,3 and 2,4 (Fig. 3.2a).

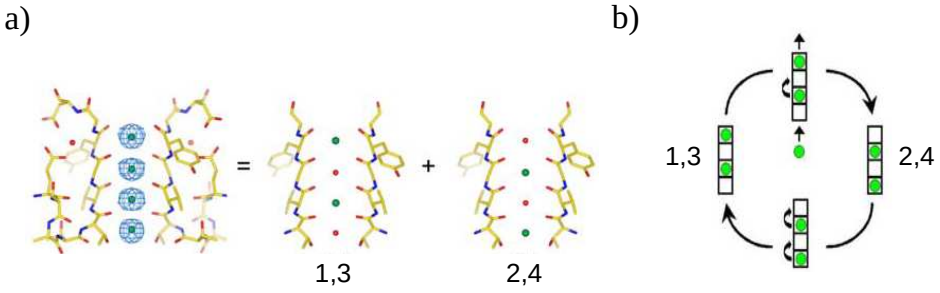

Fig. 3.2: (a) Electron density in the filter corresponds to two configurations of K+ ions (*green*) alternating with water molecules (*red*). (b) Throughput cycle for K^+ conduction (reproduced from ref. 5b).

These two configurations represent the end point of a simple conduction cycle: an ion enters the queue from one side while another one exits from the other side (Fig. 3.2b).

Moreover, by directing the *C*-terminal negative end-charge of α-helices (helix macrodipole) toward the ion pathway, while releasing a high free energy through ion rehydration of K^+, the ion is stabilized in the center of

the membrane prior to release into the intracellular space (12).

Targeting K_v1-subfamily

So far, approximately 90 genes for K^+-channels subunits have been identified in the human genome. However, this enormous diversity at genomic level, especially when combinatorial assembly of different subunits is considered, is contrasted with the relatively small number of human channels that are functionally characterized. However, since they are involved in many disease settings, considerable efforts have been made to study their properties and identify potential drug candidates. In particular, the family of voltage gated K^+ channels (K_v) has been identified as pharmacologically relevant (13).

In addition to the two α-helices of the pore domain (S5-S6), K_v channels have four S1-S4 helices, which compose the voltage sensing domain that "reads" the membrane voltage and regulates the pore (Fig. 3.3) (8).

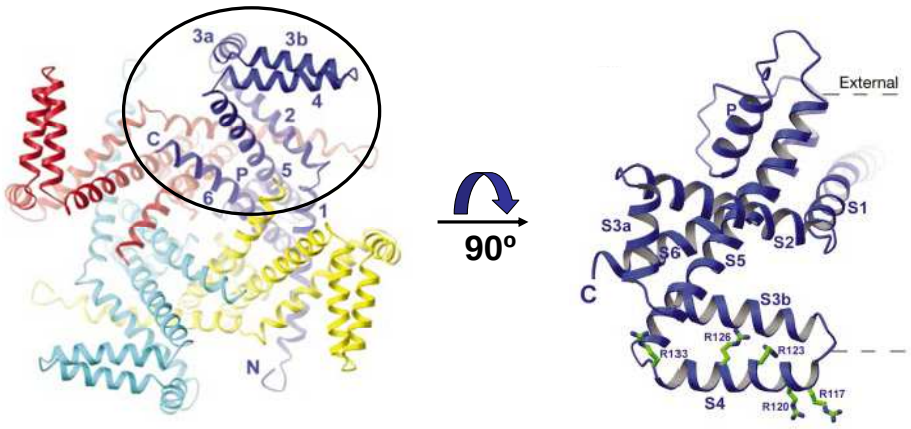

Fig. 3.3: A K_vAP subunit viewed from the top (left) and the highlighted domain from the side, with the intracellular solution below (right). Pore domain (P, S5, S6) and voltage sensitive domain (S1-S4) are highlighted, reproduced from ref. 8b.

The minimum voltage sensing region actually corresponds to S4-S3b, termed the voltage sensing *paddle*, rich in arginine residues (14). As a response to membrane voltage, the paddle switches between two conformations which are transmitted *via* S5-S6 helices to the pore, determining its open or closed conformation (15).

Triethylammonium (TEA) interacts non specifically with K_v1 channels with weak to moderate affinity. For this reason and because of its accessibility it has been employed to reveal structural and biophysical properties of voltage dependent channels (16). Moreover, to facilitate these studies, mutants of Shaker channel -a prototypical K_v1 channel from *D. megalonaster*- with enhanced susceptibility to TEA (Shaker T449Y/F) are commonly employed (17). The reason for this is that amino acids with aromatic side chains in position 449 enhance TEA binding through cation-

π interaction (18).

Also a large number of natural inhibitors from poisonous animals have been exploited to study K_v1 channel properties and several structures of toxins complexed to K_v1 channels have been reported (19). As an example, the footprint of Agitoxin (AgTx) on the extracellular surface of Shaker channel was modelled by Ericsson *et al.* (2002) based on experimental distance restraints extracted from thermodynamic mutant cycles (Fig. 3.4) (20).

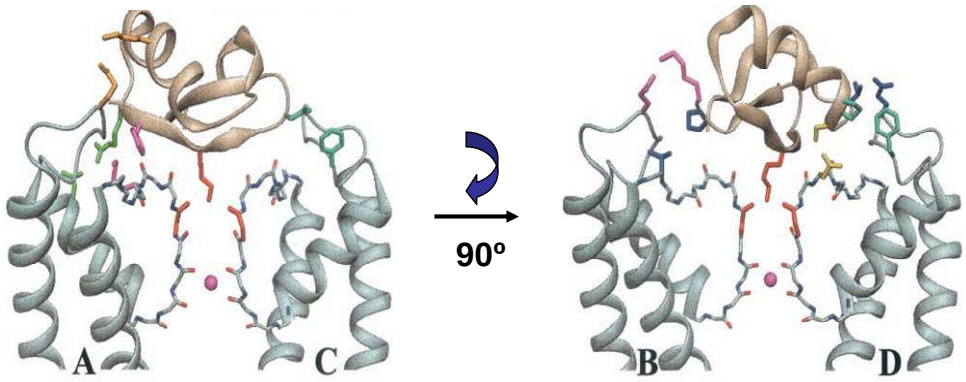

Fig. 3.4: Two views of the AgTx2-Shaker complex rotated 90° around the pore axis relative to each other. The rear and front monomers have been removed for easier visualization and the letters refer to Shaker monomers. Important side chains are highlighted in colors (reproduced from ref. 20).

From a biomedical perspective, $K_v1.3$ and $K_v1.5$ channel subtypes have revealed as very interesting targets: $K_v1.3$ is related to prevention of proliferation and clonal expansion of human T-cells. Hence, various small molecular blockers, with inhibitory activity in the nanomolar range, have

been identified as potential anti-inflammatory drugs and therapeutics for autoimmune diseases (21). Moreover, $K_v1.5$ has been implicated in a number of cardiac diseases. However, to date no selective blocker has been reported (22).

Further voltage gated K^+ channel blockers targeting the pore domain but lacking specific subtype selectivity have been described (23). However, despite the high affinity of some of these inhibitors, none of them makes full use of the four-fold symmetry of the homotetrameric channels.

3.2 Designed OH-free calix[4]arene ligands to interact with K_v1 channels

Fourfold symmetrical ligands greatly benefit from the polyvalency effect and some examples of high affinity binding to protein surfaces by have been introduced in Chapter 1 and further described in Chapter 2 (see references herein).

Trauner *et al.* (2003) studied synthetic ligands with a four-fold symmetry based on water-soluble tetraphenylporphyrins (24). These compounds were functionalized at their edges with amines, amino acids and dipeptides with positive charges at neutral pH. Competitive binding assays against ^{125}I-hongotoxin-A19Y/Y37F, as well as electrophysiological studies on *Xenopus laevis* oocytes, showed that positively charged ligands with appropriate geometry strongly interact with $K_v1.3$ channel.

However, though porphyrins fulfill the symmetry requirement, they are flat and rigid scaffolds that do not ideally complement the conical pore-entrance of the channels. In fact, the binding model based on a porphyrin lying on top of the channel and perpendicular to the pore, was recently revised by Trauner, Baldus *et al.*, who showed by solid state NMR and molecular dynamics that the core is twisted almost parallel to the channel axis, with only one positively charged side arm actually interacting with the channel pore domain (Fig. 3.5) (25).

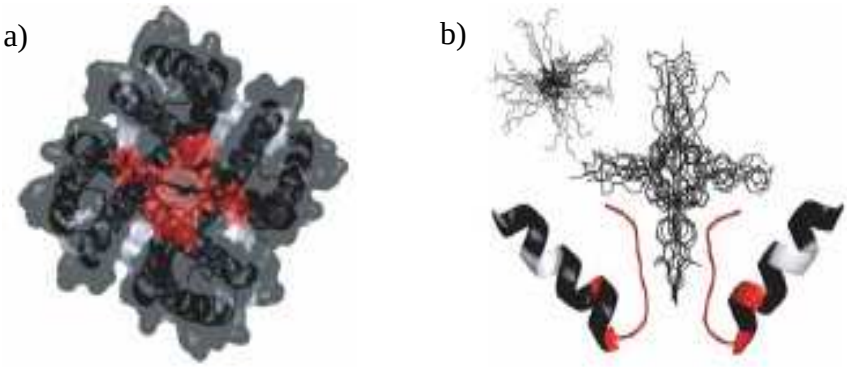

Fig. 3.5: (a) Top view of KcsA-K_v1.3 bound to the porphyrin and (b) side view with overlay of the ten lowest-energy structures according to HADDOCK docking (26), reproduced from ref. 25.

Unlike porphyrins, calix[4]arenes display conical shapes which would likely complement the shape of the extracellular face of a K_v channel. Thus, in collaboration with D. Trauner and E. Isacoff (Departments of Chemistry and Molecular & Cell Biology, UC-Berkeley), we designed C_4 symmetric ligands based on calix[4]arenes with a well-defined cavitand conformation.

We expected the affinity to arise from i) interactions of four positively charged "arms" at the upper rim of the ligands with the extracellular surface of the channel, the "turret loop" and ii) geometric complementarity of the conical calix[4]arene scaffold with the extracellular vestibule of the channel.

Preliminary docking studies, based on the crystal structures of KcsA (6) and *p*-thiourea calix[4]arene (27), confirmed that OH-free calix[4]arenes were small enough to deeply penetrate the extracellular surface of the channel, keeping the lower rim oriented towards the pore (Fig. 3.6).

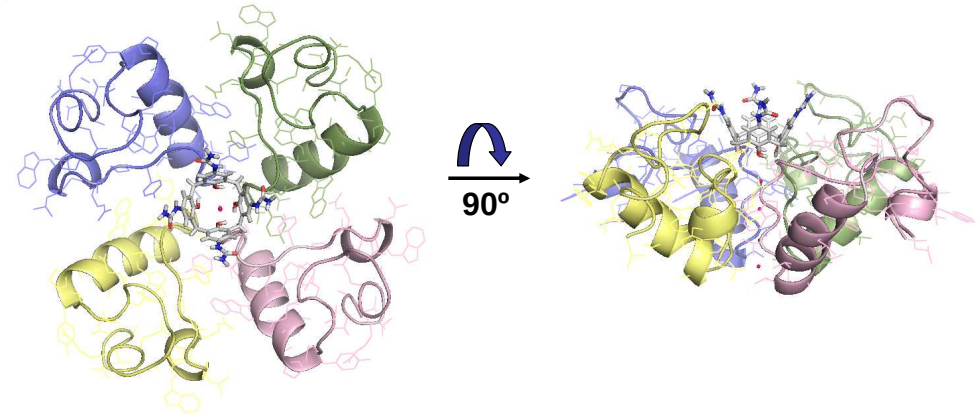

Fig. 3.6: Docking of an OH-free calix[4]arene (stick model) on KcsA (ribbon model): top view (left) and side view (right).

Hence we focused on the synthesis of a series of OH-free calix[4]arenes with positively charged groups on the upper rim as potential blockers of K_v channels. We further generated neutral and negatively charged ligands, as well as *O*-alkyl analogues, as negative controls for the binding event. Electrophysiological methods and molecular dynamics were employed to investigate the blocking properties as well as the interaction mode of the ligands.

3.3 Synthesis of K_v1 channel blockers

Our initial goal was to generate the *p*-(aminomethyl)calix[4]arene precursor **28,** which would give rise to a series of guanidinium-, amino acid- and peptide-endowed OH-free calix[4]arenes (Fig. 3.7).

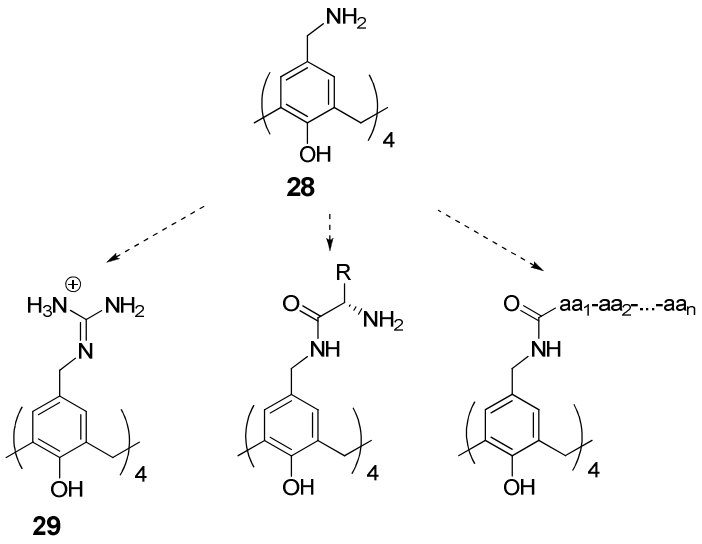

Fig. 3.7: Compound **28** as precursor for various OH-free calix[4]arenes.

To generate the tetramino precursor we first attempted a strategy *via* a tetraazide intermediate **30** (Fig. 3.8). A similar synthesis has been reported by Regnouf-de-Vains *et al.* (28), on OH-free calix[4]arenes with longer alkyl chains between the aromatic ring and the ammonium groups, based on a previous work from Gutsche *et al.* (29). Calix[4]arene **8** reacts smoothly with formaldehyde and secondary amines to yield a Mannich base, following the traditional procedure described in the literature (30). Mannich

bases are currently converted to the corresponding quaternary ammonium salts and subsequently reacted with a nucleophile to replace the amino group (31). Hence, treatment of the salt with sodium azide yielded precursor **30**.

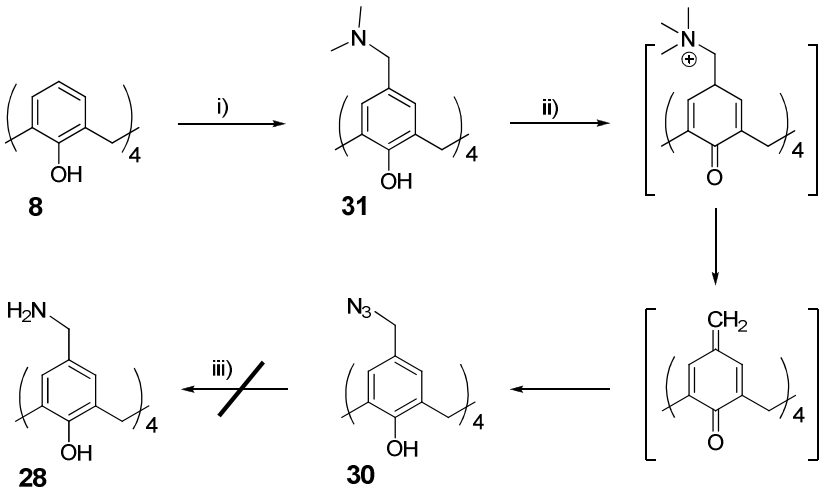

Fig. 3.8: Failed synthetic pathway *via* tetraazide intermediate **30**.

However, reduction to the expected compound **28** failed under different methods: hydrogen over palladium (32), triphenylphosphine (33), and lithium aluminium hydride (34). Likely, the acidic phenol groups interfere with the reduction reagents. Actually, although access to **28** *via* azide reduction was suggested by Gutsche *et al.* (29), neither the synthesis, nor the product were described. In fact, the product was detected by MS-ESI(+) analysis in crudes from LAH reduction, but it likely degraded during work-up, no matter the base or the salt were targeted.

Thus, we switched to a strategy in which lower rim phenols were initially protected with semi-permanent groups and deprotected only after the upper rim had been properly functionalized. *O*-protecting benzyl and *p*-methoxybenzyl groups were employed (Fig. 3.9).

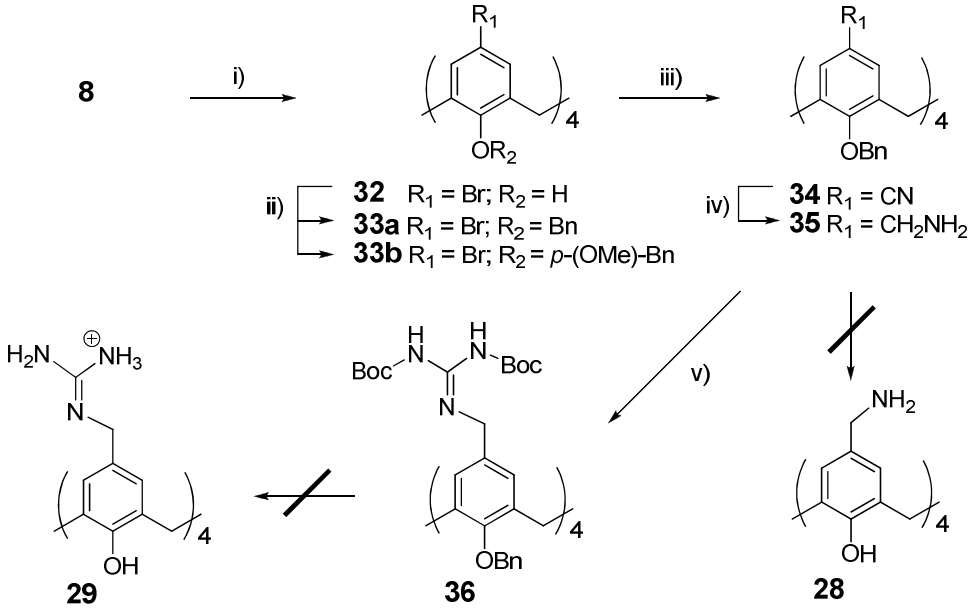

i) Br_2, $CHCl_3$, 4 h, rt (quant.) ii) **33a**: NaH, BnBr, DMF, 50 ºC, 18 h (81%); **33b**: NaH, *p*-OMe-BnBr, DMF, 50 ºC, 4 h (64%). iii) CuCn, NMP, 200 ºC, 4 h (52%). iv) 1M BH_3-THF, reflux, 16 h (92%). v) *N,N*'-bis-(tert-butoxycarbonyl)guanidine *N*''-triflate, Et_3N, CH_2Cl_2, rt, 24 h (16%).

Fig. 3.9: Failed synthesis of compounds **28** and **29** *via O*-benzyl protected precursors.

Starting from calix[4]arene **8**, *p*-bromocalix[4]arene **32** was obtained quantitatively (35). Lower rim alkylation proceeded smoothly either with benzyl bromide or with its *p*-methoxybenzyl analogue (32,36). Thereafter, cyanation was attempted on a microwave oven, as described for compounds **23a/b**, but conditions were too harsh for precursors **33a/b** and only

degradation products were harvested. However, using conventional heating and no pressure (37), enabled to generate cyano derivative **34** in satisfactory yields. This was not feasible for precursor **33b**, which degraded prior to complete nitrile incorporation.

Reduction of the cyano groups following previous described conditions yielded *p*-amino precursor **35** almost quantitatively. In this context, we tried to obtain compound **28** *via* *O*-benzyl removal on precursor **35** through hydrogenolysis (38), but again failed to isolate final product (Fig. 3.9).

Incorporation of *N,N'*-bis-(*tert*-butoxycarbonyl)guanidine *N*"-triflate on **35** led to compound **36**, in analogy to **24a/b,** although in surprisingly low yields (16%). Furthermore, upper and lower rim protecting groups removal under acidic conditions (TFA) did not proceed as expected: Whereas Boc groups were cleaved easily, as assessed by analytical HPLC, *O*-benzyl group removal proceeded more slowly. Prior to complete conversion, the final compound started to disappear, probably due to concomitant *N*-debenzylation, as shown in Fig. 3.10.

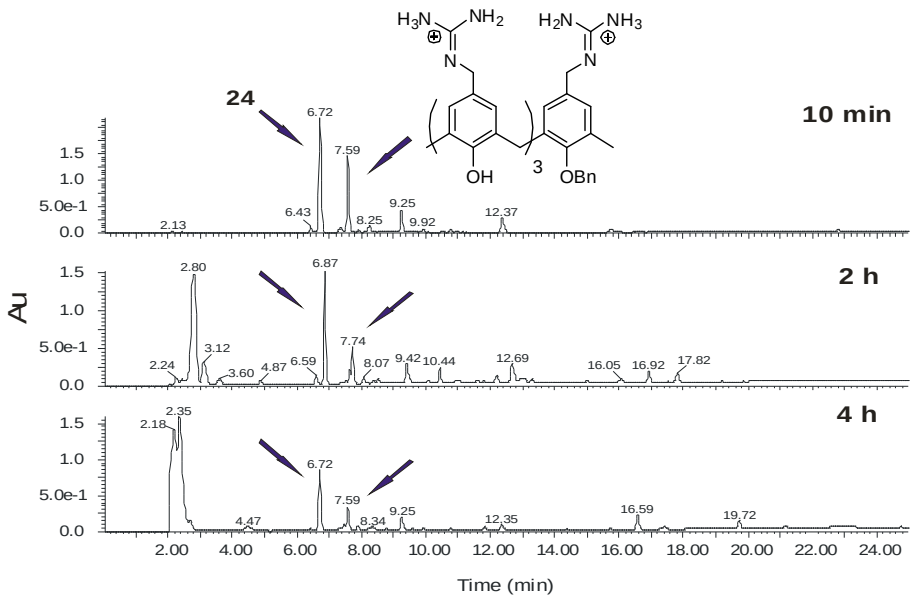

Fig. 3.10: HPLC chromatograms of Boc and *O*-Bn cleavage crude reactions of compound **36** under acid conditions after 10 min, 2 h, and 4 h. Before full conversion takes place, degradation occurs (see peak at ~ 2.5 min and others, conds.: 5-95% CH_3CN in H_2O + 0.05% TFA in 20 min, 3 µl, 1 ml/min, 220 nm).

Meanwhile the *p*-tetracarboxylic compound **37** was generated through classical nitrile oxidation (39). Thereafter incorporation of *N-tert*-butoxycarbonyl-guanidine, following a procedure described by Schmuck *et al.* (40), was attempted. Obtention of final OH-free compound **3** was straightforward, as shown in Fig. 3.11, by simultaneous upper and lower rim removal of protecting groups in a trifluoroacetic solution.

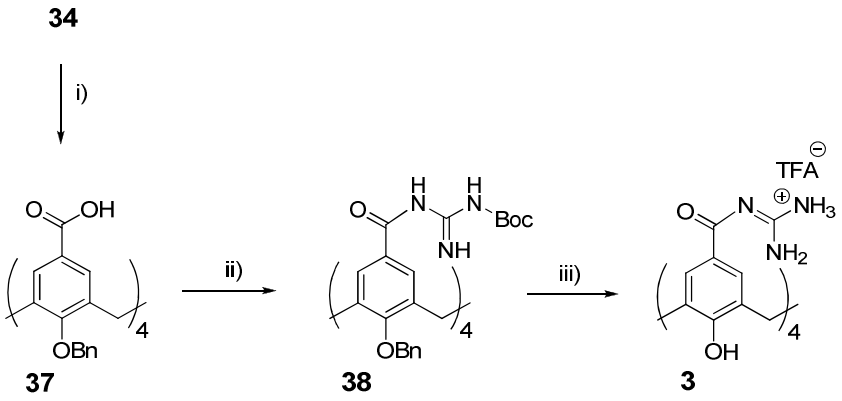

i) KOH, EtOH, reflux, overnight (96%). ii) PyBOP, NMM, GuanBoc, DMF, rt, 24 h (90%). iii) TFA: $CHCl_3$, reflux, overnight (90%).

Fig. 3.11: Synthesis of ligand **3**.

The functional acylguanidine group has an increased acidity, as compared to simple guanidinium cations, besides additional hydrogen bonds to bind to carboxylates in polar solvents (40). Thus, compound **3** was as good as molecule **28** to bind the pore entrance of K_v1 channels.

Encouraged by this result, we decided to build the series of OH-free calix[4]arenes by generating amide bonds on carboxylic precursor **37**, thus obtaining *C*-linked instead of *N*-linked functionalized ligands, a procedure previously reported by Ungaro *et al.* (41).

Carboxylic acid activation was attempted by three methods, prior to reaction with *N*-(*tert*-butoxycarbonyl)-ethylenediamine (Fig. 3.12).

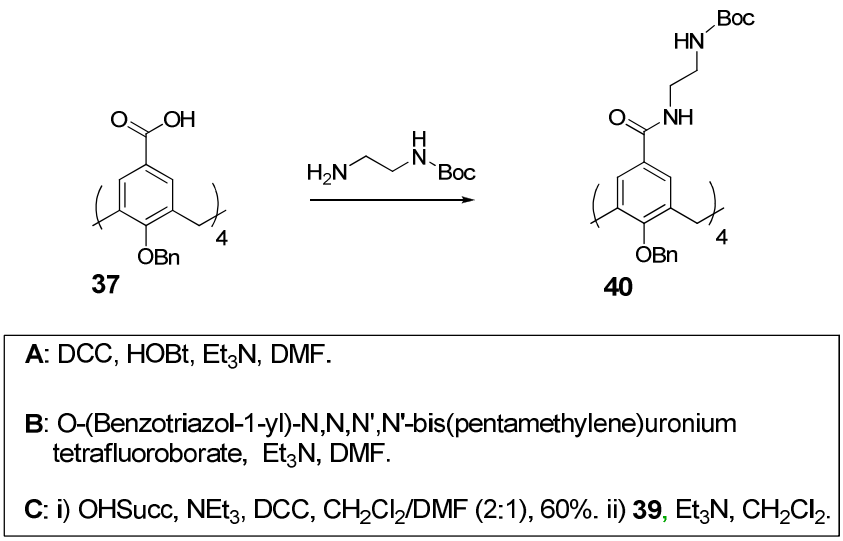

Fig. 3.12: Carboxylic acid activation.

Very low yields (6%) were obtained employing classical coupling reagents such as *N,N'*-dicyclohexylcarbodiimide (DCC) and hydroxybenzotriazole (HOBt) (**A**), but yields slightly improved (to 18%) with *O*-(benzotriazol-1-yl)-*N,N,N',N'*-bis(pentamethylene)uroniumtetrafluoroborate as coupling reagent in the presence of Et_3N (**B**). In both cases, reaction went almost to completion but crudes were cumbersome to purify by precipitation and silica gel chromatography. Hence, though method (**C**) involved two steps instead of one, the intermediate *O*-succinimidoyl ester **39** was easily isolated by precipitation from the reaction crude and both reactions occurred with satisfactory yields. Moreover, the succinimidoyl derivative **39** provided us with a stable and storable compound on which to perform additional amide couplings in a straightforward manner.

Thus, protected compounds **40-43** were obtained from **39** by incorporation of *N*-(*tert*-butoxycarbonyl)-ethylenediamine, L-Lys(Boc)-OMe, L-Arg(Pbf)-OMe and L-Ala-OMe, respectively. Further deprotection of these intermediates at the upper and lower rims resulted in cationic ligands **4-6** and in neutral compound **7** (Fig. 3.13).

Methoxy esthers did resist the acidic conditions employed for final benzyl removal as long as no water traces were present and temperature conditions were controlled. Surprisingly, amide-protected amino acids, such as L-Lys-NH_2, gave rise to secondary reactions during the acid *O*-benzyl removal step, thus amide-protected amino acids were discarded therein.

Amino acid L-Arg-OMe had to be incorporated with its guanidinium group masked, as otherwise no incorporation would occur. Fortunately, Pbf (2,2,4,6,7-pentamethyldihydrobenzofuran-5-sufonyl) was also cleaved under TFA treatment and could easily be removed during work-up.

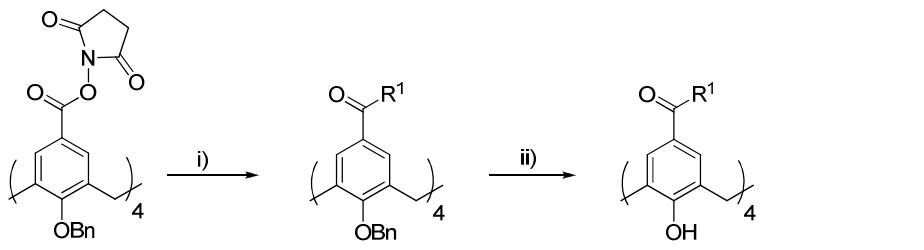

39

40 R^1 = $NHCH_2CH_2NHBoc$ (51%)
41 R^1 = Lys(Boc)-OMe (45%)
42 R^1 = Arg(Pbf)-OMe (70%)
43 R^1 = Ala-OMe (46%)

4 R^1 = $NHCH_2CH_2NH_3^+ Cl^-$ (90%)
5 R^1 = Lys-OMe^+ TFA^- (80%)
6 R^1 = Arg-OMe^+ TFA^- (60%)
7 R^1 = Ala-OMe (quant.)

i) Amide coupling: Et_3N, CH_2Cl_2/DMF, amine. ii) Deprotection: TFA: $CHCl_3$ (1:1).

Fig. 3.13 : Synthetic scheme of compounds **4-7**.

Obtention of tetraanionic negative control **9** *via* oxidation of OH-free *p*-formyl-calix[4]arene **44** with a mixture of sulfamic acid and sodium chlorite was attempted next, as described for *O*-alkyl *p*-formylcalix[4]arenes (42), but the reaction was unsuccessful. Thus **9** resulted from debenzylation of **37** (Fig. 3.14).

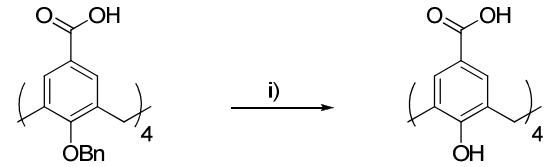

37 **9**

i) AcOH, HCl, reflux, 2 days, sealed tube, semi-preparative purification (60%).

Fig. 3.14: Synthesis of compound **9**.

Several *O*-alkyl calix[4]arenes controls (**10**-**12**) were synthesized by analogous procedures as for compound **3**, from the corresponding carboxylic acids (Fig. 3.15) (refs. 61 and 63, Chapter 2). Compound **10** contains two short loops that cannot enter the channel simultaneously but that could allow the molecule to adjust in a slightly distorted way, which cannot be possible with longer or less structured side chains, such as in **11** and **12**.

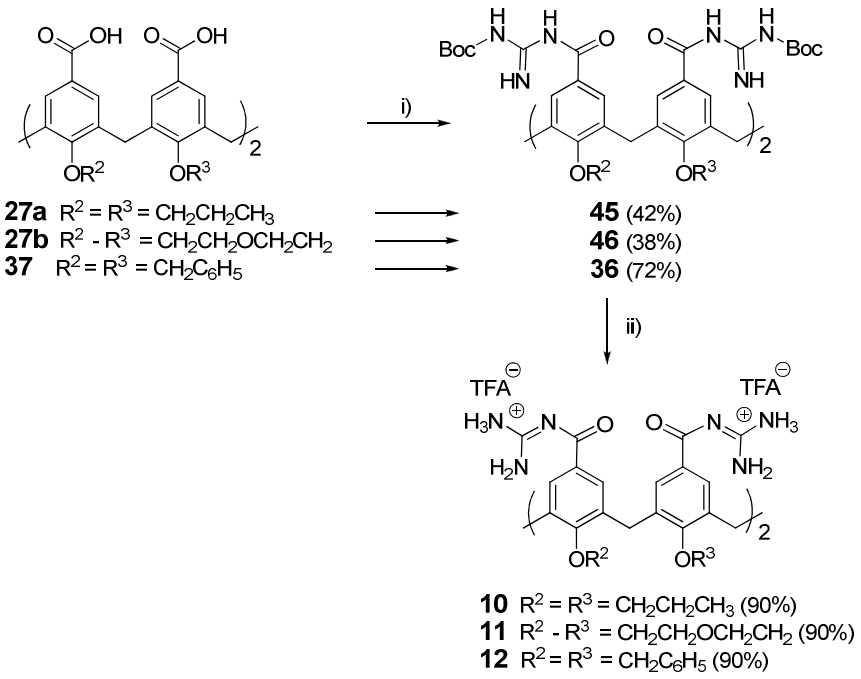

Fig. 3.15: Synthetic scheme of compounds **10**-**12**.

Finally, phenol derivative **13**, a non macrocycle negative control, was readily prepared in two steps from commercially available 4-benzyloxybenzoic acid (Fig. 3.16).

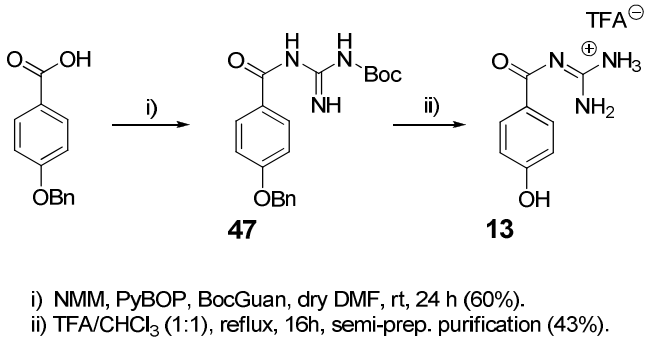

Fig. 3.16: Synthesis of control compound **13**.

Finally, in collaboration with E. Dalcanale and E. Biavardi (Department of Chemistry, University of Parma, Italy), we synthesized ligand **14,** analogous to compound **3**, but based on a resorcinarene platform (Fig. 3.17).

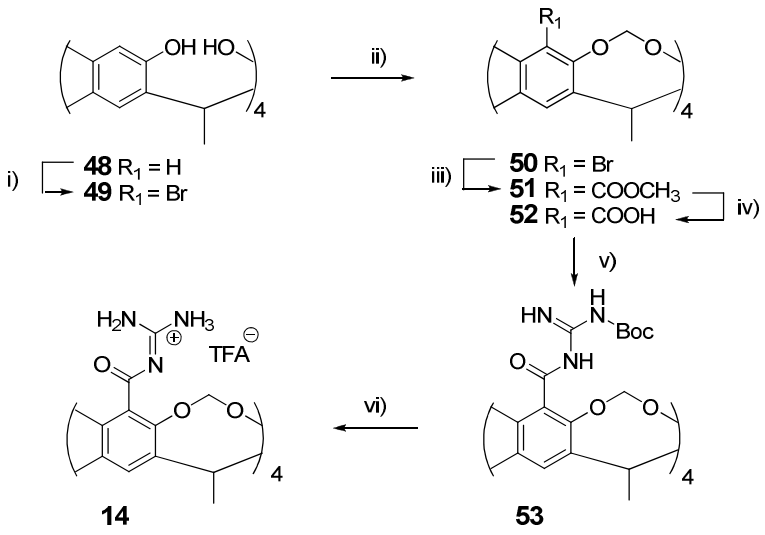

i) NBS, 2-butanone, rt, 16 h (38%). ii) CH_2BrCl, K_2CO_3, dry DMF, 60 ºC, 4 h (56%). iii) BuLi, $ClCO_2CH_3$, THF, 30%. iv) KOH, DMSO, H_2O, 90 ºC, 24 h (70%). v) PyBOP, NMM, GuanBoc, 3 days (52%). vi) TFA/CH_2Cl_2, 0-23 ºC,1 h (51%).

Fig. 3.17: Synthesis of resorcinarene **14**.

To this aim, the readily available calix[4]resorcinarene **48**, (43) was brominated in phenol's *orto*-position with NBS to give **49** as described (44). After bridging the phenol positions with dibromomethane, metal-halogen exchange was performed on compound **49** followed by methoxycarbonyl incorporation. The esthers were subsequently hydrolysed to their free acids and these were transformed into carboxyguanidinium groups, following the same procedure described for compounds **3** and **10**-

13. Reaction of the tetralithium intermediate with CO_2(g), to directly obtain the tetracarboxyl derivative was unsuccessful in our hands (45).

At this point we had succeeded to generate a series of conical calix[4]arenes, shown in Fig. 3.18, comprising seven OH-free calix[4]arenes **3**-**9** with different upper rim functionalization in addition to several *O*-alkyl calix[4]arenes **10**-**12**, one control for the C_4 symmetric design, phenol **13**, and a control for the calixarene platform, resorcinarene **14**, endowed with carboxyguanidinium groups on their wider edges.

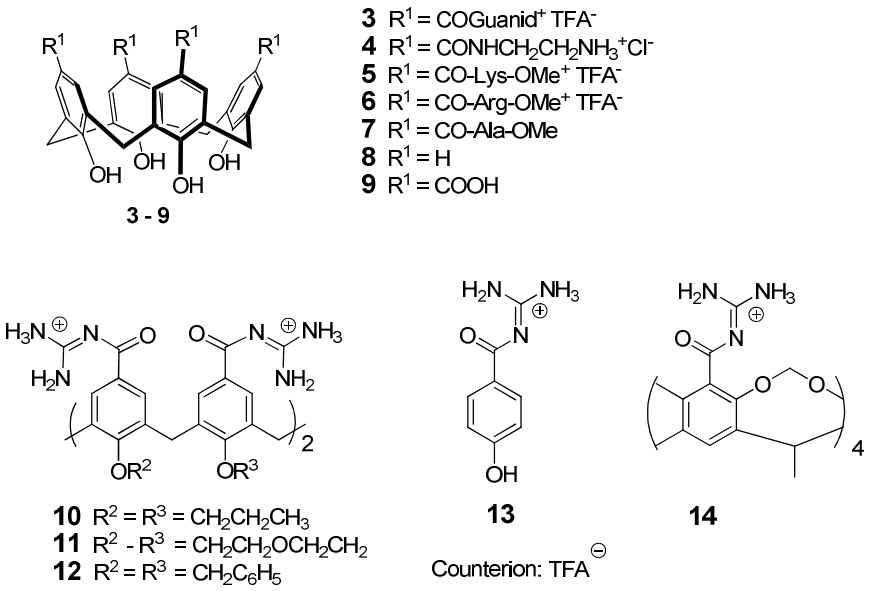

*Fig. 3.18***:** Calix[4]arenes **3-12,** phenol **13** and resorcinarene **14** studied as channel blockers.

3.4 Molecular dynamics performed at ICIQ (Dr. E. Santos)

Docking studies were performed with structures **3**, **6** and **11**, employing the coordinates of the crystal structure of the $K_v1.2$ potassium channel, (pdb: 2a79) (9), excluding chain A and part of chain B (residues 32 to 131). Thus, the integral membrane component of $K_v1.2$ was considered.

They indicated that the conical platform of OH-free calix[4]arenes was indeed well suited to deeply penetrate the extracellular outer vestibule of the channel (Fig. 3.19) (46).

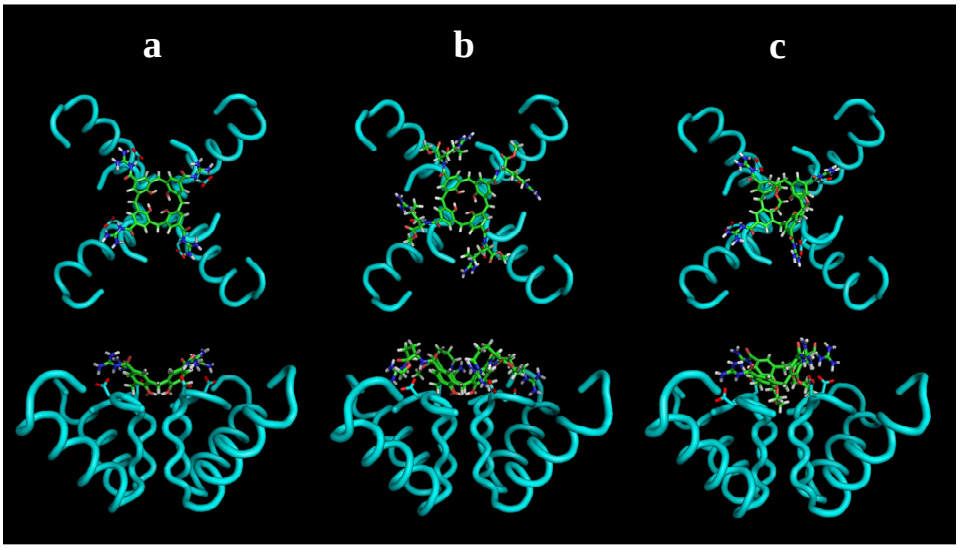

Fig. 3.19: Top and side wireframe views of calix[4]arenes **3** (**a**), **6** (**b**), and **11** (**c**) docked into the x-ray structure of the human voltage dependent $K_v1.2$ potassium channel. Only the backbone helices of the alpha subunits are shown. The Asp379 side chains are represented, showing the four ion-pair, hydrogen bonded contacts with the guanidinium residues of the calix[4]arene. Structures were optimized *in vacuo* at 300 K applying positional restraints to $K_v1.2$ (reproduced from ref. 46).

3.4 Molecular dynamics performed at ICIQ (Dr. E. Santos)

Protein-ligand stabilities were assessed by analyzing the trajectories obtained in 1500 ps molecular dynamics simulations *in vacuo* at 300 K with positional restraints. To evaluate protein-ligand binding affinity, we computed both the Xscore empirical scoring function and the variation in the guanidinium-carboxylate (Asp379) distances versus time. Xscore was used to evaluate, for each trajectory, 128 structures collected every 12 ps. The values obtained for the three calixarenes were very similar and only slightly fluctuated during the molecular dynamics simulations. The average Xscore value of all the complexes formed with **3** was 6.65. The complexes in which **6** and **11** intervened had values of 6.30 and 6.32 respectively. This demonstrated high and similar protein-ligand affinity in the three cases.

To estimate the variation of the hydrogen bond guanidinium-carboxylate distances we monitored all the NH-OC distances at every step. The two values corresponding to a same guanidinium-carboxylate interaction were averaged. Thus, the result depended on the fine orientation of both interactions. Comparison of the plots versus time pointed out a slightly larger fluctuation of the hydrogen bond distances in **3**. In this ligand the four interactions oscillated between 1.6 and 2.4 Å during the whole trajectory. In compound **6** the four of them were highly fixed at a distance of 1.6-1.7 Å. Three of the interactions in compound **11** were maintained at this distance but the remaining one highly fluctuated between 1.6 and > 3 Å. This was due to the tilted orientation of the calixarene on the $K_v1.2$ surface, which caused one of the guanidinium groups of the calixarene to keep away from the corresponding aspartate. Thus, **6** was the ligand with most favorable hydrogen bonding distances followed by **11**. In any case, the

three compounds showed to maintain all the guanidinium-carboxylate groups at standard hydrogen bonding distances.

In conclusion, molecular dynamics indicated that all three ligands bound the protein with high affinity by establishing strong hydrogen bonds and by maintaining the lower rim embedded in the channel pore. The two crown ether bridges apparently did not prevent the interaction of **11** with $K_v1.2$, but instead caused the ligand to be slightly twisted with respect to **3** and **6**.

3.5 Results from eletrophysiology studies performed at UC Berkeley (S. C. Bell and Dr. E. Y. Isacoff)

3.5.1 Introduction to voltage clamp

The two-electrode voltage clamp (TEVC) is a method that allows ion flow across the cell membrane to be measured as an electric current (I), since the transmembrane potential is held under constant experimental control with a feedback amplifier. Voltage dependent potassium channels expressed in *Xenopus* oocytes can be studied using TEVC (Fig. 3.20): The membrane of the oocyte is penetrated by two microelectrodes, one for voltage sensing, relative to the ground, and one for current injection. The user sets a "holding voltage", or "command potential", and the voltage clamp uses negative feedback to maintain the cell at this voltage. The electrodes are connected to an amplifier, which measures membrane potential and feeds the signal into a feddback amplifier. This amplifier also gets an input from the signal generator that determines the command potential, and it subtracts the membrane potential from the command potential ($V_{command}$-V_m), magnifies any difference, and sends an output to the current electrode. Whenever the cell deviates from the holding voltage, the operational amplifier generates an "error signal", that is the difference between the command potential and the actual voltage of the cell. The feedback circuit passes current into the cell to reduce the error signal to zero. Thus, the clamp circuit produces a current equal and opposite to the ionic current. This can be measured, giving an accurate reproduction of the currents flowing across the membrane (47).

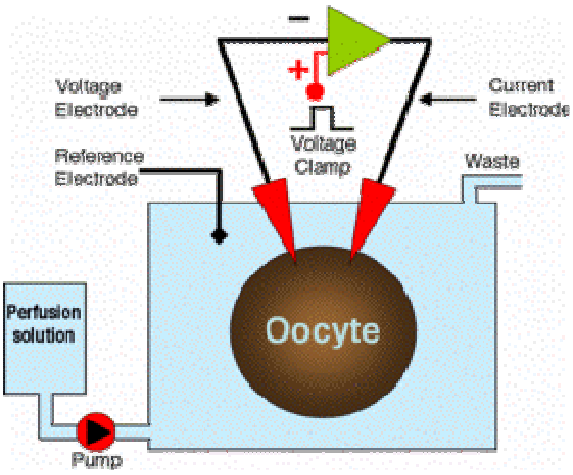

Fig. 3.20: Two-electrode voltage clamp.

X. laevis oocytes provide a convenient system to study potassium channels because they are single cells of macroscopic size (~1 mm in diameter) that possess an endogenous expression system and an efficient trafficking of proteins to the membrane.

They are obtained from ovarian lobes in the abdomen of the frogs through surgery (Fig. 3.21). The follicle wall is removed and the sorted oocytes are incubated until microinjection of messenger RNA (mRNA). Injection of the mRNA of the channel under study leads to its overexpression on the membrane of the oocyte, and minimizes the presence of endogenous channels that otherwise would interfere with electrophysiological experiments. After injection into the cytosol, the oocytes are incubated for 12 h to 3 days at 12-18 ºC, depending on the mRNA construct, the oocyte batches, the channel expression requirements etc. Thereafter oocytes are ready for TEVC studies.

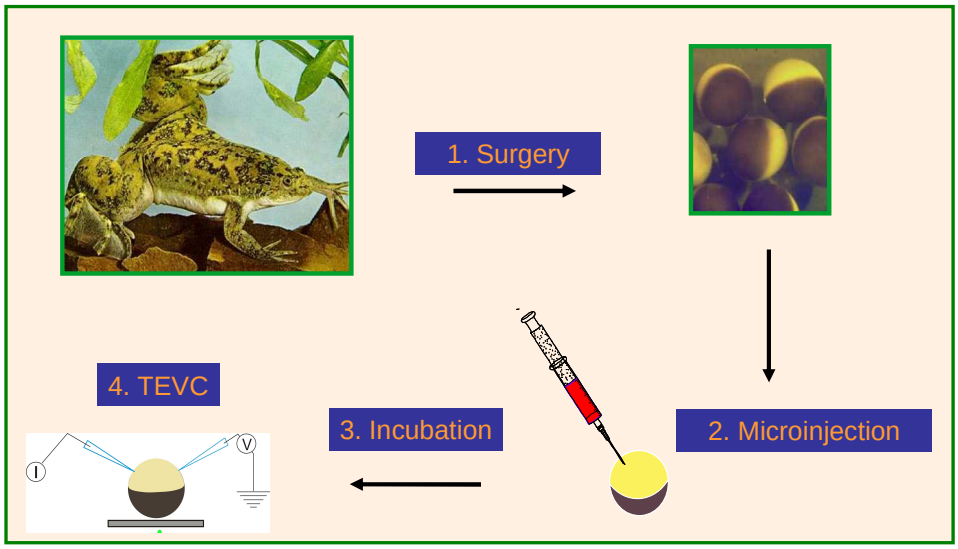

Fig. 3.21: From *Xenopus* frog to TEVC experiments.

3.5.2 TEVC results

Inhibition of K_v1 channels by calix[4]arene compounds.

TEVC experiments for this project were initiated by us during a short research stage (Aug. 07-Oct. 07) at the laboratories of Profs. D. Trauner and E. Isacoff, in the Departments of Chemistry and Molecular Biology at UC-Berkeley, and later taken up and completed by PhD student Sarah Bell (E. Isacoff's group).

Either Shaker potassium channel and $K_v1.3$, both members of the K_v1 subfamily, were expressed in oocytes. Moreover, two different Shaker

channel constructs were initially employed: Shaker H4 IR(Δ6-46) T449F (Shaker T449F) and Shaker H4 IR(Δ6-46) wt (Shaker wt). Both Shaker constructs lack an *N*-terminus domain which inactivates the channel from the intracellular side, in a voltage independent manner (*N*-type inactivation). However, they differ in that mutation T449F renders the channel more sensitive to external block by TEA.[i]

[i] The Shaker clone Sh H4 IR (Δ6-46) in the pBluescript2 KS+ vector was previously prepared by Sarah Bell (E. Isacoff's group) performing site-directed mutagenesis from the Shaker H4 IR T449F (QuikChange protocol, Strategene). The $rK_v1.3$ construct was cloned into in the pGEM-HE vector as well. Finally, all DNA was confirmed by DNA-sequencing previous to performing transcription (mMessage mMachine T7 transcription kit, Ambion).

3.5.2 TEVC results

Ionic currents were measured by TEVC in cells expressing the Shaker or $K_v1.3$ channel in the presence of each calix[4]arene compound. A typical experiment included three sequential protocols: First, current elicited by test voltages that range from -80 mV to +60 mV, are applied in 10 mV increments, from a holding potential of -80 mV, and recorded in order to evaluate the channel expression and leak of the oocyte cell under study. Once, the expected behavior is observed, the second protocol, which consists in pulses from resting (-80 mV) to open states (+20 mV), is launched to test I_{max}. After reaching the steady state, inhibitor solution is perfused and current decrease is expected. Once maximum inhibition is achieved, a washout solution is perfused to remove any reversible blocker from the oocyte surface. Finally the first protocol is repeated to evaluate if the oocyte membrane has been fully recovered. The sequence of protocols, gives rise to three different graphs represented in Fig. 3.22.

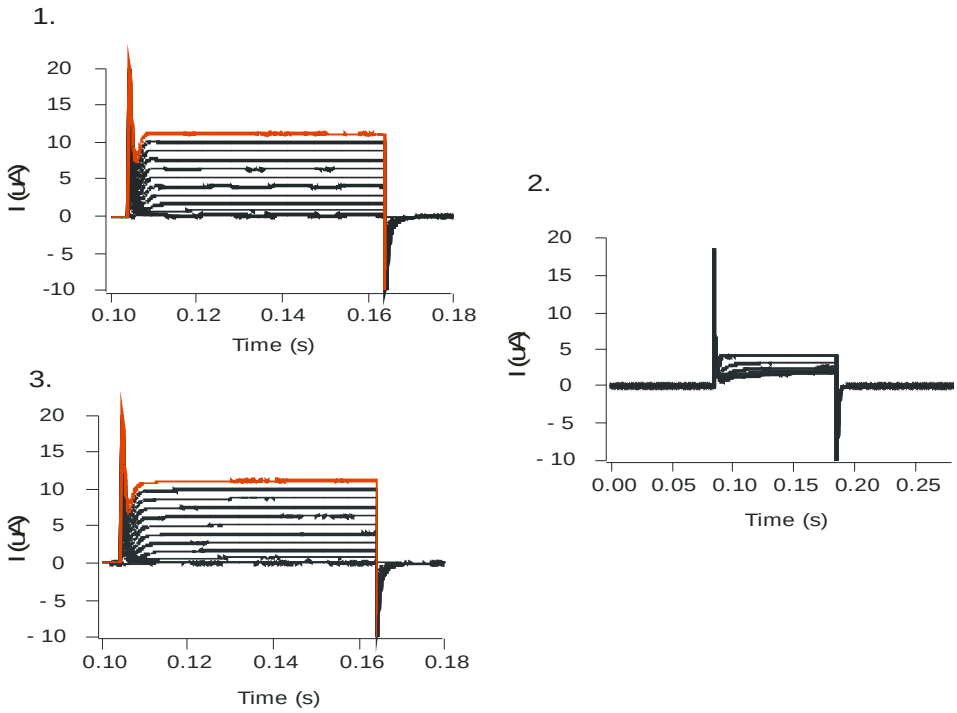

Fig. 3.22: Sequence of graphs [I(μA) *vs* time] obtained with CLAMPEX software for the three protocols described, while perfusing compound **6** (50 μM) on oocytes expressing Shaker wt.

Normalizing the current obtained during the second protocol gives rise to a graph, as the one depicted in Fig. 3.23, showing the typical response of an oocyte expressing Shaker channel, when exposed to 50 μM compound **6**.

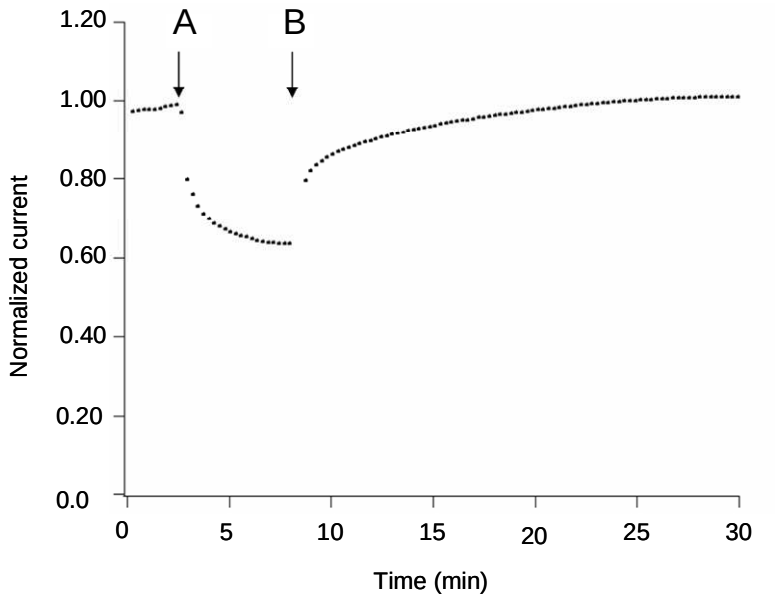

*Fig. 3.23***:** Reversible reduction of Shaker ionic current in response to application of 50 μM ligand **6** (% inhibition vs time). Ligand **6** was applied at A and washed out at B. Note that inhibition and recovery occur in two distinct phases (reproduced from ref. 46).

The percent inhibition elicited by application of compounds **3-14** was compared to that induced by the pore blocker TEA (Fig. 3.24). At this concentration, calixarenes **3-14** caused different levels of reduction in Shaker wt ionic current, which in most cases was reversible. TEA was used as a positive control of a reversible open voltage-dependent K^+ channel pore blocker (16-18).

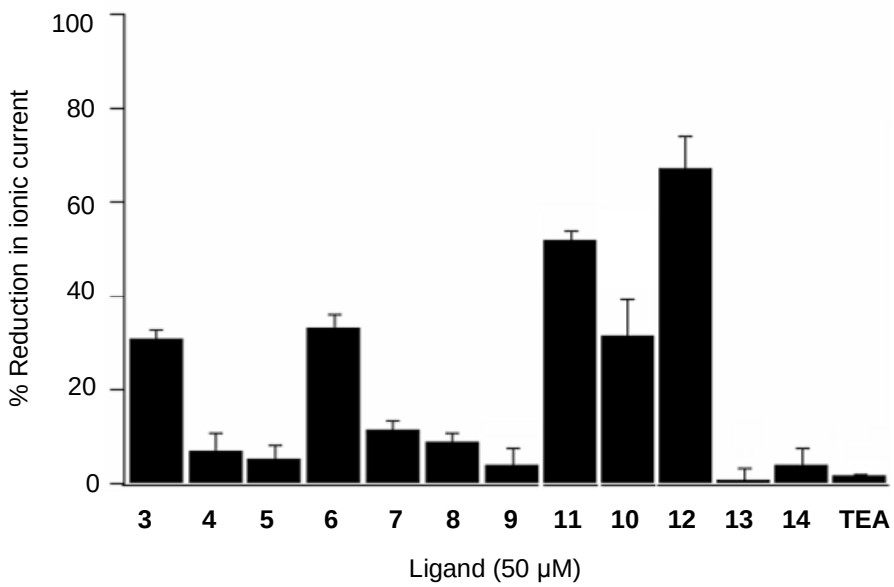

Fig. 3.24: % inhibition elicited by application of 50 µM of compounds **3-14** and TEA to *Xenopus laevis* oocytes expressing the Shaker channel. (n > 4 for each condition; error bars indicate SEM).

At 50 µM, compounds **3-14** caused different levels of reduction in Shaker ionic current, which in most cases was reversible: Compounds functionalized either with carboxylates, ammonium or neutral functional groups at the upper rim, did not exert significant reduction in Shaker ionic current. On the contrary, ligands **3** and **6** containing guanidinium groups at the upper rim of a OH-free calix[4]arene scaffold, aimed at interacting with negatively charged residues and hydrogen bonding in the turret loop, proved promising ligands. When applying *O*-alkyl derivatives **10** and **12** to oocytes expressing the Shaker channel, decreases in ionic current were also seen, but these effects were not reversible and cell health was visually compromised. Lower rim alkylation with hydrophobic residues might cause

non-specific interactions with the membrane lipids or other hydrophobic portions of the Shaker channel which could not be restored by application of the aqueous recording solution used for the washout. Quite remarkably, but in agreement with computer modeling studies, ligand **11**, carrying two crown ether loops at the lower rim, caused reduction in Shaker ionic currents in a reversible manner and even to a larger extent than the OH-free analogues **3** and **6**. It is known that crown ether bridges at vicinal lower rim positions in a calix[4]arene strongly contribute to keep the conical shape of the macrocycle, preventing it from collapsing into the so-called pinched conformations (43a). The conical shape is also maintained in the OH-free derivatives, due to the cyclic array of hydrogen bonds. At the same time, the crown ether bridges on **11** do not create a severe steric effect, since the ligand can comfortably fit at the top of the channel in a slightly tilted orientation, as was clearly seen by molecular dynamics simulations, described later.

Furthermore, the effect of the multivalency present in the calix[4]arene macrocycle was evidenced by the fact that a simple phenol such as **13** showed very little inhibition at 50 μM. Even at four times the concentration employed for ligand **3**, thus at the same effective concentration, phenol **13** did not reduce the positive current and even caused some minor negative current to arise (Fig. 3.25).

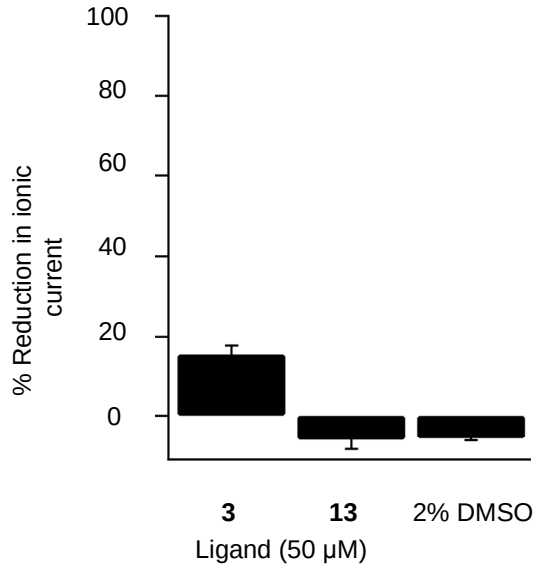

Fig. 3.25: Comparison of monomer *vs* fully assembled calixarene compound: *X. laevis* oocytes expressing Shaker wt were incubated with either 25 μM ligand **1** (n = 4), 100 μM ligand **11** (n = 5), or DMSO (2% v/v), n = 4). Data in bar graphs, error bars indicate SEM (reproduced from ref. 46).

Changes in the counter-anions (either chloride or trifluoroacetic acid) had no measurable effect on the channel binding properties of the calix[4]arenes. Furthermore, the presence of < 2% DMSO in the bath solution was not harmful to the cells (Fig. 3.25).

Finally resorcinarene analogue **14** had a minor effect on current reduction (Fig. 3.24), probably due to the insolubility of this material at 50 μM in ND96 -the buffer employed throughout the electrophysioloy studies- with 1% DMSO. Thus no conclusion could be drawn concerning the adaptability

of resorcinarene **14** architecture to Shaker surface compared to calix[4]arene **3**.

Among the most active ligands (**3**, **6** and **11**), ligand **3** had a limited solubility and ligand **11** with bulkier substituents on the lower rim did dock into the pore in a tilted orientation. Therefore, in the rest of our studies, we focused on ligand **6**.

Inhibition includes gating modification.

Ligand **4** showed a concentration dependent inhibition of both Shaker and $K_v1.3$, the two related members of the $K_v1.x$ ion channels subfamily employed in this study (Fig. 3.26). While the inhibition was greater in $K_v1.3$, the apparent affinity was similar for the two channels. The Hill coefficients for the two channels (1.0±0.3 and 1.1±0.7, respectively) were close to 1, fitting with the proposed molecular model in which a single calix[4]arene docks in the outer mouth of the pore and interacts with residue Asp379 ($K_v1.2$ sequence numbering), which is shared by all $K_v1.x$ subfamily members.

Even at saturating concentrations of calix[4]arene **4**, Shaker ionic current was not completely inhibited (Fig. 3.26), suggesting, an incomplete occlusion of the pore.

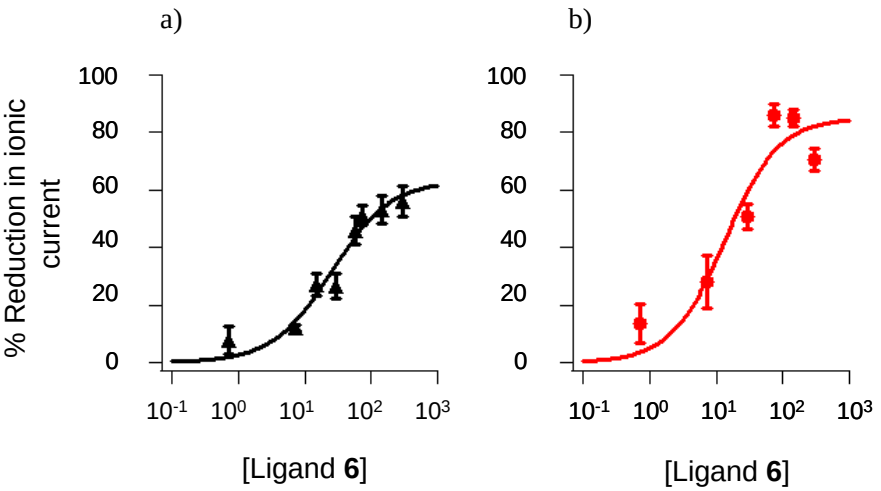

Fig. 3.26: Concentration dependence of compound **6** on macroscopic ionic currents in *X. laevis* oocytes expressing Shaker channels (a) or $K_v1.3$ channels (b). ($n \geq 3$ for each data point; error bars indicate SEM). Data fit to a single Boltzmann. Shaker: max = 63±10, K_d = 25±11 µM, m = 1.0±0.3. $K_v1.3$: max = 85±16, K_d = 14±9 µM, m = 1.1±0.7.

The effect of ligand **6** could not be entirely attributed to pore block. The rate of channel opening was slowed (Fig. 3.27a) and the voltage dependence of channel opening was shifted in the positive direction by ligand **6** (Fig. 3.27b), indicating that binding relatively stabilizes the resting state or an intermediate state preceding opening in the activation pathway.

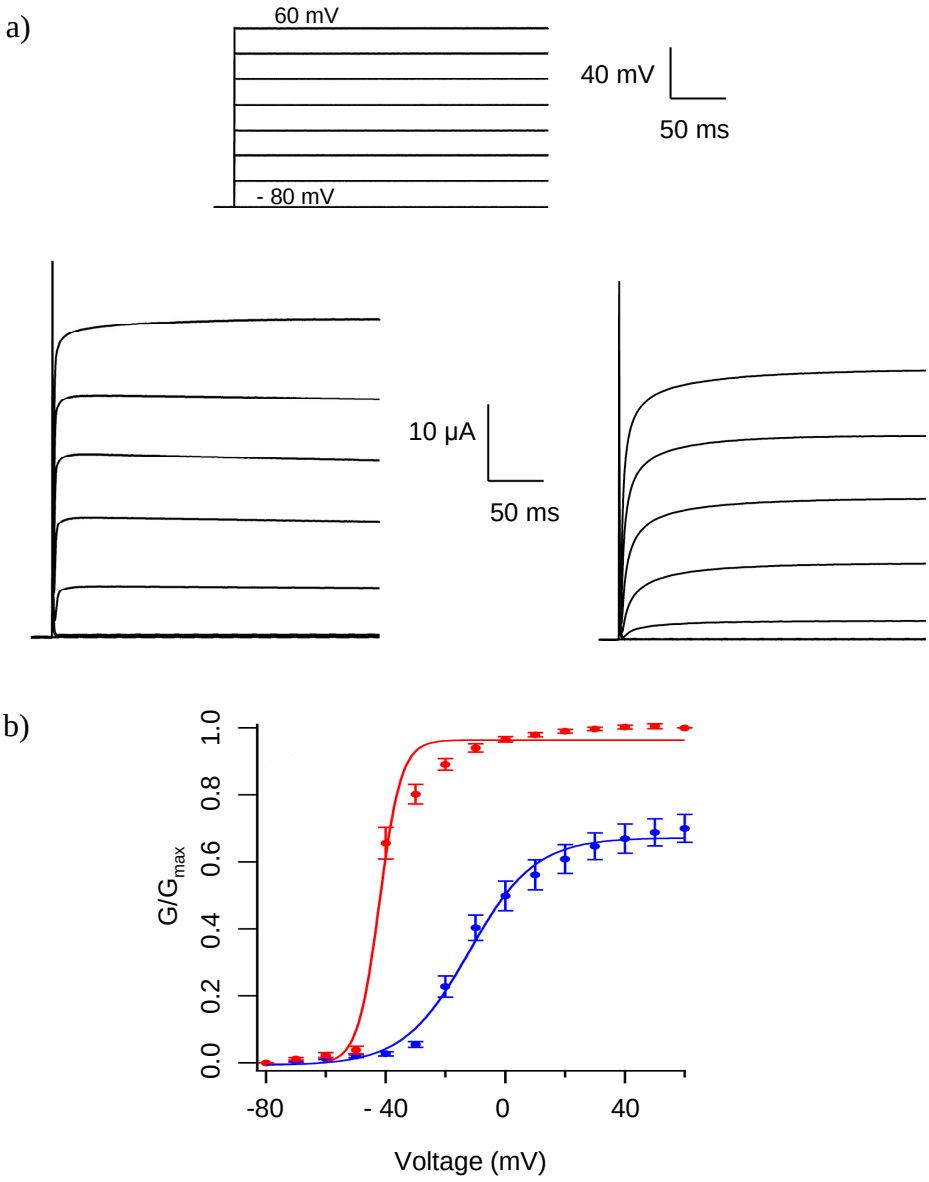

Fig. 3.27: (a) Voltage-step protocol from -80 to +60 mV: Opening kinetics are slower in the presence of 50 µM ligand **6** (right traces) compared to control (left traces). (b) Ligand **6** (50 µM) shifts the voltage dependence of channel opening to the right. Conductance measured from inward tails in 98 mM external K^+. (n = 4, error bars indicate SEM). Control solution before exposure: max = 0.97±0.04, $V_{0.5}$ = -42±1 mV, *m* = 3.6±0.9. During ligand **6** application: max = 0.68±0.02, $V_{0.5}$ = -12±1 mV, *m* = 11±1.2 (ref. 46).

The onset of current inhibition and of the gating effect occurred in parallel, with reduction in current amplitude tracked by the slowing of channel opening (Fig. 3.28 a,b).

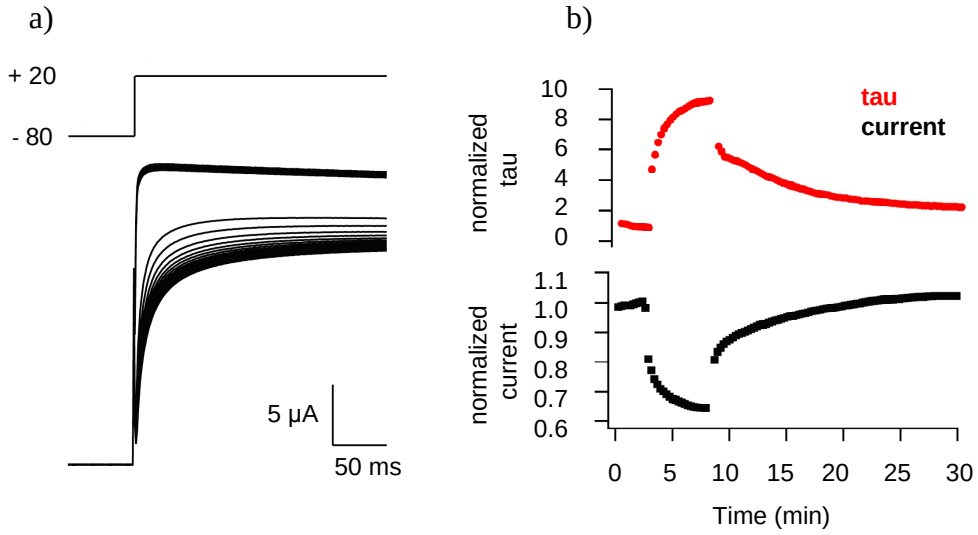

Fig. 3.28: (a) Progressive slowing of opening kinetics accompanies progressive inhibition of current amplitude upon application of 50 µM ligand **6** (steps from holding potential of -80 mV to +20mV). (b) Time course of reduction of current amplitude parallels slowing of channel opening following application of 50 µM ligand **6** (reproduced from ref. 46).

We wondered whether the gating effect reflected an influence of ligand **6** on the protein motions underlying voltage sensing. To address this we employed a technique that would distinguish between effects on the voltage sensing domain and pore blocking properties.

3.5.3 Voltage clamp fluorometry results

A structural link between reversible block and inactivation of a voltage dependent channel chimaera (KcsA-K_v1.3) has been previously reported with reversible pore blocking tetraphenylporphyrin derivatives whose positively charged arms deeply insert into the selectivity filter (24,25). Likely, the interaction of **6** with the selectivity filter of Shaker channels exerts the same inactivation effect observed for the porphyrin ligands on KcsA-K_v1.3.

For a structural proof of this allosteric effect, we employed voltage clamp fluorometry which measures structural rearrangements in the S4 voltage sensor (48). Recordings were carried out in the W434F mutation, which locks the channel in the non-conducting P-type inactivated state, but permits free motion of S4 (49). A single cysteine mutation was also introduced in the extracellular portion of the Shaker S4 segment (A359C) to allow for site-specific conjugation with tetramethylrhodamine-6-maleimide, an environmentally sensitive fluorophore, and to monitor the movement of the voltage sensing domain (50). Ligand **6** (200 μM) was found to slow the rate of S4 motion at the top of the voltage dependence curve where channels open (Fig. 3.29).

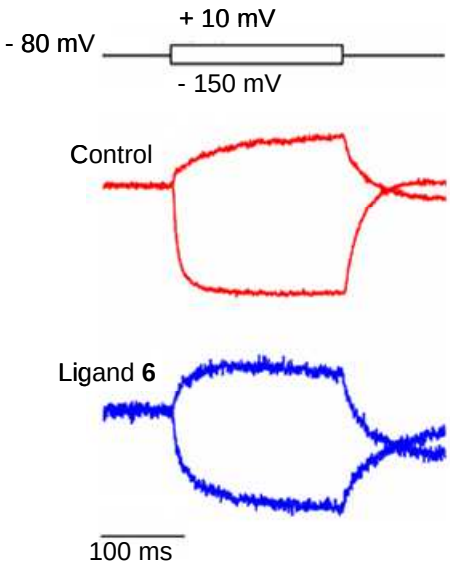

Fig.3.29: Fluorescence analysis of kinetic effects of ligand **6**. Representative normalized fluorescence traces showing Shaker voltage sensor movement in the absence (top) and presence (bottom) of ligand **6**. A slowing in kinetics upon hyperpolarization and depolarization steps is seen upon application of ligand **6** (200 µM, reproduced from ref. 46).

This result is consistent with the observation that channel opening is slowed by the ligand (Figs 3.27a,b and 3.28a,b).

3.6 Conclusions and outlook

In conclusion, we show that guanidilated OH-free and bis-crowned calix[4]arenes, constitute a versatile class of non toxic reversible voltage dependent K^+ channel ligands.

Molecular modeling predicts an interaction with the turret loop and docking in the outer mouth of the pore of K_v channels for compounds **3**, **6**, and **11**. A Hill coefficient of 1 for inhibition of the current is consistent with this model. The inhibition is incomplete at saturating concentrations. In addition, the ligand shifts the voltage dependence of gating and slows down both the opening of the gate and the voltage sensing motion of S4.

Similar allosteric behaviour have been recently described by Baldus and co-workers based on solid state NMR: conformational changes induced by different natural and abiotic pore blocking ligands of K_v channels cause subsequent changes in their gating and activation properties (25,51). Hence, similar solid state NMR studies with calixarene ligand **6** would provide us with structural data to fully understand the movements caused by calixarene **6** binding on K_v1.x conformation and confirm the C_4 symmetric binding predicted by molecular modeling.

Furthermore, based on the results obtained so far, a new generation of ligands is under study, taking advantage of the divergent synthetic strategy for upper rim functionalization of OH-free and the rigidity of bridged calix[4]arenes. Therefore, a study of the footprints of toxins like AgTx

(20,52), and δ-dendrotoxin (53) on the surface of Shaker channel will be performed. Increasing the affinity of the channel-calix[4]arene interaction through further functionalization of **6** with suitable peptide chains attached to the upper rim is currently underway. Ultimately, the development of this new class of compounds might lead to novel therapeutic agents against various ailments such as autoimmune disorders, diabetes, epilepsy, or cardiac diseases (54).

3.7 Experimenal part

General procedures: See section 2.8.

Compounds **51** and **52** were obtained and kindly provided by PhD student Elisa Biavardi at Enrico Dalcanale's group (University of Parma, Italy).

5,11,17,23-Tetraazidomethyl-25,26,27,28-tetrahydroxycalix[4]arene (30).

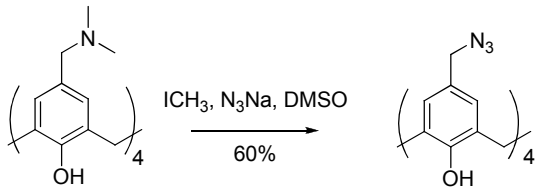

31 **30**

To a solution of compound **31** (0.15 g, 0.23 mmol) in DMSO was added ICH_3 (0.085 mL,1.38 mmol) with a syringue and the solution was stirred at rt for 40 min. Thereafter NaN_3 (0.15 g, 2.3 mmol) was added and the reaction was heated to 80 ºC and stirred for additional 4 h. Next, the reaction was cooled on an ice bath and ice/water (10 mL) was added. The aqueous solution was additionally acidified with 2M HCl until the appearence of a precipitate which was filtered and air dried. Product **30** was obtained as a yellow solid in a 60% yield. Mp: 150-152 ºC (dec). ^{1}H NMR (DMSO-d_6): δ 7.04 (s, 8H, ArH), 4.29 (bs, 4H, CH_2Ar), 4.17 (s, 8H, $ArCH_2N_3$), 4.14 (s, 8H, $ArCH_2N$); 3.58 (bs, 4H, CH_2Ar). ^{13}C NMR ($CDCl_3$) δ 148.7, 129.3 (CAr), 128.9 (CHAr), 128.3 (CAr), 54.1 ($ArCH_2N_3$), 31.9 ($ArCH_2Ar$). ESI(-) *m/z* $[M - H]^-$: 643.3 uma.

5,11,17,23-Tetradimethylamine-25,26,27,28-tetrahydroxycalix[4]arene (31).

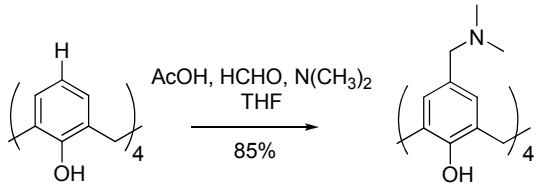

8 **31**

To a solution of **8** (0.5 g, 1.18 mmol) dissolved in THF (11 mL) were added acetic acid (1.3 mL), 40% aqueous dimethylamine (0.74 mL) and 37% aqueous formaldehyde (0.48 mL). The reaction was stirred for 24 h at rt, thereafter the solvents were removed *in vacuo*, and the residue was taken up in water (15 mL) and washed with Et_2O (3 x 15 mL). Next, the aqueous solution was neutralized with 10% K_2CO_3 solution. The suspension formed was stirred overnight at 4 ºC and finally a precipitate was obtained and filtered, yielding 85% of pure **31**. Mp: 150 ºC (dec).^{1}H NMR (DMSO-d_6): δ 6.85 (s, 8H, ArH), 4.25 (s, 4H, CH_2Ar), 3.27 (s, 8H, CH_2N), 3.16 (d, J = 12.0 Hz, 4H, CH_2Ar), 2.18 (s, 24H, CH_3N). ^{13}C NMR (DMSO-d_6) δ 154.1, 129.9 (CAr), 128.4 (ArH), 125.2 (CAr), 62.5 ($ArCH_2N$), 44.0 (CH_3N), 32.5 ($ArCH_2Ar$). ESI(+) *m/z*: $[M + H]^+$: 653.4 uma.

5,11,17,23-Tetrabromo-25,26,27,28-tetrahydroxycalix[4]-arene (32).

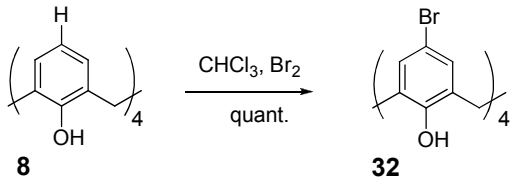

8 **32**

To a solution of compound **8** (1.5, 3.53 mmol) in $CHCl_3$ cooled down to 0

ºC, bromine (1.5 mL, 29 mmol) was added dropwise and the mixture was stirred at rt for 4 h. Thereafter, the reaction was quenched by adding 10% $NaHSO_3$ (20 mL) and the mixture was stirred vigorously for 1 h. Thereafter a precipitate was filtered and washed with $CHCl_3$ and water (quant. yield). Mp: > 350 ºC. ^{1}H NMR ($CDCl_3$) δ 9.72 (s, 4H, OH), 7.25 (s, 8H, ArH), 4.0 (bs, 8H, $ArCH_2Ar$). ESI(+) *m/z*: $[M + H]^+$: 736.8 uma.

General procedure for the synthesis of p-bromo-calix[4]arenes 33a and 33b.

To a solution of calix[4]arene **27** (0.2 g, 0.27 mmol) in DMF (12 mL) was added NaH (0.114 g, 2.85 mmol) and the reaction was heated at 55 ºC for 30 min. Thereafter the corresponding alkylating reagent was added and the reaction allowed to cool down to rt within 4 h. Quenching was performed by evaporating the solvent until dryness. Subsequently the residue was taken up in CH_2Cl_2 (8 mL) and washed with 1M HCl (2 x 8 mL), as well as once with water (8 mL) and brine (8 mL). Finally, the organic phase was dried over anhydrous Na_2SO_4, filtered and evaporated *in vacuo*. The compounds were obtained after trituration in EtOH.

5,11,17,23-Tetrabromo-25,26,7,28-tetrabenzyloxycalix[4]arene (33a).

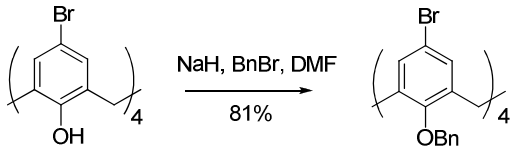

32 **33a**

Product **33a** was obtained as a fine cream-colored powder in a 81% yield. Mp: 213-216 ºC. ^{1}H NMR ($CDC1_3$): δ 7.38-7.20 (m, 20H, ArH), 6.68 (s,

8H, ArH), 4.83 (s, 8H, OCH_2Ar), 4.04 (d, J = 13.4 Hz, 4H, $ArCH_2Ar$), 2.81 (d, J = 13.4 Hz, 4H, $ArCH_2Ar$). ^{13}C NMR ($CDC1_3$): δ 154.2, 136.8 (CAr), 131.0, 129.8 (CHAr), 115.5 (CAr), 76.7, 31.0 ($ArCH_2Ar$). ESI(+) *m/z*: $[M + H]^+$ 1097.0 uma.

5,11,17,23-Tetrabromo-25,26,7,28-tetrakis[(*p*-methoxy)-benzyloxy]calix[4]arene (33b).

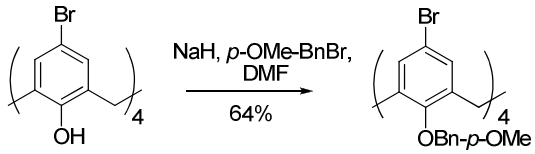

32 **33b**

Product **33b** was obtained as a fine colorless powder in a 64% yield. Mp: 235-238 ºC. ^1H NMR ($CDC1_3$): δ 7.14 (d, J = 8.6 Hz, 8H, ArH), 6.79 (d, J = 8.6 Hz, ArH), 6.73 (s, 8H, ArH), 4.85 (s, 8H, OCH_2Ar), 4.00 (d, J = 13.6 Hz, 4H, ArCH*Hax*Ar), 3.81 (s, 12H, CH_3O), 2.75 (d, J = 13.6 Hz, 4H, ArCH*Heq*Ar). ESI(+) *m/z*: $[M + H]^+$ 1217.0 uma.

5,11,17,23-Tetracyano-25,26,27,28-tetrabenzylcalix[4]arene (34).

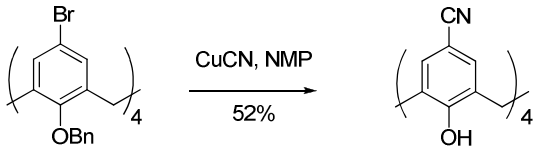

33a **34**

To a stirred solution of *p*-bromo-calix[4]arene **33a** (1 g, 0.912 mmol) in NMP (28 mL) in a 100 mL two-necked flask, CuCN (0.824 g, 9.196 mmol) was added under argon. The reaction was heated for 5 h at 200 ºC. After

cooling the solution to 50 °C, a solution of $FeCl_3$ (1.80g, 11.2 mmol) in 1M HCl (30 mL, caution!) was added and the mixture stirred for an additional 0.5 h. Thereafter, the solution was cooled down to 7 ºC and the resulting cream-colored solid was filtered and recrystallized in toluene. Compound **29** was obtained as a a fine colorless solid in a 52% yield. Mp: > 350 ºC. ^{1}H NMR (CD_3CN): δ 7.40-7.27 (m, 20H, ArH), 7.04 (s, 8H, ArH), 5.06 (s, 8H, CH_2Ar), 4.16 (d, J = 13.8 Hz, 4H, ArCH*Hax*Ar), 3.00 (d, J = 13.8 Hz, 4H, ArCH*Heq*Ar). ^{13}C NMR (CD_3CN): δ 158.5, 136.1, 135.4, 132.3, 129.7, 128.9, 128.5 (CAr, CHAr), 118.0 (CN), 107.0 (CAr), 77.26 (OCH_2Ar), 30.71 (CH_2).

5,11,17,23-Tetraminomethyl-25,26-27,28-tetrabenzyloxycalix[4]arene (35).

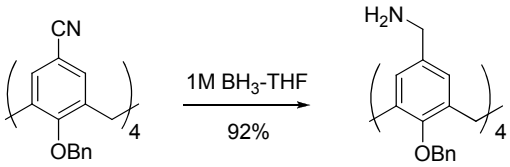

34 **35**

The same general procedure described to obtain compounds **2a** and **2b** was followed. After removal of the organic solvents, the aqueous layer was basified and extracted with CH_2Cl_2 (2 x 3 mL). The organic layer was dried over anhydrous Na_2CO_3, filtered and evaporated to dryness. Thereafter, the residue was triturated in Et_2O and final compound **35** was obtained as a colorless solid in a 92% yield. Mp: 172-175 ºC (dec). ^{1}H NMR (CD_3OH): δ 7.40-7.22 (m, 20H, ArH), 6.65 (s, 8H, ArH), 5.01 (s, 8H, OCH_2Ar), 4.30 (d, J = 13.8 Hz, 4H, ArCH*Hax*Ar), 3.49 (s, 8H, CH_2N), 2.97 (d, J = 13.8 Hz, 4H, ArCH*Heq*Ar). ^{13}C NMR (CD_3OD): δ 154.1, 136.6, 135.0, 129.3, 127.7, 126.8 (CAr, CHAr), 71.4 (OCH_2Ar), 46.7 ($ArCH_2N$), 31.0 ($ArCH_2Br$).

ESI(+) *m/z*: $[M + H]^+$: 901.5 uma.

5,11,17,23-Tetrakis(*N,N'*-bis-*tert*-butoxycarbonyl)guanidinemethyl-25,26-27,28-tetrabenzyloxycalix[4]arene (36).

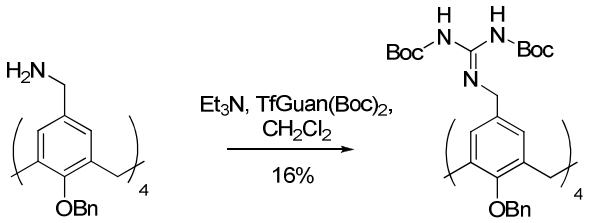

35 **36**

The same general procedure described to obtain compounds **19a** and **19b** was followed. Eluent: 100% $CH_2Cl_2 \rightarrow CH_2Cl_2/Et_2O$, 98:2. and compound **31** was obtained as a colorless foam in a 16% yield. Mp: > 350 ºC. ^{1}H NMR ($CDCl_3$): δ 8.27 (tr, 4H, NH), 7.34-7.20 (m, 20H, ArH), 6.56 (s, 8H, ArH), 4.99 (s, 8H, OCH_2Ar), 4.29 (d, J = 6.3 Hz, 8H, CH_2N), 4.13 (d, J = 12.5 Hz, 4H, ArCH*Hax*Ar), 2.87 (d, J = 12.5 Hz, ArCH*Heq*Ar), 1.51 (d, J = 6.3 Hz, 72H, $C(CH_3)_3$). ^{13}C NMR ($CDCl_3$): δ 163.8 (CO), 155.8 (CAr), 153.03 (CGuan), 137.7, 135.4, 130.8 (CAr), 129.9, 128.1 (CHAr), 82.8 ($C(CH_3)_3$), 78.9 (OCH_2Ar), 44.8 (CH_2N), 31.6 ($ArCH_2Ar$), 29.3, 28.4 ($C(CH_3)_3$). Exact Mass (ESI+): *m/z* $[M + H]^+$: calc.: 935.9949 uma, found: 935.9935 uma.

25,26,27,28-Tetrabenzyloxy[4]arene-5,11,17,23-tetracarboxylic acid (37).

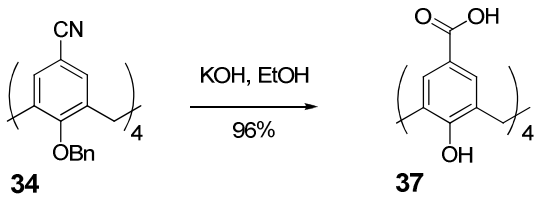

34 **37**

p-Cyano-calix[4]arene precursor (**34**) (95 mg, 0.107 mmol) was dissolved

in EtOH (11 mL) in a round 100 ml two-necked flask. KOH (6 g, 107 mmol) was dissolved in deionized water (4 mL) and added to the flask, which was heated under reflux overnight. The reaction was then acidified with concentrated HCl and the product was precipitated out, washed with H_2O (5 mL) and with Et_2O (5 mL). Final compound was obtained as a colorless solid in a 96% yield. Mp: > 350 ºC.^{1}H NMR (MeOD): δ 12.3 (s, 4H, CO_2H), 7.27-7.29 (m, 20H, ArH), 7.24 (s, 8H, ArH), 5.00 (s, 8H, CH_2Ar), 4.19 (d, J = 13.8 Hz, 4H, ArCH*Hax*Ar), 3.14 (d, J = 13.8 Hz, ArCH*Heq*Ar). ^{13}C NMR (DMSO-d_6): δ 167.2 (CO_2H), 159.26, 137.08, 135.11 (CAr), 130.17, 128.60 (CHAr), 125.19 (CAr), 76.62 (CH_2CO), 32.04 ($ArCH_2Ar$). Exact Mass (ESI+): *m/z* of $[M + Na]^+$: calc.: 983.3043, found: 983.3040.

General procedure for the synthesis of compounds 38, 45-47 and 53.

A solution of (benzotriazol-1-yloxy)tripyrrolidinophosphonium hexafluorophosphate (PyBOP, 0.33 g, 0.62 mmol) and *N*-methylmorpholine (NMM, 0.08 mL, 0.67 mmol) in dry DMF (4 mL) was added to a solution of the calix[4]arene tetraacid precursor (**32**, **22, 39** or 4-benzyloxybenzoic acid, 0.16 mmol), *N*-(*tert*-butoxycarbonyl)guanidine (0.1 g, 0.62 mmol), and NMM (0.08 mL, 0.67 mmol) in dry DMF (4 mL). The reaction mixture was stirred at rt for 24 h to several days, and then poured into water. The resulting colorless precipitate was filtered and dried. The crude compound was purified by flash chromatography in silica gel.

25,26,27,28-Tetrabenzyloxycalix[4]arene-5,11,17,23-tetrakis[*tert*-butylamino(benzamido) methylcarbamate] (38).

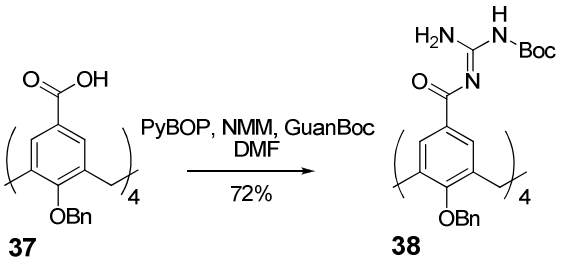

37 **38**

The reaction mixture was stirred for 24 h and pure $CHCl_3$ was employed as eluent for the chromatographic purification. The product was obtained in a 72% yield. Mp: > 350 ºC. ^{1}H NMR ($CDCl_3$): δ 7.30-7.23 (m, 28H, ArH), 4.99 (s, 8H, CH_2Ar), 4.15 (d, J = 14.5 Hz, 4H, ArCH*Hax*Ar), 3.22 (d, J = 14.5 Hz, 4H, ArCH*Heq*Ar), 1.53 (s, 36H, $C(CH_3)_3$). ^{13}C NMR (DMSO-d_6): δ 159.2 (CGuan), 137.3, 130.3, 128.6 (CAr), 31.7 ($ArCH_2Ar$), 28.4 ($C(CH_3)_3$). Exact Mass (ESI+): *m/z* of $[M + H]^+$: calc: 1525.6720 uma, found: 1525.6753 uma.

25,26,27,28-Tetra-*n*-propoxycalix[4]arene-5,11,17,23-tetrakis[*tert*-butylamino(benzamido) methylcarbamate] (45).

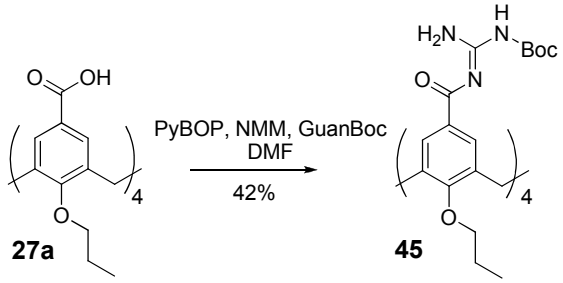

27a **45**

The reaction mixture was stirred for 4 days and was purified by flash chromatography eluting with Hex/Et_2O, 9:1. The yield of pure product **45**

was 42%. Mp: > 350 ºC (dec.). Product **45** was sparingly soluble in all common deuterated solvents, therefore its purity was checked by HPLC (50→95% CH_3CN in H_2O + 0.1% TFA for 15 min followed by a 95 to 100% gradient over 5 min). Exact Mass (ESI+): *m/z* $[M + H]^+$: calc.: 1333.6833 uma, found: 1333.6896 uma.

25,26-27,28-Biscrown-3-calix[4]arene-5,11,17,23-tetrakis[*tert*-butylamino(benzamido) methylcarbamate] (46).

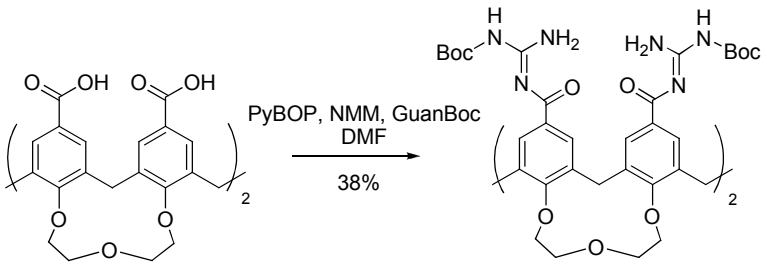

The reaction mixture was stirred for 3 days and the purification was achieved by flash chromatography in silica gel (eluent: Hex/Et_2O, 4:1). Yield was 38%. Mp: > 350 ºC. ^1H NMR ($CDCl_3$): δ 7.80 (s, 8H, ArH), 5.09 (d, *J* = 12.2 Hz, 2H, ArCH*Hax*Ar), 4.51 (d, *J* = 12.2 Hz, 2H, ArCH*Hax*Ar), 4.32-4.22 (m, 12H, CH_2O), 3.89 (tr, *J* = 10.4 Hz, 4H, CH_2O), 3.39 (tr, *J* = 13.6 Hz, 4H, ArCH*Heq*Ar), 1.51 (s, 36H, $C(CH_3)_3$). ^{13}C NMR (CD_3OD): δ 158.9 (COGuan), 152.4 (CGuan), 138.3 (CAr), 129.0, 127.3 (CHAr), 75.1, 74.3 (CH_2), 28.1 ($C(CH_3)_3$). Exact Mass (ESI+): *m/z* $[M + H]^+$: calc.: 1419.5720 uma, found: 1419.5770 uma.

4-(Benzyloxy)-*N*-(*N*-(*tert*-butoxycarbonyl)carbamimidoyl)benzamide (47).

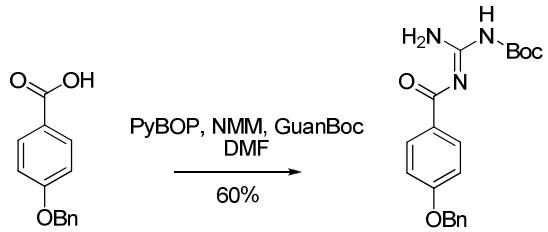

47

The reaction mixture was stirred for 24 h and pure $CHCl_3$ was employed as eluent for the chromatographic purification. The product was obtained in a 60% yield. Mp: > 350 ºC. ^{1}H NMR ($CDCl_3$): δ 8.06 (d, J = 8.5 Hz, 2H, ArH), 7.47-7.32 (m, 5H, ArH), 7.01 (d, J = 8.5 Hz, 2H, ArH), 5.14 (s, 2H, OCH_2Ar), 1.45 (s, 9H, $C(CH_3)_3$). ^{13}C NMR ($CDCl_3$): δ 153.6 (CO), 141.4 (CGuan), 131.1 (CAr), 125.4, 123.4, 123 (CHAr), 122.9 (CO), 122.2, 109.2 (CHAr), 64.8 (CH_2), 22.7 ($C(CH_3)_3$). Exact Mass (ESI+): *m/z* $[M + H]^+$: calc.: 370.1767 uma, found: 370.1779 uma.

***tert*-Butylamino(benzamido) methylcarbamate resorcinarene (53).**

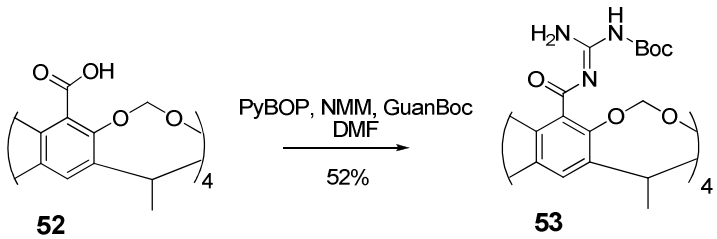

52 **53**

The reaction mixture was stirred at rt for 24 h. The crude was purified by flash column chromatography in silica gel (eluent: CH_2Cl_2/CH_3OH, 99:1→98:2) and obtained in a 52% yield. ^{1}H NMR (CD_3OD): δ 7.5 (s, 4H, ArH), 5.65 (d, J = 7.4 Hz, 4H, OC*Hax*HO), 4.95 (q, J = 7.0 Hz, 4H, CH),

4.51 (d, 4H, OCH*Heq*O), 1.82 (d, *J* = 7.0 Hz, 12H, CH_3), 1.45 (s, 36H, C(CH_3)$_3$). ^{13}C NMR (MeOD): δ 150, 139 (CAr), 100 (CH_2), 31 (CH), 27 (C(CH_3)$_3$), 15 (CH_3). Exact Mass ESI(+): *m/z* [M + Na]$^+$: calc.: 1355.5197 uma, found: 1355.5221 uma.

5,11,17,23-Tetrakis(succinimidoxycarbonyl)-25,26,27,28-tetrabenzyloxycalix[4]arene (39).

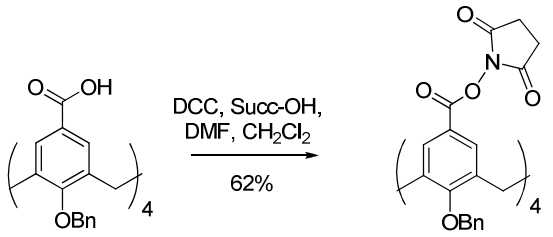

37 **39**

To a suspension of the acid precursor **37** (0.310 g, 0.32 mmol) in dry CH_2Cl_2 and DMF (1:2, 18 mL) were added *N*-hydroxysuccinimide (0.204 g, 1.77 mmol) and 1,3-dicyclohexylcarbodiimide (0.372 g, 1.80 mmol). The reaction was stirred at rt for 24 h. Then, the solvent was evaporated to dryness and the residue was sonicated in a mixture of CH_3OH and CH_2Cl_2 (1:1, 30 mL). The solid product was filtered and obtained as a grey solid (62% yield). Mp: 300 ºC (dec.). ^{1}H NMR ($CDCl_3$): δ 7.48 (s, 8H, ArH), 7.40-7.21 (m, 20H, ArH), 5.04 (s, 8H, CH_2Ar), 4.12 (d, *J* = 14.4 Hz, 4H, ArCH*Hax*Ar), 3.00 (d, *J* = 14.4 Hz, 4H, ArCH*Heq*Ar), 2.83 (s, 16H, CH_2). ^{13}C NMR ($CDCl_3$): δ 170.3 (CONR), 161.3 (CO_2), 161.0, 136.3 (CAr), 130.7, 130.4, 128.7, 128.5 (CHAr), 119.7 (CAr), 77.2 (ArCH_2O), 30.9 (ArCH_2Ar), 25.5 (CH_2). Exact Mass (ESI+) *m/z* [M + Na]$^+$ calc.: 1371.3699 uma, found: 1371.3693 uma.

General procedure for the synthesis of compounds 40-43.

Compound **34** (0.2 g, 0.15 mmol) was dissolved in a solution of dry CH_2Cl_2 and DMF (1:2, 10 mL). Et_3N (0.25 mL, 1.78 mmol) and the protected amine (1.78 mmol) were added to the solution. The reaction was stirred at rt for 48 h. The solvent was evaporated and the residue dissolved in CH_2Cl_2. The organic phase was washed once with 1N HCl (5 mL) and with H_2O (2 x 5 mL). After drying with anhydrous Na_2CO_3 and filtering, the solvent was eliminated *in vacuo* and the products were purified by flash chromatography in silica gel as follows.

25,26,27,28-Tetrabenzyloxycalix[4]arene-5,11,17,23-tetrakis(*N*-*tert*-butyl-2-benzamidoethylcarbamate) (40).

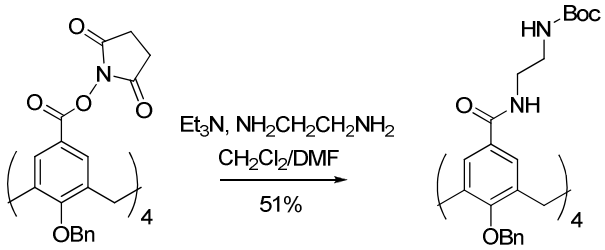

39 **40**

The reaction was performed with *N*-(*tert*-butoxycarbonyl)-ethylenediamine and for the purification the eluent was a gradient of CH_2Cl_2/acetone, 3:1→1:1. Product **15** was obtained as a colorless solid (51% yield). Mp: 145-150 ºC. ^{1}H NMR ($CDCl_3$): δ 7.37-7.21 (m, 20H, ArH), 7.04 (s, 8H, ArH), 6.84 (bs, 4H, NH), 4.98 (s, 8H, C*H*$_2$Bn), 4.1 (d, *J* = 13.6 Hz, 4H, ArCH*Hax*Ar), 3.44-4.12 (m, 16H, CH_2); 2.86 (d, *J* = 13.6 Hz, 4H, ArCH*Heq*Ar), 1.44 (s, 36H, $C(CH_3)_3$). ^{13}C NMR ($CDCl_3$): δ 168.7 (CONH), 158.1, 136.8, 135.3 (CAr), 130.1, 128.4, 127.6 (CHAr), 79.6 (*C*$(CH_3)_3$), 69.7($ArCH_2O$), 41.1, 40.4 (CH_2), 31.9 ($ArCH_2Ar$), 28.5

($C(CH_3)_3$). Exact Mass (ESI+): *m/z* $[M + Na]^+$: calc.: 1551.7539 uma, found: 1551.7468 uma.

25,26,27,28-Tetrabenzyloxycalix[4]arene-5,11,17,23-tetrakis[carbonyl-L-(*N*-*tert*-butoxycarbonyl)lysine methyl ester] (41).

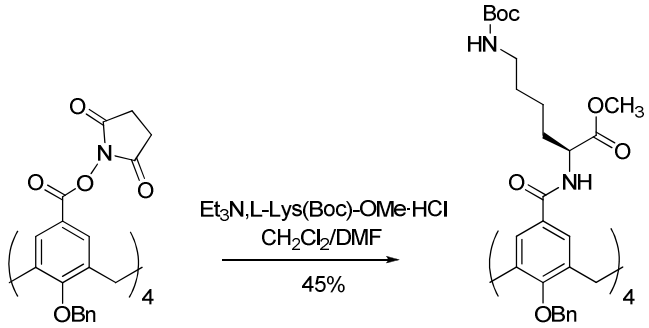

39 41

H-L-Lys(Boc)-OMe·HCl was employed as the amine reagent and chromatographic purification was performed with CH_2Cl_2/acetone 4:1 as the eluent. The product was obtained as a colorless solid (45% yield). Mp: 150-153 ºC. ^{1}H NMR ($CDCl_3$): δ 7.45-7.1 (m, 28H, ArH), 4.98 (s, 8H, CH_2Ar), 4.55 (m, 4H, CHα), 4.12 (d, 4H, *J* = 13.3 Hz, ArC*Hax*HAr), 3.76 (s, 12H, CO_2CH_3), 3.15-3.07 (m, 8H, $CH_2\varepsilon$), 2.95 (d, 4H, *J* = 13.3 Hz, ArCH*Heq*Ar), 1.90-1.75 (m, 8H, $CH_2\delta$), 1.73-1.50 (m, 8H, CH_2ß), 1.52-1.30 (m, 44H, $CH_2\gamma$, $C(CH_3)_3$). ^{13}C NMR ($CDCl_3$): δ 173.2 (CO_2CH_3), 167.0 (CONH), 157.7 (CAr), 156.1 (C), 136.6, 136.3, 135.2 (CAr), 130.1, 129.8, 129.5, 128.5, 128.3 (CHAr), 53.9 (CHα), 52.8 (CH_3O), 40.5 ($CH_2\varepsilon$), 31.5 ($ArCH_2Ar$), 30.3 (CH_2ß), 29.3 $C(CH_3)_3$, 26.7 ($CH_2\delta$), 22.9 ($CH_2\gamma$). Exact Mass (ESI+) *m/z* $[M + 2Na]^{2+}$ calc.: 987.9748 uma, found: 987.9746 uma.

25,26,27,28-Tetrabenzyloxycalix[4]arene-5,11,17,23-tetrakis[carbonyl-L-*N*-(2,2,4,6,7-pentamethyldihydrobenzofuran-5-sulfonyl)arginine methyl ester] (42).

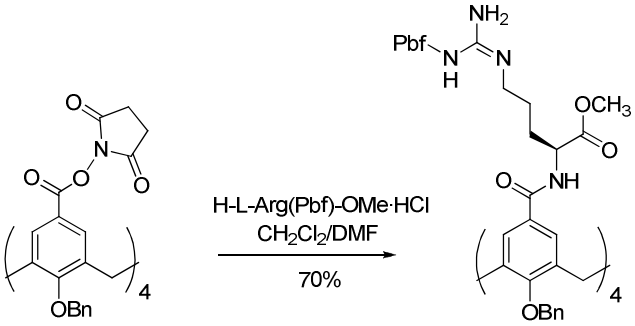

39 **42**

The diprotected amino acid employed was H-L-Arg(Pbf)-OMe·HCl and chromatographic purification was performed eluting with CH_2Cl_2/acetone, 9:1. The product was obtained as a colorless solid (70% yield). Mp: 170-172 ºC. ^{1}H NMR (CD_2Cl_2): δ 7.40-7.22 (m, 28H, ArH), 5.07-4.88 (m, CH_2Ar), 4.12 (d, 4H, J = 13.7 Hz, ArC*Hax*HAr), 3.76 (s, 12H, CO_2CH_3), 3.2 (m, 8H, $CH_2\delta$), 2.98 (d, 4H, J = 13.7 Hz, ArCH*Heq*Ar), 2.97 (s, 8H, CH_2-Pbf), 2.58 (s, 12H, CH_3-Pbf), 2.5 (s, 12H, CH_3-Pbf), 2.08 (s, 8H, CH_3-Pbf), 1.92-1.82 (m, 8H, CH_2ß), 1.58-1.48 (m, 8H, $CH_2\gamma$), 1.46 (s, 24H, CH_3-Pbf). ^{13}C NMR (DEPTQ135, CD_2Cl_2): δ 172.7 (CO_2CH_3), 167.5 (CONH), 158.7 (CAr), 156.4 (CGuan), 138.4, 136.4, 132.3, 132.3 (CAr), 129.9, 128.4, 128.3 (CHAr), 124.5, 123.9, 117.6 (CAr), 86.5 (C), 53.8 (CHα), 52.5 (CO_2CH_3), 43.3 ($CH_2\delta$), 40.4 (CH_2ß), 40.0 ($ArCH_2Ar$), 29.3 ($CH_2\gamma$), 28.7, 19.3, 18.1, 12.5 (CH_3-Pbf). Exact Mass (ESI+) *m/z* [M + 2Na]$^{2+}$ calc.: 1347.5541 uma, found: 1347.5502 uma.

25,26,27,28-Tetrabenzyloxycalix[4]arene-5,11,17,23-tetrakis(carbonyl-L-alanine methyl ester) (43).

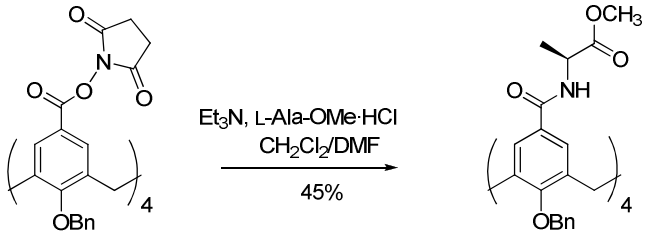

39 **43**

The protected amino acid employed was H-L-Ala-OMe·HCl and chromatographic purification was performed with CH_2Cl_2/acetone, 2.5:2 as eluent. The pure product was obtained as a colorless oil (46% yield). Mp: 268-671 ºC. ^{1}H NMR ($CDCl_3$): δ 7.35-7.18 (m, 20H, ArH), 7.09 (s, 4H, ArH), 6.99 (s, 4H, ArH), 6.64 (d, J = 7.0 Hz, 4H, NH), 6.63 (s, 4H, NH), 4.99 (d, J = 15.3 Hz, 8H, CH_2Ar), 4.55 (q, J = 7.0 Hz, 4H, CHα), 4.10 (d, J = 13.6 Hz, 4H, ArCH*Hax*Ar), 3.77 (s, 12H, CO_2CH_3), 2.91 (d, J = 13.6 Hz, 4H, ArCH*Heq*Ar), 1.46 (d, J = 7.0 Hz, 12H, CH_3). ^{13}C NMR (DEPTQ135, $CDCl_3$): δ 173.73 (CO_2CH_3), 166.9 (CONH), 157.9, 136.6, 135.2, 125.1 (CAr), 129.8, 128.4, 128.3, 128.0, 127.05 (CHAr), 76.8 (CH_2), 52.3 (CO_2CH_3), 48.7 (CHα), 31.4 ($ArCH_2Ar$), 18.1 (CH_3). Exact Mass (ESI+): *m/z* $[M + Na]^+$: calc.: 1323.5154 uma, found: 1323.5146 uma.

5,11,17,23-Tetraformyl-25,26,27,28-tetrahydroxycalix[4]arene (44).

8 **44**

The same general procedure described to synthesize compounds **21a** and **21b** was followed. The mixture was diluted with 1M HCl (50 mL) and CH_2Cl_2 (50 mL) and stirred vigorously for additional 3 h. Therafter, the organic layer was separated and washed with water (2 x 30 mL). The organic layer over anhydrous Na_2CO_3 and the solvent was removed *in vacuo*. The remaining residue was taken up in water (10 mL) and the resulting precipitate was filtered and washed until neutral pH. Pure compound **44** was obtained as a colorless solid in a 85% yield. Mp: > 350 ºC. ^{1}H NMR (DMSO-d_6): δ 9.63 (s, 4H, CHO), 8.75 (bs, 4H, OH), 7.65, (s, 8H, ArH), 3.95 (bs, 8H, $ArCH_2Ar$). ^{13}C NMR (DMSO-d_6): δ 190.4 (d, CHO), 160.1 (CAr), 130.5 (CHAr), 129.8, 128.1 (CAr), 31.2 ($ArCH_2Ar$). ESI(+) *m/z*: $[M + H]^+$: 537.2 uma.

General procedure to obtain compounds 3-7 and 10-14.

Trifluoroacetic acid (10^3 eq.) was added to a solution of the corresponding protected compounds **38**, **40-43**, **45-47** (1 eq.) dissolved in the same volume of CH_2Cl_2. The reaction was stirred at rt or carried out under reflux, depending on the substrates. Analytical HPLC was employed to monitor the reaction: 5-95% CH_3CN in water + 0.1% TFA in 20 min.

25,26,27,28-Tetrahydroxycalix[4]arene-5,11,17,23-tetrakis[*N*-(diaminomethyl)benzamide] hydrochloride (3).

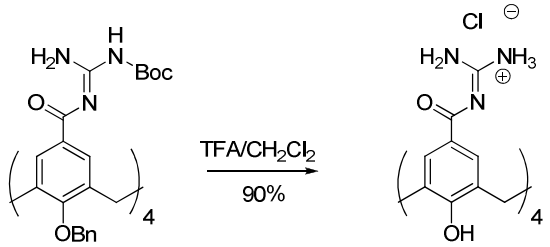

38 **3**

Compound **38** (50 mg, 0.033 mmol) was refluxed for 24 h. The solvent was evaporated and the residue was dissolved in a solution of 1M HCl (1.5 mL). The aqueous phase was then washed twice with CH_2Cl_2 (1.5 mL), the solvent was evaporated and the residue was lyophilized to afford **3** as a colorless compound (90% yield). Mp: > 350 ºC. ^{1}H NMR (DMSO-d_6): δ 11.02 (s, 4H, OH), 8.49 (br s, 4H, NHGuan), 8.40 (br s, 4H, NHGuan), 7.71 (s, 8H, ArH), 4.36 (br s, 4H, ArCH*Hax*Ar), 3.48 (br s, 4H, ArCH*Heq*Ar). ^{13}C NMR (DMSO-d_6): δ 167.44 (COGuan), 161.7 (CGuan), 157.7, 130.1 (CAr), 129.5 (CHAr), 120.9 (CAr), 32.4 (Ar*C*H_2Ar). Exact Mass (ESI+): *m/z* [M + H - 4HCl]$^+$: calc.: 765.2857 uma, found: 765.2887 uma.

5,26,27,28-Tetrahydroxycalix[4]arene-5,11,17,23-tetrakis[*N*-(2-aminoethyl)benzamide] hydrochloride (4).

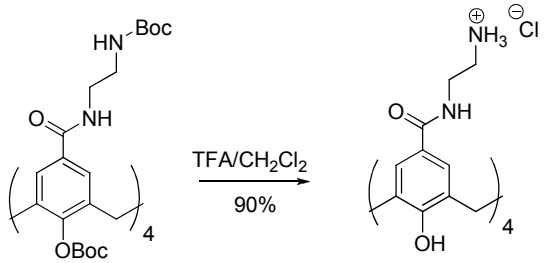

40 **4**

Reaction with **40** (115 mg, 0.075 mmol) was performed at rt for 70 min. Work-up as described above for **3,** afforded **4** as a colorless compound (73% yield). Mp: 160-170 ºC. ^{1}H NMR (D_2O): δ 7.55 (s, 8H, ArH), 3.90 (bs, 4H, $ArCH_2Ar$), 3.51 (tr, J = 5.8 Hz, 8H, CH_2CH_2), 3.11 (tr, 8H, J = 5.8 Hz, 8H, CH_2CH_2). ^{13}C NMR (DMSO-d_6): δ 170.23 (CONH), 153.32 (CAr), 128.53 (CH), 128.37, 125.9 (CAr), 39.39, 37.2 (CH_2). Exact Mass (ESI+) *m/z* [M + H - 4HCl] $^{+}$: calc.: 769.3673 uma, found: 769.3709 uma.

25,26,27,28-Tetrahydroxycalix[4]arene-5,11,17,23-tetrakis(carbonyl-L-lysine-methyl ester) trifluoroacetate (5).

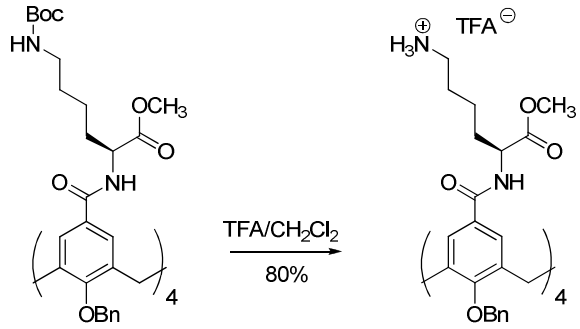

41 **5**

Reaction with **41** (40 mg, 0.02 mmol) was performed at rt for 18 h. The solvent was evaporated to complete dryness (until all traces of acid were

removed) and the residue was dissolved in water. Work-up as for **3** gave pure **5** as a colorless solid (80% yield). Mp: > 250 ºC (dec.). ^{1}H NMR (CD_3OD): δ 7.68 (s, 8H, ArH), 4.54-4.50 (m, 4H, CHα), 4.05 (bs, 8H, $ArCH_2Ar$), 3.70 (s, 12H, CO_2CH_3), 2.91 (t, J = 7.6 Hz, 8H, $CH_2\varepsilon$), 2.01-1.81 (m, 8H, $CH_2\delta$), 1.73-1.63 (m, 8H, $CH_2ß$), 1.58-1.48 (m, 8H, $CH_2\gamma$). ^{13}C NMR (DMSO-d_6): δ 172.9 (CO_2CH_3), 168.8 (CONH), 153.4 (CAr), 128.53 (CHAr), 127.7, 126.27 (CAr), 52.8 (CHα), 51.4 (CO_2CH_3), 39.1 ($CH_2\varepsilon$), 30.3 ($CH_2ß$), 26.7 ($CH_2\gamma$), 22.9 ($CH_2\delta$). Exact Mass (ESI+): *m/z* [M + 2H - 4CH_3COOH]$^{2+}$: calc.: 585.2919 uma, found: 585.2932 uma.

25,26,27,28-Tetrahydroxy-calix[4]arene-5,11,17,23-tetrakis(carbonyl-L-arginine methyl ester) trifluoroacetate (6).

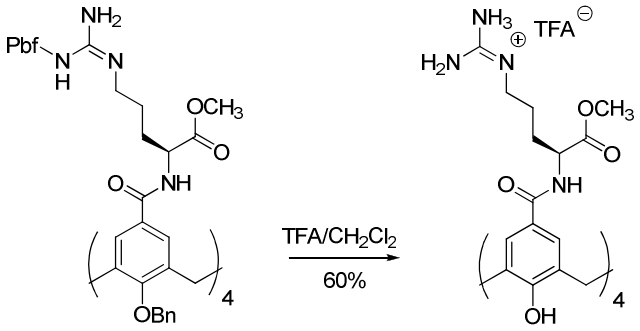

42 **6**

Reaction was performed with precursor **42** (50 mg, 0.019 mmol) at rt for 13 h. The solvent was evaporated to complete dryness (until all traces of acid were removed) and the pure product was obtained by crystallization in CH_3CN (60% yield). Mp: 245-247 ºC. ^{1}H NMR (CD_3OD): δ 7.7 (s, 8H, Ar*H*), 4.55-4.50 (m, 4H, CHα), 3.65 (s, 12H, CO_2CH_3), 3.24-3.18 (m, 8H, $CH_2\delta$), 1.99-1.78 (m, 8H, $CH_2ß$), 1.70-1.60 (m, 8H, $CH_2\gamma$). ^{13}C NMR (CD_3OD): δ 172.7 (CO_2CH_3), 168.9 (CONHR), 157.4 (CGuan), 156.4

(CAr), 128.6 (CHAr), 127.7, 126.3 (CAr), 52.6 (CHα), 51.6 (CO_2CH_3), 40.5 ($CH_2\delta$), 30.6 ($ArCH_2Ar$), 28.0 ($CH_2\beta$), 25.2 ($CH_2\gamma$). Exact Mass (ESI+): *m/z* $[M + 2H - 2CF_3COOH]^{2+}$: calc.: 755.2971 uma, found: 755.2971 uma.

25,26,27,28-Tetrahydroxycalix[4]arene-5,11,17,23-tetrakis(carbonyl-L-alanine methyl ester) (7).

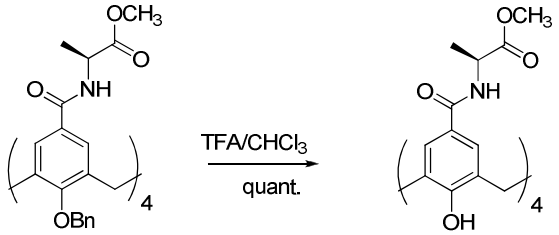

43 **7**

Reaction with compound **43** was performed in a TFA:CH_3Cl (1:1) mixture, at reflux in a closed tube for 1 h. The solvent was evaporated and the residue was sonicated in CH_3OH, filtered and lyophilized. The product was obtained as a colorless solid (quant. yield). Mp: > 350 ºC (dec.).

^{1}H NMR (CD_3OD): δ 7.67 (s, 8H, ArH), 4.52 (m, 4H, CHα), 4.04 (bs, 8H, CH_2Ar), 3.71 (s, 12H, OCH_3), 1.45 (s, 12H, CH_3). ^{13}C NMR (CD_3OD): δ 173.8 (CO_2CH_3), 168.4 (CONHR), 153.1 (CAr), 128.7 (CHAr), 127.7, 126.7 (CAr), 51.3 (CHα), 48.6 (CO_2CH_3), 15.6 (CH_3). Exact Mass ESI(-): *m/z* $[M - H]^-$: calc.: 939.3300 uma, found: 939.3343 uma.

25,26-27,28-Biscrown-3-calix[4]arene-5,11,17,23-tetrakis[*N*-(diaminomethyl)benzamide] trifluoroacetate (10).

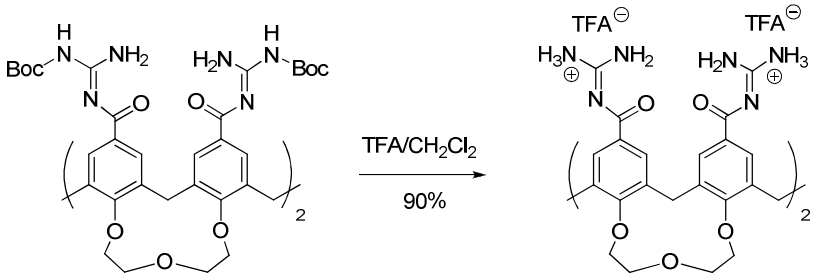

46 **10**

The reaction with precursor **46** was stirred at rt for 13 h. The solvent was evaporated and the crude was triturated in EtOAc. The product was obtained as a colorless solid (90% yield). Mp: > 350 ºC. ^{1}H NMR (CD_3OD): δ 7.81 (d, J = 13.3 Hz, 8H, ArH), 5.37 (d, J = 12.4 Hz, 2H, ArCH*Hax*Ar), 4.70 (d, J = 12.4 Hz, 2H, ArCH*Hax*Ar), 4.5 (d, J = 12.4 Hz, CH_2O), 4.37-4.23 (m, 8H, CH_2O), 3.89 (m, 4H, CH_2O), 3.5 (d, J = 12.7 Hz, 2H, ArCH*Heq*Ar), 3.43 (d, J = 12.7 Hz, 2H, ArCH*Heq*Ar). ^{13}C NMR (CD_3OD): δ 168.2 (CONH), 159.7 (CGuan), 157.3, 136.1 (CAr), 126.3 (CHAr), 76.6, 74.4 (CH_2), 30.1, 29.1($ArCH_2Ar$). Exact Mass (ESI+): *m/z* $[M + H - CF_3COOH]^+$: calc.: 1247.3593 uma, found: 1247.3546 uma.

25,26-27,28-Tetra-*n*-propoxycalix[4]arene-5,11,17,23-tetrakis[*N*-(diaminomethyl)benzamide] trifluoroacetate (11).

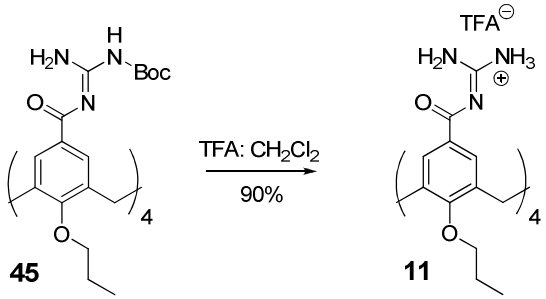

The reaction was stirred overnight at rt. The solvent was evaporated and the residue sonicated in CH_3CN. The resulting precipitate was filtered and the product obtained as a colorless solid (90% yield). Mp: > 350 ºC (dec.). ^{1}H NMR (CD_3CN): δ 8.21 (br s, 6H, NH), 7.80 (br s, 6H, NH), 7.30 (s, 8H, ArH), 4.52 (d, J = 13.9 Hz, 4H, ArCH*Hax*Ar), 3.97 (t, J = 7.3 Hz, 8H, OC*H*$_2$CH$_2$CH$_3$), 3.36 (d, 8H, J = 13.9 Hz, ArCH*Heq*Ar), 1.99-1.89 (q, J = 7.3 Hz, 8H, OCH$_2$C*H*$_2$CH$_3$), 1.0 (t, J = 7.3 Hz, 12H, OCH$_2$CH$_2$C*H*$_3$). ^{13}C NMR (CD_3CN): δ 167.9 (CONH), 161.7 (CGuan), 156.2, 135.7 (CAr), 128.8 (CHAr), 124.9 (CAr), 77.4 (O*C*H$_2$CH$_2$CH$_3$), 30.5 (ArCH$_2$Ar), 23.2 (OCH$_2$*C*H$_2$CH$_3$), 9.6 (CH_3). Exact Mass (ESI+): *m/z* of [M + H - CF_3COOH]$^+$: calc.: 1275.4521, found: 1275.4561 uma.

25,26-27,28-Tetrabenxyloxycalix[4]arene-5,11,17,23-tetrakis[*N*-(diaminomethyl)benzamide] trifluoroacetate (12).

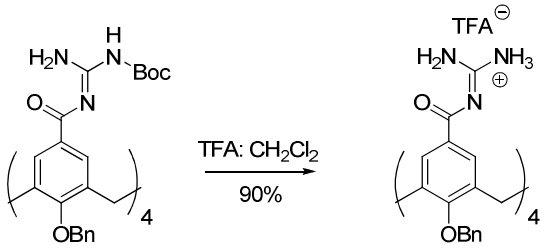

38 **12**

The reaction with compound **38** was stirred at 0-5 ºC (to avoid *O*-debenzylation) for 26 h. The reaction was quenched with distilled water, and the solvent was evaporated at rt. The residue was dissolved in CH_3OH and the solvent was eliminated *in vacuo* again. The pure compound was obtained as a colorless solid (90% yield). Mp: > 350 ºC. ^{1}H NMR (CD_3CN): δ 8.10 (bs, 6H, NH), 7.83 (bs, 6H, NH), 7.38-7.28 (m, 20H, ArH), 7.23 (s, 8H, ArH), 6.08 (bs, 1H, 8H), 5.08 (s, CH_2Ar), 4.28 (d, J = 14.3 Hz, 4H, ArCH*Hax*Ar), 3.07 (d, J = 14.3 Hz, 4H, ArCH*Heq*Ar). ^{13}C NMR (CD_3OD): δ 167.5 (CONH), 160.4 (CGuan), 156.2, 136.2 (CAr), 130.2, 128.7, 128.6, 128.3 (CHAr), 125.1 (CAr), 76.9 (CH_2Ar), 30.8 ($ArCH_2Ar$). Exact Mass (ESI+): *m/z* $[M + H - 4CF_3COOH]^+$: calc.: 1125.4848 uma, found: 1125.4806 uma.

_N_-(diaminomethyl)-4-hydroxybenzamide trifluoroacetate (13).

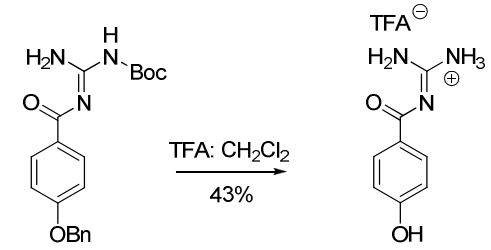

47 **13**

This compound was prepared following the same procedure as for compound **3**, except for purification on semi-preparative HPLC: the crude was dissolved in CH_3CN (32 mg/mL), and a gradient of CH_3CN in water + 0.1% CF_3COOH (5-60% for 15 min and 60 to 95% for 3 min). The compound was obtained as a colorless solid (43% yield). Mp: 282-285 ºC. ^1H NMR (CD_3OD): δ 8.57 (s, 1H, OH), 7.97 (d, J = 8.8 Hz, 2H, ArH), 6.98 (d, J = 8.8 Hz, 2H, ArH). ^{13}C NMR (CD_3OD): δ 167.7 (CGuan), 163.3 (CONH), 130.5 (CHAr), 121.8 (CAr), 115.49 (CHAr). Exact Mass (ESI+): *m/z*. $[M + H - CF_3COOH]^+$: calc.: 202.0592 uma, found: 202.0584 uma.

_N_-(diaminomethyl)benzamide trifluoroacetate resorcinarene (14).

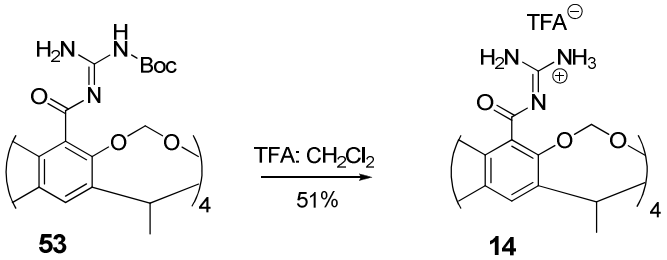

53 **14**

The reaction with precursor **53** was stirred for 1 h at 0 ºC. Semi-preparative purification was performed on an Alltech semiprep column

(Alltech C18. Length: 250 mm, ID: 22 mm), with gradient: 5-70% CH_3CN in H_2O + 0.1%. FA. Pure compound **14** was obtained as a colorless solid with trifluoroacetate as counteranion (51%). ^{1}H NMR (DMSO-d_6): δ 8.31 (s, 1H, NHGuan), 7.6 (s, 1H, ArH), 5.45 (d, *J* = 7.7 Hz, 1H, OCH*Hax*O), 4.68 (q, *J* = 7.5 Hz, 1H, CH), 4.3 (d, *J* = 7.7 Hz, 1H, OCH*Heq*O), 1.77 (d, *J* = 7.5 Hz, 3H, CH_3). Exact Mass ESI(+): *m/z* of $[M + 3FA + Na]^+$: calc.: 1093.3264 uma, found: 1093.3241uma 100%.

25,26,27,28-Tetrahydroxycalix[4]arene-5,11,17,23-tetracarboxylic acid (9).

This known compound (55), was synthesized by a novel procedure.

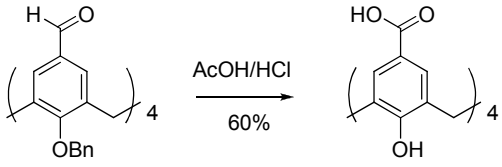

37 **9**

The benzyl derivative **37** (52 mg, 0.054 mmol) was suspended in a mixture of conc. HCl and acetic acid (1:2, 8 mL). The reaction was stirred and heated at reflux for 48 h in a sealed tube. The solvents were evaporated and the residue was dissolved in THF-water (3:1) and purified by semi-preparative HPLC (2.5 mg/mL, 30-36% CH_3CN in water + 0.1% TFA gradient in 15 min). The pure product was obtained (60% yield) as a grey powder. Mp: > 350 ºC. ^{1}H NMR (DMSO-d_6): δ 7.66 (s, 8H, ArH), 3.9 (bs, 4H, $ArCH_2Ar$). ^{13}C NMR (DMSO-d_6): δ 167.4 (COOH), 156.7 (CArOH), 130.9 (CHAr), 128.9, 122.7 (CAr), 31.24 (CH_2). Exact Mass ESI(-): *m/z* $[M]^-$: calc: 599.1190 uma, found: 599.1182 uma.

2,8,14,16-Tetrabromo-5,11,17,23-tetramethylpentacyclo-[19.3.1.1^{3,7}.1^{9,13}.1^{15,19}]octacosa-1(25),3,5,7(28), 9, 11, 13(27),15,17,19(26),21,23-dodecaene-4,6,10,12,16,18,22,24-octol (49).

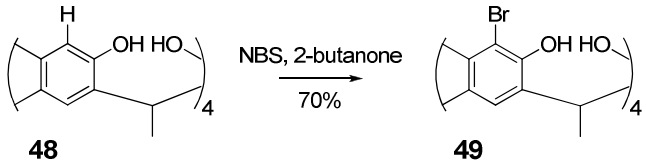

48 **49**

To a solution of precursor **48** (1.8 g, 3.3 mmol) in 2-butanone (80 mL), was added NBS (3.9 g, 22 mmol) in small portions. After stirring for 10 minutes at rt a precipitate appeared. After 4 h the solid was filtered and washed with Et_2O to obtain the final compound **49** (70% yield). Mp: > 350 ºC (dec). ^{1}H NMR (DMSO-d_6): δ 8.38 (s, 8H, ArOH), 6.81 (s, 4H, ArH), 4.62 (q, J = 6.2 Hz, 4H, CH), 1.58 (d, 12H, J = 6.2 Hz, CH_3). ESI(+) *m/z*: $[M + H]^+$: 860.9 uma.

Tetrabromo resorcinarene (50).

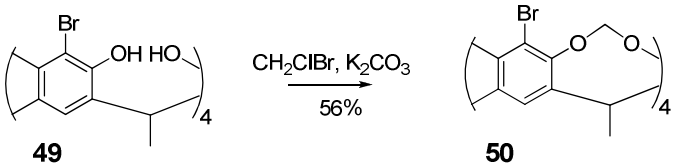

49 **50**

To a solution of **49** (0.81 g, 0.91 mmol)in dry DMF (67 mL), were added CH_2ClBr (0.94 g, 7.3 mmol) and dry K_2CO_3 (2 g, 14.5 mmol). The resulting solution was heated at 80 º C for 3 days and thereafter was diluted with water (200 mL) and acidified with 2M HCl. The dark precipitate formed was separated and dried under vacuum to give rise to a crude compound which was purified by flash chromatography in silica gel (eluent: 100% CH_2Cl_2). Product **50** was obtained in 56% yield as a

colorless solid. Mp: > 350 ºC (dec). ^{1}H NMR ($CDCl_3$): δ 7.16 (s, 4H, ArH), 5.95 (d, J = 7.2 Hz, 4H, OCHH_oO), 5.06 (q, 4H, CH), 4.39 (d, J = 7.2 Hz, 4H, OCHH_iO), 1.75 (d, J = 7.0 Hz, 12H, CH_3). ESI(+) *m/z*: $[M + H]^+$: 908.9 uma.

Electrophysiology

Surgically extracted *Xenopus laevis* oocytes were injected with 0.5-4 ng channel RNA (50 nl). The cells were incubated in ND-96 (96 mM NaCl, 2 mM KCl, 1.8 mM $CaCl_2$, 1 mM $MgCl_2$, 50 mg mL^{-1} gentamicin, 2.5 mM Na pyruvate, and 5 mM HEPES, pH 7.6) at 12-18 °C for 12-48 h prior to experiments. All electrophysiology experiments were conducted at rt.

Two electrode voltage clamp (TEVC) experiments were performed using a Dagan CA-1B amplifier (Dagan Corporation), Digidata-1440A board, and pClamp10 software. The oocytes were placed in a perfusion dish to allow for pre-wash, wash, and post-wash recordings. All recordings were performed in ND-96 recording solution (96 mM NaCl, 2 mM KCl, 1.8 mM $CaCl_2$, 1 mM $MgCl_2$, 10 mM HEPES, pH 7.2). For each experiment, the oocyte membrane voltage was held at -80 mV followed by a continuous train of 100 or 300 ms pulses to 20 mV every 15 seconds.

All compounds were dissolved in ND-96 recording solution to make a 500 µM stock solution. When needed, a maximum of 5% (v/v) DMSO was added to the stock solution to facilitate solubilization. For inhibition experiments, small quantities of the calixarene stock solutions were manually applied and mixed in a stagnant bath containing the oocyte. For

all recordings, DMSO was present at levels less than 1% (v/v). Oocytes were bathed in the calixarene solution until the current measurements taken at +20 mV reached steady-state. The compounds were washed away with ND-96 administered using a gravity perfusion system at approximately 80 mL/h.

All ionic current measurements taken at +20 mV were leak-subtracted using the following formula:

$$I_{LS} = I_{+20mV} - 0.25*(I_{-80mV})$$

The percent reduction in ionic current (B) was determined using the following formula, using leak subtracted current measured at +20 mV for steady state levels before and after addition of the calix[4]arene:

$$B = 100*[(I_{initial} - I_{ligand})/ I_{initial}]$$

Each experiment was repeated with at least 4 different oocytes, and data are shown as averages of individual experiments. Error bars indicate standard error of the mean.

For dose-response experiments, varying concentrations of ligand **6** were applied to oocytes expressing either the Shaker or $rK_v1.3$ channel. Each experiment was repeated with at least 3 different occytes, and the data were then averaged. Then, the average reduction in ionic current elicited by application of ligand **6** (B) was plotted as a function of the log of ligand **6** concentration. Error bars indicate standard error of the mean (SEM). The

plotted data were then fit using Igor Pro software with the modified Hill Equation:

$$B = B_{max} * [L]^h/(K_d^h + [L]^h)$$

where L represents the concentration of calix[4]arene used in the experiment, K_d the equilibrium dissociation constant and h the Hill Coefficient. The following values were obtained:

Channel	**B_{max}**	***K_d***	**h**
Shaker	63 ±10	25±11	1.0 ± 0.3
rK_v1.3	85±16	14 ± 9	1.1 ± 0.7

3.8 References

1. (a) Hille B (2001) Ion Channels of Excitable Membranas, 3ed, Sinauer (Sunderland). (b) Ashcroft FM (2000) Ion Channels and Disease: channelopathies, Academic Press (San Diego).

2. Gutman GA, Chandy KG, Adelman JP, Aiyar J, Bayliss DA, Clapham DE, Covarrubias DM, Desir GV, Furuichi K, Ganetzky B, Garcia ML, Grissmer S, Jan LY, Karschin A, Kim D, Kuperschmidt S, Kurachi Y, Lazdunski M, Lesage F, Lester HA, MacKinnon R, Nichols CG, O'Kelly I, Robbins J, Robertson GA, Rudy B, Sanguinetti M, Seino S, Stuehmer W, Tamkun MM, Vandenberg CA,Wei A, Wulff H, Wymore RS (2003) International Union of Pharmacology. XLI. Compendium of voltage-gated ion channels: Potassium channels. *Pharmacol Rev* 55:583-586.

3. Coetze WA, Amarillo Y, Chiu J, Chow A, Lau D, McCormack T, Moreno H, Nadal MS, Ozaita A, Pountney D, Saganich M, Vega-Saenz de Miera E, Rudy B (1999) Molecular diversity of K+ channels. *Ann NY Acad Sci* 868:233-285.

4. Shealy RT, Murphy AD, Ramarathnam R, Jakobsson E, Subramaniam S (2003) Sequence-function analysis of the K+-selective family of ion channels using a comprehensive alignment and the KcsA channel structure. *Bioph J* 84:2929-2942.

5. (a) MacKinnon R, Cohen SL, Kuo A, Lee A, Chai, BT (1998) Structural conservation in prokaryotic and eukaryotic potassium channels. *Science* 280:106-109. (b) MacKinnon R (2003) Potassium channels. *FEBS Lett.* 555:62-65.

6. (a) Doyle DA, Morais Cabral J, Pfuetzner RA, Kuo A, Gulbis JM, Cohen SL, Chait B T, MacKinnon R (1998) The structure of the potassium channel: molecular basis of K+ conduction and selectivity. *Science* 280:69-77.

7. (a) Jiang Y, Lee A, Chen J, Cadene M, Chait BT, MacKinnon R (2002) Crystal structure and mechanism of a calcium-gated potassium channel. *Nature* 417:515-522. (b) Jiang Y, Lee A, Chen J, Cadene M, Chait BT, Mackinnon R (2002) The open pore conformation of potassium channels. *Nature* 417:523-527.

8. (a) Jiang Y, Lee A, Chen J, Ruta V, Cadene M, Chait BT, MacKinnon R (2003) X-ray structure of a voltage-dependent K+ channel. *Nature* 423:33-41. (b) Ruta V, Jiang Y, Lee A, Chen J, MacKinnon R (2003) Functional analysis of an archaebacterial voltage-dependent K+ channel. *Nature* 422:180-185.

9. Long SB, Campbell EB, MacKinnon R (2005) Crystal structure of a mammalian voltage-dependent Shaker family K+ channel. *Science* 309:897-903.

10. Long SB, Tao X, Campbell EB, MacKinnon R (2007) Atomic structure of a voltage-dependent K+ channel in a lipid membrane-like environment. *Nature* 450:376-382.

11. Gouaux E, MacKinnon R (2005) Principles of selective ion transport in channels and pumps. *Science* 310:1461-1465

12. Bernèche S, Roux B (2001) *Nature* 414:73-76.

13. Sanguinetti MC, Spector PS (1997) Potassium channelopathies. *Neuropharm* 36:755-762.

14. Alabi AA, Bahamonde MI, Jung HJ, Kim JI, Swartz KJ (2007) Portability of paddle motif function and pharmacology in voltage sensors. *Nature* 450:370-376.

15. Tombola F, Patak MM, Gorostiza P, Isacoff EY (2007) The twisted ion-permeation pathway of a resting voltage-sensing domain. *Nature* 445:456-549.

16. (a) Armstrong CM (1971) Interaction of tetraethylammonium ion derivatives with the potassium channels of giant axons. *J Gen Physiol* 58:413-437.
(b) Heginbotham L, MacKinnon R (1992) The aromatic binding site for tetraethylammonium ion on potassium channels. *Neuron* 8:483-491.
(c) Thompson J, Begenisich T (2003) External TEA block of shaker K+ channels is coupled to the movement of K+ ions within the selectivity filter. *Gen Physiol* 122:239-246.

17. Blaustein RO, Cole PA, Williams C, Miller C (2000) Tethered blockers as molecular 'tape measures' for a voltage-gated K+ channel. *Nat Struct Biol* 7:309-311.

18. Ahern CA, Eastwood AL, Lester HA, Dougherty DA, Horno R (2006) A cation-pi interaction between extracellular TEA and an aromatic residue in potassium channels. *J Gen Physiol* 128:649-657.

19. (a) Garcia ML, Hanner M, Kaczorowski GJ (1998) Scorpion toxins: tools for studying K+ channels. *Toxicon* 36:1641-1650.
(b) Imredy JP, MacKinnon R (2000) Energetic and structural interactions between delta-dendrotoxin and a voltage-gated potassium channel. *J Mol Biol* 296:1283-1294.
(c) Lange A, Giller K, Hornig S, Martin-Eauclaire M-F, Pongs O, Becker S, Baldus M (2006) Toxin-induced conformational changes in a potassium channel revealed by solid-state NMR. *Nature* 440:959-962.

20. Ericsson MA, Roux B, (2002) Modeling the structure of agitoxin in complex with the Shaker K+ channel: a computational approach based on experimental distance restraints extracted from thermodynamic mutant cycles. *Biophys J* 83:2595-609.

21. (a) Goetz MA, Zink DL, Dezeny G, Dombrowski A, Polishook JD, Felix JP, Slaughter RS, Singh SB (2001) Diterpenoid pyrones, novel blockers of the voltage-gated potassium channel Kv1.3 from fungal fermentations. *Tetrahedron Lett.* 42:1255-1257.
(b) Schmitz A, Sankaranarayanan PA, Schmidt-Lassen K, Homerick D, Hänsel W, Wulff H (2005) Design of PAP-1, a selective small molecule Kv1.3 blocker, for the suppression of effector memory T cells in autoimmune diseases. *Mol Pharm* 68:1254-

1270.
(c) Wang X, Liao Y, Zou A, Li L, Tu D (2007) Blockade action of ketanserin and increasing effect of potassium ion on Kv1.3 channels expressed in Xenopus oocytes. *Pharm Res* 56:148-254.

22. Shieh CC, Coghlan M, Sullivan JP, Gopalakrishnan M (2000) Potassium channels: molecular defects, diseases, and therapeutic opportunities. *Pharma Rev* 52:557-593.

23. Gordon E, Cohen JL, Engel R, Abbott GW (2006) 1,4-Diazabicyclo[2.2.2]octane derivatives: a novel class of voltage-gated potassium channel blockers. *Mol Pharm* 69:718-726.

24. Gradl SN, Felix JP, Isacoff EY, Garcia ML, Trauner D (2003) Protein surface recognition by rational design: nanomolar ligands for potassium channels. *J Am Chem Soc* 125:12668-12669.

25. Ader C, Schneider R, Hornig S, Velisetty P, Wilson EM, Lange A, Giller K, Ohmer I, Martin-Eauclaire M-F, Trauner D, Becker S, Pongs O, Baldus M (2008) A structural link between inactivation and block of a K+ channel. *Nat Struct Mol Biol* 15:605-612.

26. Dominguez C, Boelens R, Bonvin AM (2003) HADDOCK: A protein-protein docking approach based on biochemical or biophysical information. *J Am Chem Soc* 125:1731-1737.

27. Casnati A, Sansone F, Ungaro R (2003) Peptido- and glycocalixarenes: playing with hydrogen bonds around hydrophobic cavities. *Acc Chem Re* 36:246-254.

28. Mourer M, Duval RE, Finance C, Regnouf-de-VainsJ.-B (2006) Functional organisation and gain of activity: the case of the antibacterial tetra-para-guanidinoethyl-calix[4]arene. *Bioorg Med Chem Lett* 16:2906-2963.

29. Gutsche CD, Nam KC (1988) Calixarenes. 22. Synthesis, properties, and metal complexation of aminocalixarenes. *J Am Chem Soc* 110:6153-6162.

30. Gutsche CD, Levine JA, Sujeeth PK (1985) Calixarenes. 17. Functionalized calixarenes: The Claisen rearrangement route. *J Org Chem* 50:5802-5806.

31. Short JH, Dunnigan DA, Ours CW (1973) Synthesis of phenethylamines from phenylacetonitriles obtained by alkylation of cyanide ion with mannich bases from phenols and other benzylamines. *Tetrahedron* 29:1931-1939.

32. Payne RJ, Bulloch EMM, Abell AD, Abell C (2005) Design and synthesis of aromatic inhibitors of anthranilate synthase. *Org Biomol Chem* 3:3629-3635.

33. Niikura K, Anslyn EV (1999) Azacalixarene: synthesis, conformational analysis, and recognition behavior toward anions. *J Chem Soc, Perkin Trans* 2: *2*, 2769-2775

34. (a) Hossain Md T, Timberlake JW (2001) Rearrangements in the reduction of 3-

iodobicyclo[1.1.1]pentyl azide with lithium aluminum hydride: Mechanistic evidence of intermediates. *J Org Chem* 66**:**4409-4412.
(b) Vaultier M, Knouzi N, Carrie R (1983) Reduction d'azides en amines primaires par une methode generale utilisant la reaction de staudinger. *Tetrahedron Lett* 24:763-764.

35. Gutsche CD, Pagoria PF (1985) Calixarenes. Calixarenes. 17. Functionalized calixarenes: The Claisen rearrangement route. *J Org Chem* 50:5795-5802.

36. Wei RG, Arnaiz DO, Chou Y-L, Davey D, Dunning L, Lee W, Lu S-F, Onuffer J, Ye B, Phillips G (2007) CCR5 receptor antagonists: discovery and SAR study of guanylhydrazone derivatives. *Bioorg Med Chem Lett* 17:231-234.

37. Casnati A, Sartori A, Pirondini L, Bonetti F, Pelizzi N, Sansone F, Ugozzoli F, Ungaro R (2006) New tetrafunctionalized cone calix[4]arenes as neutral hosts for anion recognition. *Supramol Chem* 18:199-218.

38. Sato S, Hiroe K, Kumazawa T, Jun-ichi O. (2006) Total synthesis of two isoflavone C-glycosides: genistein and orobol 8-C-beta-D-glucopyranosides. *Carbohydr Res* 341:1091-1095.

39. Sasina JS, Brewster E, Caran KL, Bentley AM, Shuker S (2006) Heterodimerization studies of calix[4]arene derivatives in polar solvents *Org Lett* 8:2913-2915.

40. Schmuck C, Machon U (2006) 2-(Guanidiniocarbonyl)furans as a new class of potential anion hosts: Synthesis and first binding studies *Chem Eur J* 11:1109-1118.

41. (a) Lazzarotto M, Sansone F, Baldini L, Casnati A, Cozzini P, Ungaro R (2001) Synthesis and properties of upper rim C-linked peptidocalix[4]arenes. *Eur J Org Chem* 595-602.
(b) Sansone F, Baldini L, Casnati A, Lazzarotto M, Ugozzoli F, Ungaro R (2002) Biomimetic macrocyclic receptors for carboxylate anion recognition based on C-linked peptidocalix[4]arenes. *Proc Natl Acad Sci USA* 99:4842-4847.
(c) Baldini L, Sansone F, Faimani G, Massera C, Casnati A, Ungaro R (2008) Self-assembled chiral dimeric capsules from difunctionalized N,C-linked peptidocalix[4]arenes: Scope and limitations. *Eur J Org Chem* 869-886.

42. (a) Arduini A, Fabbi M, Mantovani M, Mirone L, Pochini A, Secchi A, Ungaro R (1995) Calix[4]arenes blocked in a rigid cone conformation by selective functionalization at the lower rim. *J Org Chem* 60:1454-1457.
(b) van Loon JD, Arduini A, Coppi L, Verboom W, Pochini A, Ungaro R, Harkema S, Reinhoudt DN (1990) Selective functionalization of calix[4]arenes at the upper rim *J Org Chem* 55:5639-5646.
(c) Gutsche CD, Pagoria PF (1995) Calixarenes. 16. Functionalized calixarenes: the direct substitution route. *J Org Chem* 50:5795-5802.

43. Atwood L, Szumna A (2003) Cation-pi interactions in neutral calix[4]resorcinarenes. *J Supramol Chem* 2:479-482.

44. (a) Timmerman P, Nierop KGA, Brinks EA, Verboom W, van Veggel FCJM, van Hoorn WP, Reinhoudt DN (1995) Hydrophobic concave surfaces and cavities by combination of calix[4]arenes and resorcin[4]arenes. *Chem-Eur J* 1:132-143.
(b) Román E, Peinador C, Mendoza S, Kaifer A (1999) Improved synthesis of cavitands. *J Org Chem* 64:2577-2578.

45. Moran JR, Karbach S, Cram DJ (1982) Cavitands: Synthetic molecular vessels. *J Am Chem Soc* 104:5826-5828

46. Martos V, Bell SC, Santos E, Trauner D, Isacoff EY, de Mendoza J (2008) Calix[4]arene-based conical-shaped ligands for voltage dependent potassium channels. *Proc Natl Acad Sci USA*, submitted.

47. Halliwell JV, Plant TD, Robbins J, Standen NB (1994) In Microelectrode Techniques, ed Odgen D, The Company of Biologists (Cambridge), pp 17-35.

48. Mannuzzu LM, Moronne MM, Isacoff EY (1996) Direct physical measure of conformational rearrangement underlying potassium channel gating. *Science* 271:213-216.

49. (a) Perozo E, MacKinnon R, Bezanilla F, Stefani E (1993) Gating currents from a nonconducting mutant reveal open-closed conformations in Shaker K+ channels. *Neuron* 11:353-358.
(b) Loots E, Isacoff EY (1998) Protein rearrangements underlying slow inactivation of the Shaker K+ channel. *J Gen Physiol* 112:377-389.

50. (a) Glauner KS, Mannuzzu LM, Gandhi CS, Isacoff EY (1999) Spectroscopic mapping of voltage sensor movement in the Shaker potassium channel. *Nature* 402:813-817.
(b) Mannuzzu LM, Isacoff EY (2000) Independence and cooperativity in rearrangements of a potassium channel voltage sensor revealed by single subunit fluorescence. *J Gen Physiol* 115:257-268.

51. Zachariae U, Schneider R, Velisetty P, Lange A, Seeliger D, Wacker S, Karimi-Nejad Y, Vriend G, Becker S, Pongs O (2008) The molecular mechanism of toxin-induced conformational changes in a potassium channel: relation to C-type inactivation. *Structure* 16:747-754

52. Gross A, MacKinnon R (1996) Agitoxin footprinting the shaker potassium channel pore. *Neuron* 16:399-406.

53. Imredy J, Chen C, MacKinnon R.(1998) A snake toxin inhibitor of inward rectifier potassium channel ROMK1. *Biochemistry* 37:14867-14874.

54. Coghlan MJ, Carroll WA, Gopalakrishnan M (2001) Recent developments in the biology and medicinal chemistry of potassium channel modulators: update from a decade of progress. *J Med Chem* 44:1627-1653.

55. (a) Yilmaz Y, Vural U (1991) Synthesis of new substituted calix[4]arenes and their

complexes with iron(III). *Synth React Inorg Met-Org Chem* 21:1231-1241.
(b) Dalgarno SJ,Warren JE, Antesberger J, Glass TE, Atwood JL (2007) Large diameter non-covalent nanotubes based on the self-assembly of para-carboxylatocalix[4]arene. *New J Chem* 31:1891-1894.

Chapter 4

Solid phase synthesis of chiral bicyclic guanidinium oligomers for cellular uptake

4.1 Cell permeability of bicyclic guanidinium oligomers

Chiral bicyclic guanidinium oligomers are lipophilic polycationic molecules based on guanidinium subunits whose moieties are incorporated into a decaline bicyclic framework. The resulting guanidine has several remarkable properties: it bears orientation-restricted NH protons which avoid *anti* conformations non suitable for hydrogen-bonding, it has an amphipatic character provided by a "lipophilic backbone", and it is endowed with two stereogenic centers (Fig. 4.1).

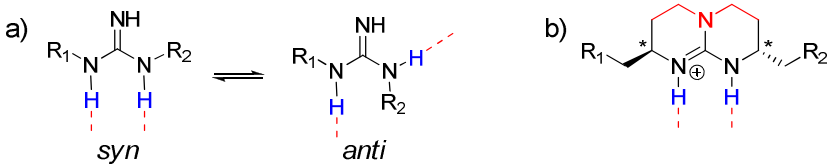

Fig. 4.1: (a) *Anti* and *syn* conformations of guanidinium group and (b) bicyclic guanidinium moiety.

These characteristics account for the design of several chiral oxoanion receptors based on monomeric units of the bicyclic guanidine (1). Both, chirality and stable ionic complex as well as hydrogen bond formation in

non aqueous media, promote the folding of chiral bicyclic guanidinium tetramers (thereafter referred as tetraguanidinium) around suitable anionic templates. Reported examples of this behavior are the self-assembly of double stranded sulfate helicates (2), the stabilization of α-helical peptides endowed with carboxylic amino acids in i, i + 3 position (3), as well as the interaction with alpha helices of the p53 tetramerization domain (p53TD) (4).

In addition, the amphipatic nature of bicyclic guanidinium oligomers conveys to them membrane permeability properties.

Chemical characteristics of guanidinium rich transporters (GRTs)

The ability of a drug or probe to cross a biological barrier has historically been viewed as a function of its intrinsic physical properties. This view has hampered the evaluation and development of many agents which did not meet the cell-uptake requirements. Production of molecular transporters to overcome these biological barriers would be highly desirable in drug development. In this context, a number of cell-penetrating peptides (CPPs) derived from HIV-1 Tat protein (5), Antennapedia protein (Antp) of Drosophila (6), and related peptides have been extensively studied to improve the absorption, distribution, metabolism, and elimination (ADME) properties of poorly bioavailable drugs including small molecules (7), proteins (8), nucleic acids and genes (9).

Several groups have undertaken systematic structure-function studies with a series of artificial arginine peptides inspired in Tat_{49-57}, (Fig. 4.2). They

concluded that the optimal number of arginines for cell-penetration in polyarginines lies between 7 and 15, depending on the techniques and cell lines employed (10). Expectedly, *all*-D peptides are even more efficient due to their greater stability towards proteolysis.

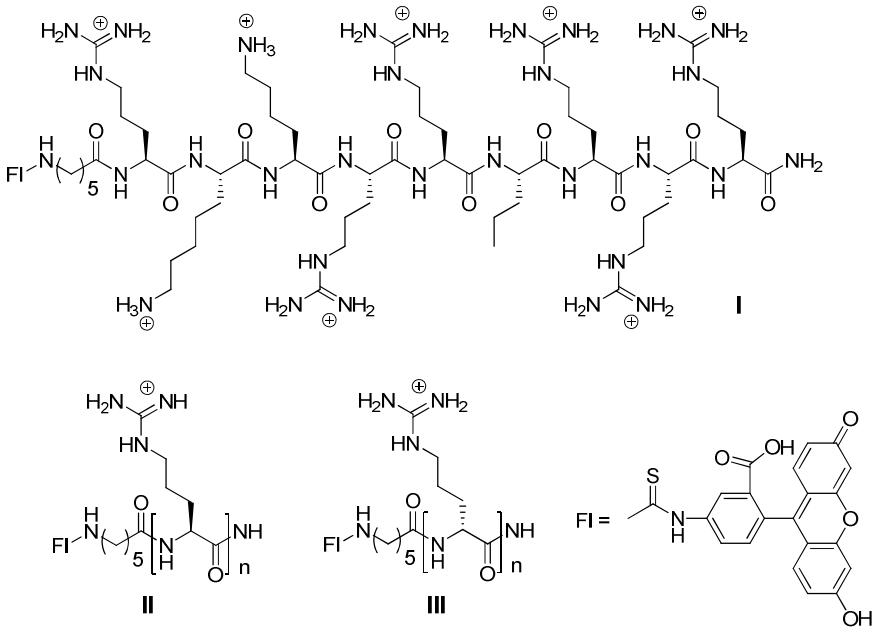

Fig. 4.2: Structure-function studies with fluorescent peptides (**I-III**) inspired in Tat_{49-57} (counterions not indicated).

Moreover, cellular uptake by peptides containing lysines or ornithines instead of arginines was comparatively less efficient, reflecting the importance of arginine for cellular uptake in natural and non-natural CPPs (11). Promising internalization studies and optimized synthesis for D-Arg(8) (12), have fostered its entry into clinical studies (13).

In the mean time, cellular uptake by a number of artificial peptoids (14), oligocarbamates (15), and β-peptides (16), rich in guanidinium groups have

been reported by different researchers (Fig. 4.3).

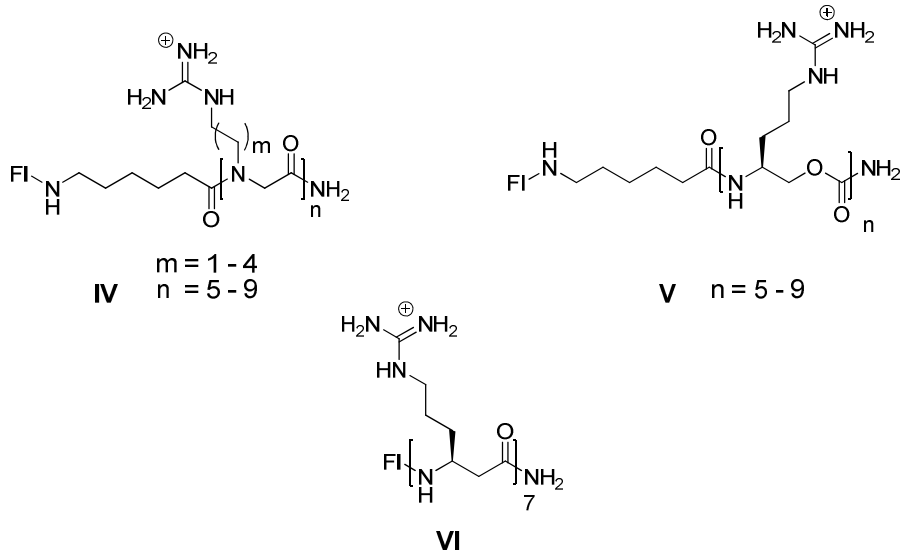

Fig. 4.3: Structure-function studies with fluorescent peptoids (**IV**), oligocarbamates (**V**) and β-peptides (**VI**, counterions not specified).

These guanidinium-rich molecular transporters (GRTs) differ structurally in many respects to CPPs, except for the key conserved oligoguanidinium functional group. Internalization studies with these molecules showed that neither the nature of the backbone, its stereochemistry nor the side chain position or spacing to the guanidinium head groups are critical for cell internalization. However, they clearly influence the efficiency of uptake (17). Flexibility and amphipaticity are both factors that contribute to the increase in uptake as reported by different studies on synthetic GRTs (18). Most interesting, the nature of the scaffold may determine tissue specificity as well as cell localization of the entering conjugate, offering strategies for specific tissue or cell organel targeting (19). Therefore the diversity and number of scaffolds reported to target fused molecules into cells or into

animal tissues (20) range from highly branched oligosaccharides (21) to polyproline helices (22), dendrimers (23), peptide nucleic acids (24), calix[4]arenes (25), cationic lipids (26), and even polymers (27) (Fig. 4.4).

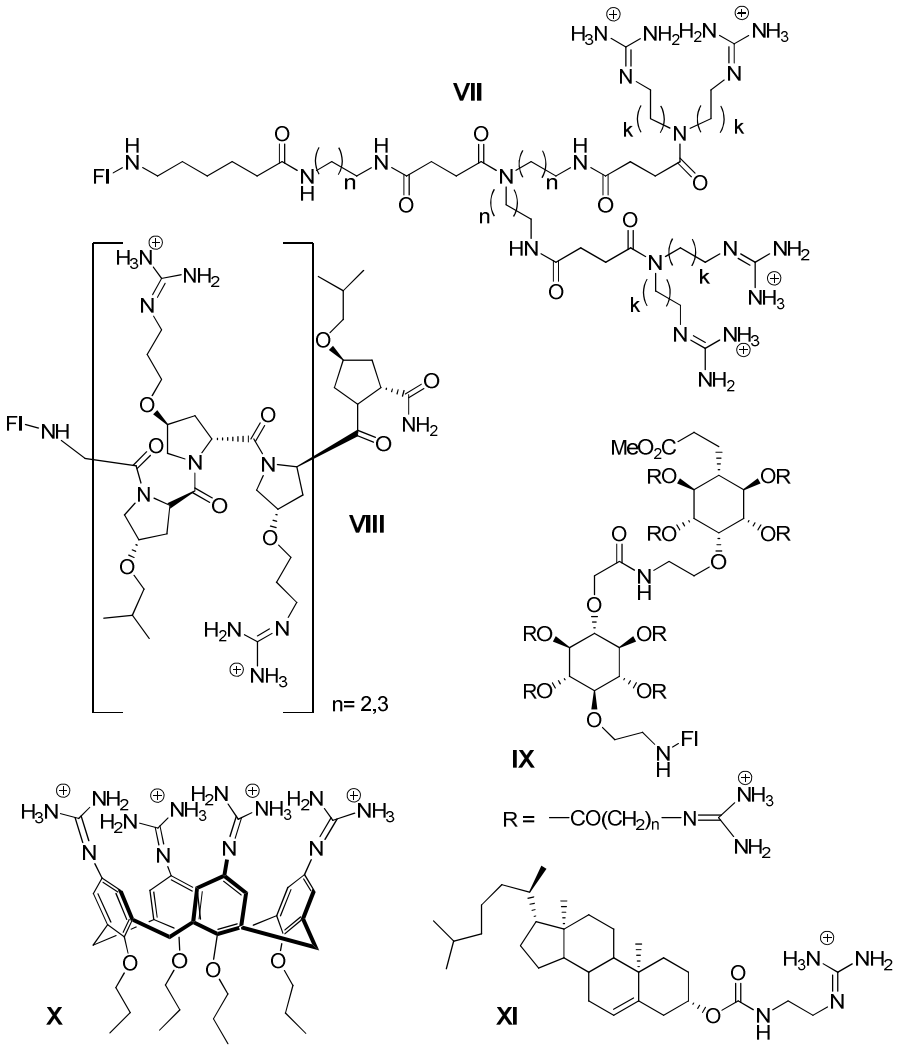

Fig. 4.4: Examples of guanidinium rich scaffolds: Dendrimers (**VII**), Proline helices (**VIII**), Guanidinoglycosides (**IX**), Calix[4]arenes (**X**), Cationic lipids (**XI**).

In most cases the cargo is linked covalently to a vector, but there are also

interesting examples of non covalent conjugation and transport which benefit from the ability of guanidines to bind tightly to negatively charged cargos (DNA, RNA or anionic supramolecules) (28).

Mechanisms of cellular uptake

Given the structural variety of GRTs carrying a wide range of cargos, from small molecule probes to metals, drugs, peptides, oligosaccharides, proteins and plasmid DNA, a universal GRT uptake mechanism is unlikely. Moreover, other crucial variables involved in cellular uptake such as cell types, nature of the counterions, or experimental conditions, hamper the identification of a single entry mechanism (29). However, there are common aspects to several mechanistic possibilities and these derive from the special properties of the guanidinium group.

It is of general agreement that association of the GRTs to the cell membrane takes place prior to translocation. Compared to ammonium, the guanidinium group is able to form well-oriented hydrogen bonds and is protonated over a wider range of pHs, which provides a rationale for the differing abilities of oligolysines and oligoarginines to associate and to cross cellular membranes (14). As the guanidinium function combines the positive charge with a bidentate hydrogen bond donor, it is ideally poised to interact with negatively charged cell surface constituents, such as phospholipids head groups, fatty acids, proteins and heparan sulfate proteoglycans (HPPGs) (Fig. 4.5).

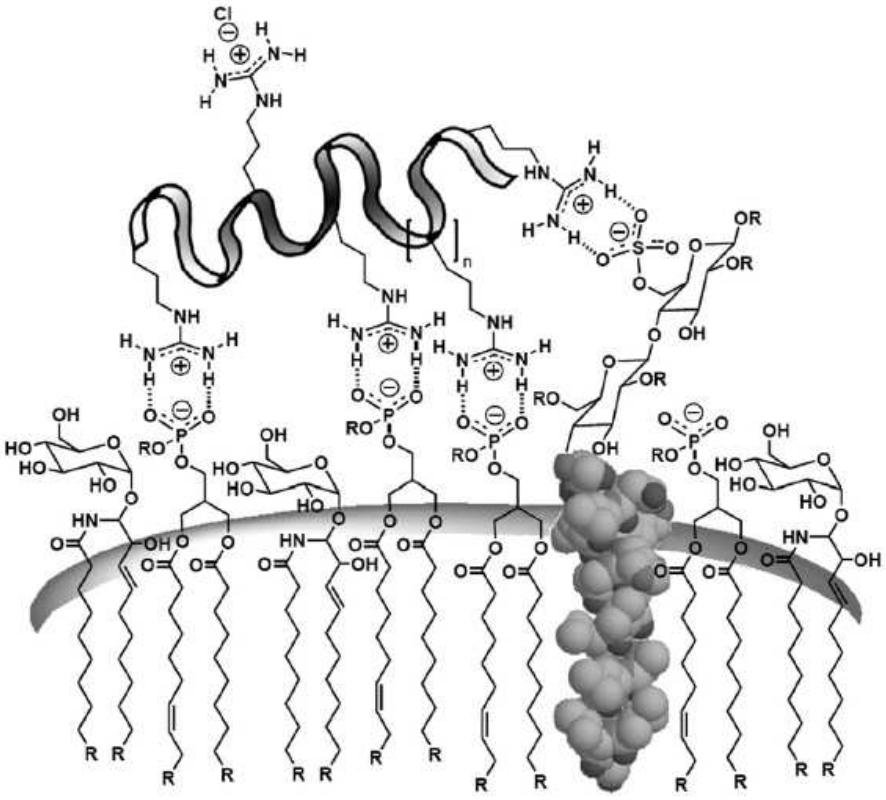

Fig. 4.5: Schematic representation of some common associations of a polycationic guanidinium transporter with anionic cell membrane constituents (reproduced from ref. 30).

The driving force for the initial association is supposed to be the dramatic increase in stability of the guanidinium-oxoanion pair as the medium changes from water to the non-polar membrane environment (for instance, ~ 2.6-6.0 kcal/mol for phosphate) (30).

Considerable effort has been devoted to elucidate the uptake mechanism of different GRTs, because of its relevance on intracellular trafficking processes, which in turn determine the rate at which a cargo is degraded or

delivered to a given organel.

With some exceptions, receptor mediated transport is ruled out for GRTs, which makes sense considering account the broad range of structural variations compatible with their internalization. Instead, endocytosis and diffusion processes which are less structure-specific, have been detected as major processes. The chemical nature and size of the transported conjugate as well as the cell type seem to be determinant for the mechanism of entry. Different endocytic processes have been identified and generally visualized by confocal microscopy, but no predictions can be made so far. Therefore, clathrin-mediated, caveolin-mediated or macropinocytic transport are distinguished, depending on the proteins associated to the membrane involved in the endocytic transport (Fig. 4.6).

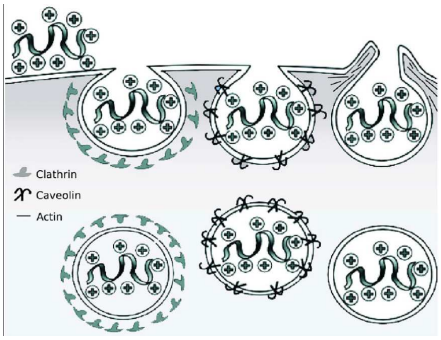

Fig. 4.6: Proposed endocytotic uptake mechanism. From left to right: clathrin-mediated endocytosis, caveolin-mediated endocytosis, macropinocytosis (reproduced from ref. 30).

Most often a clathrin mediated endocytosis is reported, but even concentration changes in the CPPs may permutate the endocytic mechanism

from a clathrin to a caveolae mediated one. For bigger conjugates, caveolae or macropinocytosis are generally observed (18,31).

Moreover, all endocytic mechanisms are energy-dependent, thus easily distinguished from direct diffusion by the kinetics of internalization and their dependence on temperature. When cellular uptake is not inhibited at low temperatures it is attributed to direct diffusion. A direct diffusion of charged species through the cell membrane seems to contradict the intrinsic rules of biological barriers. However, association between the guanidinium charged species and the amphipatic counterions on the cellular surface would lead to non polar complexes, able to cross the lipid bilayer and dissociate once in the cytosol (32). This hypothesis has been shown experimentally by the groups of Matile (33) and Wender (34): Simple water-octanol partitioning experiments reveal that the presence of amphipatic anions, such as sodium laureate, a surrogate of a membrane constituent- is simply enough to transfer a water-soluble arginine strand from water to a non polar octanol phase that mimics the membrane (Fig. 4.7).

The importance of the bidentate hydrogen bond formation in this process was investigated by Wender *et al.* examining the influence of mono- and dimethylation of the guanidinium group on cellular internalization. Decrease of cellular uptake was 80% and 95% respectively, confirming the observation that cationic charge is not enough for efficient diffusion.

The same research group studied the impact of the membrane potential on the passage of the ion pair complex and demonstrated a direct relation

between membrane potential, which naturally favors the movement of positive charged species into the cell, with GRT internalization (Fig. 4.7).[32]

a) b)

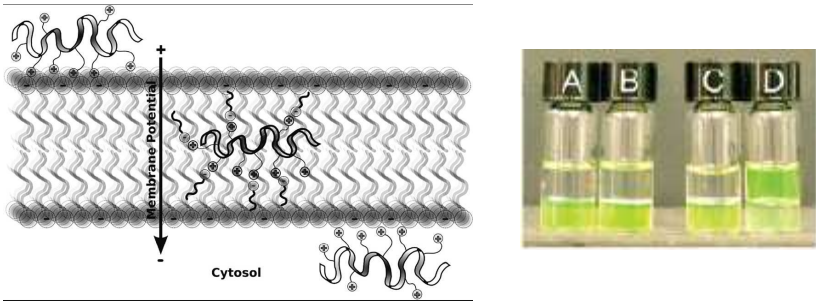

Fig. 4.7: a) Diffusion translocation uptake mechanism proposed by Wender *et al.* b) Octanol/water (upper and lower phases, respectively) partitioning of Fl-aca-Orn_8-$CONH_2$ and Fl-aca-D-Arg_8-$CONH_2$ alone (A, B) and after addition of sodium laurate (C, D) (reproduced from refs. 30 and 30).

Finally, some authors suggest that compounds able to fold into amphipatic secondary structures are best suited for cellular uptake, although this has not been confirmed as a general requisite for GRT internalization (35).

Cell-permeable bicyclic tetraguanidinium oligomers

Tetraguanidinium compounds **XII** and **XIII**, labeled covalently with carboxyfluoresceine (CF), were recently synthesized in our group and tested for cellular uptake in collaboration with the group of Ernest Giralt (PCB) (Fig. 4.8).

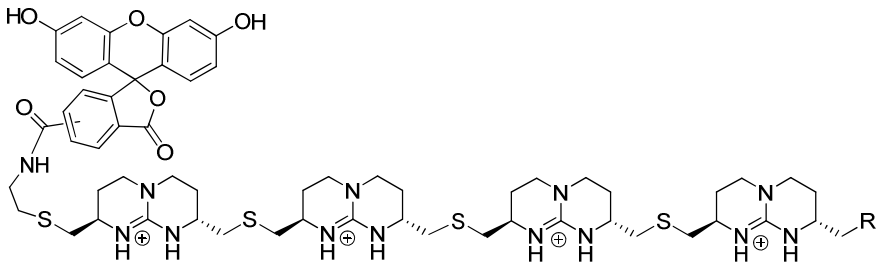

Fig. 3.8: Structure of tetraguanidinium oligomers **XII** and **XIII.**

Rapid and dose-dependent internalization of fluorescent compounds **XII** and **XIII** in HeLa cells was observed on a fluorescent microplate reader after 1 hour incubation at 37 ºC. The uptake was compared with Tat_{49-57} 9-mer and Antp, both labelled with carboxyfluorescein (CF) at their NH_2-termini, as positive controls, and with CF as a negative control. Interestingly, silylated conjugate **XII** (*R* = $SiPh_2{}^tBu$) outperforms its hydroxyl-free analogue **XIII** (*R* = OH) as well as peptide controls even at low micromolar concentration (5 µM) (Fig. 4.9a). Cell viability assays with 1-(4,5-dimethylthiazol-2-yl)-3,5-diphenylformazan (MTT) at up to 10 µM concentrations showed that the best internalized compound **XII**, incubated for 24 h with HeLa cells, reduced cell viability to 28% at 10 µM (Fig. 4.9b). In view of reducing toxicity, further internalization experiments were performed at a concentration range of 1-0.1 µM. In good agreement with the preliminary data obtained using a microplate fluorimeter, flow cytometry revealed that **XII** was better internalized than CF-Antp, while **XIII** and CF-Tat were both internalized to a similar extent (Fig. 4.9c).

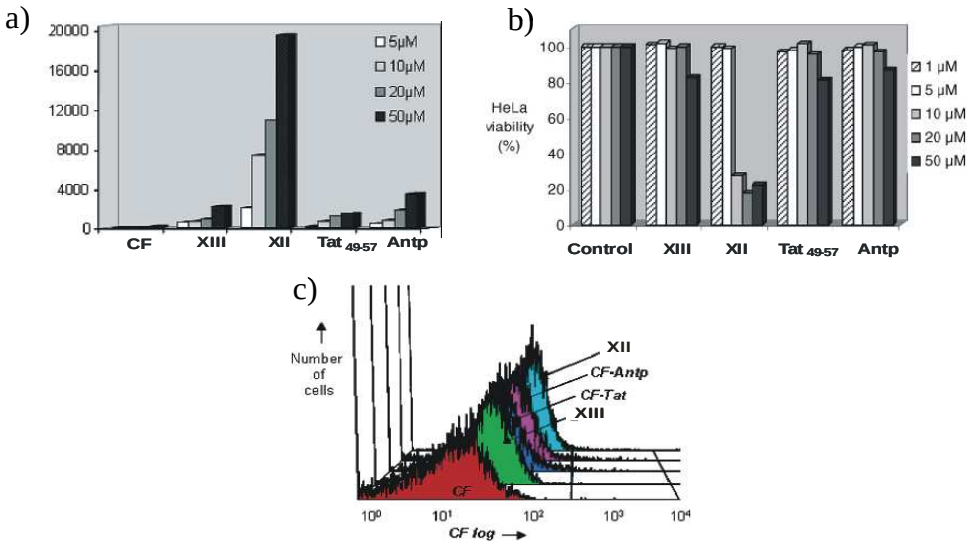

Fig. 4.9: a) Fluorescence measured in a microplate fluorescence reader after incubation of HeLa cells with tetraguanidinium oligomers **XII** and **XIII**, CF-Tat, CF-Antp, and CF at 5-50 µM concentrations. b) Cytotoxicity of **XII**, **XIII**, CF-Tat, and CF-Antp. Viability was quantified by MTT staining after 24 h of incubation. c) Fluorescence obtained FACS after incubating cells with **XII**, **XIII**, CF-Tat, CF-Antp, or CF at 1 µM for 1 h at 37 °C (reproduced from ref. 37).

To gain insight into the mechanism of internalization of compound **XII**, flow cytometry experiments were also performed at 4 ºC. Cellular uptake proved to be energy dependent as uptake of **XII** was substantially reduced. However, kinetics of the internalization indicated that some passive diffusion of the complex was taking place as well. Thus, we suggested that both pathways were indeed taking place simultaneously, as it has been observed for other GRTs. Furthermore, confocal laser scanning microscopy studies revealed that compound **XII** co-localized with MitoTracker Orange, a dye that accumulates in active mitochondria (Fig. 4.10).

a) b)

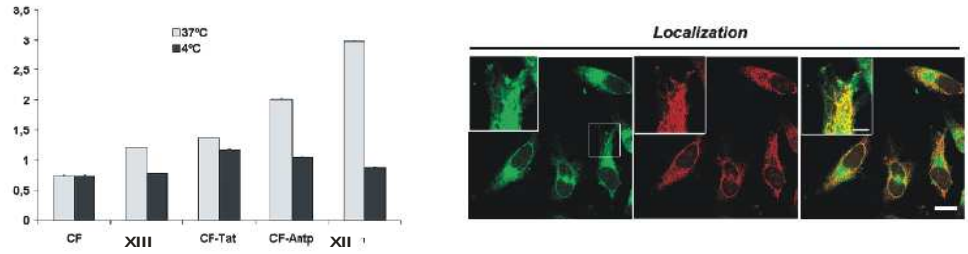

Fig. 4.10: a) Fluorescence measured by flow cytometry after incubating HeLa cells with **XII**, **XIII**, CF-Tat and CF-Antp (1 µM) at 37 °C or 4 °C; b) Distribution of **XII** and colocalization with the mitochondrial marker MitoTracker Orange (reproduced from ref. 37).

This particular behavior could find interesting therapeutic applications (36). Therefore, a new family of GRTs based on bicyclic guanidinium subunit, with improved mitochondrial selectivity, was necessary (37).

More recently, the *O*-silyl tetraguanidinium oligomer was conjugated with a different linker to form an emissive terbium complex for optical imaging (collaboration with David Parker, the University of Durham, UK) (Fig. 4.11).

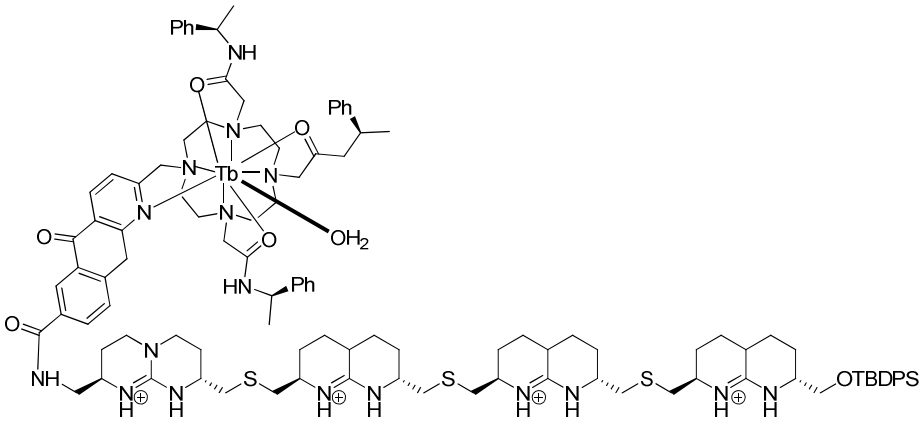

XIV Counterion: $Cl^{\ominus}$

Fig. 4.11: Covalent conjugate of emissive terbium complex and *O*-silyl, bicyclic tetraguaninium **(XIV)**.

Although the chemical nature of the cargo and the linker were different as compared to conjugate **XII**, similar uptake behaviors were observed for complex **XIV** through two-photon fluorescence microscopy: Thus, compound **XIV** showed efficient permeabilization and mitochondrial localization but optical imaging experiments with this probe were compromised by toxicity at low micromolar concentrations (IC_{50} = 12 µM). Moreover, **XIV** was observed in all cell lines assayed: HeLa, NIH-3T3 and CHO, pointing to a general use of bicyclic guanidinium tetramers as cell permeabilizing agents. However, as already mentioned, toxicity at low micromolar concentrations for either complexes **XII** and **XIV** hampered further progress of these vectors (38). In order to identify optimal compounds, with efficient permeability, reduced cell toxicity, and specific cellular localization, a systematic structure-function study was necessary, as has been reported for other families of GRTs. Variation of the terminal moieties, the linkers or the length of the strands should give rise to a series

of compounds for evaluation in cell uptake assays (Fig. 4.12).

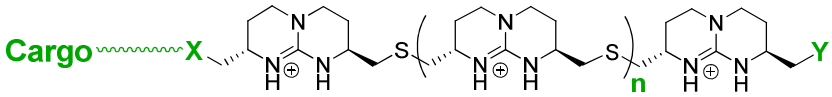

Fig. 4.12: Modification sites (highlighted in green) for systematic structure-function studies.

4.2 Development of solid phase (SP) synthetic strategies

Until now, solution phase synthesis of symmetric and non symmetric guanidinium oligomers has been successfully employed in our group to obtain strands of up to six bicyclic guanidinum subunits (37,39). However, to synthesize series with site specific modifications, a solid phase synthesis (SPS), inspired in the classical peptide synthesis developed by Merrifield in 1963, was envisaged (40).

Solid phase peptide synthesis (SPPS) is based on the sequential addition of α-amino acids (protected at their amino end and eventually at the side chains) to an insoluble support or resin (Fig. 4.13). The scheme is based on the incorporation of the desired number of monomers through a series of coupling, capping and deprotection steps, followed by cleavage of the peptide from the solid support. The crude is analyzed by HPLC, as exemplified in Fig. 4.13 (41), and finally the desired peptide is purified by precipitation or chromatography.

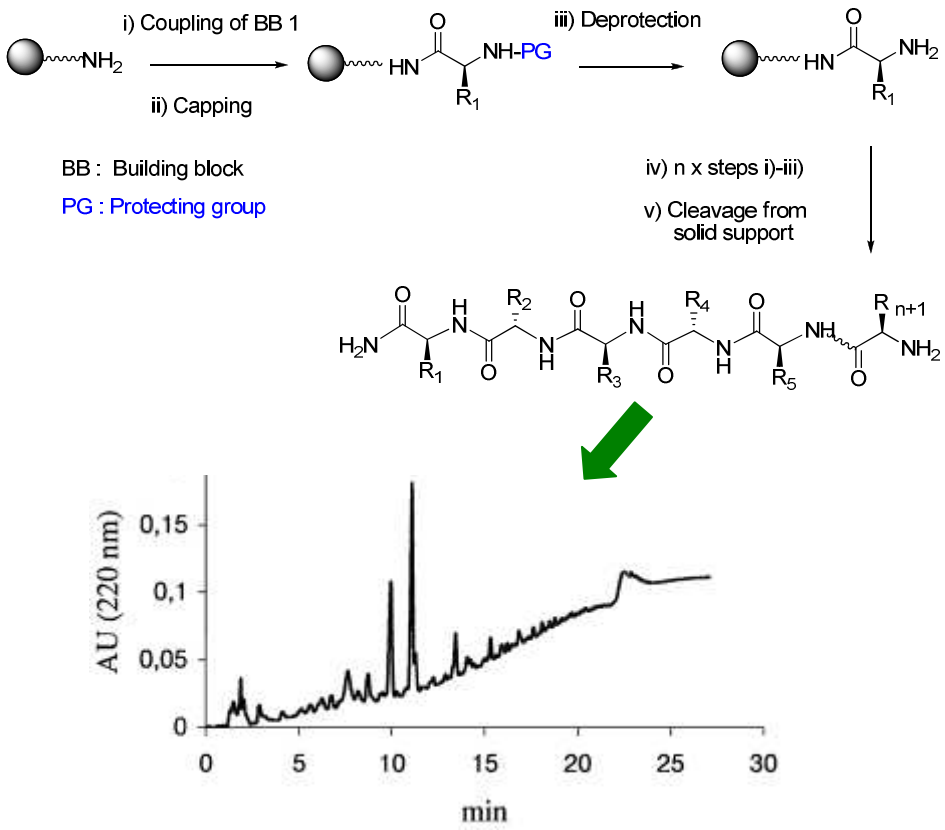

Fig. 4.13: a) Simplified representation of SPPS b) Example of an analytical HPLC profile (reproduced from ref. 41).

In addition to peptides, synthesis of organic compounds on solid support presents many advantages. First, reactions may be carried out in the presence of an excess of reagents to drive the reaction to completion. The reagents are simply washed away at each step and no synthetic intermediates are isolated. Second, the capping step takes place with quantitative yield and reduces secondary products that may originate from non complete coupling. Third, the final purification is the only one performed over the whole synthesis. Thus, solid phase synthesis (SPS) is convenient in terms of efficiency, ease of experimental work-up and

purification procedures.

However, there are as well some disadvantages linked to solid support synthesis. For instance, the difficulty in the structural analysis of the supported species. Also, linkers and protecting groups have to remain stable under the various conditions taking place along the process, including harsh cleavage protocols. Therefore, their robustness has to be guaranteed. Finally, and most challenging, reactions have to take place in high to quantitative yields, otherwise after repeated coupling almost no final product is harvested.

Over the last three decades, considerable technological and synthetic effort has been invested to optimize SPS for combinatorial and high-throughput chemistry (42). As a result, this original concept has expanded from natural peptides to cyclic peptides, DNA, PNAs, oligosaccharides, peptoids and small drug compounds. In addition, during the last decade the *in situ* analysis of anchored compounds has been made possible through spectroscopic techniques, such as IR, RAMAN and also High Resolution Magic-Angle Spinning (HRMAS). As a result, the role of SPS in fundamental organic chemistry research is gaining importance (43).

To the best of our knowledge, the synthesis of bicyclic guanidinium strands has not been tested on solid phase conditions, nor has this scaffold been applied on solid support before. Therefore, taking into consideration the inherent advantages and drawbacks of SPS, as well as the particular nature of the oligomers we aimed to obtain, the following premises were established:

1. To choose a convenient bicyclic guanidinium building block (BB) for reiterative coupling on solid phase.
2. To provide sites for diverse end-functionalization, linker and cargo anchorage.
3. To propose a qualitative follow-up test as well as a quantitative capping reaction.

In the following sections several attempts to build a solid-phase synthetic strategies for bicyclic guanidinium oligomers fulfilling these requirements, will be described.

In addition, in the last section of this chapter, preliminary results with an amino acid analogue of a bicyclic guanidinium subunit, will be presented.

4.2.1 Initial trials on solid phase

4.2.1.1 Objectives

Almost half of the work described in this chapter was performed by us in the laboratory of Miriam Royo and Fernando Albericio, at the Combinatorial Chemistry Department, Barcelona Science Park (PCB). The remainin work was developed at ICIQ's laboratories.

Our first trials on SPS were performed with two building blocks which were already available in the group, namely BB **15** and **16** (Fig. 4.14) (44).

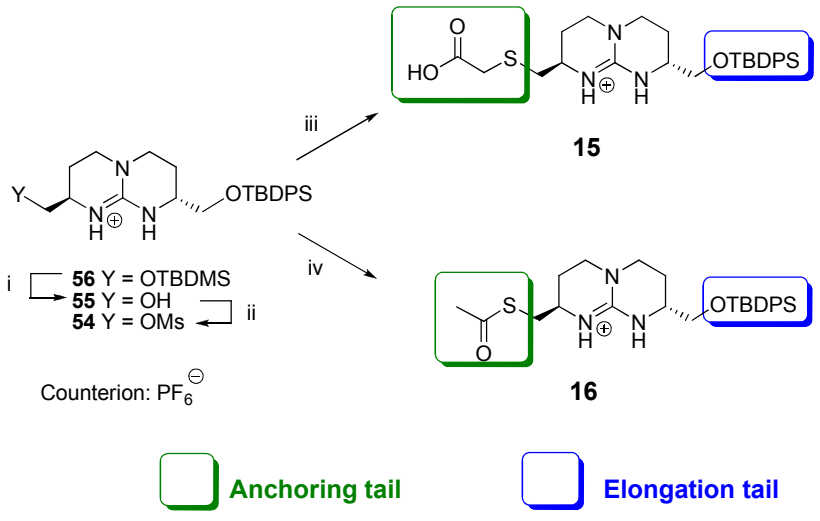

i) H_2O/AcOH/THF (1:3:1), rt, 20 h (98%). ii) Ms_2O, NMM, CH_2Cl_2, rt, 2 h (98%). iii) Mercaptoacetic acid, K^tBuO, THF, rt, 4 h (82%). iv) $KSCOCH_3$, CH_3CN, MW: 140 ºC, 10 min (97%).

Fig. 4.14: Building Blocks **15** and **16.**

Synthesis of compounds **15** and **16** proceed from the orthogonally diprotected bicyclic guanidinium precursor **56**, which was obtained, on a large scale, in eight steps from the amino acids *R*-asparagine and *R*-methionine (45). Molecule **56** was deprotected at its OTBDMS end, and the free alcohol **55** was activated as mesyl. Next, compound **54** was functionalized through nucleophilic substitution with mercaptoacetic acid or with thioacetate, respectively. BB **15,** endowed with a mercaptoacetic acid tail, is suited for anchorage to an amine functionalized resin, whereas BB **16** bears a protected nucleophile as anchoring moeity.

Concerning the solid support, we selected Bal-linker, [5-(4-formyl-3,5-dimethoxyphenoxy) butyric acid], as a traceless linker for attachment of the bicyclic guanidinium unit **15**. BAL-resin was prepared by coupling [5-(4-formyl-3,5-dimethoxyphenoxy)] butyric acid to a 4-methylbenzhydrylamine polystyrene (MBHA) resin through a HOBt/DIPCDI mediated coupling, within a Fmoc solid phase strategy (46). This particular linker provides a potential site for cargo anchoring through a primary amine, whose coupling is carried out by on-resin reductive amination, as described by Albericio and coworkers (47). Initially we employed four carbon length amines as cargo models: 3-methylbutylamine and butylamine (Fig. 4.15).

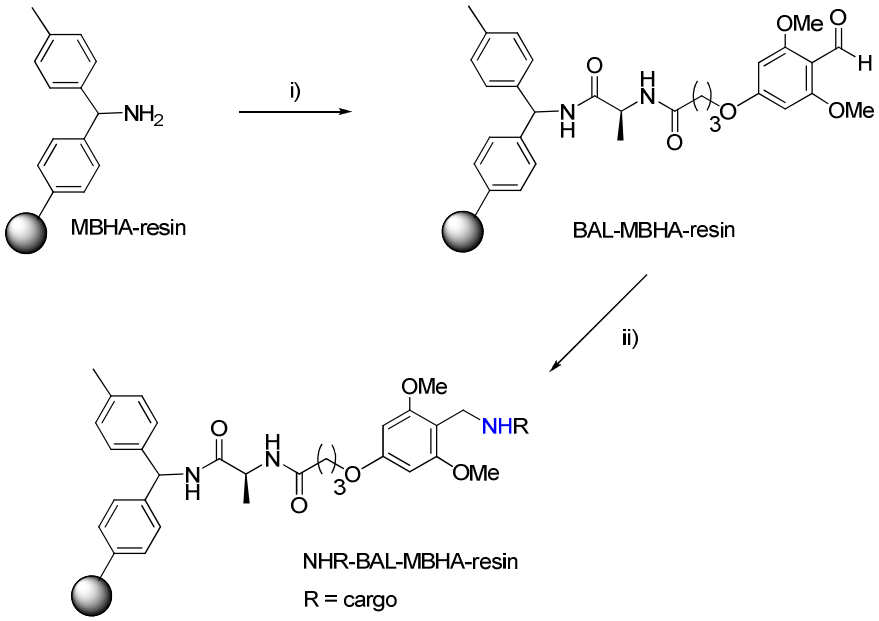

i) BAL, DIPCDI/HOBt, DMF, rt, overnight. ii) a) NHR, AcOH 1% DMF; b) $NaCNBH_3$.

Fig. 4.15: Synthesis of NHR-BAL-MBHA resin.

The following synthetic sequence for bicyclic guanidinium oligomer synthesis was designed: First, anchorage of BB **15** would be performed through amide coupling to NHR-BAL-MBHA resin. Thereafter, deprotection of the hydroxy group, followed by its activation as an electrophile on solid support would pave the way for the next bicyclic BB **16** attachment through nucleophilic attack. Compound **16** bears a thioacetate that can be converted into a sulfide in a basic medium, providing a strong nucleophile for anchorage to the electrophilic resin. Iteration of previous *O*-silyl deprotection and alcohol activation steps would, in theory, enable for sequential coupling steps and afford strands of different lengths (Fig. 4.16).

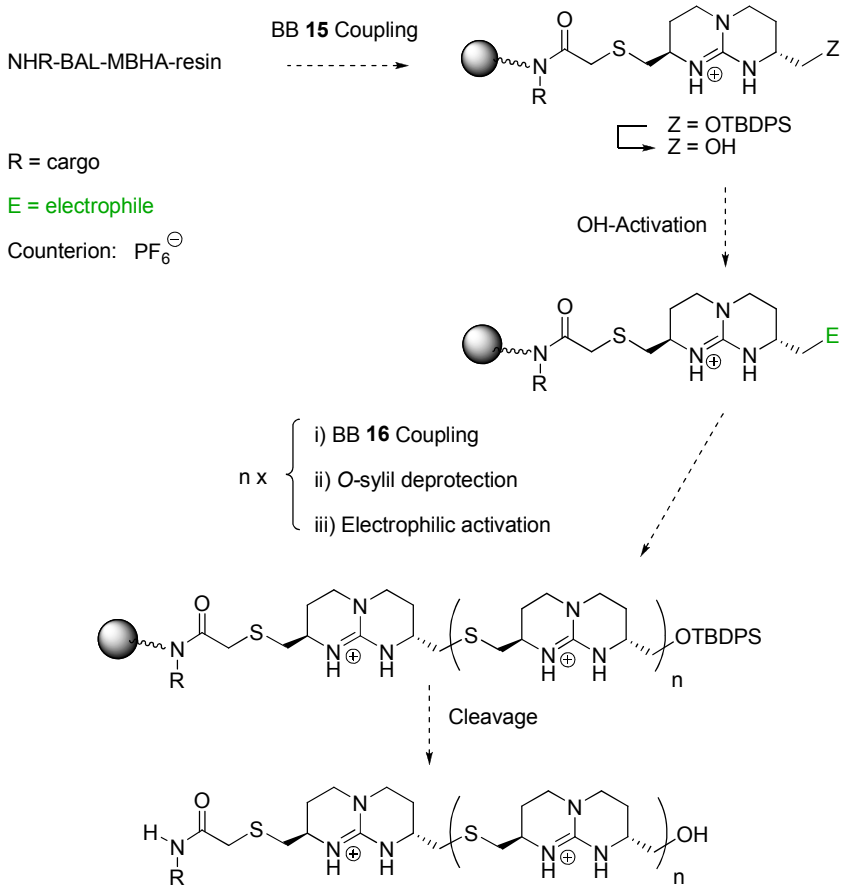

Fig. 4.16: Synthetic scheme for bicyclic oligomer synthesis based on BBs **15** and **16** and NHR-Bal-MBHA resin.

4.2.1.2 Results and discussion

Amide coupling of BB **15** was carried out under HOBt/DIPDCI conditions overnight at room temperature (rt) and successfully monitored by a ninhydrine test. Moreover we verified that the presence of the guanidine core does not interfere with the test. Compounds were finally cleaved in 100% TFA (1h at rt) and the crude mixtures were analyzed by

LC-MS with light scattering detection (Fig. 4.17).

a)

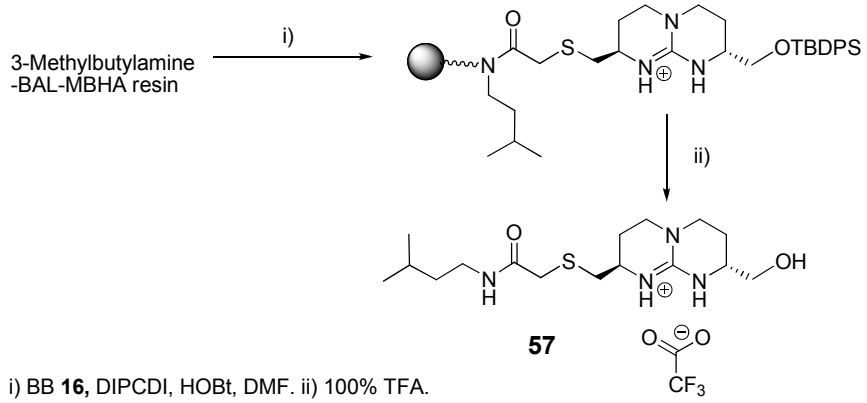

b)

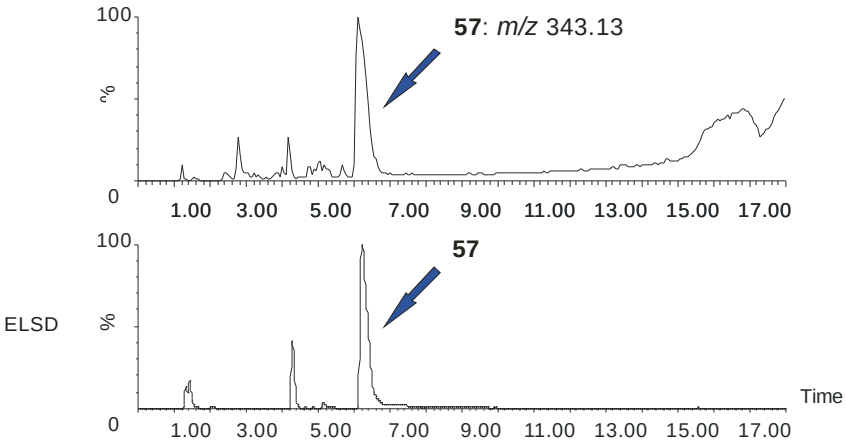

Fig. 4.17: a) Reaction scheme and b) LC-MS analysis of crude compound **57:** ESI(+) spectrum (top), ELSD chromatogram (bottom) (Conditions: 0-100 % CH_3CN in H_20 with 0.1% HCOOH for 15 min).

Deprotection of OTBDPS-group employing 1M tetrabutylammonium fluoride (TBAF) was completed in a couple of hours at rt. We tried to monitor this reaction by a qualitative color test for hydroxyl groups, which

is carried out on-bead and shows violet staining with primary alcohols. The reaction is based on the formation of a tosylate, its displacement by *p*-nitrobenzylpyridine and conversion of the resin-bound pyridinium salt into a strongly colored internal salt by treatment with base (48). However this test was not reliable in our case. Later trials showed that conversion of this hydroxyl group into a sulfonate was indeed not trivial. Thus, after confirming deprotection by LC-MS, we attempted to convert the hydroxyl group into a good leaving group such as chloride, bromide or sulfonate, followed by nucleophilic substitution with benzylthiol (3 eq.) under basic conditions (3 eq. Cs_2CO_3), Fig. 4.18.

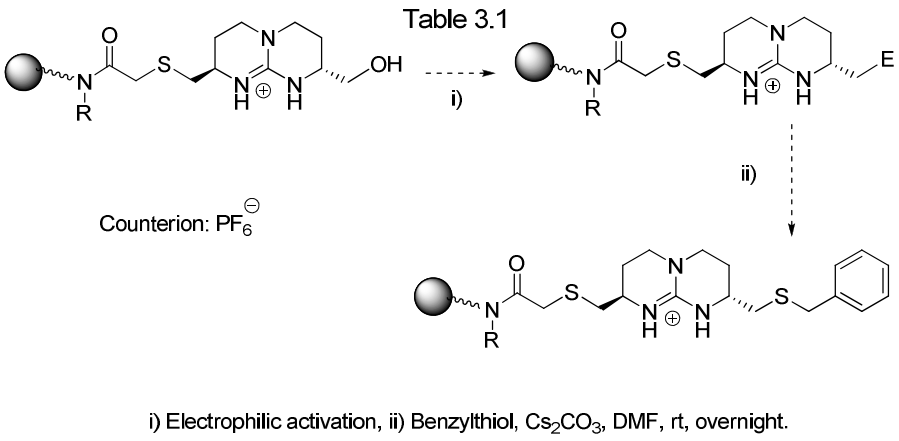

Fig. 4.18: Electrophilic activation followed by nucleophilic attack by benzylthiol under basic conditions.

Table 4.1 shows different reagent, solvent and time conditions assayed for this purpose:

Table 4.1: Attempted electrophilic activation of anchored alcohol.

	Reagents	**Solvent**	**Time at rt**
a	7.5 eq PBr_3	THF/CH_2Cl_2 (2:1)	4 h , 8 h, 10 h
b	3.5 eq CBr_4, 3.5 eq TPP	CH_2Cl_2	4 h, 8 h, 10 h
c	3 eq. DIPCDI, 2% Cu(I)Cl, 4.5 eq. NBS	THF	4 h
d	3 eq. DIPCDI, 2%Cu(II)Tf_2, 4.5 eq. NBS	THF	4 h
e	3 eq. DIPCDI, 2% Cu(I)Cl, 4.5 eq. NCS	THF	4 h
f	3 eq. DIPCDI, 2% Cu(II)Tf_2, 4.5 eq. NCS	THF	4 h
g	7.5 eq. DsCl, 10 eq. Et_3N	CH_2Cl_2	4 h
h	7.5 eq. TsCl, 10 eq. Et_3N	CH_2Cl_2	4 h
i	7.5 eq. MsCl, 10 eq. Et_3N	CH_2Cl_2	4 h
j	7.5 eq. MsCl, 10 D*i*PEA, DMAP	CH_2Cl_2	4 h

Initially we unsuccessfully tried to achieve the bromide incorporation with carbon tetrabromide (entry **a**) and phosphorus tribromide (entry **b**). Thus, we searched for alternative procedures for conversion of hydroxyl groups into halides.

A mild one-pot procedure was described recently (49). The reaction takes place in two steps: the alcohol is first activated as *O*-alkylisourea *via* DIPCDI under mild acidic conditions and then *N*-halosuccinimide (NXS, X = Br, Cl) is employed as halide source to convert the alcohol into a chloride or bromide derivative. Following the described protocol in solution, we obtained 50% conversion on compound **54**. Next, we tested this procedure

on the solid support (entries **c**-**f**) varying the Lewis acid, but in this case, no brominated nor chlorinated products were detected in the cleavage crude [MALDI and ESI(+)]. Next, we attempted to obtain different sulfonates (entries **g**-**j**). For entry **j**, the expected mass (LC-MS), after nucleophilic attack and cleavage, was observed (Fig. 4.19).

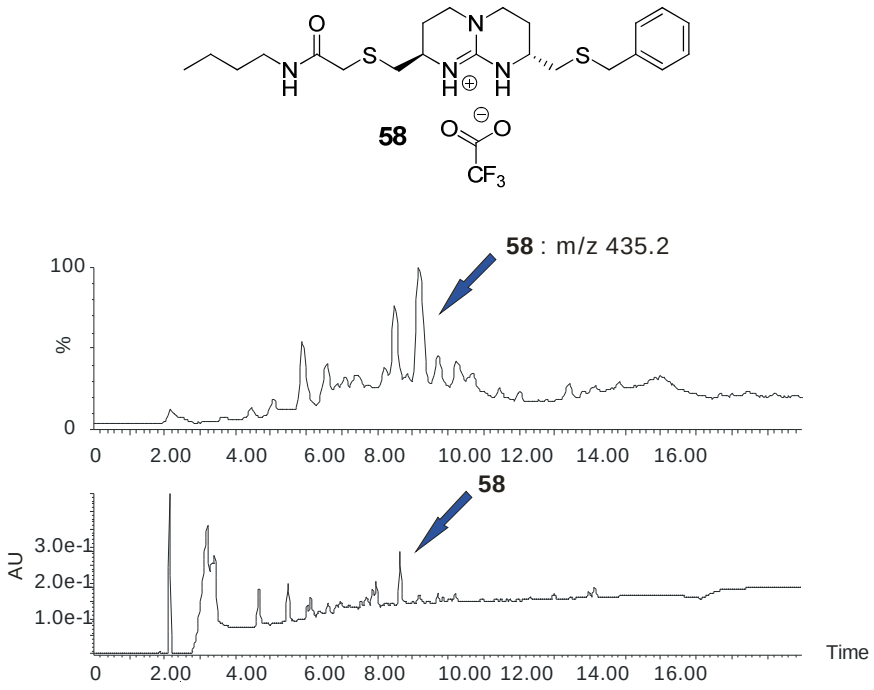

Fig. 4.19: LC-MS analysis of crude compound **58**. ESI(+) (top) and UV_{220} (bottom) (Conditions: 0-100 % CH_3CN in H_20 with 0.1% HCOOH in 15 min).

Addition of DMAP (entries **g**-**h**) may have led to the same outcome as for entry **j**, but this was not further studied. We analyzed crude compound **58** in more detail, and besides **58** its precursor **59** was identified (Fig. 4.20).

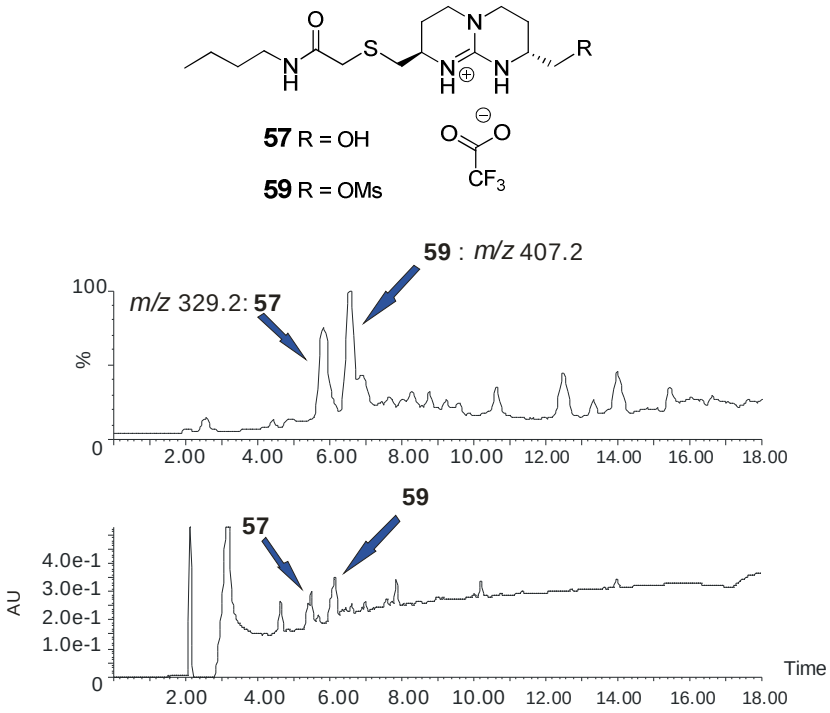

Fig. 4.20: LC-MS analysis of crude compound **59**. ESI(+) (top) and UV_{220} (bottom), (0-100% CH_3CN in H_20 with 0.1% HCOOH in 15 min).

The presence of **57** could be due to mesyl hydrolysis during the acidic cleavage conditions, though uncomplete conversion of the alcohol could not be excluded. The products in the cleavage crudes described above were not obtained in quantitative yields, but they were easily identified by LC-MS. Therefore, we attempted the anchorage of the next bicyclic guanidinium unit, BB **16**, through a thioether linkage. In solution, analogous reactions have been previously performed in our research group, whereby cesium carbonate (Cs_2CO_3) can be employed as base to deprotect the sulfide *in situ*, prior to nucleophilic attack on the mesyl group.

Our first trial to couple a second unit (DMF, rt) was monitored for three days (Fig. 4.21).

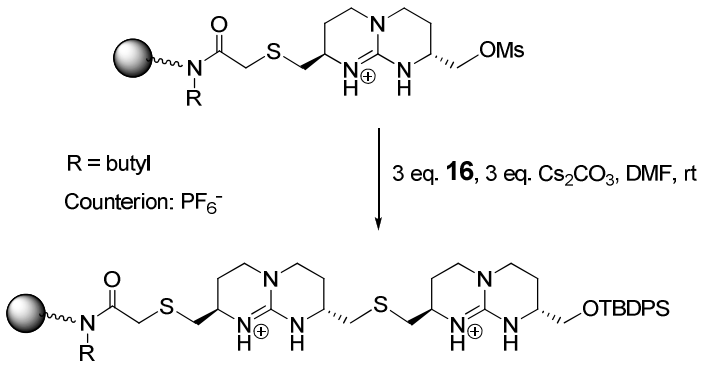

Fig. 4.21: Synthetic scheme for BB **16** coupling.

Despite an excess BB **16** was employed (three-fold), precursor **57** was present in the crude besides the expected product **60** (Fig 4.22), and the reaction did not further proceed after 20 h.

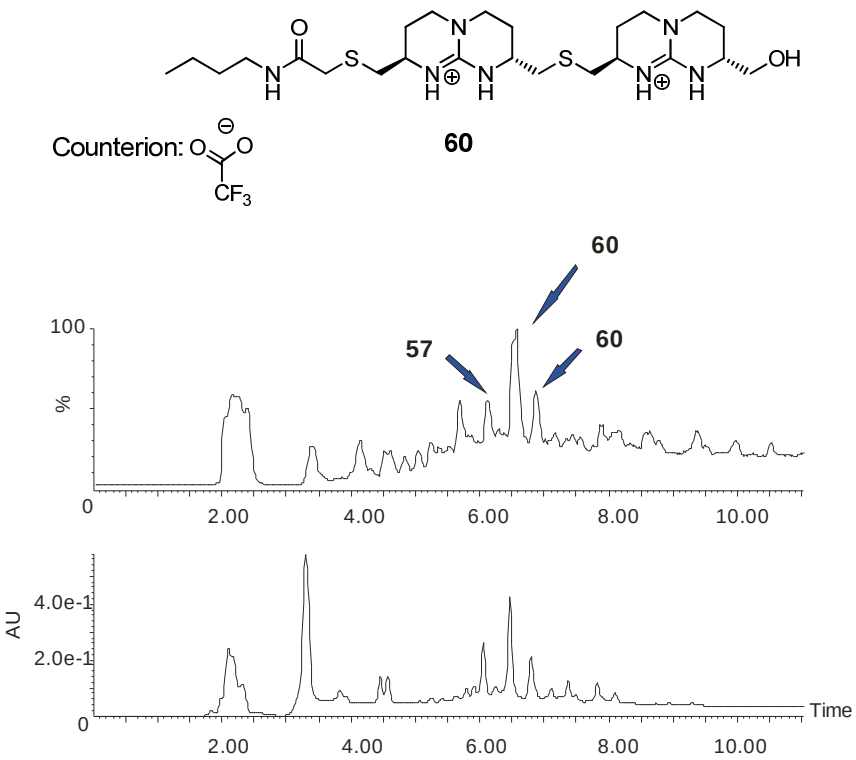

Fig. 4.22: Chemical structure **60** and LC-MS analysis of the crude mixture. MS (top) and UV_{220} (bottom), (0-100% CH_3CN in H_20 with 0.1% HCOOH in 15 min).

Repeating protocols of hydroxyl deprotection, electrophile conversion and coupling of BB **16,** led once more to the identificaction (LC-MS) of the triguanidinium derivative **61**. However, many unidentified subproducts were also detected (Fig. 4.23).

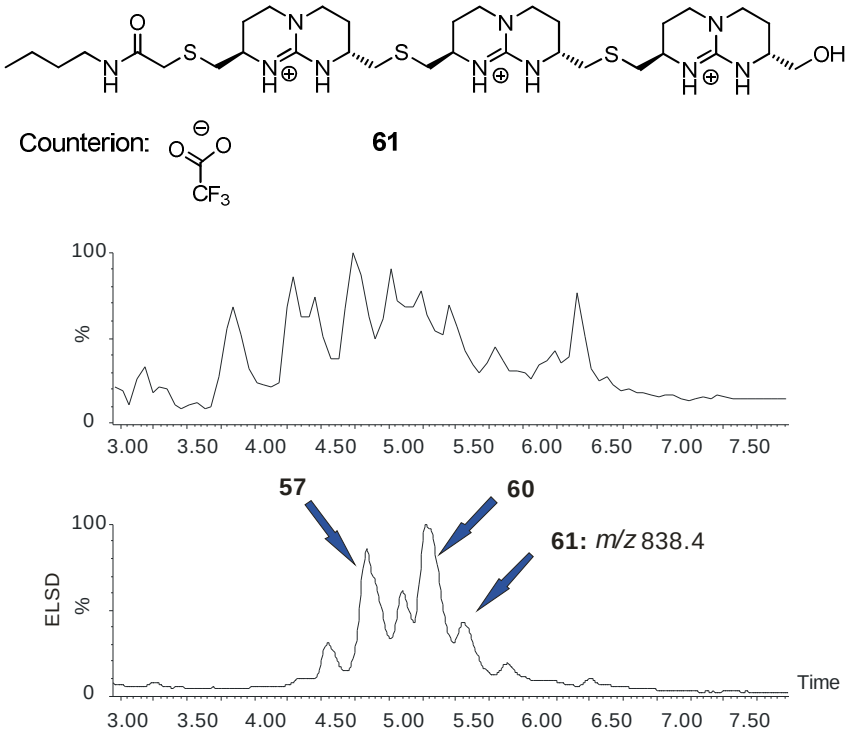

Fig. 4.23: LC-MS analysis after the third bicyclic unit coupling and cleavage: ESI(+) (top) and ELSD chromatogram (bottom) (0-100% CH_3CN in H_20 with 0.1% HCOOH in 15 min).

After these preliminary results, the coupling reaction was optimized, taking into consideration the following parameters: phosphine reducing agent, time, temperature, microwave conditions and renewal of reagents.

No starting product was detected in the filtrate after the reaction, but disulfide subproduct **62**, resulting from intermolecular disulfide formation between deprotected molecules of **16**, was highly represented. This indicates that nucleophilic attack and disulfide formation were actually competing reactions (Fig. 4. 24).

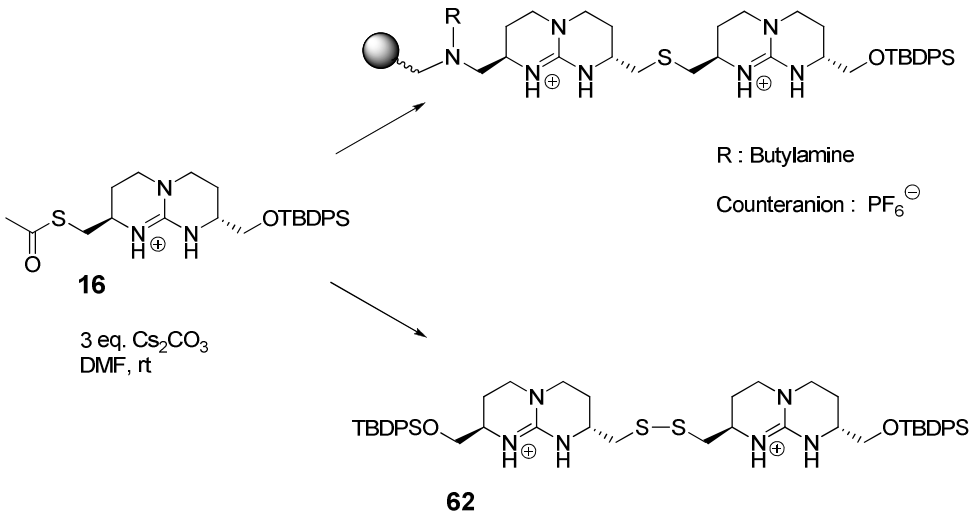

Fig. 4.24: Competing reactions during coupling.

To prevent disulfide formation, we added reducing phosphines to the reaction: *n*-butylphosphine [n-$P(Bu)_3$] or triphenylphosphine [$P(Ph)_3$] (50). Contrary to our expectations, addition of 5 to 8 eq. of $P(Ph)_3$ or n-$P(Bu)_3$ did not improve the coupling yields. Further experiments aimed at reducing reaction time did not improve yields, either. On the contrary, better results were obtained with longer reaction times (up to 72 h) at rt.

Next, the temperature of the reaction was increased to 50 ºC for 24 h and also some trials in the microwave reactor were attempted. However, both approaches failed to improve the coupling yield, as assessed by the LC-MS analysis of the respective cleavage crudes. Finally we renewed the reaction solution after 24 h, and again after 24 h and 48 h, and compared the results to a reference resin without renewals, in the following conditions: 3 eq. of **16**, 3 eq. of Cs_2CO_3, 5 eq. of n-$P(Bu)_3$ in DMF at rt for 72 h. We expected to improve the yields as the number of renewals of the reaction mixture was

increased. Light scattering chromatograms (ELSD) obtained after cleavage of the different samples are shown in Fig. 4.25.

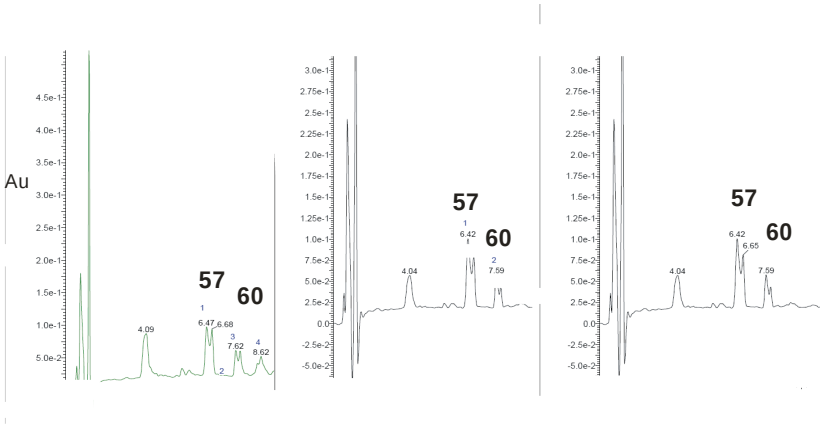

Fig. 4.25: ELSD chromatograms of crude compound after 72 h reaction (*red*), with one renewal after 24 h (green) and with two renewals (*black*).

The reference reaction yielded a 1:4 mixture of starting and final products after 72 h, as estimated from the areas of the corresponding peaks (identified by LC-MS). Renewal of the reaction mixture once after 24 hours improved this yield slightly but a second renewal did not. Thus, further renewals were not attempted to avoid waste of starting material.

In summary, our approach based on BBs **15** and **16** demonstrated that the synthesis was indeed possible, but we were unable to develop consistent protocols for the transformations. The major drawback was the coupling rate, much too slow under the conditions employed. Part of the failure was also associated to the difficulty to control disulfide formation during nucleophilic coupling. Moreover, use of building blocks requiring

functionalization prior to further elongation, increases the probability of incomplete conversion.

Dahan *et al.* reported on a solid phase synthesis of thioether dendrons based on nucleophilic attack of an aromatic sulfide -deprotected *in situ*- on a resin-bound benzyl halide. Further sulfide anchorage required previous hydrolysis and reduction of the ester followed by electrophilic activation of the resulting phenols through halide conversion (51). Though further anchorage required prior functionalization, high yields were reported for this dendron synthesis. This is mainly due to the high reactivity of the aryl reagents employed, which enabled quantitative nucleophilic coupling of the sulfide-bearing monomers. In comparison, alkyl thiolates based on bicyclic guanidinium scaffolds are less reactive, thus they require a better adapted strategy .

Therefore, we focused on the synthesis of bifunctionalized building blocks containing a good leaving group on one side and a thiolate precursor on the other one. In this way, we envisaged to limit synthetic steps to coupling and deprotection reactions. Moreover, we reasoned that the oxidation state of the nucleophilic sulfur might be easier to control if it is bound to the resin.

4.2.2 Synthesis of *ideal* building blocks (BB)

4.2.2.1 Objectives

Initial trials on solid phase described in Section 4.2.1 paved the way for the design of new building blocks functionalized with an electrophile at one side and a thiolate precursor at the other. Elongation of bicyclic guanidinium oligomers would be achieved by iterative repetition of three main steps: incorporation of a bicyclic subunit at the electrophilic end, deprotection of its sulfur moiety and coupling of the next BB (Fig. 4.26).

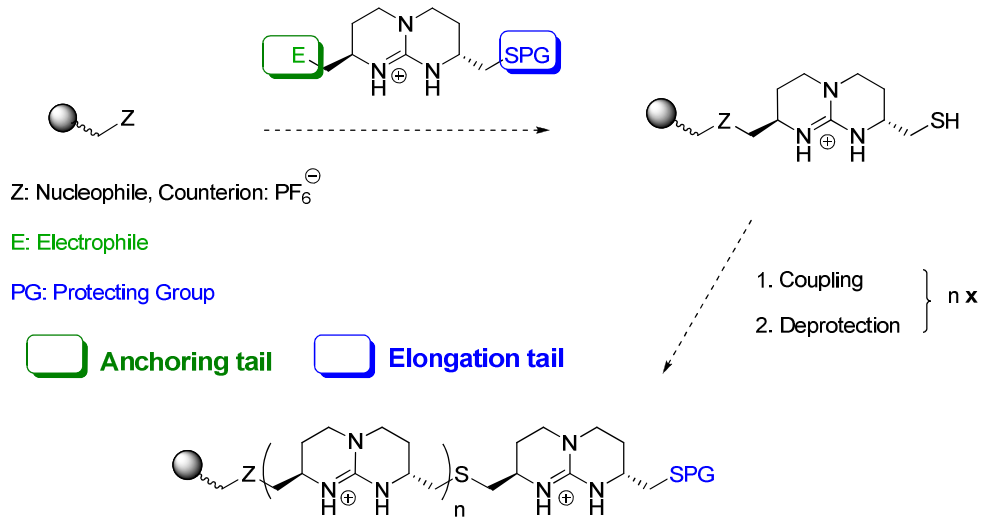

Fig 4.26: Merrifield-like synthesis of bicyclic oligoguanidiniums.

For this goal, we decided to synthesize a number of ideal BBs in the minimum synthetic steps and with the highest possible yields. We attempted the difunctionalization of the bicyclic guanidinium scaffold with different

sulfur protecting groups (Fig. 4.27) (52).

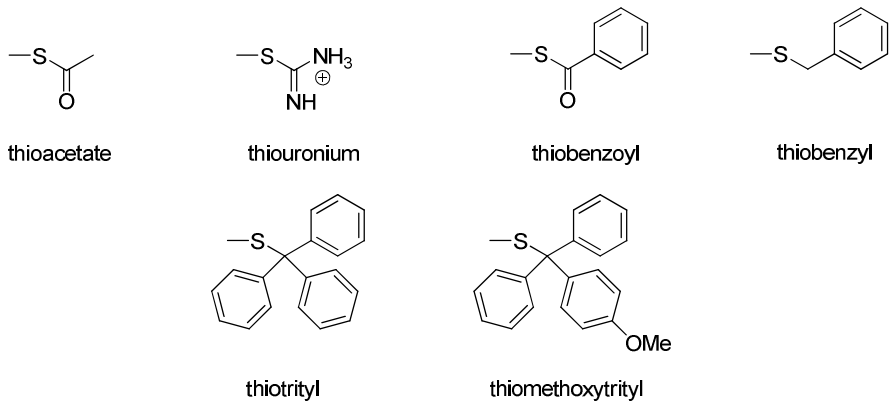

Fig 4.27: Selected thiol protecting moeities.

The same synthetic strategy was followed in all cases: First the protected sulfur was attached through nucleophilic substitution to the bicyclic guanidinium **54**, then the *O*-silyl group was deprotected and finally transformed into a suitable eletrophile (Fig. 4.28).

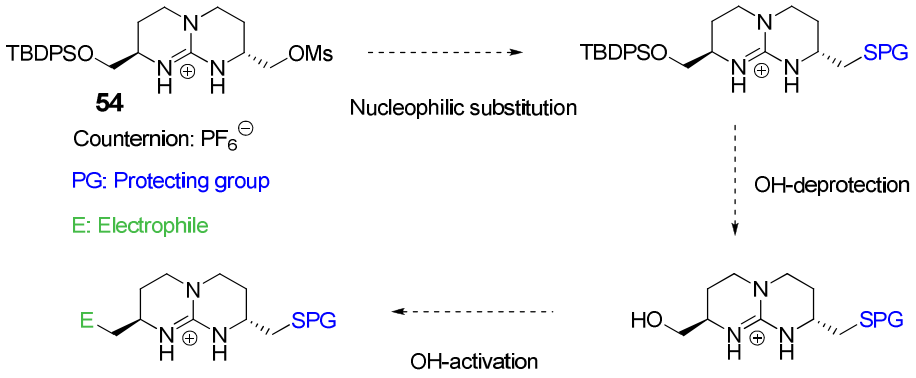

Fig. 4.28: Synthetic scheme for difunctionalized BBs.

4.2.2.2 Results and discussion

Thiourea attempt

First we aimed at obtaining BB **63,** functionalized with thioacetate, as we had experience on the handling of this chemical group and its use had been previously reported in solid phase (Fig 4.29) (53).

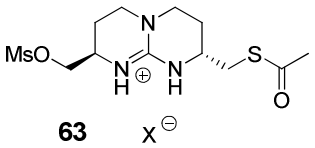

Fig 4.29: Compound **63**.

However our first attempts failed in the *O*-silyl deprotection. In the presence of fluorides (such as TBAF or CsF), simultaneous deprotection of the thioacetate group took place, leading to disulfide **64** (Fig. 4.30).

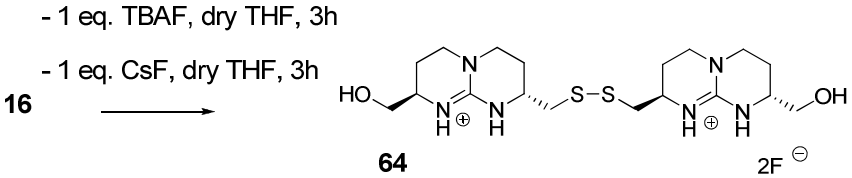

Fig 4.30: Simultaneous *O*-silyl and thioacetate deprotection in the presence of fluorides.

Milder deprotection conditions, with a solution of 3% HCl in acetonitrile or HF-pyridine, yielded mixtures of the starting compound **16**, the expected product **65**, and disulfide **64**. Isolation of product **65** was investigated by reducing the mixture to two compounds and exploiting the

differences in solubility (**16** is soluble in organic solvents, whereas **65** and **64** are water soluble). Trials at different temperature and time conditions are summarized in Table 4.2.

Table 4.2: Thioacetate deprotection in 3% HCl under various conditions.

3% HCl in CH_3CN	Temperature	hours	Products in aq. phase
a	5 ºC	7 h	Mixture*
b	-5 ºC	7 h	Mixture*
c-f	-5 ºC	1 h	Pure product
		2 h	Pure product
		3 h	Mixture*
		4 h	Mixture*

*Mixture of compounds **64** and **65**.

Though conditions for entry **c** enabled isolation of compound **65** in a pure form from the aqueous phase, a large amount of starting product was left unreacted in the organic phase. Therefore, as yields did not exceed 21%, the thioacetate-synthetic route was abandoned.

Isothiouronium attempt

Thiouronium is a well known precursor for a thiolate (54). Incorporation of thiourea was assayed following conditions described by our group on different electrophilic precursors **54**, **66** and **67** (2). However, all trials failed (Table 4.3) and most often the starting product was recovered.

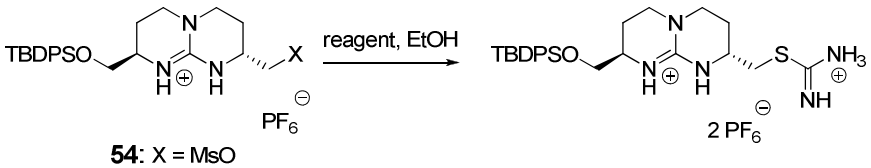

54: X = MsO

66: X = Cl

67: X = Br

68

Table 4.3: Trials to incorporate a thiouronium moiety.

	Reagent	Conditions	Time	Result
a	1.2 eq. thiourea	22 ºC, atm pressure	2 h o/n	recover starting material
b	1.2 eq. thiourea	110 ºC, sealed tube,	4 h	recover starting material
c	1.2 eq. thiourea	µW: 110 ºC, 200 W, 100 PSI	10, 20, 60 min	recover starting material
d	14 eq. thiourea	110 ºC, sealed tube	24 h, 4 days	no final product
f	1.2 eq. imidazolidine-2-thione	µW: 110 ºC, 200 W, 100 PSI	10 min	recover starting material

As a positive control, the reactivity of the thiourea reagent was checked on benzylbromide and the expected product was obtained quantitatively. Moreover imidazolidine-2-thione was employed as an alternative reagent (entry **f**) (55), but failed, too. As we were unable to progress further, we proceeded towards further alternatives for sulfur protection.

Thiobenzoate coupling

We generated the potassium thiobenzoate salt under basic conditions following a described procedure (56) in order to incorporate thiobenzoate as the sulfur-containing moeity. Deprotection of the hydroxyl group with HF-Pyridine reagent and further methylsulphonate generation, lead to building block **17** in good overall yield (53%, Fig. 4.30).

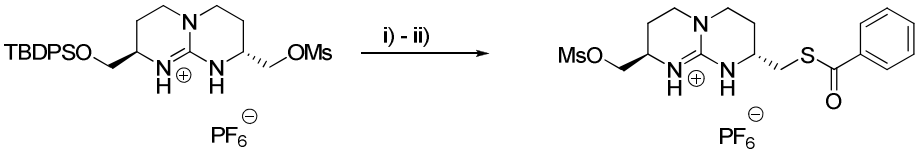

54 **17** (3 steps: 53%)

i) $C_6H_5COS^-K^+$, CH_3CN, MW, 140 ºC, 10 min (86%). ii) a) **69**, HF-Py, dry THF, rt, 24 h; b) MsO_2, NMM, dry THF, rt, 3 h (61%).

Fig 4.30: Synthesis of BB **17.**

The reported deprotection conditions in solution were confirmed under two different conditions: 0.5 M sodium hydroxide or 10% aqueous ammonia solutions in DMF (52).

Benzylmercaptane and Tritylmercaptane coupling

Nucleophilic substitutions on **54** by Benzylmercaptane (BnSH), Tritylmercaptane (TrtSH) and 4-Methoxytrityl mercaptane (MmtSH) were achieved in basic conditions (0.25 M sodium methoxyde in methanol) (Fig 4.31).

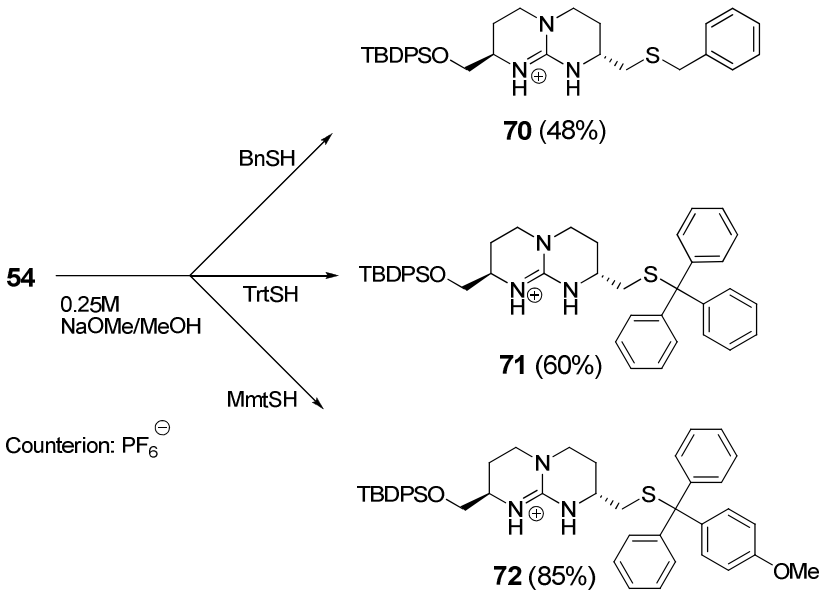

Fig 4.31: Functionalization with aromatic mercaptane moieties.

However only the synthesis of methoxytrityl functionalized building block **18** was driven to completion (Fig. 3.32) as the deprotection conditions for Bn (52) and Trt (57) protecting groups on thioethers are not suited for orthogonal solid phase strategies, based on Fmoc group.

i) MmtSH, MeONa/MeOH, 22-50 ºC, o/n. ii) **73**, Ms_2O, dry CH_2Cl_2, rt, 2 h (80%).

Fig 4.32: Synthesis of BB **18**.

O-silyl deprotection took place in the same basic medium as the initial nucleophilic substitution; therefore BB **18** was obtained in high yields after only two reaction steps from precursor **54**. Moreover, methoxytrityl (Mmt) can be removed using very dilute TFA solutions in the presence of TIS as scavenger (5% TFA, 5% TIS in CH_2Cl_2), which we confirmed in solution (58).

In conclusion, we synthesized two different bicyclic guanidinium BBs **17** and **18** with good yields. Deprotection of the respective sulfur-protected moeities was confirmed in solution and was strictly orthogonal: Thiobenzoate liberates the sulfide in basic media while Mmt does it under acid conditions. In this way we might develop analoguous strategies based on distinct handles and solid supports. In the next section we will discuss the choice of resins and linkers, the synthetic drawbacks as well as the achievements made with BB **17** and BB **18.**

4.2.3 Attempts with bifunctionalized BBs

4.2.3.1 Objectives

Building Blocks **17** and **18** differ *only* in their sulfur protecting groups. This means that similar conditions for nucleophilic substitution on their electrophilic end may be employed for their initial coupling to SP. However, deprotection of the *S*-protecting groups requires different conditions, thus different resins or linkers.

Ideally, the selected solid support should as well offer an anchorage point for cargo attachment, though the cargo might also be attached to the final sulfur. Finally a reaction to cap non reacted coupling sites, in both cases, should help to prevent the formation of deletion sequences, which could jeopardize the final purification.

4.2.3.2 Results and discussion

Amine-functionalized resins are the most common commercially available resins, so initial trials to anchor BBs **17** and **18** through S_N reaction to a solid support were done on Aminomethyl and Rink amine-MBHA polystyrene resins. Different basic conditions with organic bases (D*i*PEA, Pyridine) were assayed. However, only in the presence of potassium carbonate and crown ether some anchorage of the building blocks was detected on Rink amide-MBHA resin. Since coupling still occurred with low yield, we focused on nucleophilic anchorage on thiol functionalized resins.

Thiol-4-methoxytrityl resin is commercially available and its cleavage takes place under mild acidic conditions: 1-8% TFA, 5% TIS in CH_2Cl_2 (Fig. 4.33a). Thus this resin is suited for BB **17** but not for BB **18**, whose sulfur moiety is removed as well under the same conditions.

Therefore we selected a different anchoring system for BB **18,** namely Fmoc-Cys(Mmt)-Rink amide-MBHA resin (Cys resin, Fig. 4.33b). This support provides an additional attachment point for cargo molecules *via* the α-amino group of the cysteine.

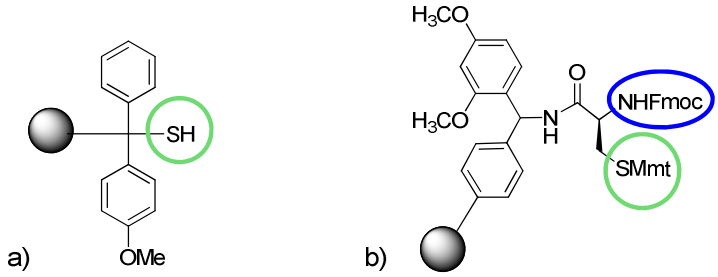

Fig. 4.33: Thiol 4-methoxytrityl resin (a) and Fmoc-Cys(Mmt)-Rink amide-MBHA resin or Cys resin (b).

Coupling results with BB 17

Attachment of **17** to thiol-4-methoxytrityl resin was achieved either in the presence of 3 eq. of cesium carbonate (Cs_2CO_3) or with Et_3N. Diluted TFA cleavage conditions and LC-MS analysis confirmed previous anchorage of compound **17** (Fig. 4.34).

a)

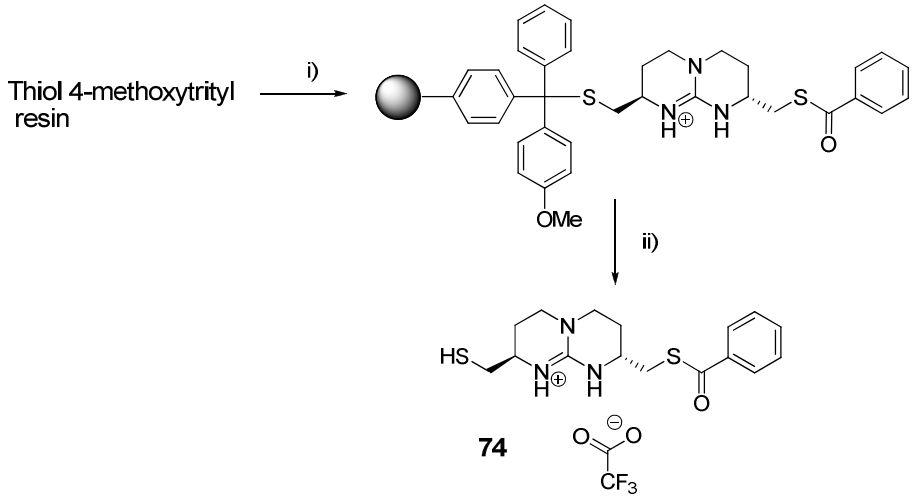

b)

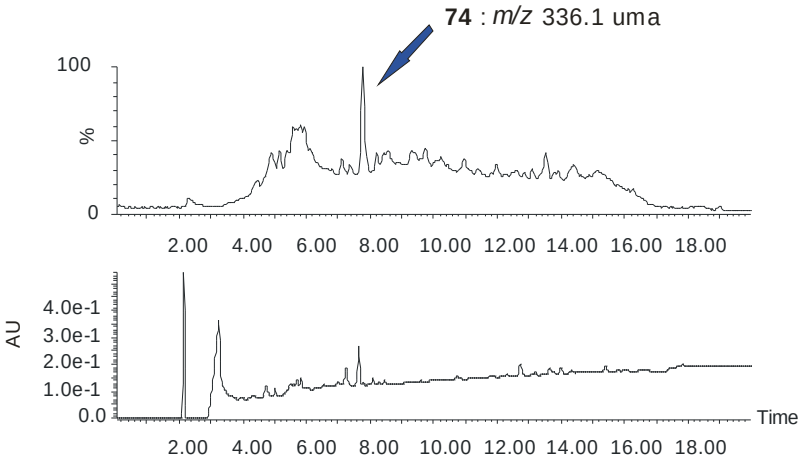

Fig. 4.34: (a) Reaction scheme and (b) LC-MS analysis of crude compound **74**. MS (top) and UV_{220} (bottom) (Conds: 0-100 % CH_3CN in H_20 with 0.1% HCOOH in 15 min).

However, to assess disulfide bond formation during the reaction we employed the Ellman test, a fast and easy color test to detect resin-bound thiols in a qualitative and/or quantitative manner (Fig 4.35) (59).

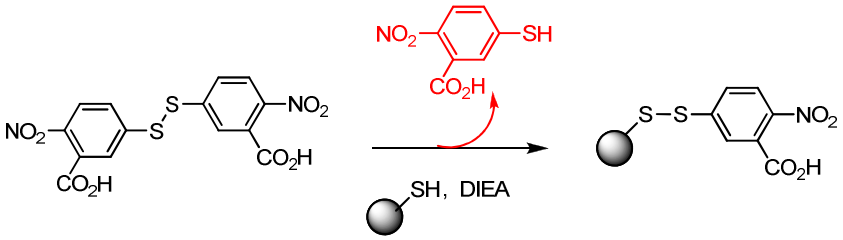

Fig. 4.35: Ellman test reveals the presence of free thiols by liberating into solution a red dye.

After coupling BB **74** in the described reaction, Ellman test indicated that no more free thiols were present on the resin. This could be due to completion of nucleophilic reaction or to both nucleophilic substitution and disulfide bridge formation during coupling. To evaluate this, reduction of the resin was first attempted with the following agents: $P(Ph)_3$, n-$P(Bu)_3$ and 1,4-Dithiothreitol (DTT). Only treatment with a DTT (8 eq.) solution in DMF revealed free thiols on the resin after Ellman test. Hence, disulfide bridges were indeed forming between thiols of the resin beads at the conditions employed.

Benzyl bromide was employed beforehand as a model electrophile to optimize coupling conditions (Fig. 4.36). After nucleophilic reaction under different conditions, we checked the presence of free thiols *via* Ellman test, preceeded by additional treatment with DTT (Table 4.4).

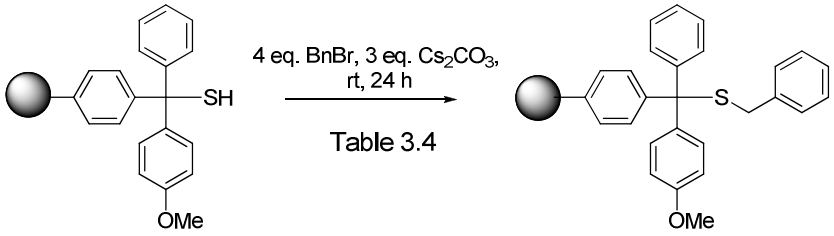

Fig. 4.36: Initial trials with BnBr.

Table 4.4: Testing disulfide bond formation after coupling.

	Reductive agent	**Ellman test after coupling**	**Ellman test after DTT treatment**
a	5 eq. n-$P(Bu)_3$	negative	positive
b	12 eq. n-$P(Bu)_3$	negative	positive
c	2 eq. of DTT	negative	positive

However, disulfide formation was observed under all conditions described in Table 4.4.

Next, bases other than Cs_2CO_3 were assayed on the same reaction. In this context the limiting factor is solubility in DMF: Of all the inorganic bases reported for nucleophilic reactions with mercaptans in solution (60,61), only potassium *tert*-butoxide (K^tBuO) was actually soluble in wet DMF, therefore we used K^tBuO besides the organic base Et_3N, varying the number of equivalents of BnBr and n-$P(Bu)_3$, as depicted in Table 4.5.

Table 4.5: Different bases and reduction conditions to avoid disulfides.

	Base	**Reductive agent**	**BnBr**	**Ellman test after reaction**	**Ellman test after DTT treatment**
a	3.5 eq. K^tBuO pH 9	4 eq. n-$P(Bu)_3$	2 eq.	negative	positive
b		4 eq. n-$P(Bu)_3$	5 eq.	negative	positive
c		0 eq. n-$P(Bu)_3$	5 eq.	negative	positive
d	3 eq. Et_3N pH 9-10	4 eq. n-$P(Bu)_3$	2 eq.	negative	positive
e		4 eq. n-$P(Bu)_3$	5 eq.	negative	positive
f		0 eq. n-$P(Bu)_3$	5 eq.	negative	positive

However, once again all cases gave a positive Ellman test after DTT treatment, indicating the formation of disulfides under all investigated coupling conditions.

This could be by the combination of two factors: i) High local concentration of free thiols (functionalization of the resin: 1.8 mmol/g) which might strongly favor disulfide bond formation over nucleophilic attack and ii) sterical hindrance of tertiary thiolate, which reduces its nucleophilic strength.

Hence, asssuming that substitution at the highly hindered trityl thiol might be difficult, long reaction times or highly activated reagents may be required to effect complete transformation. However, neither adding n-$P(Bu)_3$ as reducing reagent, nor changing basic conditions did alter the high

rate of disulfide formation during BB **17** coupling. Maybe the phosphonium moiety was actually unable to react with water, due to the highly hydrophobic nature of the thiol-4-methoxytrityl resin, causing the reduction cycle not to be closed.

Interestingly, incorporation of methoxytrityl mercaptan on mesyl compound **54** in solution occurred in a high yield under the previously described conditions (Fig. 4.32). Most often, however, efficient conditions in solution cannot be transferred "literally" to solid phase and viceversa.

In fact, several authors consider that a solid-phase system is actually *ideal* for intramolecular disulfide bond formation: Rigid fixation of molecules on the solid-phase restricts their mobility and decreases intermolecular contacts, which ensures predominant occurrence of intramolecular reactions (62). However, a reported way to avoid the intramolecular reaction is to apply the so-called "pseudo-dilution" which consists of reducing the initial functionalization of the resin at will by applying capping conditions in quantitative yields (63). Pseudo-dilution may indeed offer an alternative to progress with this synthetic strategy, but was not assayed in the context of this thesis.

Coupling results with BB 18

Meanwhile, we assayed the strategy based on BB **18** and the selected Cys-resin, represented in Fig. 4.33b. *A priori,* conditions in this case were better suited to our purpose, because the initial resin functionalization was low (< 0.7 mmol/g) and because the nucleophile was a primary thiolate.

Also the handle provided a straightforward anchoring point for cargo molecules.

Initial attempts to couple an electrophile *via* thioether formation on Cys-resin were performed after Fmoc deprotection and acetylation of the α amine, because NHFmoc does not survive the basic coupling conditions required, Fig. 4.37.

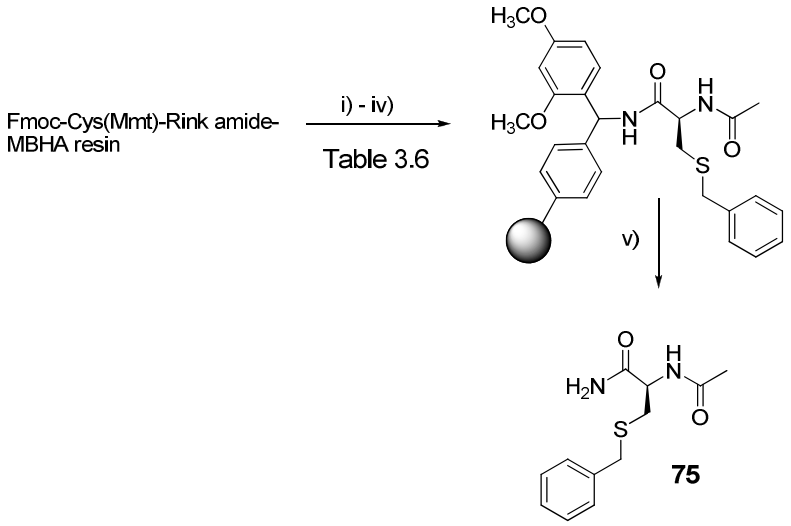

Fig. 4.37: Initial trials on Cys resin with benzyl bromide.

Furthermore, as for previous strategy, benzyl bromide was employed beforehand as model electrophile to optimize coupling conditions (Fig. 4.37 and Table 4.6).

Table 4.6: Attempts to couple quantitatively BnBr to Fmoc-Cys(Mmt)-Rink amide-MBHA resin.

	Base	Reductive agent (eq.)	BnBr	Ellman test after reaction	Ellman test after DTT
a	3.5 eq. K^tBuO pH 9	4 eq. n-$P(Bu)_3$	2	–	+
b		0 eq. n-$P(Bu)_3$	2	–	+
c		4 eq. n-$P(Bu)_3$	5	–	+
d		0 eq. n-$P(Bu)_3$	5	–	–
e	3 eq. Et_3N pH 10	4 eq. n-$P(Bu)_3$	2	–	+
f		0 eq. n-$P(Bu)_3$	2	–	+
g		4 eq. n-$P(Bu)_3$	5	–	+
h		0 eq. n-$P(Bu)_3$	5	–	–

Promising results, according to the Ellman test, were obtained for entries **d** and **h** and the results were confirmed on anal. HPLC after cleavage (Fig. 4.38).

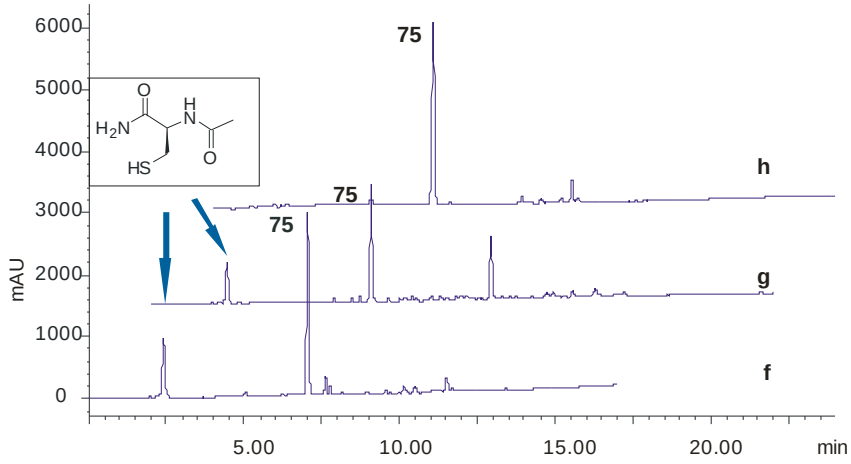

Fig. 4.38: Crude profiles for entries **f**-**h** and compounds identified by ESI(+). From bottom to top: entries **f**, **g** and **h**. (Conds: 5-95% CH_3CN in H_2O, 0.1% TFA, in 15 min, UV_{220}).

In the presence of 5 eq. of benzyl bromide, reaction was completed in either of the basic conditions. Moreover, as better results were obtained in the absence of n-$P(Bu)_3$, this reagent was definitely discarded for nucleophilic coupling on solid support.

The expected product **75** was obtained almost pure in the case of entry **h**, as observed by HPLC and confirmed by ESI(+) and ^{1}H-NMR analysis (see Appendix, Fig. A4.1), whereas chromatograms for entries **f** and **g** showed residual compound from non completed reaction. Hence, conditions for entry **h** were optimum to functionalize the resin with quantitative yield.

Next, similar conditions were employed with 3 eq. of BB **18** (Fig. 4.39 and Table 4.7).

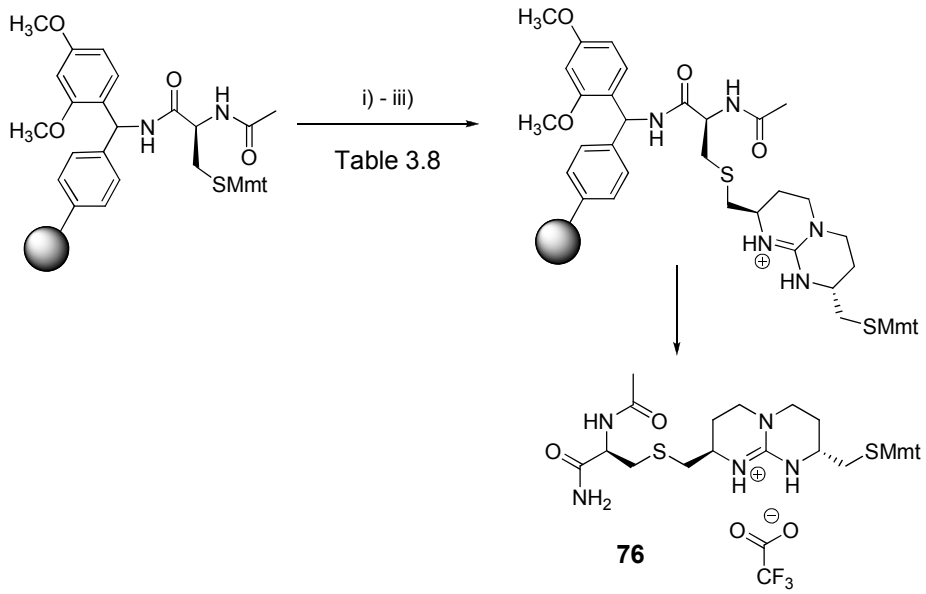

i) 5% TFA, 5% TIS, CH_2Cl_2. ii) **BB** **18** coupling. iii) DTT and Ellman test. iv) 100% TFA.

Fig. 4.39: Initial trials with BB **18** on Cys resin.

Table 4.7: Trials to couple BB **18** to Cys resin.

	Base	**Time**	**Ellman test after reaction**	**Ellman test after DTT**
a	3.5 eq. K^tBuO pH 9	3 h	–	(+)
b		o/n	–	(+)
c	3 eq. Et_3N, pH 10	3 h	+	+
d		o/n	+	+

We observed that in the case of K^tBuO (entries **a** and **b**) a slightly positive result was obtained after DTT treatment, regardless of the reaction time, while for Et_3N no nucleophilic coupling seemed to occur (entries **c** and **d**). HPLC as well as ^1H NMR analysis of the cleavage crudes indeed

revealed that BB **18** had been anchored with satisfactory yields for entries **a** and **b**, while no product was identified for entries **c** and **d** (Fig. 4.40).

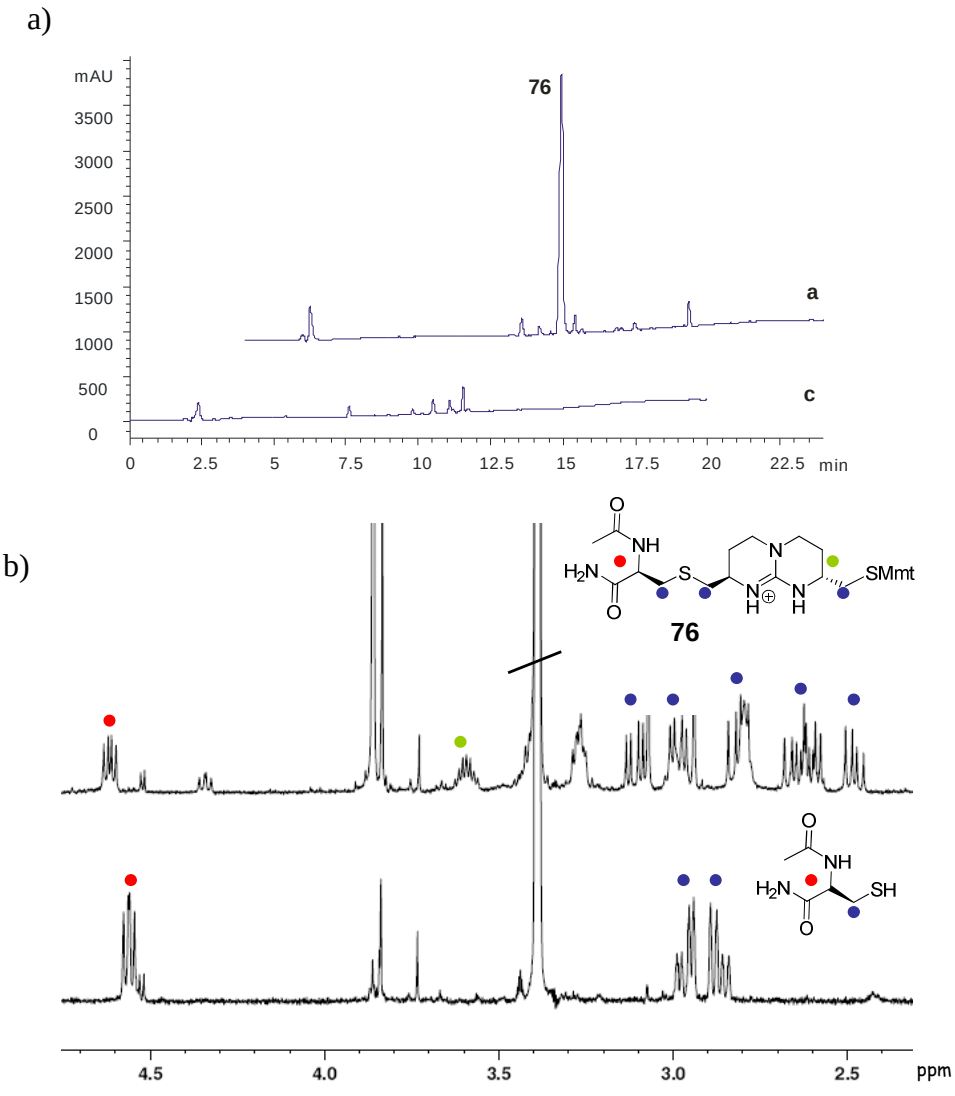

Fig. 4.40: (a) anal. HPLC crude profiles (Conds: 5-95% CH_3CN in H_2O, 0.1% TFA, in 20 min, UV_{214}) for entries **a** and **c**, and (b) detail from ^1H NMR spectra of crude compound **76** in CH_3OD, entries **a** (top) and **c** (bottom).

However, we had not succeeded in coupling BB **18** with quantitative yield, therefore the previous described coupling conditions with benzyl bromide as capping reaction were employed (Fig. 4.41).

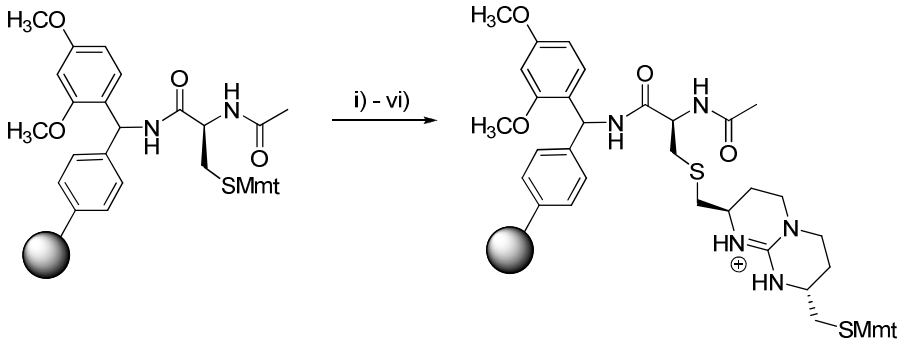

i) 5% TFA, 5% TIS, CH_2Cl_2. ii) DTT. iii) BB **18**, K^tBuO. iv) DTT. v) BnBr, Et_3N. vi) DTT.

Fig. 4.41: Synthetic scheme incorporating capping reaction after BB **18** coupling.

After all synthetic steps described in Fig. 4.38, we obtained a negative Ellman test, indicating that all sulfur coupling sites had been successfully capped. After cleavage the crude was analyzed by HPLC and ^{1}H NMR (Fig. 4.42).

a)

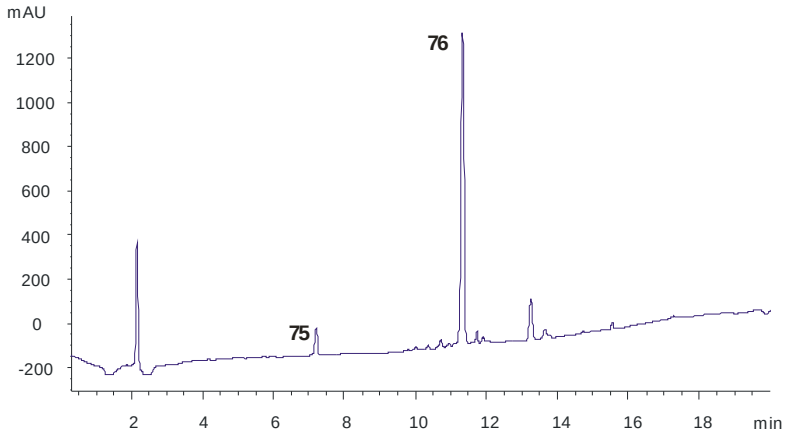

b)

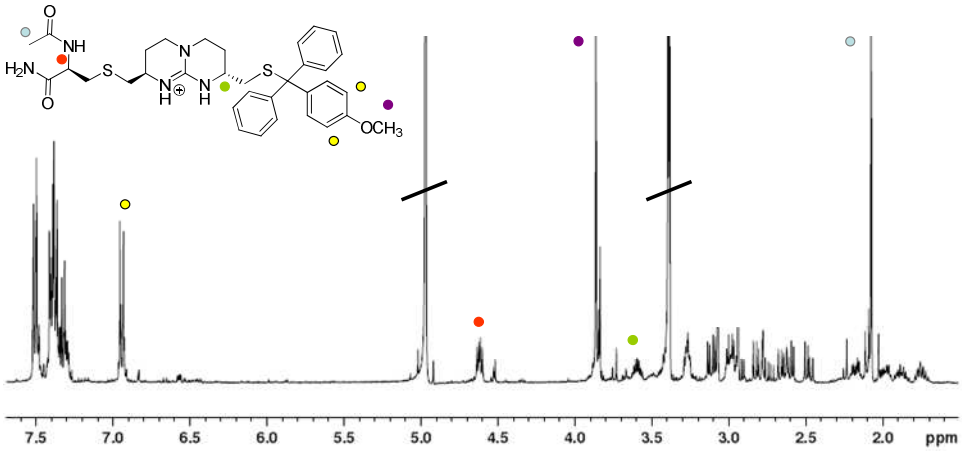

Fig. 4.42: (a) HPLC profile of crude compound **76** (Conds: 5-95% CH_3CN in H_2O, 0.1% TFA, in 20 min, UV_{214}), and (b) ^1H NMR spectrum of crude compound **76** in CH_3eOD.

Compound **75** could not be clearly identified on the ^1H NMR spectrum as the proton signals for CH_α where the same for products **75** and **76** while the remaining proton signals overlapped. However, in the UV chromatogram compound **75** was identified as a tiny peak at 7.2 min, product **76** as the major peak at 11.3 min and a third peak corresponding to methoxytrityl at

13.3 min. At first instance we thought the methoxytrityl peak originated from non complete wash out after on-resin removal of SMmt. The same synthetic steps were repeated several times and aliquots for cleavage after the first, the second and the fourth coupling were taken (Fig. 4.43).

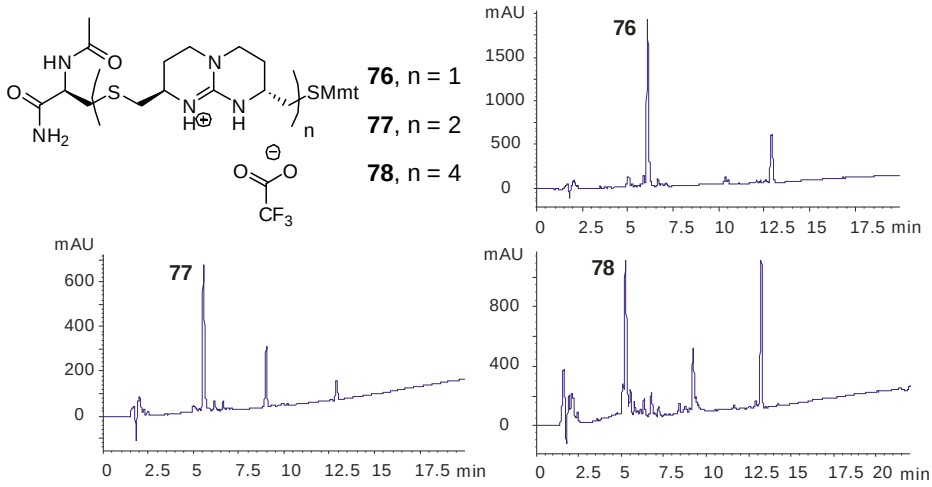

Fig. 4.43: Crude profiles of crude compounds **76**-**78**.

As confirmed by LC-MS, in each case, the major peak corresponded to the expected compound. At this point, several aspects are difficult to understand: first we were unable to identify the capping subproducts on analytical HPLC, second aromatic signals from 4-methoxytrityl were integrating comparatively more than the rest of the signals in ^{1}H-NMR spectra, and third many difficulties were encountered during the purification procedures. At this point we performed a negative control to discard partial deprotection of Mmt at the cleavage conditions (Fig. 4.44).

a)

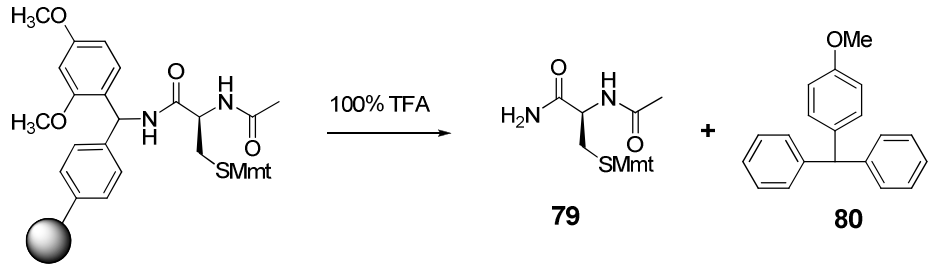

b)

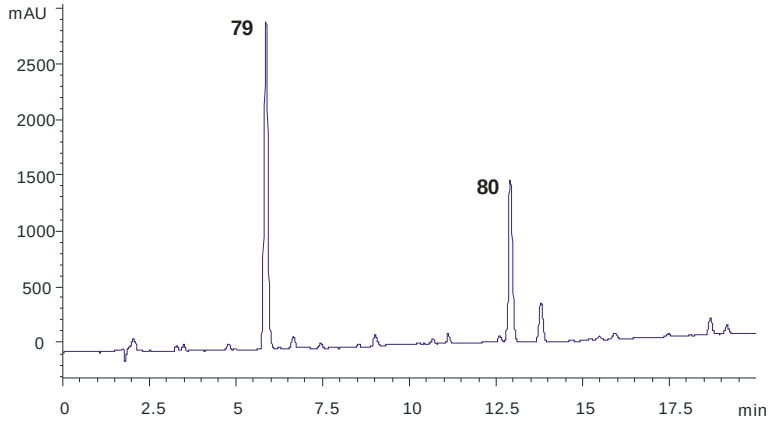

Fig. 4.44: (a) Reaction scheme and (b) HPLC profile of crude compound **79**, showing 4-methoxytrityl residues in the cleavage crude.

The appearance of a peak at 13.1 min, revealed that partial Mmt deprotection was taking place in the absence of scavenger TIS, which makes sense since TIS leads cleavage to completion but TFA is the actual cleavage agent.

Likely, if deprotection of Mmt was taking place, oligomeric subproducts, not visible in the UV-chromatograms due to the intensity of Mmt as fluorophore, were actually generating. Therefore two more steps to the synthetic strategy were added, consisting of hydrolyze the final Mmt and

coupling a non hydrolizable group, e.g. benzylbromide, before the final cleavage, (Fig. 4.45).

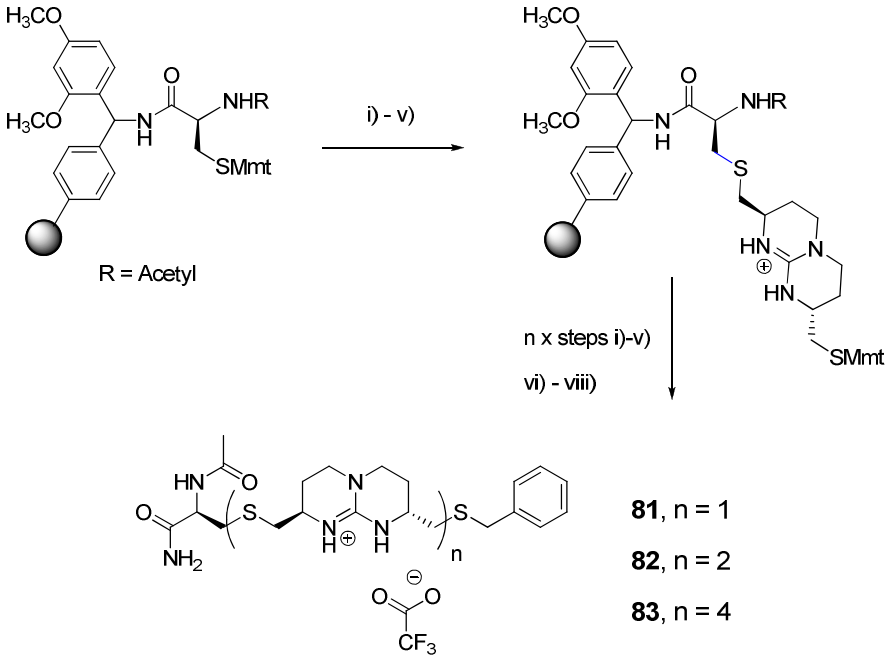

i) 5% TIS, 5% TFA in CH_2Cl_2. ii) DTT. iii) BB **18**, K^{t}BuO. iv) = ii). v) BnBr, Et_3N. vi) = i). vii) = v). viii) 100% TFA.

Fig. 4.45: Improved synthetic strategy to avoid partial Mmt deprotection (DTT treatments omitted).

The same procedure was repeated several times and aliquots were taken for cleavage after the first, the second and the fourth coupling (Fig. 4.46).

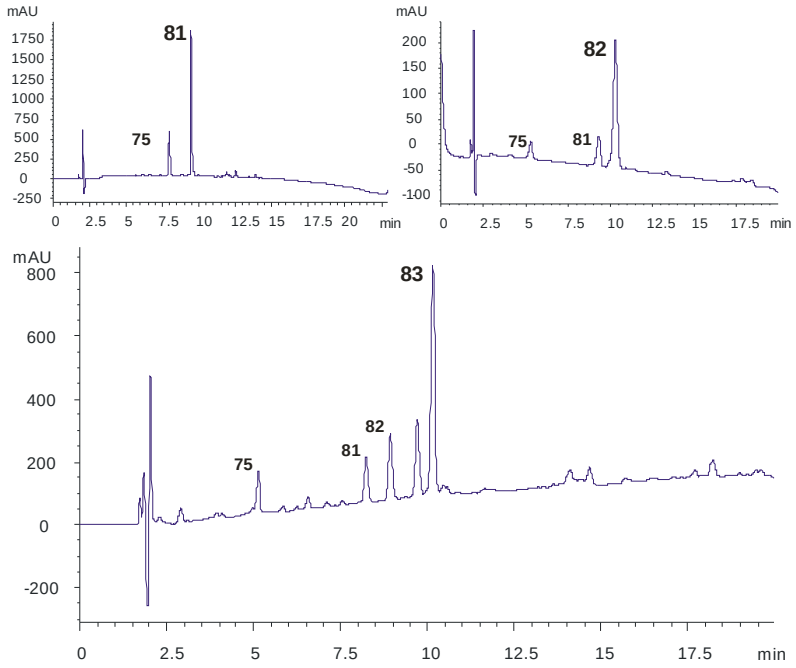

Fig. 4.46: Crude profiles of compounds **81-83**, UV_{210} (Conds: 20-50% CH_3CN in H_2O with 0.1% TFA in 17 min, UV_{210}).

The products were purified by semi-preparative HPLC and obtained in the following final yields: **81** (33%), **82** (21%) and **83** (12%) (see Appendix, Figs. A4.2-A4.4).

According to HPLC chromatograms in Fig. 4.46, conversion at each step was ≥75%. Therefore all intermediate products were identified as minor peaks in crude compound **83**.

The coupling yield might be improved by repeating the coupling step for a second time after DTT treatment. However, in view of the easy purification of the final product and the synthetic difficulty of preparing BB **18**, a single coupling followed by a capping step was preferred.

Alternatively, we tried to recover it from the reaction mixture, but ESI(+) and ^{1}H-NMR analysis of the final reaction mixture showed that the content of non reacted BB **18** was smaller than expected. Part of BB **18** hydrolyses in the reaction mixture to its OH precursor **73** and partially reacts with DMF, thus generating a mixture of similar compounds whose separation is cumbersome (see Appendix Fig. A4.5).

To evaluate if the overall strategy was still worthwhile, several parameters were taken into account: yields of the reactions, consumption of starting material, time investment, ease and reproducibility of the protocols and last but not least, adaptability of the synthetic result to the final goal. In this case non complete coupling and non recovery of excess BB **18** was balanced by the feasibility of the protocols and the short time investment. Furthermore, semipreparative purification protocols enabled the isolation of strands of different length from the same cleavage crude. Thus this strategy may be suited to generate, in a short time, a series of oligoguanidiniums for their preliminary evaluation as internalizing vectors, whereby optimized conditions would be needed for large scale synthesis of the most promising candidates.

However, a building block endowed with two subunits of bicyclic guanidiniums would be convenient to grow faster towards longer oligoguanidiniums. Therefore a diguanidinium BB was synthesized, by applying to the diguanidinium mesyl derivative **85** the same conditions as for compound **54**, Fig. 4.47 (37).

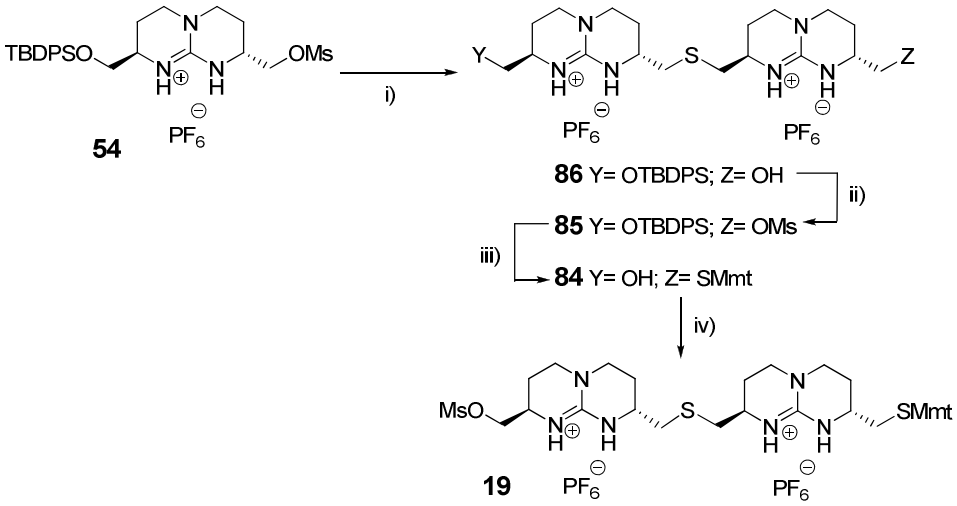

(i) a) $KSCOCH_3$, MsOH, THF/water (3:1), reflux, 24 h, $KHCO_3$ (72%); b) **54**, n-$P(Bu)_3$, Cs_2CO_3, CH_3OH/THF (2:1), rt, 5 h (70%) (**ii**) NMM, Ms_2O, dry CH_2Cl_2, rt, 2 h (85%). (**iii**) NaOMe 0.25M, SHMmt, rt-50 ºC, 18h (79%). iv) NMM, Ms_2O, dry CH_2Cl_2, rt, 2 h, (83%).

Fig. 4.47: Synthetic scheme of BB **19**.

Preliminary coupling of BB **19** was assayed on a resin functionalized with a tetraguanidinium oligomer and nucleophilic conditions were kept the same (Fig. 4.48).

a)

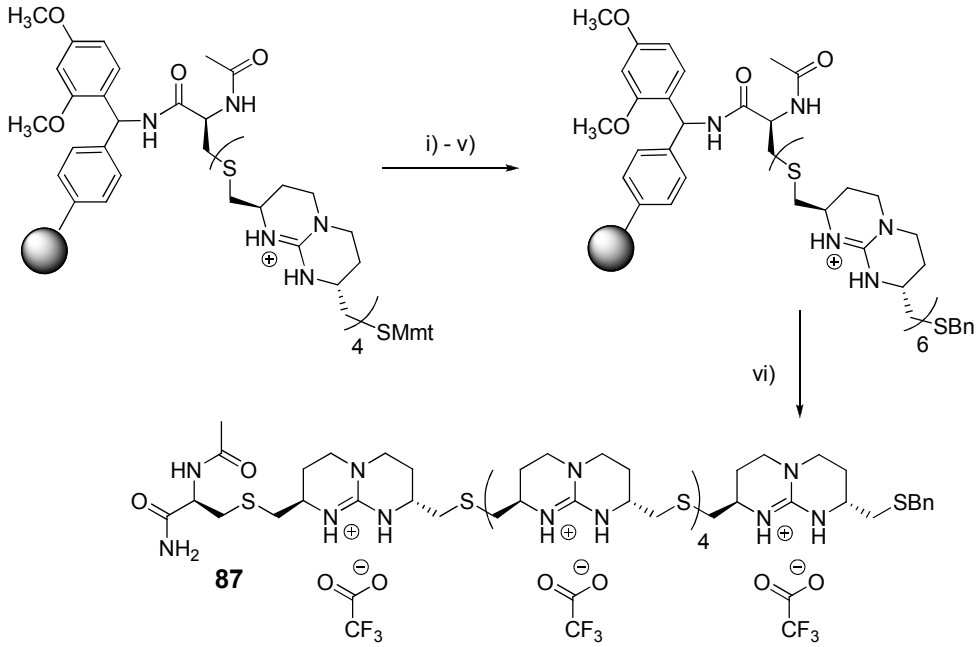

i) 5% TFA, 5% TIS, CH_2Cl_2. ii) BB **19**, K^{t}BuO. iii) BnBr, Et_3N. iv) = i). v) = iii). vi) 100% TFA.

b)

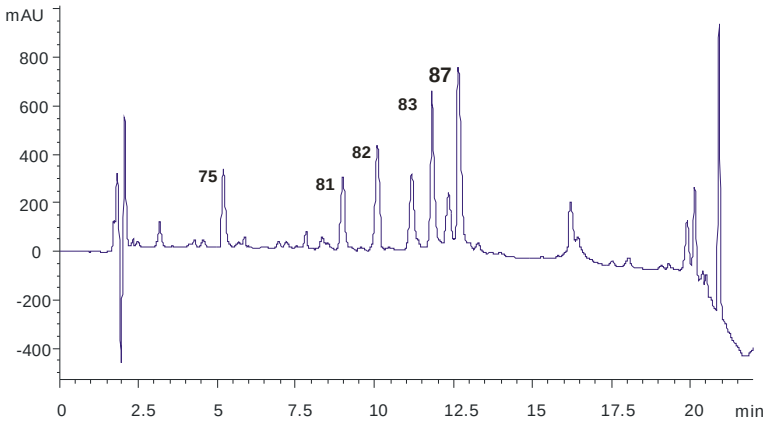

Fig. 4.48: (a) Reaction sheme of compound **87** (DTT treatments are omitted) and (b) anal. HPLC chromatogram obtained after cleavage (Conds: 20-45% CH_3CN in H_2O with 0.1% TFA in 17 min, UV_{210}).

The hexaguanidinium derivative was obtained from the tetraguanidinium precursor as confirmed by ESI(+), (see Appendix, Fig. A4.6). Apparently, coupling of BB **19** was less efficient as compared to coupling of BB **18**. However, BB **19** should be considered in the future as an alternative to BB **1** for longer oligomers.

So far, elongation of a bicyclic guanidinium was achieved on the proposed solid phase system. According to this strategy, anchorage of cargos should take place before vector elongation, as Fmoc is not compatible as a semipermanent protection of the cysteine α-amino group, because it does not survive the couping conditions.

However, introduction of the cargo should take place more conveniently at the end of the chain elongation to avoid incompatibilities with the vector synthesis. Alternatively, Alloc, which is orthogonal to Mtt and Rinkamide resin, and stable to the basic conditions used for the elongation step, was attempted.

Alloc-L-Ala-OH, obtained in two steps from H-Ala-O^{t}Bu*HCl was introduced at the Cys resin prior to incorporation of BB **1**. Once attached, Mmt was removed and nucleophilic coupling of BB **18** was performed (Fig. 4.49b and c). This Alloc-Ala-OH residue was introduced to further separate the cargo from the vector, which could facilitate cargo anchorage without disrupting the biological process.

a)

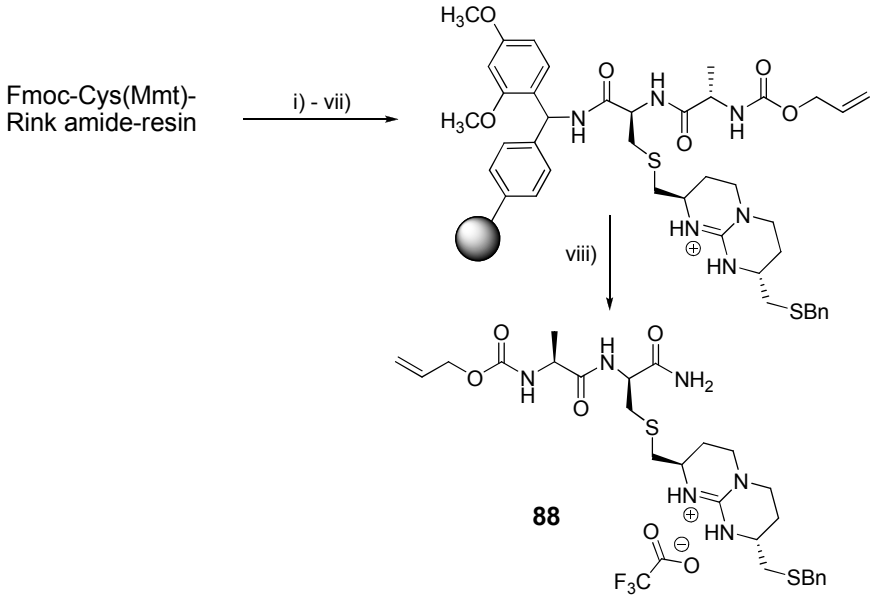

i) 20% Piperidine in DMF. ii) Alloc-Ala-OH, HOBt, DIPCDI. iii) 5% TFA, 5% TIS in CH_2Cl_2. iv) BB **18,** K^tBuO. v) BnBr, Et_3N. vi) = iii). vii) = v). viii) 100% TFA.

b)

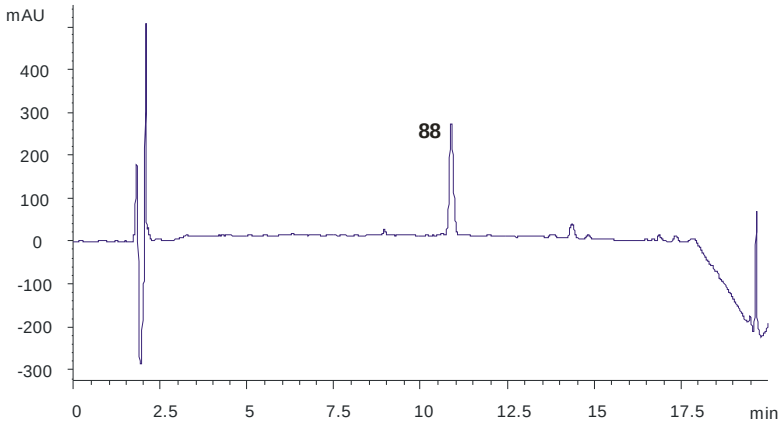

Fig. 4.49: (a) incorporation of **88** to the synthetic scheme (DTT treatments are omitted), and (b) analytical HPLC profile of crude compound **88** (Conds: 20→50% CH_3CN in H_2O with 0.1% TFA in 17 min, UV_{210}).

Figure 4.49 shows only one peak, demonstrating the stability of the Alloc protection. Finally compound **88** was purified by semipreparative HPLC (40% yield, see Appendix Fig. A4.7).

Furthermore, removal of Alloc from the solid support has been reported under inert conditions in the presence of phenyl-silane and tetrakis(triphenylphosphine)palladium, which is compatible with the guanidinium oligomer (64). This should allow the introduction of the cargo at any step of the synthetic process.

In fact, in the next section deprotection of NHAlloc in the presence of a bicyclic guanidinium unit will be described.

4.2.4. Attempt with amino acid-type BB

4.2.4.1 Objectives

Going a step further towards the mimicking of Merrifield's peptide synthesis, we considered replacing the thioether bond between bicyclic subunits with an amide bond, in collaboration with Dr. Pilar Castreño (ICIQ). We have already demonstrated that bicyclic guanidinium unit anchorage through formation of an amide bond was possible (Fig. 4.16). Next, we targeted a bifunctionalized BB with a carboxylic function on one terminus and a protected amine on the other (Fig. 4.50).

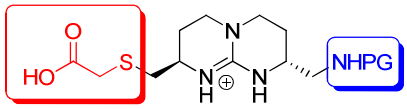

Fig. 4.50: Representation of the searched bicyclic guanidinium unit.

Synthesis of amino acid type bicyclic guanidinium 20

As amino-protecting groups three different moeties were evaluated: Fmoc, Mmt and Alloc. However, only BB **20**, bearing an Alloc moiety, was successfully obtained. Starting from the readily available mesyl compound **54**, a primary amine was incorporated by nucleophilic substitution in aqueous ammonia (**91**). Next, the free amine was functionalized with Alloc with allylchloroformate reagent and precursor **90** was obtained (65). Thereafter the silyl group (OTBDPS) was removed to activate the alcohol

again as mesyl. Finally the mercaptoacetic acid moiety was linked through nucleophilic substitution, which led to final compound **20** (Fig. 4.51).

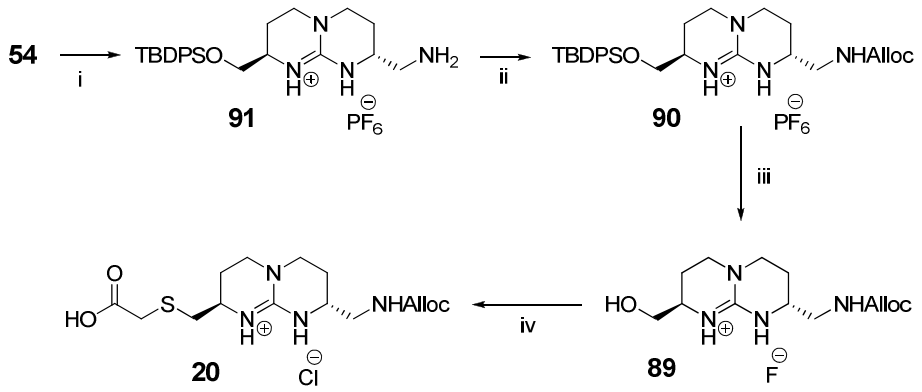

i) 30% NH_4^+ in CH_3OH, rt, 1 h, quant. ii) Allylchloroformate, $NaHCO_3$, 1,4-dioxane/H_2O, 0 ºC-rt, 1 h, 93%. iii) CsF, THF, rt, 24 h, quant.. iv) a) MsCl, dist. Et_3N, dry CH_2Cl_2 and THF (1:3), inert atm, rt, 18 h; b) Mercaptoacetic acid, K^tBuO, dry THF, rt, 4 h, 54%.

Fig. 4.51: Synthetic scheme for BB **20**.

4.2.4.2 Results and discussion

The Alloc-protected BB **20** was successfully coupled to NH_2-Cys(Mmt)-Rink amide-MBHA resin with DIPCDI/HOBt as coupling agents, while amide under HATU/PyBOP conditions failed (data not shown). Removal of the Alloc group was performed as described (24) and monitored by the ninhydrine test. Next, classical acetylation of primary amines and final cleavage of the product, led to the crude profile represented in Fig. 4.52. Finally compound **92** was purified by semi-preparative HPLC (see Appendix Fig. A4.8).

a)

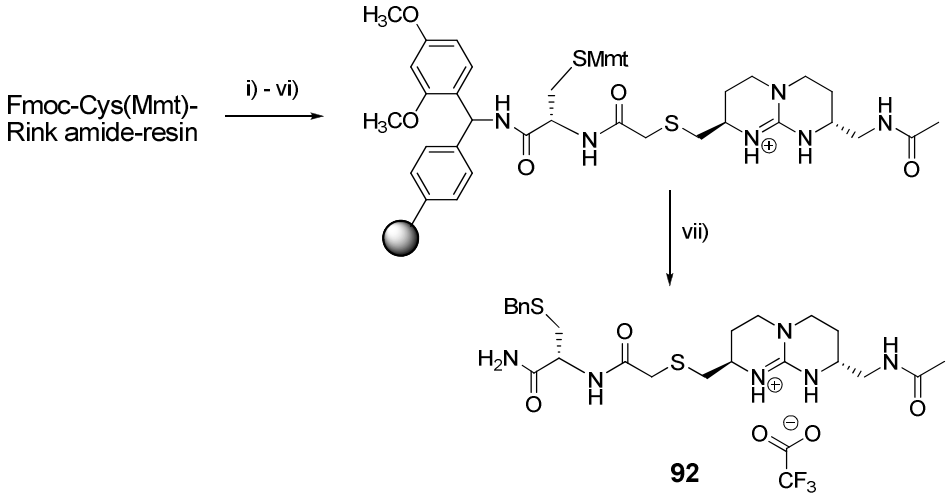

i) 20% Piperidine in DMF. ii) **20**, HOBt, DIPCDI. iii) $Pd(Ph)_3)_4$, $PhSiH_2$. iv) Ac_2O, D*i*PEA. v) 5% TIS, 5% TFA, CH_2Cl_2. vi) BnBr, Et_3N. vii) 100% TFA.

b)

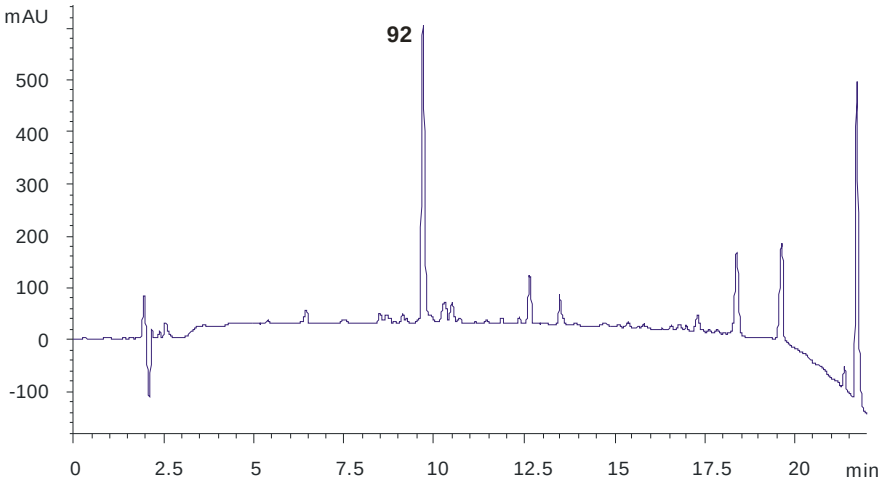

Fig. 4.52: (a) Synthesis of **92** (top) and (b) anal. HPLC profile of crude compound **92** (bottom) (Conds: 5-60% CH_3CN in H_2O with 0.1 % TFA in 17 min, 60-95% in 3 min, UV_{210}).

Finally compound **92** was purified by semi-preparative HPLC (see Appendix, Fig. A4.8).

This attempt shows that classical procedures from Fmoc synthesis, such as amide coupling, NHAlloc deprotection and amine capping by acetylation, are compatible with bicyclic guanidinium scaffolds. This opens the possibility to prepare guanidinium containing oligomers through amino acid building blocks (Fig. 4.53) and/or branched oligomers through two different chemistries.

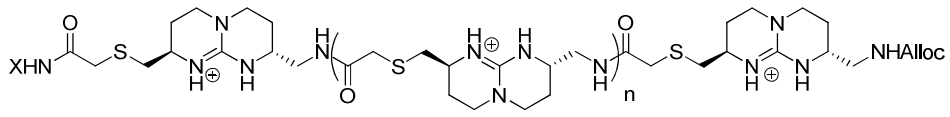

X: linker

n = 0, 1, 2, 3, 4...

Fig. 4.53: New strands of bicyclic guanidinium based on amino acid BB **20**.

Compared to strands bound by thioether bridges, these chains have more flexible linkers. In the context of GRTs, flexibility is associated to increased internalization rates (66), so these new bicyclic guanidinium oligomers constitute promising targets for drug delivery.

4.3 Conclusions and outlook

In this chapter we have described the solid phase synthesis of polythioether oligomers based on bicyclic guanidinium subunits, with the ultimate goal to design libraries of diverse bicyclic GRTs.

The iterative coupling of thioether-bound bicyclic guanidniniums was assayed with different molecules, supports and reactions. The first attempt was useful to tune cleavage and analytical conditions for the bicyclic guanidinium scaffold. However, this strategy was hampered by several obstacles that prompted the use of new strategies, based on difunctionalized building blocks **17** and **18**.

Iterative anchorage of BB **17** on commercially available thiol 4-methoxytrityl resin failed, probably due to partial anchorage and high initial functionalization of the starting resin. Better results may be achieved by lowering the initial number of exposed thiols with, *i.e. via* acylation -which has been reported to form thioesters with quantitative yield- (67), and by improving nucleophilic coupling conditions.

The third strategy, based on an Cys(Mmt)-Rink amide-MBHA support, provided for both the guanidinium moiety coupling *via* thioether formation and cargo attachment through the α-amino group. The key of this strategy was the use of a BB with a protected function, in combination with the presence of another function carrying a semipermanent protecting group for

the incorporation of the cargo, as well as a compatible resin as a permanent protecting group.

So far, high, but not quantitative yields, have been achieved with a reaction sequence which includes: i) reduction treatments with dithiothreitol before nucleophilic coupling to ensure the reduced state of the thiols, ii) a capping reaction based on benzyl bromide incorporation and iii) NHAlloc as semipermanent group for α-amino protection.

To the best of our knowledge, this constitutes the first example of solid-phase synthesis of thioethers conceptually following the Merrifield approach, in just two steps by removal of a protecting group and incorporation of the building block. So far, this synthesis is suited to generate a versatile series of bicyclic guanidinium strands, varying in linkage, oligomer length and chemical nature of the cargo, to be evaluated in future preliminary transfection assays.

Furthermore, we tested standard SPPS protocols for their use on an amino acid type bicyclic guanidinium scaffold. Preliminary results are promising and point to the development of new oligomeric compounds based on more flexible amide linkers. Interestingly, BB **20** and related compounds may be applied to any SPPS. In fact, their incorporation in artificial peptides could provide with new chemical properties affording strands with non natural amino acids.

4.4 Experimental part

4.4.1 Solution phase synthesis

General procedures: See section 2.8, except for:

Thiol-4-methoxytrityl resin purchased in Novabiochem, Novabiochem cat. number: 01-64-0077.

SHMmt was first purchased by Novabiochem (cat number: 01-63-0092) but it was recently discontinued. Since then it is synthesized in our lab as described herein.

(2*R*,8*R*)-2-*tert*-butyldiphenylsilanoxymethyl-8-hydroxymethyl-3,4,6,7,8,9-hexahydro-2*H*-pyrimido[1,2-*a*]pyrimidin-1-ium hexafluorophosphate (55).

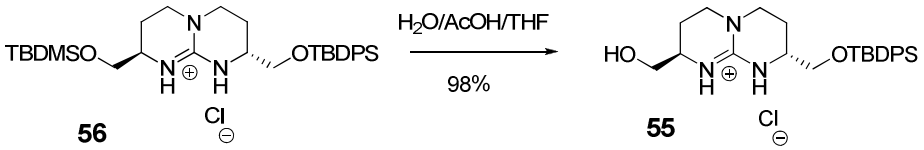

A solution of **56** (6.00 g, 10.20 mmol) in H_2O/AcOH/THF (1:3:1, 150 mL) was stirred for 20 h at rt. After removing the solvent, the crude was dissolved in CH_2Cl_2 (150 mL) and washed subsequently with saturated solutions of Na_2CO_3 (100 mL) and NH_4Cl (3 × 100 mL). The organic phase was dried (Na_2SO_4) and after evaporating the solvent, the remaining oil was triturated with toluene/diethyl ether at 4 °C, resulting in **55** as a colorless solid in a 98% yield. Mp: 130-132 °C. $[\alpha]^{20}_D$ - 42 (*c* = 0.85, $CHCl_3$). ^{1}H NMR ($CDCl_3$) δ 9.23 (s, 1H, NH), 7.78 (s, 1H, NH), 7.67-7.63 (m, 4H, ArH), 7.46-7.40 (m, 6H, ArH), 3.83 (dd, *J* = 3.5, 12.5 Hz, 1H, CH_2OSi),

3.73 (dd, *J* = 5.2, 12.5 Hz, 1H, CH_2OSi), 3.63-3.47 (m, 4H, CH_2O, CHα), 3.36-3.21 (m, 4H, $CH_2\gamma$), 2.13-1.86 (m, 5H, OH, $CH_2\beta$), 1.07 (s, 9H, $C(CH_3)_3$). ^{13}C NMR ($CDCl_3$) δ 151.2 (CGuan) 135.5, 135.4 (CAr), 132.6, 129.8, 128.9, 127.8 (CHAr), 65.3, 63.7 (CH_2O), 50.6, 49.3 (CHα), 45.6, 44.6 ($CH_2\gamma$), 26.7 ($C(CH_3)_3$), 22.7 ($CH_2\beta$), 19.1 ($C(CH_3)_3$). ESI(+) *m/z* [M + H - HCl] : 474.5. Anal. Calcd. for $C_{25}H_{36}N_3O_2SiCl$: C 62.9, H 7.7, N 8.5; found C 63.3, H 7.65, N 8.9.

The chloride anion of the resulting product could be changed into the hexafluorophosphate by dissolving 4 g (1.7 mmol) in CH_2Cl_2 (100 mL) and washing with a 2M KOH solution (2 × 50 mL) and subsequently with 0.1M NH_4PF_6 (2 × 50 mL).

(2*R*,8*R*)-2-*tert*-butyldiphenylsilanoxymethyl-8-methanesulfonyloxymethyl-3,4,6,7,8,9-hexahydro-2*H*-pyrimido[1,2-*a*]-pyrimidin-1-ium hexafluorophosphate (54).

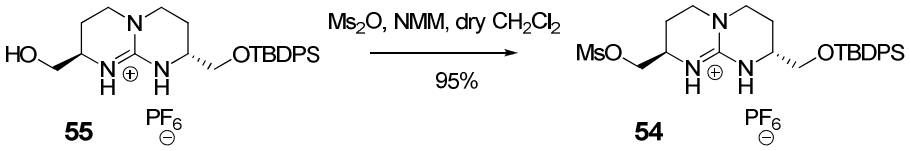

To a solution of alcohol **55** (400 mg, 0.75 mmol) in dry CH_2Cl_2 (20 mL) was added methanesulfonic anhydride (Ms_2O, 336 mg, 1.88 mmol) in dry THF (5 mL). The mixture was treated with *N*-methylmorpholine (NMM: 330 µL, 3.00 mmol) and stirred for 2 h at rt. The organic solution was washed with a 0.1M NH_4PF_6 solution (2 × 30 mL), filtered over cotton and concentrated *in vacuo*. Purification by column chromatography on silica gel (eluent: CH_2Cl_2/CH_3OH, 98:2) afforded **54** as a colorless solid in a 98%

yield. Mp 60-63 °C. $[\alpha]^{25}_{D}$ - 43 (*c* = 0.5, $CHCl_3$). ^{1}H NMR ($CDCl_3$) δ 7.63 (m, 4H, ArH), 7.62 (m, 6H, ArH), 6.24 (s, 1H, NH), 6.08 (s, 1H, NH), 4.30 (m, 1H, CH_2OMs), 4.17 (m, 1H, CH_2OMs), 3.80 (m, 1H, CHα), 3.65 (m, 2H, CH_2OSi), 3.57 (m, 1H, CHα), 3.33 (m, 4H, CH_2γ), 3.08 (s, 3H, CH_3-OMs), 2.05-1.89 (m, 4H, CH_2β), 1.06 (s, 9H, $C(CH_3)_3$). ^{13}C NMR ($CDCl_3$) δ 150.6 (CGuan), 135.5 (CAr), 132.5, 130.0, 128.9 (CHAr), 69.5 (CH_2OMs), 66.2 (CH_2OSi), 50.1, 47.7 (CHα), 45.3, 44.9 (CH_2γ), 37.1 (CH_3), 26.7 ($C(CH_3)_3$), 22.4, 21.9 (CH_2β), 19.1 ($C(CH_3)_3$). Exact Mass *m/*z $[M + H - HPF_6]^+$: calc.: 516.2352 uma; found 516.2354 uma.

(2*R*,8*R*)-2-*tert*-butyldiphenylsilanoxymethyl-8-carboxymethylsulfanylmethyl-3,4,6,7,8,9-hexahydro-2*H*-pyrimido[1,2-*a*]pyrimidin-1-ium chloride (15).

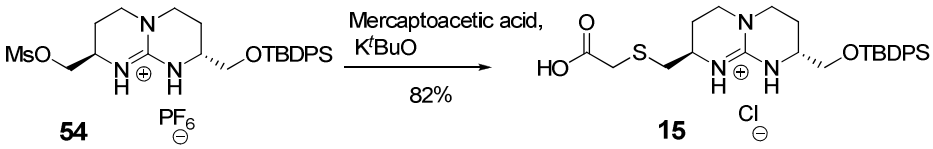

To a stirred solution of **54** (680 mg, 1.03 mmol) in dry THF (50 mL) was added a solution of sodium mercaptoacetic acid (363 mg, 3.08 mmol) and K^{t}BuO (341 mg, 2.88 mmol) in CH_3OH (20 mL). The resulting mixture was stirred for 4 h at rt. The solvent was removed, and the solid residue dissolved in CH_2Cl_2 (100 mL), washed with 1N $NaHCO_3$ (100 mL), water (100 mL), 1M HCl (100 mL) and then dried over Na_2SO_4. After filtration and evaporation the residue was triturated in EtAcO to afford **15** as a colorless solid in a 82% yield. Mp: 166-168 °C. $[\alpha]^{25}_{D}$ - 50 (*c* = 0.5, CH_3OH). ^{1}H NMR ($CDCl_3$) δ 8.27 (s, 1H, NH), 8.16 (s, 1H, NH), 7.65-7.60

(m, 4H, ArH), 7.41-7.39 (m, 6H, ArH), 3.77 (dd, *J* = 4.0, 11.0 Hz, 1H, CH_2OSi), 3.59 (m, 3H, CH_2OSi, CHα), 3.43 (d, *J* = 15.0 Hz, 1H, SCH_2CO), 3.36 (d, *J* = 15.0 Hz, 1H, SCH_2CO), 3.28-3.23 (m, 4H, $CH_2\gamma$), 2.95-2.71 (m, 2H, CH_2S), 2.12-1.85 (m, 4H, $CH_2\beta$), 1.07 (s, 9H, $C(CH_3)_3$). ^{13}C NMR ($CDCl_3$) δ 171.9 (CO), 150.9 (CGuan), 135.5, 135.4 (CAr), 132.6, 129.8, 127.8 (CHAr), 65.3 (CH_2OSi), 49.3, 48.0 (CHα), 45.1, 44.7 ($CH_2\gamma$), 36.7 (CH_2S), 34.5 (SCH_2CO), 26.7 ($C(CH_3)_3$) 24.8, 22.5 ($CH_2\beta$), 19.1 ($C(CH_3)_3$). ESI(+) *m/z* [M + H - Cl]: 512.4. Anal. Calcd. for $C_{27}H_{38}N_3O_3SSiCl \cdot H_2O$: C 57.1, H 7.1, N 7.4, S 5.6; found C 57.5, H 6.8, N 7.3, S 5.5.

(*2R*,*8R*)-2-*tert*-butyldiphenylsilanyloxymethyl-8-acetylsulfanylmethyl-3,4,6,7,8,9-hexahydro-2*H*-pyrimido-[1,2-*a*]-pyrimidin-1-ium hexafluorophosphate (16).

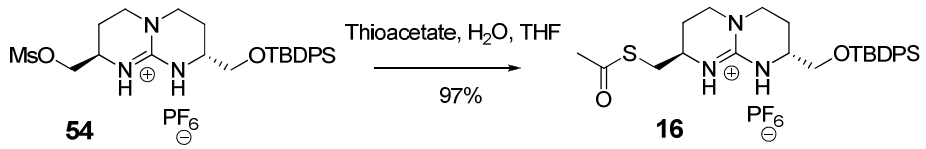

A solution of compound **54** (60 mg, 0.09 mmol) and potassium thioacetate (32 mg, 0.27 mmol) in CH_3CN (4 mL) was placed in a 6 mL sealed tube. The reaction mixture was stirred and heated with microwaves at 140 ºC for 10 min (200 W, max. 300 PSI). After cooling to rt the solvent was evaporated. The resulting crude was dissolved in CH_2Cl_2 and washed with 0.1M NH_4PF_6 (2 × 10 mL). The organic phase was filtered over cotton and concentrated *in vacuo* to give a crude residue which was purified by column chromatography on silica gel (eluent: CH_2Cl_2/CH_3OH,

99.5:0.5→98:2), affording **16** as a colorless solid in a 97% yield. Mp: 98-100 °C. $[\alpha]^{25}_{D}$ - 42 (*c* = 0.3, $CHCl_3$). ^{1}H NMR ($CDCl_3$) δ 7.61-7.58 (m, 4H, ArH), 7.40-7.35 (m, 6H, ArH), 6.10 (s, 1H, NH), 6.08 (s, 1H, NH), 3.63-3.62 (m, 2H, CH_2O), 3.52-3.50 (m, 2H, CHα), 3.38-3.25 (m, 4H, $CH_2\gamma$), 3.04 (dd, *J* = 6.1, 14.3 Hz, 1H, CH_2S), 2.98 (dd, *J* = 6.7, 14.3 Hz, 1H, CH_2S), 2.34 (s, 3H, CH_3CO), 2.07-1.96 (m, 2H, $CH_2\beta$), 1.89-1.81 (m, 2H, $CH_2\beta$), 1.04 (s, 9H, $C(CH_3)_3$). ^{13}C NMR ($CDCl_3$) δ 195.8 (CO), 150.8 (CGuan), 135.6, 134.4 (CAr), 132.6, 130.1, 127.9 (CHAr), 65.4 (CH_2O), 49.7, 48.5 (CHα), 45.1, 45.0 ($CH_2\gamma$), 32.5 (CH_2S), 30.5 (CH_3CO), 26.8 ($C(CH_3)_3$), 24.5, 22.7 ($CH_2\beta$), 19.2 ($C(CH_3)_3$). Exact Mass *m/z* [M + H - HPF_6]$^+$: calc.: 496.2454; found 496.2429 uma.

(*2R*,*8R*)-2-*tert*-butyldiphenylsilanyloxymethyl-8-chloromethyl-3,4,6,7,8,9-hexahydro-2*H*-pyrimido-[1,2-*a*]-pyrimidin-1-ium hexafluorophosphate (66).

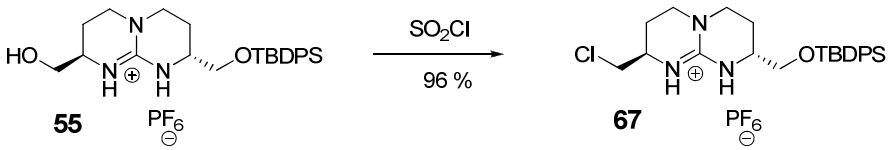

55 **67**

A solution of alcohol **55** (133.5 mg, 0.282 mmol) in $SOCl_2$ (3.0 mL) and pyridine (0.5 mL) was refluxed under for 3 h. Thereafter the solvent was eliminated and the resulting oil was dissolved in CH_2Cl_2 (20 mL) and washed with a saturated solution of $NaHCO_3$ (20 mL) and with 0.1 M NH_4PF_6 (20 mL). The organic layer was dried, concentrated and purified by column chromatography on silica gel (eluent: CH_2Cl_2/CH_3OH, 97.5:2.5→95:5) to obtain pure product **67** as a colorless solid with almost

quantitative yield. Mp: 79-82 ºC. ^{1}H NMR ($CDCl_3$): δ 7.60-7.53 (m, 4H, ArH), 7.42-7.28 (m, 6H, ArH), 6.43 (bs, 1H, NH), 6.22 (bs, 1H, NH), 3.76-3.39 (m, 6H, CH_2O, CH_2Cl, CHα), 3.30-3.13 (m, 4H, $CH_2\gamma$), 2.09-1.77 (m, 4H, $CH_2\beta$), 1.00 (s, 9H, $C(CH_3)_3$). ^{13}C NMR ($CDCl_3$): 150.7 (CGuan), 135.1 (CAr), 132.2, 129.5, 127.5 (CHAr), 64.9 (CH_2O), 48.9 CH_2Cl), 45.0 (CHα), 44.3 ($CH_2\gamma$), 26.4 ($C(CH_3)_3$), 23.0, 22.3 ($CH_2\beta$), 18.7 ($C(CH_3)_3$). ESI(+) *m/z*: [M + H - HCl]: 456.2 uma.

(*2R,8R*)-2-*tert*-butyldiphenylsilanyloxymethyl-8-bromomethyl-3,4,6,7,8,9-hexahydro-2*H*-pyrimido-[1,2-*a*]-pyrimidin-1-ium hexafluorophosphate (67).

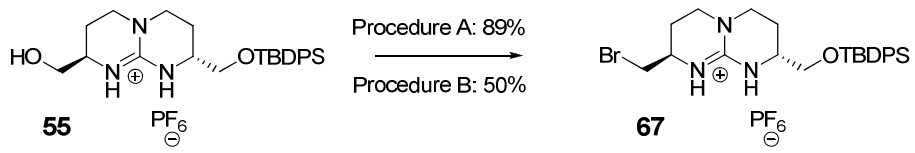

Procedure A:

A solution of alcohol **55** (0.14 g, 0.3 mmol), $P(Ph)_3$ (0.2 g, 0.76 mmol) and CBr_4 (0.25 g, 0.46 mmol) was stirred under for 24 h in dry CH_2Cl_2 (6 mL). The reaction was quenched by washing the organic phase with water (1 x 5 mL) and with 0.1 M NH_4PF_6 (2 x 5 mL). Next the organic layer was dried over Na_2SO_4 and concentrated under vaccum. The residue was purified by column chromatography on silica gel (eluent: 100% EtOAc→CH_2Cl_2/CH_3OH: 97.5:2.5→95:5) and pure product **67** was obtained as a colorless solid in a 89% yield.

Procedure B:

Alcohol **55** (30 mg, 0.063 mmol) and $Cu(OTf)_2$ (2% mol) were dissolved in 0.5 ml THF and *N*, *N'*-dicyclohexylcarbodiimide (CDI, 20 µL, 0.127 mmol) was added. The solution was stirred at rt for 3 h and the same amount of CDI was added again. The reaction was further stirred at rt for 2 h. Next, *N*-bromosuccinimide (43 mg, 0.254 mmol) was added dissolved THF (2 mL), and the reaction was refluxed for 10 h. Next, the solvent was evaporated and the crude dissolved in CH_2Cl_2 (1 mL). The organic phase was washed with 0.1 M NH_4PF_6 (2 x 1 mL), dried with Na_2SO_4, filtered and concentrated *in vacuo*. Next, the crude was purified by column chromatography on silica gel (eluent: CH_2Cl_2/CH_3OH: 97.5:2.5→95:5). Finally, **67** was obtained as a colorless solid in a 50% yield. Mp: 60-64 ºC. ^{1}H NMR (CD_3Cl): δ 7.71-7.60 (m, 4H, CHAr), 7.45-7.35 (m, 6H, CHAr), 6.42 (s, 1H, NH), 6.21 (s, 1H, NH), 3.80 (dd, *J* = 13.4, 6.7 Hz, 1H, CH_2O), 3.72-3.53 (m, 5H, CH_2O, CH_2Br, CHα), 3.32-3.20 (m, 4H, $CH_2\gamma$), 2.21-1.88 (m, 2H, $CH_2\beta$), 1.06 (s, 9H, $C(CH_3)_3$). ^{13}C NMR: δ 150.7 (CGuan), 135.3, 135.2 (CAr), 132.3, 129.7, 127.6 (CHAr), 65.0 (CH_2O), 49.1, 48.8 (CHα), 44.5, 44.4 ($CH_2\gamma$), 33.2 (CH_2Br), 26.2 ($C(CH_3)_3$), 24.0, 22.4 ($CH_2\beta$), 18.8 ($C(CH_3)_3$). ESI(+): *m/z* $[M + H - PF_6]^+$: 502.2 uma.

(*2R,8R*)-2-hydroxymethyl-8-acetylsulfanylmethyl-3,4,6,7,8,9-hexahydro-2*H*-pyrimido-[1,2-*a*]-pyrimidin-1-ium hexafluorophosphate chloride (68).

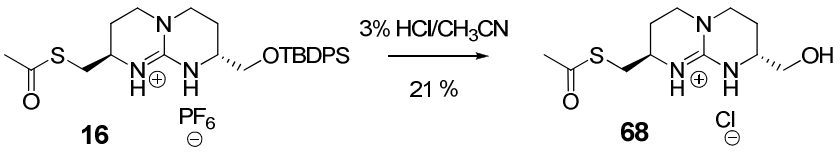

A solution of compound **16** (20 mg, 0.03 mmol) was stirred for 1 h at -5

ºC in 3% HCl-CH_3CN (1:2, 1.87 ml). The solvent was evaporated and the residue was dissolved in distilled water (8 mL). Thereafter, the aqueous phase was washed with CH_2Cl_2 (2 x 8 mL) and evaporated. Finally the residue was dried thouroughly, affording pure compound **68** as a colorless solid in a 21 % yield. ^{1}H NMR (CH_3OD): δ 3.66 (dd, J = 10.5, 3.8 Hz, 1H, CH_2O), 3.57-3.55 (m, 1H, CH_2O), 3.48-3.35 (m, 8H, CHα, $CH_2\gamma$), 3.11 (d, J = 6.1 Hz, 2H, CH_2S), 2.39 (s, 3H, CH_3COS), 2.15-2.01 (m, 2H, $CH_2\beta$), 1.91-1.76 (m, 2H, $CH_2\beta$). Exact Mass (ESI+) *m/z* $[M + H - HCl]^+$: calc.: 258.1276 uma, found: 258.1284 uma.

(2*R*,8*R*)-2-*tert*-butyldiphenylsilyloxymethyl-8-benzoylthiomethyl-3,4,6,7,8,9-hexahydro-2*H*-pyrimido[1,2-*a*]pyrimidin-1-ium hexafluorophosphate (69).

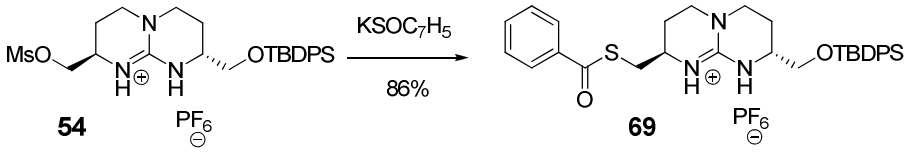

Mesyl precursor **54** (150 mg, 0.227 mmol) was dissolved in CH_3CN (3 mL) and introduced into a microwave tube to which potassium thiobenzoate (0.06 mg, 0.34 mmol) was added. The reaction was heated at 140 ºC (200 W, max. 300 PSI) for 10 min. Thereafter salts were filtered and solvent was evaporated. The resulting solid was dissolved in CH_2Cl_2 (5 mL) and the organic phase was washed with water (2 x 5 mL) and 0.1M NH_4PF_6 (2 x 5 mL). The organic layer was filtered over cotton and the solvent was concentrated *in vacuo*. Column chromatography on silica gel (eluent: CH_2Cl_2/ CH_3OH, 100:0→96:4) afforded pure product **69** as a colorless

solid in a 86% yield. $[\alpha]^{20}_{D}$: + 20.1 (*c* = 0.5, CH_3CN, st. dev.: 0.7). Mp: 70-72 ºC. ^{1}H NMR (CH_3OD): δ 7.96 (d, *J* = 8.2 Hz, 2H, ArH-COS), 7.66-7.62 (m, 4H, ArH-Si), 7.59 (d, 1H, *J* = 7.6 Hz, ArH-COS), 7.49-7.39 (m, 8H, ArH-COS, ArH-Si), 6.42 (s, 1H, NH), 6.21 (s, 1H, NH), 3.74-3.64 (m, 3H, CH_2O, CHα), 3.62-3.54 (m, 1H, CHα), 3.50-3.42 (m, 1H, $CH_2\gamma$), 3.38-3.29 (m, 4H, $CH_2\gamma$, CH_2S), 3.24 (dd, *J* = 5.6, 14.0 Hz, 1H, CH_2S), 2.16-2.06 (m, 1H, $CH_2\beta$), 2.06-1.98 (m, 1H, $CH_2\beta$), 1.97-1.87 (m, 2H, $CH_2\beta$), 1.07 (s, 9H, $CH_3{}^t$Bu). ^{13}C NMR (CH_3OD): δ 150.4 (CGuan), 135.6 (CAr), 135.5, 134.0 (CHAr), 133.6 (CAr), 130.1, 128.8, 128.0, 127.5 (CHAr), 65.5 (CH_2O), 50.1 (*C*HαCH$_2$O), 49.1 (*C*HαCH$_2$S), 45.4, 45.3 ($CH_2\gamma$), 32.2 (CH_2S), 26.8 (C(*C*H$_3$)$_3$), 24.4, 22.6 ($CH_2\beta$), 19.2 (*C*(CH$_3$)$_3$). Exact Mass *m/z* [M + H - HPF_6]$^+$: calc.: 558.2611 uma, found: 558.2585 uma.

(2*R*,8*R*)-2-methylsulfonyloxymethyl-8-benzoylthiomethyl-3,4,6,7,8,9-hexahydro-2*H*-pyrimido[1,2-*a*]pyrimidin-1-ium hexafluorophosphate (17).

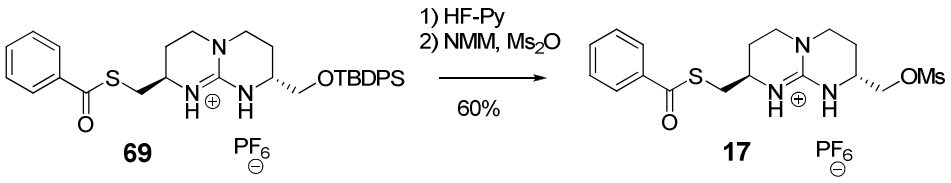

To a solution of compound **69** (331 mg, 0.470 mmol) in THF (25 mL) at 0 ºC, was added dropwise HF-Pyridine (2.2 mL). The reaction was stirred for 10 h at rt. The solvent was removed and the remaining residue was dissolved in CH_2Cl_2 (10 mL). Next, the organic layer was washed with water (2 x 10 mL) and with 0.1M NH_4PF_6 (2 x 10 mL). The organic layer

was dried over anhydrous Na_2CO_3, filtered and evaporated *in vacuo*. Next, the remaining solid was dissolved in CH_2Cl_2 (10 mL), and NMM (0.205 mL, 1.88 mmol) and Ms_2O (205 mg, 1.18 mmol) were added. After stirring at rt for 2 h, the organic layer was washed with water (2 x 5 mL) and with 0.1M NH_4PF_6 (2 x 5 mL). Finally, the residue was precipitated in $CHCl_3$ and pure compound **17** was obtained as a colourless solid in a 61% yield. $[\alpha]^{20}_D$: - 90.94 (*c* = 0.5, CH_3CN, stand. dev.: 0.5). Mp: 170-174 ºC. ^{1}H NMR (CD_3CN): δ 8.02 (d, *J* = 8.4 Hz, 2H, ArH-S), 7.71 (tr, *J* = 7.3 Hz, 1H, ArH-S), 7.57 (tr, *J* = 7.9 Hz, 2H, ArH-S), 6.24 (d, *J* = 13.9 Hz, 2H, NH), 4.29 (dd, *J* = 4.3, 10.5 Hz, 1H, CH_2O), 4.13 (dd, *J* = 7.3, 10.3 Hz, 1H, CH_2O), 3.83-3.76 (m, 1H, C*H*αCH_2O), 3.74-3.67 (m, 1H, CHαCH_2S), 3.47-3.27 (m, 6H, $CH_2\gamma$, CH_2S), 3.09 (s, 3H, CH_3), 2.19-2.06 (m, 2H, $CH_2\beta$), 2.00-1.85 (m, 2H, $CH_2\beta$). ^{13}C NMR (CD_3CN): δ 191.1 (CO), 150.6 (CGuan), 136.6 (CAr), 134.3, 129.1, 127.3 (CHAr), 70.8 (CH_2O), 48.6 (*C*HαCH_2O), 47.6 (*C*HαCH_2S); 44.5 ($CH_2\gamma$); 36.8 (CH_3SO_3), 32.6 (CH_2S), 24.2, 21.7 ($CH_2\beta$). Exact Mass (ESI+) *m/z* $[M + H - HPF_6]^+$: calc.: 398.1208 uma, found: 398.1208 uma.

General procedure for the synthesis of compounds 70-72.

To a solution of 0.25 M $NaOCH_3$ (25 eq.), the appropriate mercaptane (2.5 eq.) was added and stirred for 20 min. Thereafter, compound **54** (1 eq.) was added dissolved in CH_3OH and the reaction mixture was stirred at rt for 5 h. After evaporation of the solvent, the remaining residue was dissolved in CH_2Cl_2 and the organic phase was washed with water and with 0.1M NH_4PF_6, dried over anhydrous Na_2CO_3, filtered and concentrated at reduced pressure. Purification of the crudes was achieved by column

chromatography on silica gel with the respective eluents.

(2*R*,8*R*)-2-*tert*-butyldiphenylsilanoxymethyl)-8-benzylthiomethyl-3,4,6,7,8,9-hexahydro-2*H*-pyrimido[1,2-*a*]pyrimidin-1-ium hexafluorophosphate (70).

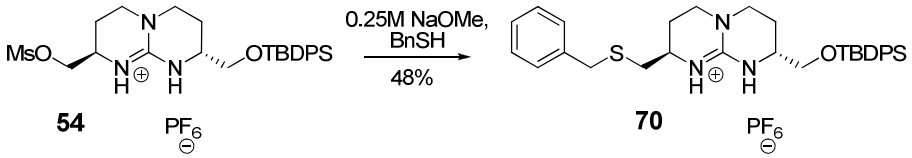

Prepared following the described procedure in 0.25M NaOMe (3 mL), with benzylmercaptane (9 µl, 0.076 mmol) and compound **54** (20 mg, 0.03 mmol), dissolved in CH_3OH (0.5 mL). Purification by column chromatography on silica gel (eluent: CH_2Cl_2/CH_3OH, 100:0→98:2) afforded **70** as a light yellow oil in a 48% yield. ^{1}H NMR (CD_3Cl): δ 7.68-7.62 (m, 4H, CHArSiO), 7.49-7.40 (m, 6H, CHArSi), 7.36-7.31 (m, 4H, CHAr-BnS), 7.25 (m, 1H, CHAr-BnS), 6.21 (s, 1H, NH), 6.07 (s, 1H, NH), 3.75 (m, 2H, SCH_2Ph), 3.73-3.63 (m, 2H, CH_2O), 3.57-3.49 (m, 1H, CHα), 3.41-3.33 (m, 1H, CHα), 3.31-3.20 (m, 4H, $CH_2\gamma$), 2.68 (dd, J = 4.4, 13.7 Hz, 1H, CH_2S), 2.56 (dd, J = 7.6, 13.7 Hz, 1H, CH_2S), 2.10-1.94 (m, 2H, $CH_2\beta$), 1.94-1.77 (m, 2H, $CH_2\beta$), 1.08 (s, 9H, $C(CH_3)_3$). ^{13}C NMR (CD_3Cl): δ 149.8 (CGuan), 135.5 (CAr), 134.9 (CAr), 134.4, 130.6, 130.3, 129.6, 129.6, 128.7, 128.0, 127.3 (CHAr), 65.5 (CH_2O), 48.1 (CHαCH_2O), 47.9 (CHαCH_2S), 45.4, 45.0 ($CH_2\gamma$), 36.9 (CH_2S), 35.8 (SCH$_2$Ph), 26.8 (C(CH_3)$_3$), 24.8, 22.6 ($CH_2\beta$), 19.2 ($C(CH_3)_3$). ESI(+) m/z [M + H - HPF_6]$^+$: 544.2.

(2*R*,8*R*)-2-*tert*-butyldiphenylsilyloxymethyl-8-tritylthiomethyl-3,4,6,7,8,9-hexahydro-2*H*-pyrimido[1,2-*a*]pyrimidin-1-ium hexafluorophosphate (70).

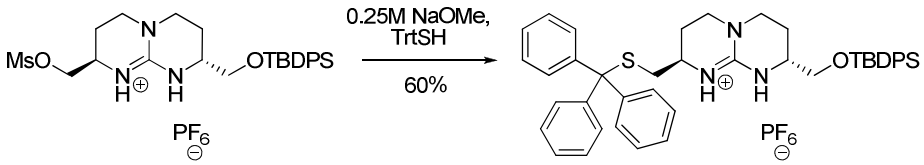

54 **70**

Prepared following the described procedure in 0.25M NaOMe (15 mL), with tritylmercaptane (TrtSH, 104 mg, 0.38 mmol) and compound **54** (100 mg, 0.15 mmol), dissolved in CH_3OH (2 mL). Purification by column chromatography on silica gel (eluent: CH_2Cl_2/CH_3OH, 100:0→99.5:0.5) afforded **70** as a yellow solid in a 60% yield. ^{1}H NMR (CD_3Cl): δ 7.62-7.57 (m, 4H, CHArSiO), 7.44-7.35 (m, 11H, CHArSiO, CHAr-Trt), 7.32-7.19 (m, 10H, CHAr-Trt), 6.17 (s, 1H, NH), 5.99 (s, 1H, NH), 3.69-3.58 (m, 2H, CH_2O), 3.53-3.46 (m, 1H, CHα), 3.25-3.16 (m, 2H, $CH_2\gamma$), 3.12-3.03 (m, 2H, $CH_2\gamma$), 2.86-2.78 (m, 1H, CHα), 2.53-2.46 (dd, J = 5.5, 13.7 Hz, 1H, CH_2S), 2.43-2.35 (dd, J = 8.4, 13.7 Hz, 1H, CH_2S), 2.00-1.81 (m, 3H, $CH_2\beta$), 1.76-1.66 (m, 1H, $CH_2\beta$), 1.08 (s, 9H, ($C(CH_3)_3$). ^{13}C NMR ($CDCl_3$): δ 150.2 (CGuan), 144.7, 144.6, 136.5, 135.8 (CAr), 133.1), 130.8, 130.3, 129.3, 127.9, 127.5, 126.9, 113.7 (CHAr), 67.5 (C), 65.5 (CH_2O), 49.7 (CHαCH$_2$O), 48.0 (CHαCH$_2$S), 45.2, 45.1 ($CH_2\gamma$), 35.6 (CH_2S), 26.8 ($C(CH_3)_3$), 24.6, 22.5 ($CH_2\beta$), 19.2 ($C(CH_3)_3$). ESI(+) *m/z* $[M + H - HPF_6]^+$: 696.4 uma.

(2*R*,8*R*)-2-*tert*-butyldiphenylsilyloxymethyl-8-(4-methoxyphenyldiphenylmethylthiomethyl)-3,4,6,7,8,9-hexahydro-2*H*-pyrimido[1,2-*a*]pyrimidin-1-ium hexafluorophosphate (72).

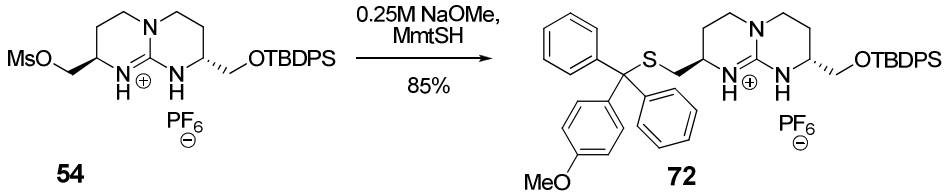

Prepared following the described procedure in 0.25M NaOMe (45 mL), with MmtSH (208 mg, 0.9 mmol) and compound **54** (400 mg, 0.6 mmol), dissolved in CH_3OH (5 mL). Purification by column chromatography on silica gel (eluent: CH_2Cl_2/CH_3OH, 100:0→99.5:0.5) afforded **72** as a yellow solid (85%). Mp: 98-100 ºC. $[\alpha]^{20}D$: - 45.7 (*c* = 0.37, CH_3CN, stand. dev.: 1.3). ^1H NMR ($CDCl_3$): δ 7.68-7.61 (m, 4H, CHAr-Si), 7.48-7.38 (m, 10H, CHAr-Si, CHAr-Mmt), 7.36-7.28 (m, 6H, CHAr-Mmt), 7.26-7.20 (m, 2H, CHAr-Mmt), 6.86 (d, *J* = 9.0 Hz, 2H, CHAr-Mmt), 6.14 (s, 1H, NH), 5.99 (s, 1H, NH), 3.81 (s, 3H, CH_3O), 3.71-3.60 (m, 2H, CH_2O), 3.53-3.46 (m, 1H, CHα), 3.29-3.16 (m, 2H, $CH_2\gamma$), 3.12-3.06 (m, 2H, $CH_2\gamma$), 2.94-2.85 (m, 1H, CHα), 2.55-2.47 (dd, *J* = 5.3, 13.1 Hz, 1H, CH_2S), 2.46-2.39 (dd, *J* = 8.4, 13.1 Hz, 1H, CH_2S), 2.00-1.81 (m, 3H, $CH_2\beta$), 1.76-1.66 (m, 1H, $CH_2\beta$), 1.08 (s, 9H, $C(CH_3)_3$). ^{13}C NMR ($CDCl_3$): δ 158.4 (CO), 150.2 (CGuan), 144.6, 144.5, 136.1, 135.6, 132.6 (CAr), 130.8, 130.1, 129.4, 128.1, 128.0, 126.9, 113.7 (CHAr), 67.1 (C), 65.5 (CH_2O), 55.3 (CH_3O), 49.9 ($CH\alpha CH_2O$), 48.1 ($CH_\alpha CH_2S$), 45.2, 45.0 ($CH_2\gamma$), 35.7 (CH_2S), 26.8 ($C(CH_3)_3$), 24.6, 22.5 ($CH_2\beta$), 19.2 ($C(CH_3)_3$).

Exact Mass ESI(+): *m/z* [M + H - HPF_6]$^+$: calc.: 726.3550, found: 726.3515.

(2*R*,8*R*)-2-methanesulfonyloxymethyl-8-(4-methoxyphenyldiphenylmethylthiomethyl)-3,4,6,7,8,9-hexahydro-2*H*-pyrimido[1,2-*a*]pyrimidin-1-ium hexafluorophosphate (18).

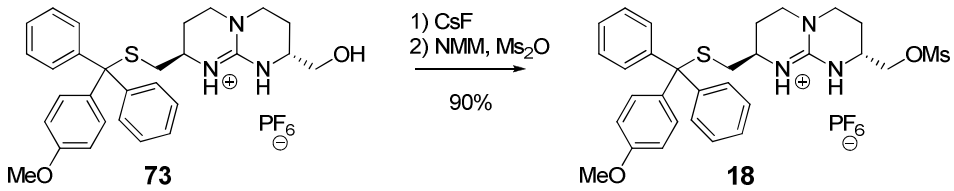

Alcohol **73** (250 mg, 0.39 mmol) was dissolved in CH_2Cl_2 (20 mL) and NMM (0.204 ml, 1.87 mmol) and then Ms_2O (0.204 g, 1.17 mmol) were sequentially added. The reaction was stirred at rt for 3 h. Next, the organic phase was washed with water (2 x 8 mL) and with 0.1 M NH_4PF_6 (2 x 8 mL). After drying the organic phase over Na_2CO_3 and filtering over cotton, the solvent was removed and the oily residue was purified by column chromatography on silica gel (eluent: 100% CH_2Cl_2→CH_2Cl_2/CH_3OH, 99.5:0.5) and pure compound **18** was obtained as a yellow solid in a 90% yield. Mp: 98-100 ºC. $[\alpha]^{20}_D$: - 12.2 (*c* = 4.42 mg/mL in CH_3CN; St. Deviation: 0.67). ^{1}H NMR (CD_3Cl): δ 7.45-7.41 (m, 4H, ArH), 7.36-7.30 (m, 6H, ArH), 7.28-7.21 (m, 2H, ArH), 6.86 (d, *J* = 9.0 Hz, 1H, NH), 6.24 (s, 1H, NH), 6.0 (s, 1H, NH), 4.29 (dd, *J* = 4.3, 10.5 Hz, 1H, CH_2O), 4.13 (dd, *J* = 7.3, 10.3 Hz, 1H, CH_2O), 3.82-3.76 (m, 1H, CHα), 3.81 (s, 3H, CH_3O), 3.37-3.29 (m, 2H, $CH_2\gamma$), 3.27-3.18 (m, 1H, CHα), 3.17-3.10 (m, 1H, $CH_2\gamma$), 3.10 (s, 3H, CH_3O), 2.94-2.85 (m, 1H, $CH_2\gamma$), 2.46 (d, *J* = 5.3 Hz, 2H, CH_2S), 2.12-2.00 (m, 1H, $CH_2\beta$), 1.99-1.87 (m, 2H, $CH_2\beta$), 1.80-

1.67 (m, 1H, $CH_2\beta$). ^{13}C NMR ($CDCl_3$): δ 158.4 (CO), 150.5 (CGuan), 144.6, 144.6, 136.2 (CAr), 130.7, 129.3, 128.1, 126.8, 113.4 (CHAr), 69.7 (CH_2O), 67.1 (C), 55.3 (CH_3O), 47.9 (*C*HαCH$_2$O), 47.4 (*C*HαCH$_2$S), 44.9 ($CH_2\gamma$), 37.2 (CH_3O), 35.8 (CH_2S), 24.4, 22.1 ($CH_2\beta$). Exact Mass (ESI+) *m/z* $[M + H - HPF_6]^+$ calc.: 566.2147 uma, found: 566.2133 uma.

(2*R*,8*R*)-2-hydroxymethyl-8-(4-methoxyphenyldiphenylmethylthiomethyl)-3,4,6,7,8,9-hexahydro-2*H*-pyrimido[1,2-*a*]pyrimidin-1-ium hexafluorophosphate (73).

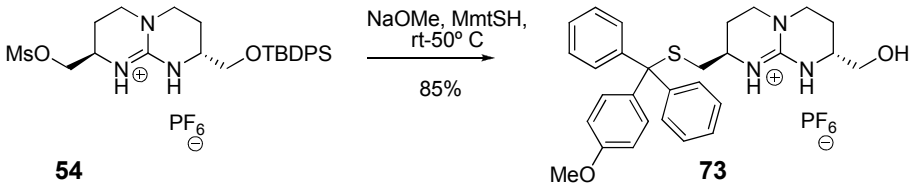

To a solution of 0.25 M NaOMe (42 ml, 10.6 mmol) was added MmtSH (280 mg, 0.91 mmol) and stirred at rt for 5 min. Thereafter, mesyl precursor **54** (280 mg, 0.42 mmol) was added dissolved in CH_3OH (5 mL) and the reaction mixture was stirred at rt for 1 h. Next, reaction was heated at 50 ºC overnight. After evaporation of the solvent, the remaining residue was dissolved in CH_2Cl_2 (15 mL) and the organic phase was washed with water (10 mL) and with NH_4PF_6 (3 x 10 mL), dried over anhydrous Na_2CO_3, filtered over cotton and concentrated at reduced pressure. Purification of the crude was performed by column chromatography on silica gel (eluent: 100% $CH_2Cl_2 \rightarrow CH_2Cl_2/CH_3OH$, 97:3). The product **73** was obtained as a colourless solid in a 85% yield. Mp: 85-95 ºC. ^1H NMR ($CDCl_3$): δ 7.42-7.40 (m, 4H, ArH), 7.35-7.7.27 (m, 6H, ArH), 7.26-7.20 (m, 2H, ArH), 6.85

(d, *J* = 8.3 Hz, 2H, ArH), 6.30 (s, 1H, NH), 6.00 (s, 1H, NH), 3.79 (s, 3H, CH_3O), 3.64-3.59 (m, 1H, CHα), 3.56-3.41 (m, 2H, CH_2O), 3.39-3.32 (m, 1H, $CH_2\gamma$), 3.21-3.11 (m, 3H, $CH_2\gamma$), 2.86-2.78 (m, 1H, CHα), 2.51-2.40 (m, 2H, CH_2S), 1.88-1.78 (m, 2H, $CH_2\beta$), 1.69-1.59 (m, 2H, $CH_2\beta$). ^{13}C NMR ($CDCl_3$): δ 158.4 (CAr), 150.4 (CGuan), 144.7, 136.2 (CAr), 130.8, 129.4, 128.1, 127.0, 113.4 (CHAr), 66.9 (C), 64.8 (CH_2), 55.3 (CH_3), 49.9 (*C*HαCH$_2$O), 47.8 (*C*HαCH$_2$S), 45.4, 44.7 ($CH_2\gamma$), 36.6 (CH_3O), 25.2, 22.2 ($CH_2\beta$). Exact Mass (ESI+) *m/z* $[M + H - HPF_6]^+$: calc.: 488.2364 uma, found: 488.2372 uma.

(4-Methoxyphenyl)diphenylmethanethiol.

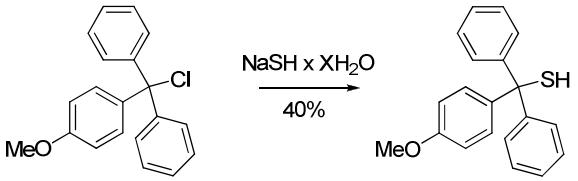

4-Methoxytrityl chloride MmtSH

The hydrated salt NaSH (1 g, aprox. 12.3 mmol) was dissolved in water (12 mL) and acetone (12 mL) under argon atmosphere and the solution was buBBled for some minutes with argon. Then, a solution of 4-Methoxytrityl chloride (1g, 3.5 mmol) was added with a canula rapidly at rt. Almost instantly a white precipitate appeared. After 45 min stirring, the solid was filtered and washed with water under inert atmosphere. After drying *in vacuo*, the product was obtained as a slightly pink solid (40% yield). ^1H NMR ($CDCl_3$): δ 7.34-7.25 (m, 10H, ArH), 7.21 (d, *J* = 8.8 Hz, 2H, ArH), 6.84 (d, *J* = 8.8 Hz, 2H, ArH), 3.83 (s, 3H, CH_3). ^{13}C NMR ($CDCl_3$): δ 158.3, 147.5, 139.5 (CAr), 130.6, 129.4, 127.8, 126.8, 113.1 (CHAr), 62.6

(C), 55.3 (CH_3). Exact Mass *m/z* [M - H]$^-$: calc.: 305.1000 uma, found: 305.1015 uma

(2*R*,8*R*)-8-[(2*R*,8*R*)-2-hydroxymethyl-3,4,6,7,8,9-hexahydro-2*H*-pyrimido[1,2-*a*]pyrimidin-2-ylmethylsulfanylmethyl-1-ium hexafluorophosphate]-8-*tert*-butyldiphenylsilanyloxymethyl-3,4,6,7,8,9-hexahydro-2*H*-pyrimido[1,2-*a*]pyrimidin-1-ium hexafluorophosphate (86).

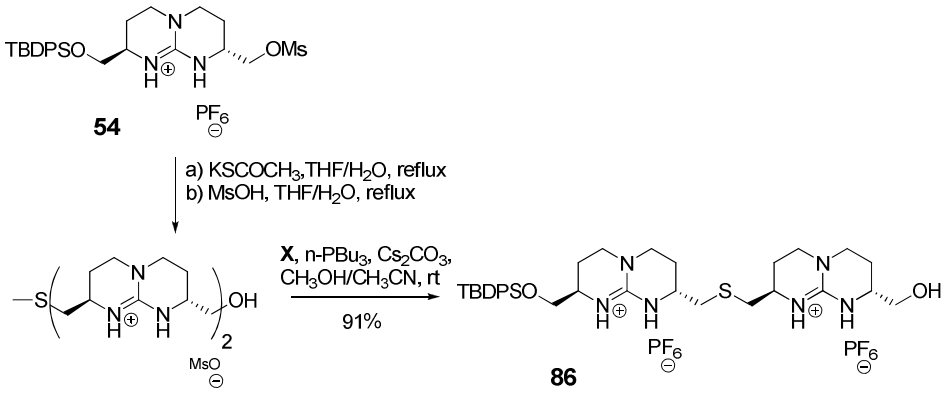

A solution of mesyl compound **54** (253 mg, 0.38 mmol) and potasium thioacetate (222 mg, 1.90 mmol) in a mixture THF/H_2O (3:1, 20 mL) was refluxed for 7 h. After cooling it to rt, MsOH (246 µL, 3.8 mmol) was added and the mixture was refluxed for 16 h. After cooling to rt, Et_2O (10 mL) were added to the solution and the aqueous phase was extracted and washed with $CHCl_3$ (2 × 20 mL) and finally with Et_2O (20 mL). After concentration of about 50% of aqueous layer, $KHCO_3$ (456 mg, 4.56 mmol) was added and the solvent evaporated to dryness. Then, CH_3OH (50 mL) was added to the residue, the precipitate was removed by filtration and the solvent evaporated under reduced pressure. This procedure was repeated several times increasing the amount of CH_2Cl_2 in the solvent mixture until pure CH_2Cl_2, resulting in a slightly yellow solid. To a solution of this

product, Cs_2CO_3 (111 mg, 0.34 mmol) in CH_3OH (20 mL) and n-PBu_3 (53.6 µL, 0.20 mmol) was added and the mixture was stirred for 40 min. Then a solution of **86** (225 mg, 0.34 mmol) in THF (5 mL) was added and the mixture was stirred for 2 h. After evaporation of the solvent, the crude residue was dissolved in CH_2Cl_2 (20 mL) and washed with a 0.1M NH_4PF_6 solution (2 × 30 mL). The organic layer was filtered over cotton and concentrated *in vacuo*. Purification by column chromatography on silica gel (eluent: CH_2Cl_2/CH_3OH, 96:4→94:6) afforded **54** as a colorless solid in a 92% yield. Mp: 100-104 °C. $[\alpha]^{25}_D$ -93 (*c* = 0.4, $CHCl_3$). ^{1}H NMR ($CDCl_3$) δ 7.64-7.24 (m, 4H, ArH), 7.43-7.38 (m, 6H, ArH), 6.47 (s, 1H, NH), 6.35 (s, 2H, NH), 6.23 (s, 1H, NH), 3.72-3.23 (m, 16H, CH_2O, CHα, $CH_2\gamma$), 2.86 (dd, *J* = 3.5, 13.7 Hz, 1H, CH_2S), 2.82 (dd, *J* = 4.0, 13.4 Hz, 1H, CH_2S), 2.65-2.63 (m, 2H, CH_2S), 2.54 (dd, *J* = 3.8, 13.6 Hz, 1H, CH_2S), 2.12-1.81 (m, 8H, $CH_2\beta$), 1.05 (s, 9H, $C(CH_3)_3$). ^{13}C NMR ($CDCl_3$): δ 150.7, 150.3 (CGuan), 135.2 (CAr), 132.7, 132.5, 129.8, 127.7 (CHAr), 65.4, 65.2 (CH_2OSi, CH_2O), 50.1, 49.8, 47.7, 47.6 (CHα), 45.3, 44.8 ($CH_2\gamma$), 36.0, 35.7 (CH_2S), 26.7 ($C(CH_3)_3$), 26.5, 25.8, 22.4, 22.2 ($CH_2\beta$), 19.1 ($C(CH_3)_3$). Exact Mass *m/z* $[M + 2H - 2HPF_6]^{2+}$: calc.: 318.1821 uma; found 318.1816 uma.

(2*R*,8*R*)-8-[(2*R*,8*R*)-2-methanesulfonyloxymethyl-3,4,6,7,8,9-hexahydro-2*H*-pyrimido[1,2-*a*]pyrimidin-2-ylmethylsulfanylmethyl-1-ium hexafluorophosphate]-8-*tert*-butyldiphenylsilanyloxymethyl-3,4,6,7,8,9-hexahydro-2*H*-pyrimido[1,2-*a*]pyrimidin-1-ium hexafluorophosphate (85).

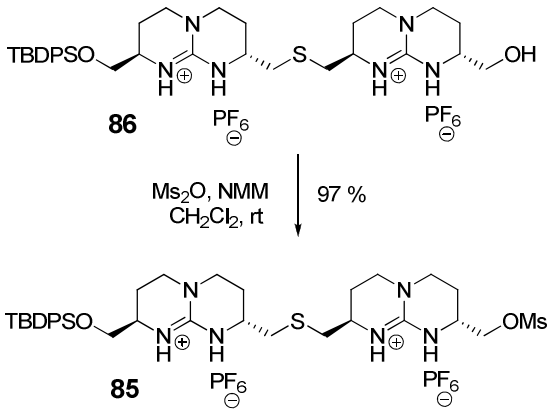

To a solution of alcohol **86** (107 mg, 0.11 mmol) and NMM (93.4 µL, 0.88 mmol) in dry CH_2Cl_2 (10 mL) was added a solution of Ms_2O (100 mg, 0.55 mmol) in CH_2Cl_2 (4 mL) and the mixture was stirred for 4 h. The solvent was evaporated under reduced pressure and the resulting crude dissolved in CH_2Cl_2 (4 mL) and washed successively with 0.1M NH_4PF_6 (2 × 30 mL). The organic layer was dried over anhydrous Na_2CO_3, filtered and concentrated *in vacuo*. Purification by column chromatography on silica gel (eluent: CH_2Cl_2/CH_3OH, 96:4) afforded **85** as colorless solid in a 97% yield. Mp: 76-80 °C. $[\alpha]^{25}_D$ - 83 (*c* = 0.5, $CHCl_3$). ^{1}H NMR ($CDCl_3$) δ 7.68-7.66 (m, 4H, ArH), 7.43-7.38 (m, 6H, ArH), 6.37 (s, 1H, NH), 6.28 (s, 2H, NH), 6.22 (s, 1H, NH), 4.22-4.01 (m, 2H, CH_2O), 3.72-3.68 (m, 2H, CH_2O), 3.47-3.23 (m, 12H, $CH\alpha$, $CH_2\gamma$), 3.02 (s, 3H, CH_3O), 2.84-2.80 (m, 1H, CH_2S), 2.68-2.63 (m, 2H, CH_2S), 2.56-2.52 (m, 1H, CH_2S), 2.13-1.79 (m, 8H, $CH_2\beta$), 1.06 (s, 9H, $C(CH_3)_3$). ^{13}C NMR ($CDCl_3$) δ 151.4, 151.2

(CGuan), 135.8 (CAr), 132.7, 132.8, 130.3, 127.7 (CHAr), 68.4, 65.6 (CH_2OSi, CH_2O), 50.1, 49.8, 47.7, 47.4 (CHα), 45.7, 44.8 ($CH_2\gamma$), 37.5 (CH_2S), 37.0 (CH_3O) 36.9 (CH_2S), 26.7 ($C(CH_3)_3$), 26.5, 25.9, 22.6, 22.4 ($CH_2\beta$), 19.2 ($C(CH_3)_3$). Exact Mass *m/z* $[M + H - HPF_6]^+$: calc.: 859.3059 uma; found 859.3067 uma.

(2*R*,8*R*)-8-[(2*R*,8*R*)-2-(4-methoxyphenyldiphenylmethylthiomethyl)-3,4,6,7,8,9-hexahydro-2*H*-pyrimido[1,2-*a*]pyrimidin-2-ylmethylsulfanylmethyl-1-ium hexafluorophosphate]-8-hydroxymethyl-3,4,6,7,8,9-hexahydro-2*H*-pyrimido[1,2-*a*]pyrimidin-1-ium hexafluorophosphate (84).

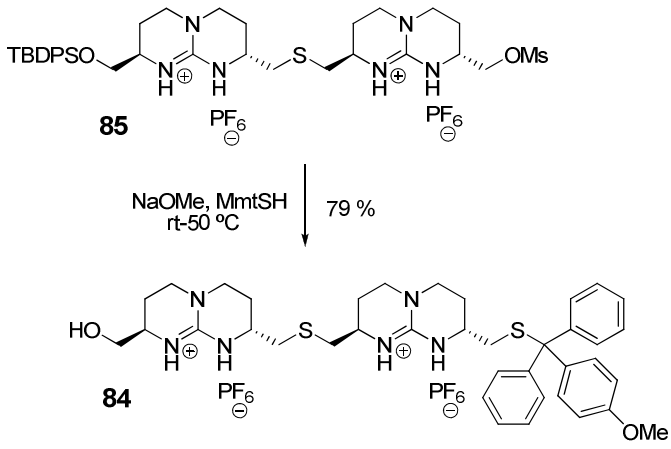

MmtSH (66 mg, 0.194 mmol) was dissolved in a solution of 0.25 M $NaOCH_3$ (13 ml, 3.23 mmol) and stirred at rt for 5 min under inert atmosphere Next, a solution of precursor **85** (280 mg, 0.42 mmol) in dry CH_3OH (2 mL) was added with a syringe. The reaction was stirred at rt for 1 h and then heated at 50 ºC for 18 h. After removal of the solvent, the remaining residue was dissolved in CH_2Cl_2 (6 mL) and the organic phase

was washed with water (5 mL) and with 0.1M NH_4PF_6 (3 x 5 mL). After drying the organic layer with anhydrous Na_2CO_3, it was filtered and concentrated. Purification of the crude was performed by silica flash chromatography (eluent: CH_2Cl_2/CH_3OH, 99.5:0.5→97:3). Pure compound **84** was obtained as a colorless solid in a 79% yield. Mp: 92-96 ºC. ^{1}H NMR (CD_2Cl_2): δ7.48-7.43 (m, 4H, ArH), 7.38-7.32 (m, 6H, ArH), 7.30-3.25 (m, 2H, ArH), 6.88 (d, *J* = 8.7 Hz, 2H, ArH), 6.38 (bs, 1H, NH), 6.30 (bs, 1H, NH), 6.17 (bs, 1H, NH), 5.92 (bs, 1H, NH), 6.00 (bs, 1H, NH), 3.82 (s, 3H, CH_3O), 3.80-3.74 (m, 1H, CHα), 3.62-3.51 (m, 4H, CHα, $CH_2\gamma$), 3.49-3.40 (m, 2H, $CH_2\gamma$), 3.40-3.28 (m, 3H, CHα, CH_2S), 3.26-3.10 (m, 2H, $CH_2\gamma$), 2.95-2.85 (m, 3H, CHα, CH_2S), 2.66-2.57 (m, 2H, CH_2S), 2.53-2.44 (m, 2H, CH_2S), 2.22-2.09 (m, 1H, $CH_2\beta$), 2.08-2.00 (m, 1H, $CH_2\beta$), 1.99-1.80 (m, 4H, $CH_2\beta$), 1.76-1.65 (m, 1H, $CH_2\beta$).^{13}C NMR (CD_2Cl_2): δ 158.5 (CAr), 150.8, 150.1 (CGuan), 144.7, 136.2 (CAr), 130.8, 129.4, 128.1, 126.9, 113.3 (CH_2Ar), 66.9 (C), 64.3 (CH_2O), 55.3 (CH_3O), 50.7, 48.2, 47.8, 47.6 (CHα), 45.7, 45.5, 45.1 ($CH_2\gamma$), 36.5, 36.2, 35.9 (CH_2S), 26.0, 25.7, 24.8, 22.4 ($CH_2\beta$). Exact Mass *m/z* $[M + H - HPF_6]^+$ calc.: 685.3358 uma, found: 685.3345 uma.

(2*R*,8*R*)-8-[(2*R*,8*R*)-8-(4-methoxyphenyldiphenylmethylthiomethyl)-3,4,6,7,8,9-hexahydro-2*H*-pyrimido[1,2-*a*]pyrimidin-2-ylmethylsulfanylmethyl-1-ium hexafluorophosphate]-2-methanesulfonyloxymethyl-3,4,6,7,8,9-hexahydro-2*H*-pyrimido[1,2-*a*]pyrimidin-1-ium hexafluorophosphate (20).

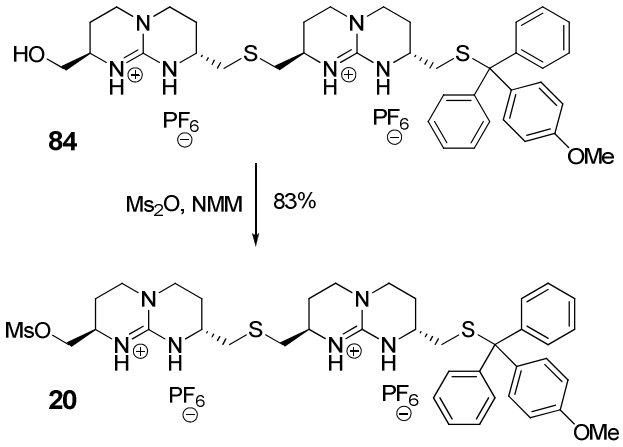

To a solution of alcohol **84** (150 mg, 0.15 mmol) and NMM (0.62 µl, 0.597 mmol) in dry CH_2Cl_2 (10 mL), Ms_2O (63 mg, 0.374 mmol) was added dissolved in dry CH_2Cl_2 (2 mL). The reaction was stirred at rt for 3 h. The solvent was removed, and after addition of CH_2Cl_2 (5 mL), the organic phase was washed with 0.1M NH_4PF_6 (2 x 5 mL). Next, the organic layer was dried over anhydrous Na_2CO_3, filtered and concentrated. Finally the crude was purified by column chromatography in silica gel (eluent: CH_2Cl_2/ CH_3OH, 98:2) affording pure **20** as a colorless solid in a 83% yield. Mp: 96-100 ºC. $[\alpha]^{20}_D$: - 80.8 (*c* = 1, CH_3CN, stand. dev.: 0.12). ^1H NMR (CD_2Cl_2): δ 7.49-7.43 (m, 4H, ArH), 7.39-7.31 (m, 8H, ArH), 6.88 (d, *J* = 9.4 Hz, 2H, ArH), 6.47 (bs, 1H, NH), 6.43 (bs, 1H, NH), 6.24 (bs, 1H, NH), 6.00 (bs, 1H, NH), 4.32 (dd, *J* = 4.4, 10.2 Hz, 1H, CH_2O), 4.17 (dd, *J* = 6.6,

10.5 Hz, CH_2O), 3.82 (s, 3H, CH_3O), 3.64-3.51 (m, 2H, CHα), 3.51-3.26 (m, 7H, CHα, $CH_2\gamma$), 3.24-3.12 (m, CHα, $CH_2\gamma$), 3.11 (s, 3H, CH_3O), 2.97-2.84 (m, 3H, CHα, CH_2S), 2.67-2.58 (m, 2H, CH_2S), 2.51-2.46 (m, 2H, CH_2S), 2.22-2.10 (m, 2H, $CH_2\beta$), 2.02-1.80 (m, 4H, $CH_2\beta$), 1.74-1.65 (m, 1H, $CH_2\beta$). ^{13}C NMR (CD_2Cl_2): δ 158.4 (CAr), 150.5, 150.0 (CGuan), 144.7, 136.2 (CAr), 130.8, 129.5, 128.1, 127.0, 113.4 (CHAr), 69.9 (C), 67.0 (CH_2), 55.4 (CH_3), 48.2, 47.9, 47.8 (CHα), 45.7, 45.5, 45.0, 44.9 ($CH_2\gamma$), 37.1 (CH_3O), 36.4, 36.3, 36.0 (CH_2S), 25.7, 25.6, 24.5, 22.0 ($CH_2\beta$). Exact Mass (ESI+) *m/z* $[M + H - HPF_6]^+$ calc.: 763.3134 uma, found: 763.3161 uma.

L-Alloc-Ala-OH.

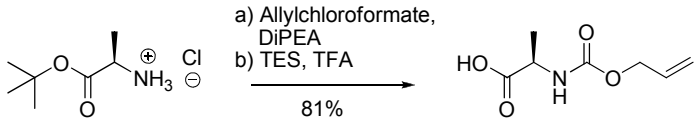

H-Ala-O^{t}Bu*HCl **L-Alloc-Ala-OH**

To a stirred solution of H-Ala-O^{t}Bu*HCl (0.1 g, 0.55 mmol) and allylchloroformate (0.1 µL, 0.83 mmol) in dry CH_2Cl_2 (1.5 mL) at 0 ºC, D*i*PEA (0.29 µL, 1.7 mmol) was added dropwise. Stirring was continued for 4 h. Thereafter, reaction was quenched by washing the organic phase with 1M HCl solution (3 x 1.5 mL) and H_2O (2 x 1.5 mL). Next, the organic phase was dried over anhydrous Na_2SO_4 and filtered over cotton. The solvent was removed by evaporation and the residue was dried prior to performing *tert*-butyl removal. Next, CH_2Cl_2 (11 mL) triethylsilane (TES) (0.14 g, 0.611 mmol) and TFA (30.5 mmol, 2.27 mL) were sequentially added to the residue. The reaction was stirred at rt for 5 h. Thereafter the solvent was evaporated and the remaining residue was dissolved in CH_2Cl_2

(2 mL) and extracted from the organic phase with distilled water (6 x 2 mL). Finally the aqueous phase was evaporated and final oil was obtained with 81% overall yield. $[\alpha]^{20}_{D}$: -27.1 (*c* = 1, CH_3OH, stand. dev.: 0.3). ^{1}H NMR (CH_3OD): δ 5.93 (sex, *J* = 5.3 Hz, 1H, CH-Alloc), 5.32 (d, *J* = 19.3 Hz, 1H, CH-Alloc), 5.20 (d, *J* = 11.04 Hz, 1H, CH-Alloc), 4.90 (bs, 1H, NH), 4.55 (d, *J* = 5.3 Hz, 2H, CH_2-Alloc), 4.19 (q, *J* = 7.2 Hz, 1H, CHα), 1.39 (d, *J* = 7.2 Hz, 3H, CH_3). ^{13}C NMR (CH_3OD): δ 175.3, 157.1 (C), 133.0 (CH), 116.3, 65.5 (CH_2), 49.6 (CH), 16.7 (CH_3). Exact Mass (ESI+): *m/z* $[M + Na]^+$: calc.: 196.0586 uma, found: 196.0585 uma.

(2*R*,8*R*)-2-*tert*-butyldiphenylsilanyloxymethyl-8-aminomethyl-3,4,6,7,8,9,-hexahydro-2*H*-pyrimido[1,2-*a*]pyrimidin-1-ium hexafluorophosphate (91).

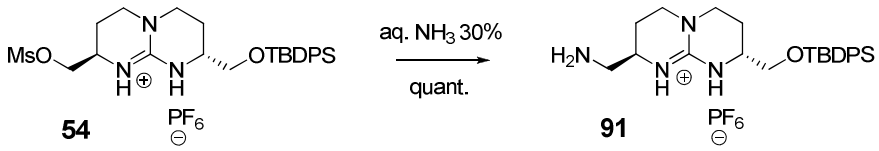

To a solution of compound **54** (0.54 g, 0.82 mmol) in CH_3OH (10 mL) was added a solution of 30% aq. ammonia (12 mL). The reaction was stirred at rt for 10 min, thereafter CH_3OH/CH_2Cl_2 (1:1, 2 mL) was added in order to aid solubilization. After 40 min, the CH_3OH was evaporated without heating the reaction. Next, the aqueous phase was extracted with CH_2Cl_2 (4 mL). The organic layer was further washed with 0.1M NH_4PF_6 (2 x 4 mL) and finally dried with anhydrous Na_2CO_3, filtered and evaporated to dryness. The product **91** was obtained as colorless foaming oil with quant. yield. ^{1}H NMR ($CDCl_3$): δ 7.66-7.60 (m, 4H, 1H, ArH),

7.41-7.31 (m, 6H, ArH), 4.02 (bs, 2H, NH), 3.85-3.53 (m, 4H, CH_2O, CHα), 3.28-3.02 (m, 6H, CH_2N, $CH_2\gamma$), 2.15-1.83 (m, 4H, $CH_2\beta$), 1.05 (s, 9H, $C(CH_3)_3$). ^{13}C NMR (CH_3OD): δ 150.6 (CGuan), 135.0 (CAr), 132.2, 129.5, 127.9, 127.4 (CHAr), 64.9 (CH_2O), 48.9 (CHα), 44.7 (CH_2N), 44.2 ($CH_2\gamma$), 26.4 ($C(CH_3)_3$), 19.1 ($C(CH_3)_3$). ESI(+): *m/z* $[M + H - HPF_6]^+$: 437.3 uma.

(2*R*,8*R*)-2-*tert*-butyldiphenylsilanyloxymethyl-8-allyloxycarbonylaminomethyl-3,4,6,7,8,9-hexahydro-2*H*-pyrimido[1,2-*a*]pyrimidin-1-ium hexafluorophosphate (90).

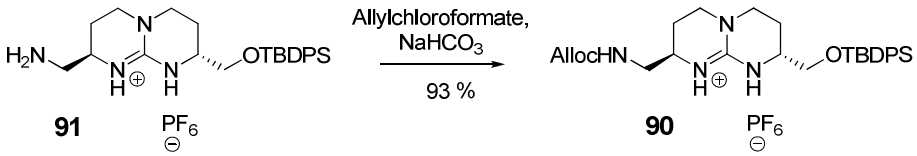

To a solution of amine **91** (186 mg, 0.319 mmol) in dioxane/water 1:1 (4 mL), cooled down to 0 ºC, was added $NaHCO_3$ (67 mg, 0.799 mmol) and allylchloroformate (58 mg, 0.479 mmol). The reaction was stirred at rt for 2 h. Next, the dioxane was evaporated and the product was extracted from water with EtOAc (5 mL) and the organic layer was further washed with 0.1M NH_4PF_6 (2 x 5 mL). Next, the organic phase was dried with anhydrous Na_2CO_3, filtered and eliminated *in vacuo*. The crude compound was purified by silica flash chromatography (eluent: CH_2Cl_2/CH_3OH, 2:98→4:98) and **90** was obtained as a colorless solid in a 93% yield. Mp: 86-89 ºC. ^1H NMR ($CDCl_3$): δ 7.63 (m, 4H, ArH), 7.62 (m, 6H, ArH), 6.24 (s, 1H, NH), 6.08 (s, 1H, NH), 6.06-5.96 (sex, *J* = 5.2 Hz, 1H, CH-Alloc), 5.37 (d, *J* = 17.2 Hz, 1H, CH-Alloc), 5.25 (d, *J* = 10.4 Hz, 1H, CH-Alloc),

4.54 (d, *J* = 5.2 Hz, 3.74-3.67 (m, 1H, CH_2O), 3.62-3.50 (m, 3H, CH_2O, CHα), 3.51-3.44 (m, 4H, $CH_2\gamma$), 3.32 (d, *J* = 6.2 Hz, CH_2NH_2), 2.17-2.05 (m, 2H, $CH_2\beta$), 1.94-1.84 (m, 2H, $CH_2\beta$), 1.04 $C(CH_3)_3$. ESI(+): *m/z* $[M + H - HPF_6]^+$: 521.7 uma.

(2*R*,8*R*)-2-hydroxymethyl-8-allyloxycarbonylaminomethyl-3,4,6,7,8,9-hexahydro-2*H*-pyrimido[1,2-*a*]pyrimidin-1-ium hexafluorophosphate (89).

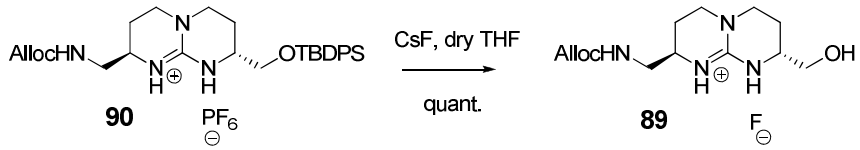

To a solution of compound **90** (0.87 g, 1.31 mmol) in THF (18 mL) cesium fluoride (CsF) (0.59 g, 3.92) was added, and the reaction was stirred at rt for 2 days. The solvent was evaporated and the residue dissolved in EtOAc (9 mL). Next, the organic layer was extracted with water (4 x 5 mL). The aqueous phase was evaporated and the residue was dissolved in a mixture of CH_3OH/CH_2Cl_2 (9:1). A precipitate was filtered and the filtrate was recovered and concentrated *in vacuo*. This procedure was repeated several times with increasing amount of CH_2Cl_2, until reaching CH_3OH/CH_2Cl_2 (1:4). Solvent was evaporated to dryness and product **89** was obtained with quantitative yield. ^{1}H NMR (CH_3OD): δ 6.07-5.97 (sex, *J* = 5.2 Hz, 1H, CH-Alloc), 5.39 (d, *J* = 17.2 Hz, 1H, CH-Alloc), 5.27 (d, *J* = 10.4 Hz, 1H, CH-Alloc), 4.56 (d, *J* = 5.2 Hz, 3.74-3.67 (m, 1H, CH_2O), 3.62-3.52 (m, 3H, CH_2O, CHα), 3.51-3.44 (m, 4H, $CH_2\gamma$), 3.32 (d, *J* = 6.2 Hz, CH_2NH_2), 2.17-2.07 (m, 2H, $CH_2\beta$), 1.94-1.84 (m, 2H, $CH_2\beta$). ^{13}C NMR (CH_3OD): δ 156.3 (CO), 149.5 (CGuan), 131.5 (CH), 114.6, 63.7, 62.1 (CH_2), 48.8, 47.1 (CHα), 43.5, 43.2, 42.5 (CH_2N, $CH_2\gamma$), 21.5, 21.0

($CH_2\beta$). ESI(+): *m/z* $[M + H - HF]^+$: 283.2 uma.

(2*R*,8*R*)-2-carboxymethylsulfanylmethyl-8-allyloxycarbonylaminomethyl-3,4,6,7,8,9-hexahydro-2*H*-pyrimido[1,2-*a*]pyrimidin-1-ium chloride (20).

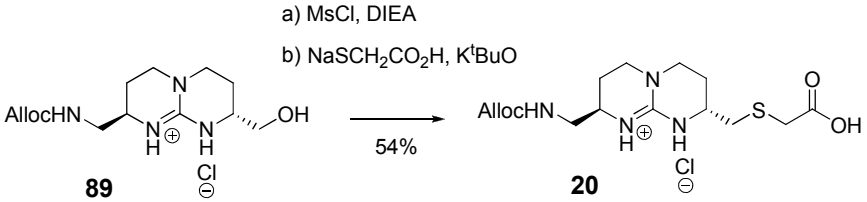

To a solution of compound **89** (0.4 g, 0.93 mmol) in dry CH_2Cl_2 (7 mL) and under inert atm, freshly distilled Et_3N (0.39 mL, 2.8 mmol) was added. The suspension was cooled to 0 ºC and MsCl (0.22 mL, 2.8 mmol), previously dissolved in CH_2Cl_2 (1 mL), was added dropwise. The reaction was warmed to rt. After 0.5 h, dry THF (3 mL) was added and the reaction was stirred overnight. Thereafter the solvent was evaporated to dryness. Next, dry THF (20 mL) was added dropwise as well as a solution of sodium mercaptoacetic acid (363 mg, 3.08 mmol) and K^tBuO (341 mg, 2.88 mmol) in CH_3OH (10 mL). The resulting mixture was stirred at rt for 4 h. Thereafter the reaction was filtered and the filtrate was evaporated. Then, a solution of CH_3OH/CH_2Cl_2 (9:1, 10 mL) was added, the precipitate was removed by filtration and the solvent evaporated under reduced pressure. This procedure was repeated several times increasing the amount of CH_2Cl_2 in the solvent mixture until pure CH_2Cl_2 was employed. Finally, product **20** was passed through a Cl-anion exchange column and was obtained as a colorless solid in a 54% yield. $[\alpha]^{20}_D$ -31.3º (*c* = 1, CH_3OH, stand. dev.: 0.31). Mp: 85-90 ºC. ^1H NMR (CH_3OD): δ 5.95-5.86 (sex, *J* = 5.2 Hz, 1H,

CHAlloc), 5.32 (d, *J* = 17.3 Hz, 1H, CHAlloc), 5.20 (d, *J* = 10.0 Hz, 1H, CHAlloc), 4.56 (bs, 2H, CH_2-Alloc), 3.67-3.60 (m, 1H, CHα), 3.58-3.49 (m, 1H, CHα), 3.46-3.37 (m, 4H, CH_2γ), 3.35 (d, *J* = 4.1 Hz, 2H, CH_2SCO), 3.26 (d, *J* = 6.2 Hz, CH_2NH_2), 2.93 (dd, *J* = 5.3, 14.1 Hz, 1H, CH_2S), 2.75 (dd, *J* = 8.0, 14.1 Hz, 1H, CH_2S), 2.21-2.14 (m, 1H, CH_2β), 2.11-2.04 (m, 1H, CH_2β), 1.96-1.79 (m, 2H, CH_2β). ^{13}C NMR (CH_3OD): δ 158.2 (CO), 151.2 (CGuan), 132.8 (CH), 117.6, 66.0 (CH_2), 51.5, 48.3 (CHα), 44.9, 39.3, 36.8, 36.3 (CH_2N, CH_2γ, CH_2S), 25.1 (CH_2β). Exact Mass: *m/z* [M + H - HCl]$^+$: calc.: 357.1597 uma, found: 357.1588 uma.

4.4.2 Solid phase synthesis

General procedures.

Initial swelling of resins.

p-Methylbenzhydrylamine (MBHA):

Table 3.8: Standard protocol for initial swelling of MBHA resin.

Reagent	Operation	times	min
60% TFA in CH_2Cl_2	swelling	2	1, 20
CH_2Cl_2	washings	5	1
5% D*i*PEA in CH_2Cl_2	neutralization	3	3
CH_2Cl_2	washings	5	1
DMF	washings	5	1

Thiol 4 methoxytrityl resin:

Treatments with DMF (3 × 1 min), CH_2Cl_2 (3 × 1 min), DMF (3 × 1 min).

*Synthesi*s. Reagent calculations were done following the scheme:

Number of eq. **x** mmol of functional groups/g of resin **x** g of resin employed **x** MW (mg/mmol) (**x** density^{-1}). Generally ~ 6 ml of solvent were used per gram of resin. Before reaction, resin was swelled in the solvent of the reaction, generally DMF. Fmoc deprotection was performed twice (1 x 1 min, 1 x 15 min) using a 20% piperidine solution in DMF. Capping of amines was carried out using a standard capping reagent consisting in the mixture of acetic anhydride (5 eq.) and D*i*PEA (5 eq.) in CH_2Cl_2 (20 min). Mmt deprotection was performed employing a solution of DTT (8 eq.) in

DMF (3 x 20 min*).*

On-bead analysis. The presence of primary amines was checked by the Kaiser test (ninhydrine test) (68). After reaction resin was washed: 3 x 1 min with the reactions's solvent, 3 x 1 min with CH_2Cl_2, 3 x 1 min with CH_3OH, 3 x 1 min with CH_2Cl_2. The presence of free thiols was checked by the Ellman test (69) after DTT treatment to assure for disulfide reduction. A tiny amount of resin was introduced into a vial were it was irst treated fwith a solution of 0.5 % DTNB in DMF (150 µl) and then with some drops of D*i*PEA. Subsequent orange coloration of the solution embedding the beads indicate the presence of free thiols, whereas no colour change indicates full nucleophilic functionalization of the thiols.

Standard cleavage protocol. A minimum of 0.01 g of resin were cleaved in a syringe with a cold solution of 5% H_2O in TFA at rt for 1h. The cleavage filtrate was recovered and the solution evaporated by applying nitrogen current.

HPLC-ESI(+) analysis for compounds **57-61**. the recovered filtrates were dried by applying nitrogen current. The samples were dissolved in 100 µL H_2O, CH_3CN or CH_3OH, HPLC grade, depending on the solubility, and were analyzed by HPLC-ESI(+) with RP Symmetry column 3.9 x 150 X-Terra C18 3.5 µm (4.6 x 100 mm); with as eluent CH_3CN in H_2O with 0.1 % HCOOH; UV_{220}, inj.: 5 µL; flow: 1 mL/min. The samples were injected into a Waters Alliance 2696 system. Flow proceeded from the column through a Waters 996 photodiode array (PDA) detector, which monitored wavelengths from 210 to 400 nm. From the PDA, the 1 mL/min flow was split using a flow splitter (0.5 mL/min each) to the Waters 2420 ELS detector (ELSD) and the electrospray Waters Micromass ZQ MS detector.

HPLC analysis and purification for compounds **74-80, 88,** and **92**: the

recovered filtrates were dried by applying nitrogen current. The samples were dissolved in 100 µL CH_3CN/CH_3OH (1:1), HPLC grade, and analysed on RP-C_{18} column Symmetry300^{TM} C_{18} 5µm 4.6 x 150 mm, $UV_{210-220}$, 5 µl inj., 1 ml/min flux, on HPLC: Agilent Technologies Serie 1200. Semipreparative-HPLC purification was performed on Waters HPLC 600 equipment with a quaternary pump (0.01-20 mL/min).

NHR-BAL-MBHA resin (R = Butylamine or 3-Methylbutylamine).

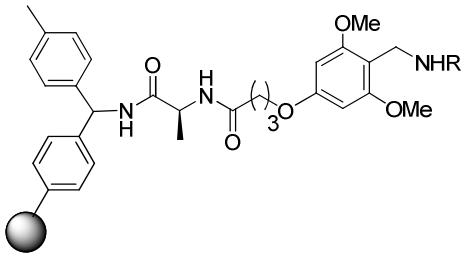

To MBHA resin (0.5 g, 0.34 mmol) swollen in DMF (3 mL) was added a solution of BAL (0.182 g, 0.68 mmol), HOBt (0.105 mg, 0.68 mmol), DIPCDI (0.102 mL, 0.68 mmol) dissolved in the minimum amount of DMF. The syringe was placed on a shaker overnight at rt. The reaction was checked by ninhydrine test and aldehyde test (70). Next, the primary amine coupling was performed with Butylamine or 3-Methylbutylamine by adding to the resin, embedded in a solution of 1% AcOH in DMF, first the amine (1 mmol) and then $NaCNBH_3$ (63 mg, 1 mmol). The reaction was shaken on an orbital shaker at rt for 4 h. Finally it was again checked by ninhydrine and aldehyde test.

(2*R*,8*R*)-2-hydroxymethyl-8-(3-methylbutyl)amidomethylsulfanylmethyl-3,4,6,7,8,9-hexahydro-2*H*-pyrimido[1,2-*a*]pyrimidin-1-ium trifluoroacetate (57).

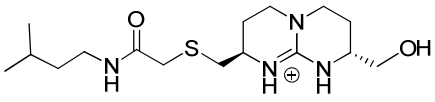

57 TFA$^{\ominus}$

To Methylbutylamine-BAL-MBHA (0.4 g, 0.27 mmol) resin swollen in DMF was added a solution of **15** (0.44 g , 0.81 mmol), HOBt (0.121 g, 0.81 mmol) and DIPCDI (0.125, 0.81 mmol). The syringe was shaken for 2 days at rt. After washes, the reaction was checked by ninhydrine test. Acetylation was performed to cap any remaining free amine groups with a solution of Ac_2O (1.36 mmol) and D*i*PEA (1.36 mmol). The resin was washed and cleaved according to general procedure. Analytical HPLC was employed to detect product **57** in the cleavage crude: Conds: 0→100 % CH_3CN in H_20 with 0.1% HCOOH in 15 min, ESI (+) *m/z* [M + H - TFA]: 343.2 uma. Compound 7 was not further purified.

(2*R*,8*R*)-2-benzylsulfanylmethyl-8-butylamidomethylsulfanylmethyl-3,4,6,7,8,9-hexahydro-2*H*-pyrimido[1,2-*a*]pyrimidin-1-ium trifluoroacetate (58).

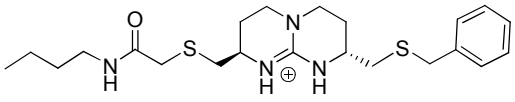

58 TFA$^{\ominus}$

Coupling of **15**, deprotection of OTBDPS and electrophilic activation was performed as described for compounds **57** and **58** on Butylamine-BAL-MBHA resin (0.05 g, 0.034 mmol). Thereafter, in the minimum amount of DMF under inert atmosphere, was added a solution of benzylthiol (12 µL, 0.102 mmol) and Cs_2CO_3 (39 mg, 0.102 mmol) in DMF (0.5 mL). The reaction was shaken at rt for 24 h on an orbital stirrer. After washes, standard cleavage was performed and the crude was analyzed by HPLC: 0→100% CH_3CN in H_20 with 0.1% HCOOH in 15 min, ESI(+) *m/z* [M + H - TFA]$^+$: 435.2 uma. Compound **58** was not further purified.

(2*R*,8*R*)-2-methanesulfonyloxymethyl-8-butylamidomethylsulfanylmethyl-3,4,6,7,8,9-hexahydro-2*H*-pyrimido[1,2-*a*]pyrimidin-1-ium trifluoroacetate (59).

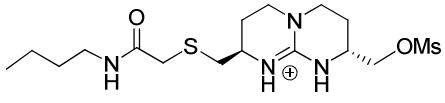

59 TFA$^{\ominus}$

Coupling of **15** proceeds as described for compound **57** on Butylamine-

BAL-MBHA resin (0.1 g, 0.068 mmol). Therafter the resin was embedded in THF (0.4 mL) to which were added 1M TBAF-THF (0.34 mL, 0.34 mmol), the syringe was shaken at rt for 3 h. Next, a solution of MsCl (40.5 µL, 0.53 mmol), D*i*PEA (115 µL, 0.7 mmol) and 4% DMAP (40 mg in 1 mL dry THF) in THF:CH_2Cl_2 (2 mL) was added to the resin swollen in the minimum amount of THF. After washes, standard cleavage was performed and the cleavage crude was analyzed by HPLC: 0→100% CH_3CN in H_20 with 0.1% HCOOH in 15 min, ESI(+) *m/z* [M + H - TFA]$^+$: 407.2 uma. Compound **9** was not further purified.

(2*R*,8*R*)-8-[(2*R*,8*R*)-8-hydroxymethyl-3,4,6,7,8,9-hexahydro-2*H*-pyrimido[1,2-*a*]pyrimidin-2-ylmethylsulfanylmethyl-1-ium hexafluorophosphate]-2-butylamidomethylsulfanylmethyl-3,4,6,7,8,9-hexahydro-2*H*-pyrimido[1,2-*a*]pyrimidin-1-ium trifluoroacetate (60).

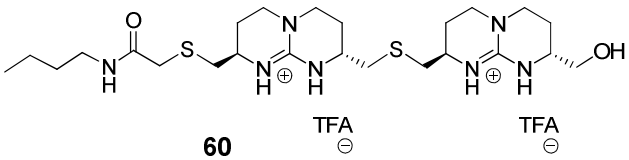

60

Coupling of **15**, deprotection of OTBDPS and electrophilic activation was performed as described for compound **59** on Butylamine-BAL-MBHA resin (0.05 g, 0.034 mmol). Next a solution of **16** (65.4 mg, 0.034 mmol) and Cs_2CO_3 (39 mg, 0.102 mmol) in DMF (0.5 mL), was added to the resin swollen in the minimum amount of DMF under inert atmosphere. The reaction was shaken at rt for 72 h. After washes, standard cleavage was performed and the cleavage crude was analyzed by HPLC; Conds: 0→100% CH_3CN in H_20 with 0.1% HCOOH in 15 min; ESI(+) *m/z* [M + H

- TFA]$^+$: 640.2 uma and [M + H + HPF - 2TFA]$^+$: 672.2 uma. Compound **60** was not further purified.

Tri(bicyclic guanidinium) oligomer 61.

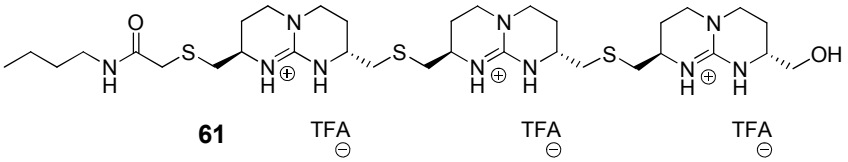

Coupling of **15** was performed as described for compound **57** on Butylamine-BAL-MBHA resin (0.05 g, 0.034 mmol). Removal of OTBDPS, electrophilic activation and BB **16** coupling protocols, according to compound **60**, were repeated twice. After washes, standard cleavage was performed and the crude was analyzed by HPLC; Conds: 0→100% CH_3CN in H_20 with 0.1% HCOOH in 15 min; ESI(+) *m/z* [M + H - TFA]$^+$: 838.4 uma. Compound **61** was not further purified.

(2*R*,8*R*)-2-benzoylthiomethyl-8-sulfhydril-3,4,6,7,8,9-hexahydro-2*H*-pyrimido[1,2-*a*]pyrimidin-1-ium trifluoroacetate (74)

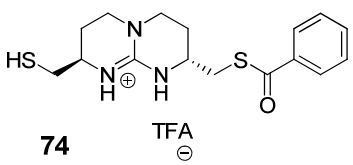

Swelled Thiol 4-methoxytrityl resin (0.06 g, 0.11 mmol) was embedded in the minimum amount of DMF and a solution with Cs_2CO_3 (106 mg, 0.33 mmol) and BB **17** (180 mg, 0.33 mmol) in DMF (1 mL) was added. The syringe was shaken on an orbital stirrer at rt for 24 h. Next, the resin was

washed and cleaved with a solution of 8% TFA and 5% Triisopropylsilane (TIS) in CH_2Cl_2 (1 mL). Next, the cleavage crude was analyzed on HPLC (Conds: 0→100 % CH_3CN in H_20 with 0.1% HCOOH in 15 min, UV_{214}) and the final compound was identified by LC-MS. The product **74** was not further purified. ESI(+) *m/z* $[M + H - TFA]^+$: 336.12 uma.

Fmoc-Cys(Mmt)-Rink-amide-MBHA resin.

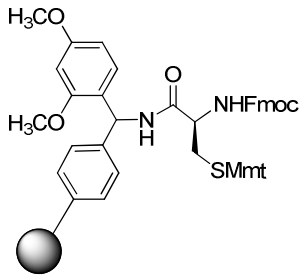

Prior to coupling, MBHA resin (1 g, 0.68 mmol) was washed with DMF (5 x 1 min). Thereafter Rink amine linker was anchored by adding a solution of Rink amine (1.1 g, 2.04 mmol), HOBt (304.2 mg, 2.04 mmol) and DIPCDI (314 µl, 2.04 mmol) dissolved in DMF (6 mL) to a syringe placed on a shaker at rt for 18 h. After washes, anchored Fmoc group was deprotected. Next, amino acid Fmoc-Cys(Mmt)-OH (1.26 g, 2.04 mmol) was coupled under the same conditions.

On 0.1 g of resin (0.068 mmol), additional Fmoc deprotection, acetylation and cleavage in 100% TFA at rt for 1h, were performed. After evaporating and drying *in vacuo,* loading of the resin was approximated to 80% (0.054 mmol).

(*R*)-2-acetamido-3-(benzylthio)propanamide (75).

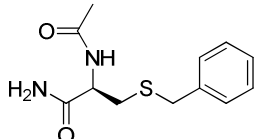

75

Fmoc-Cys(Mmt)-Rink-amide-MBHA resin (0.04 g, 0.027 mmol) was deprotected and capped at its α amine group. Next, SMmt was removed, followed by treatment with DTT. Prior to coupling, the resin was washed under inert atmosphere with dry DMF (3 x 1 min). Thereafter a solution of Et_3N (12 µl, 0.027 mmol) and BnBr (16 µl, 0.027 mmol) in dry DMF was added, and the syringe was placed on a shaker for 3 h at rt. Thereafter the resin was cleaved (TFA 100%, rt, 1 h). The cleaved product **75** was analyzed by anal HPLC (5→95% CH_3CN in H_2O, 0.1% TFA, in 15 min, UV_{220}) and obtained as a colorless oil without further purification in a 65% yield. ^1H NMR (CH_3OD): δ 7.39-7.29 (m, 4H, CHAr), 7.27-7.20 (m, 1H, CHAr), 4.67 (t, 1H, CHα), 3.8 (m, 2H, CH_2Bn), 2.87 (dd, J = 5.8,13.8 Hz 1H, CH_2S), 2.67 (dd, J = 8.2, 13.8 Hz, 2H, CH_2S), 2.03 (s, 3H, CH_3O), 1.81-1.71 (m, 2H, $CH_2\beta$). ESI(+) *m/z* $[M + H]^+$: 253.1 uma.

(2*R*,8*R*)-2-(4-methoxyphenyldiphenylmethylthiomethyl)-8-(1-acetamido-1-carboxamidoethylsulfanylmethyl)-3,4,6,7,8,9-hexahydro-2*H*-pyrimido[1,2-*a*]pyrimidin-1-ium trifluoroacetate (76).

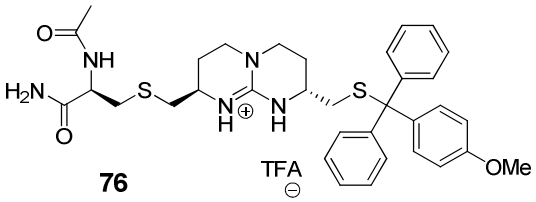

76

Fmoc-Cys(Mmt)-Rink-amide-MBHA resin (0.05 g, 0.034 mmol) was deprotected and capped at its α amino terminus. Next, SMmt was deprotected, followed by treatment with DTT. Prior to nucleophilic coupling, the resin was washed under inert atm with dry DMF (3 x 1 min). Next, a solution of K^{t}BuO (11 mg, 0.102) and BB **18** (72 mg, 0.102 mmol) in dry DMF (0.4 mL) was added, and the syringe was placed at rt on a shaker for 3 h. Thereafter washes and DTT treatment were performed. Capping of the resin were carried out following the same nucleophilic coupling conditions of BnBr, described for compound **75**. Finally, 100% TFA cleavage afforded a crude compound which was analyzed by anal. HPLC (5→95% CH_3CN in H_2O with 0.1% TFA in 15 min, UV_{220}) and **76** was obtained as colorless oil without further purification in a 41% yield. ^{1}H NMR (CH_3OD): δ 7.43-7.39 (m, 4H, ArH), 7.32-7.2 (m, 8H, ArH), 6.87-6.84 (d, J = 8.9 Hz, 2H, ArH), 4.55-4.51 (s, 1H, CHα), 3.8 (s, 3H, CH_3O), 3.54-3.47 (m, 1H, CH_2α), 3.45-3.37 (m, 2H, CH_2γ), 3.20-3.10 (m, 1H, CH_2S), 3.06-2.96 (m, 2H, CH_2S, CH_2γ), 2.94-2.85 (m, 3H, CH_2S, CH_2γ, CH_2α), 2.76-2.69 (m, 2H, CH_2S), 2.59-2.49 (m, 1H, CH_2S), 2.21-2.14 (m, 1H, CH_2β), 2.02 (s, 3H, CH_3CONH), 2.02-1.94 (m, 1H, CH_2β), 1.92-1.83

(m, 1H, $CH_2\beta$), 1.79-1.69 (m, 1H, $CH_2\beta$). ESI(+): *m/z* [M + H - TFA]$^+$: 632.2 uma.

(2*R*,8*R*)-2-benzylsulfanylmethyl-8-(1-acetamido-1-carboxamidoethylsulfanylmethyl)-3,4,6,7,8,9-hexahydro-2*H*-pyrimido[1,2-*a*]pyrimidin-1-ium trifluoroacetate (81).

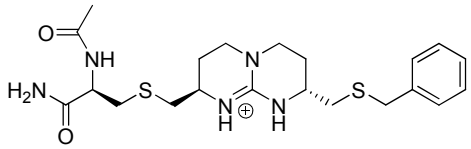

81 TFA$^\ominus$

Synthesis of compound **81** was performed as for product **76** starting from Fmoc-Cys(Mmt)-Rink-amide-MBHA resin (0.05 g, 0.034 mmol). Before final cleavage additional SMmt deprotection and BnBr capping were performed. Finally, 100% TFA cleavage afforded a crude compound which was analyzed by anal. HPLC (Conds: 5-95% CH_3CN in H_2O with 0.1% TFA in 20 min, UV_{210}). Further semipreparative purification (20→90% CH_3CN in H_2O with 0.1% TFA in 17 min, UV_{210}) yielded pure product **81** as colorless oil in a 33% yield. ^{1}H NMR (CD_3CN): δ 7.39-7.34 (m, 4H, ArH), 7.33-7.28 (m, 1H, ArH), 7.14 (bs, 1H, NH), 7.11 (bs, 1H, NH), 7.03 (bs, 1H, NH), 6.68 (bs, 1H, NH), 6.08 (bs, 1H, NH), 3.80 (s, 2H, SCH_2Ph), 3.54-3.47 (m, 1H, CHα), 3.46-3.38 (m, 1H, CHα), 3.37-3.27 (m, 4H, $CH_2\gamma$), 3.08-2.98 (m, 2H, CH_2S), 2.76-2.68 (m, 2H, CH_2S), 2.58-2.51 (m, 2H, CH_2S), 2.12-2.04 (m, 2H, $CH_2\beta$), 2.03 (s, 3H, CH_3O), 1.81-1.71 (m, 2H, $CH_2\beta$). ^{13}C NMR (CD_3CN): δ 150.86 (CGuan), 138.4 (CAr), 128.9, 128.6, 127.2 (CHAr), 48.5, 47.6, 45.5 (CHα), 45.0 ($CH_2\gamma$), 37.1, 35.9 (CH_2S), 25.8 ($CH_2\beta$), 25.4 (CH_3). Exact Mass (ESI+): *m/z* [M + H - TFA]$^+$: calc.:

450.1997 uma, found: 450.1993 uma.

(2*R*,8*R*)-8-[(2*R*,8*R*)-8-benzylsulfanylmethyl-3,4,6,7,8,9-hexahydro-2*H*-pyrimido[1,2-*a*]pyrimidin-2-ylmethylsulfanylmethyl-1-ium hexafluorophosphate]-2-(1-acetamido-1-carboxamidoethylsulfanylmethyl)-3,4,6,7,8,9-hexahydro-2*H*-pyrimido[1,2-*a*]pyrimidin-1-ium trifluoroacetate (82).

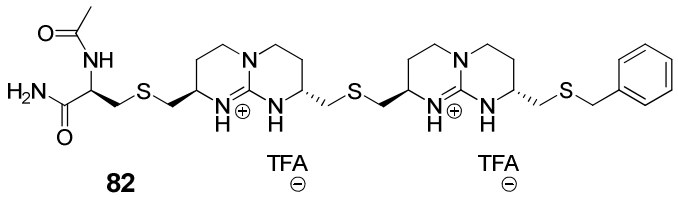

82

The same procedure as for product **81** was carried out starting from 0.08 g of Fmoc-Cys(Mmt)-Rink-amide-MBHA resin (0.08 g, 0.054), repeating the steps between the first Mmt deprotection and capping twice with BnBr. 100% TFA cleavage afforded a crude compound which was analyzed by anal. HPLC (Conds: 20→40% CH_3CN in H_2O with 0.1% TFA in 17 min, UV_{210}). Further semipreparative purification under the same conditions yielded pure product **82** as colorless oil in a 21% yield. ^{1}H NMR (CH_3OD): δ 7.44-7.36 (m, 4H, ArH), 7.36-7.29 (m, 1H, ArH), 4.64-4.60 (q, J = 5.3 Hz, 1H, CHα), 3.87 (s, 2H, SCH_2Ph), 3.71-3.61 (m, 3H, CHα), 3.58-3.37 (m, 1H, CHα, $CH_2\gamma$), 3.12 (dd, J = 5.3, 14.0 Hz, 1H, CH_2S), 3.00-2.92 (m, 3H, CH_2S), 2.85 (dd, 1H, J = 8.9, 14.0 Hz, CH_2S), 2.80-2.71 (m, 4H, CH_2S), 2.64 (dd, J = 7.5, 13.8 Hz, 1H, CH_2S), 2.28-2.17 (m, 2H, $CH_2\beta$), 2.10 (s, 3H, CH_3O), 1.99-1.85 (m, 2H, $CH_2\beta$). ^{13}C NMR (CD_3CN): δ 150.8 (CGuan), 138.2 (CAr), 128.7, 128.3, 126.9 (CHAr), 52.8, 47.9, 47.7, 47.6, 45.1 (CHα), 45.0, 44.9 ($CH_2\gamma$), 36.4, 36.1, 35.6, 34.0, 30.7, 30.6 (CH_2S),

25.3, 26.2 ($CH_2\beta$), 21.2 (CH_3). Exact Mass (ESI+): *m/z* $[M + H - TFA]^+$: calc.: 647.2984 uma, found: 647.2984 uma.

Tetra(bicyclic guanidinium) oligomer 83.

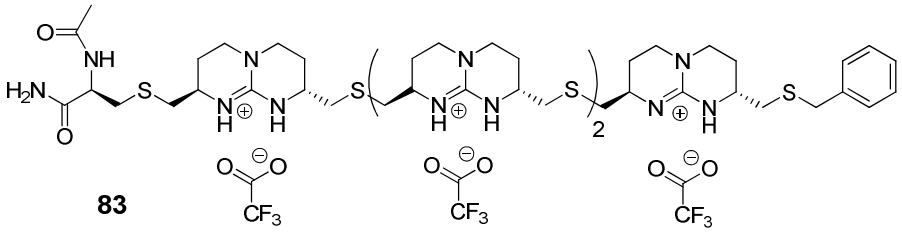

83

The same procedure as for product **81** was followed starting from Fmoc-Cys(Mmt)-Rink-amide-MBHA (0.08 g, 0.054 mmol), repeating four times the steps between the first Mmt deprotection and capping with BnBr. 100% TFA cleavage afforded a crude compound which was analyzed by anal. HPLC (Conds: 20→50% CH_3CN in H_2O with 0.1% TFA in 17 min, UV_{210}). Further semipreparative purification (Conds: 25% CH_3CN in H_2O with 0.1% TFA for 17 min, then in 3 min from 25→28%, UV_{210}) yielded pure product **83** as colorless oil in a 12% yield. ^1H NMR (CH_3OD): δ 7.46-7.36 (m, 4H, CHAr), 7.35-7.30 (m, 1H, CHAr), 4.65-4.59 (m, 1H, CHα), 3.76-3.60 (m, 8H, CHα), 3.58-3.42 (m, 16H, CHγ), 3.12 (dd, *J* = 5.3, 14.0 Hz, 2H, SCH_2Ph), 3.01-2.90 (m, 7H, CH_2S), 2.87-2.70 (m, 9H, CH_2S), 2.63 (dd, *J* = 7.7, 13.7 Hz, 2H, CH_2S), 2.29-2.18 (m, 8H, $CH_2\beta$), 2.11 (s, 3H, CH_3O), 2.04-1.89 (m, 8H, $CH_2\beta$). Exact Mass (ESI+): *m/z* $[M + Na]^+$: calc.: 1519.4492 uma, found: 1519.4525 uma.

Hexa(bicyclic guanidinium) oligomer 87.

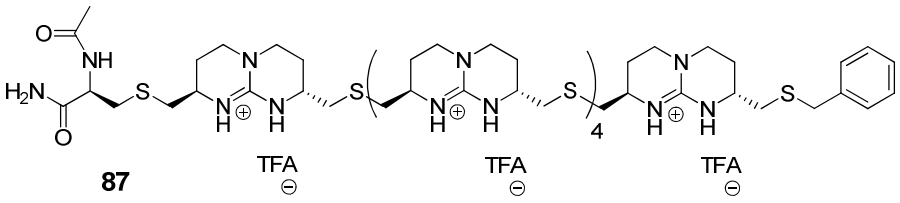

87

The same procedure as for compound **81** was repeated with 0,04 g Fmoc-Cys(Mmt)-Rink-amide-MBHA starting resin (0.04 g, 0.027 mmol)**,** until incorporating four times BB **1** and capping with BnBr. Next, BB **19** was anchored after DTT treatment, under the same coupling conditions described before. After 100% TFA cleavage, the crude compound **87** was analyzed by anal. HPLC (Conds: 20→45% CH_3CN in H_2O with 0.1% TFA in 17 min, UV_{210}) and ESI(+). The product **87** was identified among several oligomer precursors (see Fig. 3.45, Fig. A3.2), but not further purified. ESI(+) *m/z* $[M + 2H - 2TFA]^{2+}$: 946.3 uma.

Compound 88.

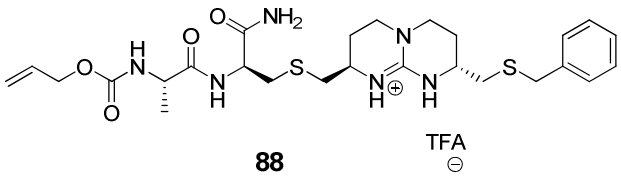

88

Fmoc-Cys(Mmt)-Rink-amide-MBHA resin (0.035 g, 0.024 mmol) was deprotected at its amino terminus and coupling of L-Alloc-Ala-OH was performed as described earlier for Rink amine to MBHA resin. Next, the SMmt was removed, BB **18** anchored through nucleophilic substitution and the thiol end capped with BnBr, following protocols described before.

Finally, crude compound **88** was analyzed by anal. HPLC (20→50% CH_3CN in H_2O with 0.1% TFA in 17 min, UV_{210}) and further purified by semi preparative HPLC (Conds: 20→50% CH_3CN in H_2O with 0.1% TFA in 15 min, 50-95% in 4 min, UV_{210}), although yield could not calculated, as a not enough amount of final compound was recovered. ^1H NMR (CH_3OD): δ 7.46-7.23 (m, 5H, CHArS), 6.01-5.89 (m, 1H, CH-Allyl), 5.33 (d, *J* = 17.5 Hz, 1H, CH_Allyl), 5.21 (d, *J* = 11.7 Hz, CH-Allyl), 3.81 (s, 2H, SCH_2Ph), 3.59-3.36 (m, 6H, $CH_2\alpha$, $CH_2\gamma$), 3.25-3.06 (m, 1H, CH_2S), 3.01-2.94 (m, 2H, CH_2S), 2.87-2.80 (m, 1H, CH_2S), 2.73-2.68 (m, 1H, CH_2S), 2.63-2.53 (m, 1H, CH_2S), 2.23-2.08 (m, 2H, $CH_2\beta$), 1.90-1.77 (m, 2H, $CH_2\beta$), 1.38 (d, *J* = 7.0 Hz, 3H, CH_3-Ala). Exact Mass (ESI+): *m/z* $[M + H - TFA]^+$ calc.: 563.2474 uma, found: 563.2477 uma.

Compound 92.

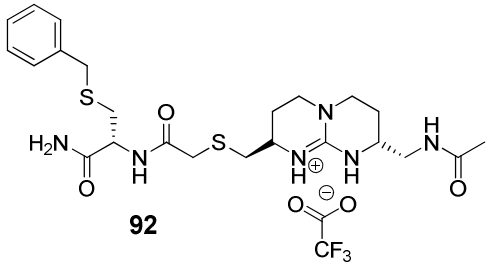

92

Fmoc-Cys(Mmt)-Rink-amide-MBHA resin (0.035 g, 0.024 mmol) was deprotected at its amino terminus. Next, a solution of BB **20** (36 mg, 0.072 mmol), HOBt (11 mg, 0.072 mmol) and DIPCDI (11 µL, 0.072 mmol) dissolved in DMF (0.4 mL) was added to the resin and the syringe was shaken at rt for 18 h. Alloc deprotection was performed as reported (70), with treatments of 0.05 eq. of $Pd(P(Ph)_3)_4$ and 5 eq. of $PhSiH_3$ under

inert atm (3 x 15 min) at rt. Thereafter the free primary amine was acetylated. Before final cleavage the thiol group (SMmt) was deprotected and capped with BnBr as described before. The crude compound **92** was analyzed by HPLC (5→60% CH_3CN in H_2O with 0.1 % TFA in 17 min, 60→95% in 3 min, UV_{210}) and further purified by semipreparative HPLC (15→30% CH_3CN in H_2O with 0.1 % TFA in 20 min, UV_{210}), but yield could not be calculated as a very tiny amount of product was recovered. Exact Mass (ESI+) *m/z* $[M + H - TFA]^+$ calc.: 507.2212 uma, found: 507.2216 uma.

4.5 References

1. (a) Alcázar V, Segura M, Prados P, de Mendoza J (1998) A preorganized macrocycle based on a bicyclic guanidinium subunit with six convergent hydrogen bonds for anion recognition. *Tetrahedron Lett* 39:1033-1036.
   (b) Breccia P, Van Gool M, Pérez-Fernández R, Martín-Santamaría S, Gago F, Prados P, de Mendoza J (2003)) Guanidinium receptors as enantioselective amino acid membrane carriers. *J* nitrate complexation by guanidinium-based macrocycles. *New J Chem* 31:736-740.
   (c) Blondeau P, Benet-Buchholz J, de Mendoza J (2007) Enthalpy driven nitrate complexation by guanidinium-based macrocycles. *New J Chem* 31:736-740.

2. Sánchez-Quesada J, Seel C, Prados P, de Mendoza J (1996) Anion helicates: Double strand helical self-assembly of chiral bicyclic guanidinium dimers and tetramers around sulfate templates. *J Am Chem Soc* 118:277-278.

3. (a) Peczuh MW, Hamilton AD, Sánchez-Quesada J, de Mendoza J, Haack T, Giralt E (1997) Design, synthesis and evaluation of synthetic receptors for the recognition of aspartate pairs in an alpha-helical conformation. *J Am Chem Soc* 119:9327-9328.
   (b) Orner PB, Salvatella X, Sánchez-Quesada J, de Mendoza J, Giralt E, Hamilton AD (2002) De novo protein surface design: Use of cation-π interactions to enhance binding between an α-helical peptide and a cationic molecule in 50% aqueous solution. *Angew Chem Int Ed* 41:117-119.

4. Salvatella X, Martinell M, Gairí M, Mateu MG, Feliz M, Hamilton AD, de Mendoza J, Giralt E (2004) A tetraguanidinium ligand binds to the surface of the tetramerization domain of protein p53. *Angew Chem Int Ed* 43:196-198.

5. Fawell S, Seery J, Daikh Y, Chen LL, Pepinsky B, Barsoum J (1994) Tat-mediated delivery of heterologous proteins into cells. *Proc Natl Acad Sci USA* 91:664-668.

6. Derossi D, Joliot AH, Chassaing G, Prochiantz A (1994) The third helix of Antennapedia homeodomain translocates through biological membranes. *J Biol Chem* 269:10444-10450.

7. Rothbard JB, Garlington S, Lin O, Kirschberg T, Kreider E, McGrane PL, Wender PA, Khavari PA (2000) Conjugation of arginine oligomers to cyclosporin A facilitates topical delivery and inhibition of inflammation. *Nat Med* 6:1253-1257.

8. (a) Wadia JS, Stan RV, Dowdy SF (2004) Transducible TAT-HA fusogenic peptide enhances escape of TAT-fusion proteins after lipid raft macropinocytosis. *Nat Med* 10:310-315.
   (b) Nakase I, Niwa M, Takeuchi T, Sonomura K, Kawabata N, Koike Y, Takehashi M, Tanaka S, Ueda K, Simpson JC, Jones AT, Sugiura Y, Futaki S (2004) Cellular uptake of arginine-rich peptides: Roles for macropinocytosis and actin rearrangement. *Mol Ther* 10: 1011-1022.

9. Tung C-H, Weissleder R (2003) Arginine containing peptides as delivery vectors. *Adv Drug Del Rev* 99:281-294.

10. a) Mitchell DJ, Kim DT, Steinman L, Fathman CG, Rothbard JB (2000) Polyarginine enters cells more efficiently than other polycationic homopolymers. *J Pept Res* 56:318-325.
(b) Zaro JL, Shen W-C (2003) Quantitative comparison of membrane transduction and endocytosis of oligopeptides. *Biochem Biophys Res Commun* 307:241–247.

11. Futaki S (2002) Arginine-rich peptides: Potential for intracellular delivery of macromolecules and the mystery of the translocation mechanisms. *Int J Pharm* 245:1-7.

12. Wender PA, Jesssop TC, Pattabiraman K, Pelkey ET, VanDeusen CL (2001) An Efficient, scalable synthesis of the molecular transporter octaarginine via a segment doubling strategy. *Org Lett* 3:3229-3232.

13. (a) Samuel BU, Hearn B, Mack D, Wender PA, Rothbard J, Kirisits MJ, Mui E, Wernimont S, Roberts CW, Muench SP, Rice DW, Prigge ST, Law AB, McLeod R (2003) Delivery of antimicrobials into parasites. *Proc Natl Acad Sci USA* 100:14281-14286.
(b) Dubikovskaya EA, Thorne SH, Pillow TH, Contag CH, Wender PA (2008) Overcoming multidrug resistance of small-molecule therapeutics through conjugation with releasable octaarginine transporters. *Proc Natl Acad Sci USA* 105:12128-12133.

14. Wender PA, Mitchell DJ, Pattabiraman K, Pelkey ET, Steinman L, Rothbard JB (2000) The design, synthesis, and evaluation of molecules that enable or enhance cellular uptake: Peptoid molecular transporters. *Proc Natl Acad Sci USA* 97:13003-13008.

15. Wender PA, Rothbard JB, Jessop TC, Kreider EL, Wylie BL (2002) Oligocarbamate molecular transporters: Design, synthesis, and biological evaluation of a new class of transporters for drug delivery. *J Am Chem Soc* 124:13382-13383.

16. Rueping M, Mahajan Y, Sauer M, Seebach D (2002) Cellular uptake studies with beta-peptides. *ChemBioChem* 3:257-259.

17. Rothbard JB, Kreider E, Vandeusen CL, Wright L, Wylie BL, Wender PA (2002) Arginine-rich molecular transporters for drug delivery: Role of backbone spacing in cellular uptake *J Med Chem* 45:3612-3618.

18. Pujals S, Fernández-Carneado J, López-Iglesias C, Kogan MJ, Giralt E (2006) Mechanistic aspects of CPP-mediated intracellular drug delivery: Relevance of CPP self-assembly. *Bioch Bioph Acta* 1758:264–279.

19. (a) Goun EA, Shinde R, Dehnert KW, Adams-Bond A, Wender PA, Contag CH, Franc BL (2006) Intracellular Cargo delivery by an octaarginine transporter adapted to target prostate cancer. *Bioconjug Chem* 17:787-796.
(b) Maiti KK, Jeon OY, Lee WS, Takeuchi T, Watkins C, Fretz M, Kim DC, Futaki S,

Jones A, Kim KT, Chung SK (2007) Guanidine-containing molecular transporters: Sorbitol-based transporters show high intracellular selectivity toward mitochondria. *Angew Chem Int Ed* 46:5880-5884.

20. Jiang T, Olson ES, Nguyen QT, Roy M, Jennings PA, Tsien RY (2004) Tumor imaging by means of proteolytic activation of cell-penetrating peptides. *Proc Nat Acad Sci USA* 101:17867–17872.

21. Luedtke NW, Carmichael P, To Y (2003) Cellular uptake of aminoglycosides, guanidinoglycosides, and poly-arginine. *J Am Chem Soc* 125:12374-12345.

22. Fillon YA, Anderson JP, Chmielewski J (2005) Cell penetrating agents based on a polyproline helix scaffold. *J Am Chem Soc* 127:11798-11803.

23. (a) Chung HH, Harms G, Seong CM, Choi BH, Min CH Taulane JP Goodman M (2004) Dendritic oligoguanidines as intracellular translocators. *Pept Sci* 76:83-96.
(b) Wender PA, Kreider E, Pelkey ET, Rothbard J, Van Deusen CL (2005) Dendrimeric molecular transporters: Synthesis and evaluation of tunable polyguanidino dendrimers that facilitate cellular uptake. *Org Lett* 7:4815-4818.

24. (a) Dragulescu-Andrasi A, Zhou P, He GF, Ly DH (2005) Cell-permeable GPNA with appropriate backbone stereochemistry and spacing binds sequence-specifically to RNA. *Chem Commun* 244-246.
(b) Ohmichi T, Kuwahara N, Sasaki M, Hasegawa T, Nishikata H (2005) Nucleic acid with guanidinium modification exhibits efficient cellular uptake. *Angew Chem Int Ed* 44:6682-6685.
(c) Deglane G, Abes S, Michel T, Prevot P, Vives E, Debart F, Barvik I, Lebleu B, Vasseur JJ (2006) Impact of the guanidinium group on hybridization and cellular uptake of cationic oligonucleotides. *ChemBioChem* 7:684-692.

25. Sansone F, Dudic M, Donofrio G, Rivetti C, Baldini L, Casnati A, Cellai S, Ungaro R (2006) DNA Condensation and cell transfection properties of guanidinium calixarenes: dependence on macrocycle lipophilicity, size, and conformation. *J Am Chem Soc* 128:14528-14536.

26. (a) Vigneron JP, Oudrhiri N, Fauquet M, Vergely L, Bradley JC, Basseville M, Lehn P, Lehn JM (1996) Guanidinium-cholesterol cationic lipids: efficient vectors for the transfection of eukaryotic cells. *Proc Natl Acad Sci USA* 93:9682-9686.
(b) Martin B, Sainlos M, Aissaoui A, Oudrhiri N, Hauchecorne M, Vigneron JP, Lehn JM, Lehn P (2005) The design of cationic lipids for gene delivery. *Curr Pharm Res* 11:375-394.

27. Kolonko EM, Kiessling LL (2008) A polymeric domain that promotes cellular internalization. *J Am Chem Soc* 130:5626–5627.

28. (a) Perret F, Nishihara M, Takeuchi T, Futaki S, Adina AN, Coleman AW, Sakai N, Matilé S (2005) Anionic fullerenes, calixarenes, coronenes, and pyrenes as activators

of oligo/polyarginines in model membranes and live cells *J Am Chem Soc* 127:1114-1115.
(b) Nakase I, Niwa M, Takeuchi T, Sonomura K, Kawabata N, Koike Y, Takehashi M, Tanaka S, Ueda K, Simpson JC, Jones AT, Sugiura Y, Futaki S (2004) Cellular uptake of arginine-rich peptides: roles for macropinocytosis and actin rearrangement. *Mol Ther* 10:1011-1022.

29. (a) Mann DA, Frankel AD (1991) Endocytosis and targeting of exogenous HIV-1 Tat protein. *EMBO J* 10:1733-1739.
(b) Richard JP, Melikov K, Vives E, Ramos C, Verbeure B, Gait MJ, Chernomordik LV, Lebleu B (2003) Cell-penetrating peptides. A reevaluation of the mechanism of the cellular uptake. *J Biol Chem* 278:585-590.

30. Wender PA, Galliher WC, Goun EA, Jones LR, Pillow TH (2008) The design of guanidinium-rich transporters and their internalization mechanisms. *Adv Drug Del Rev* 60:452-472.

31. Rejman J, Oberle V, Zuhorn IS, Hoekstra D (2004) Size-dependent internalization of particles via the pathways of clathrin- and caveolae-mediated endocytosis. *Biochem J* 377:159-169.

32. Rothbard JB, Jessop TC, Wender PA (2005) Adaptive translocation: The role of hydrogen bonding and membrane potential in the uptake of guanidinium-rich transporters into cells. *Adv Drug Del Rev* 495-504.

33. (a) Sakai N, Matile S (2003) Anion-mediated transfer of polyarginine across liquid and bilayer membranes. *J Am Chem Soc* 125:14348-14356.
(b) Takeuchi T, Futaki S, Matile S (2005) Direct and rapid cytosolic delivery using cell-penetrating peptides mediated by pyrenebutyrate. *ChemBioChem* 6:114-122.

34. Rothbard JB, Jessop TC, Lewis RS, Murray BA, Wender PA (2004) Role of membrane potential and hydrogen bonding in the mechanism of translocation of guanidinium-rich peptides into cells. *J Am Chem Soc* 126:9506-9507.

35. Ho A, Schwarze SR, Mermelstein SJ, Waksman G, Dowdy SF, (2001) Synthetic protein transduction domains: Enhanced transduction potential in vitro and in vivo. *Cancer Res* 61:474-477.

36. Smith RAJ, Porteous CM, Gane AM, Murphy MP (2003) Delivery of bioactive molecules to mitochondria in vivo. *Proc Natl Acad Sci USA* 100:5407-5412.

37. Fernández-Carneado G, Van Gool M, Martos V, Castel S, Prados P, de Mendoza J, Giralt G (2005) Highly efficient, nonpeptidic oligoguanidinium vectors that selectively internalize into mitochondria. *J Am Chem Soc* 27:869-874.

38. Kielar F, Congreve A, Law G-l, New EJ, Parker D, Wong K-L, Castreño P, de Mendoza J (2008) Two-photon microscopy study of the intracellular

compartmentalisation of emissive terbium complexes and their oligo-arginine and oligo-guanidinium conjugates. *Chem Commun* 2435-2437.

39. (a) Peréz-Fernández R (Oct 2005) Protein-ligand interactions, self-assembly and dynamic combinatorial libraries for biological applications based on chiral bicyclic guanidines. PhD Thesis, Universidad Autónoma de Madrid (UAM).
(b) Valero J (June 2007) New ligands for the tetramerization domain of p53. DEA, Universitat Rovira i Virgili (URV).

40. (a) Merrifield RB (1963) Solid phase peptide synthesis. I. The synthesis of a tetrapeptide. *J Am Chem Soc* 85:2149-2154.
(b) Merrifield RB (1985) Solid Phase Synthesis (Nobel Lecture). *Angew Chem Int Ed Engl* 24:799-810.

41. Goetz M, Rusconi F, Belghazi M, Schmitter JM, Dufourc EJ (2000) Purification of the c-erbB2/neu membrane spanning segment: a hydrophobic challenge. *J Chromatogr Biomed Sci App* 737:55-61.

42. Seneci P (2000) Solid phase synthesis and combinatorial technologies, John Wiley & Sons (New York).

43. Keifer PA (1997) High-resolution NMR techniques for solid-phase synthesis and combinatorial chemistry. *Drug Discov Today* 2:468-478.

44. Breccia P, Boggetto N, Pérez-Fernández R, Van Gool M, Takahashi M, René L, Prados P, Badet B, Reboud-Ravaux M, de Mendoza J (2003) Dimerization inhibitors of HIV-1 protease based on a bicyclic guanidinium subunit. *J Med Chem* 46:5196-5207.

45. (a) Echavarren A, Galán A, de Mendoza J, Salmerón A, Lehn J-M (1888) Anion-receptor molecules: synthesis of a chiral and functionalized binding subunit, a bicyclic guanidinium group derived from L- or D-asparagine. *Helv Chim Acta* 71:685-693.
(b) Kurzmeier H, Schmitchen FP (1990) Abiotic anion receptor functions. A facile and dependable access to chiral guanidinium anchor groups. *J Org Chem* 55:3749-3755.

46. Chan WC, White PD (2000) Fmoc solid phase peptide synthesis: a practical approach, Oxford University Press (Oxford).

47. (a) Fernández-Forner D, Huerta JM, Ferrer M, Casals G, Ryder H, Giralt E, Albericio F (2002) Solid-phase syntheses of N-substituted carbamates. Reaction monitoring by gel-phase ^{13}C NMR using a ^{13}C enriched BAL-linker. *Tetrahedron Lett* 43:3543-3546.
(b) Yraola F, Ventura R, Vendrell M, Colombo A, Fernández JC, de la Figuera N, Fernández-Forner D, Royo M, Foros P, Albericio F (2004) A re-evaluation of the use of Rink, BAL, and PAL resins and linkers *QSAR Comb Sci* 23:145-151.

48. Kuisle O, Lolo M, Quiñoá E (1999) Monitoring the solid-phase synthesis of depsides and depsipeptides. A color test for hydroxyl groups linked to a resin. *Tetrahedron* 55:14807-14812.

49. (a) Li Z, Crosignani S, Linclau B (2003) A mild, phosphine-free method for the conversion of alcohols into halides (Cl, Br, I) via the corresponding O-alkyl isourea. *Tetrahedron Lett* 44:8143-8147.
(b) Crosignan S, Nadal B, Li Z, Linclau B (2003) A novel stereoselective one-pot conversion of alcohols into alkyl halides mediated by N,N-diisopropylcarbodiimide. *Chem Commun* 260-261.

50. (a) Humphrey RE, Potter JL (1965) Reduction of disulfides with tributylphosphine. *Anal Chem* 37:164-165.
(b) Urpí F, Vilarrasa J (1986) New synthetic 'tricks': Advantages of using triethylphosphine in some phosphorus-based reactions. *Tetrahedron Lett* 27:4623-4624.
(c) Ayers JT, Anderson SR (1999) A preparative scale reduction of alkyl disulfides with tributyl phosphine and water. *Synth Commun* 29:351-358.

51. Dahan A, Weissberg A, Portnoy M (2003) Preparation of novel polythioether dendrons on a solid support. *Chem Commun* 1206-1207.

52. Greene TW, Wuts PGM (1999) Protective Groups in Organic Synthesis, 3rd ed, John Wiley & Sons (New York).

53. Wu X, Pitsch S (1999) Functionalization of the sugar moiety of oligoribonucleotides on solid support. *Bioconjugate Chem* 10:921-924.

54. (a) Koval IV (2005) Synthesis, structure, and physicochemical characteristics of thiols. *Russian J Org Chem* 41:631-648.
(b) Pachamuth K, Schmidt RR (2006) Synthetic routes to thiooligosaccharides and thioglycopeptides. *Chem Rev* 106:160-187.

55. Masquelin T, Sprenger D, Baer R, Gerber F, Mercadal Y (1998) A novel solution and solid-phase approach to 2,4,5-tri- and 2,4,5,6-tetrasubstituted pyrimidines and their conversion into condensed heterocycles. *Helv Chim Acta* 81:646-660.

56. Kato S, Oguri M, Ishida M (1983) A convenient preparation of anhydrous alkali metal thiocarboxylates. *Z Naturforsch* 38b:1585-1590.

57. Bang D, Pentelute BL, Gates ZP, Kent SB (2006) Direct on-resin synthesis of peptide-αthiophenylesters for use in native chemical ligation. *Org Lett* 8:1049-1052.

58. Mourtas S, Gatos D, Kalaitizi V, Katakalov C, Barlos K (2001) S-4-Methoxytrityl mercapto acids: synthesis and application. *Tetrahedron Lett* 42:6965-6967.

59. Badyal JP, Cameron AM, Cameron NR, Coe D, Cox R, Davis BG, Oates LJ, Oye G, Steel PG (2001) A simple method for the quantitative analysis of resin bound thiol groups. *Tetrahedron Lett* 42:8531-8533.

60. Takeshi-Kondo T, Nishiyama A, Ueyama N, Murao H, Manabe H, Ueda Y (2000, Jan.

4) Patent number: 6,011,170.

61. Brotzel F, Mayer H (2007) Nucleophilicities of amino acids and peptides. *Org Biomol Chem* 5:3814–3820.

62. (a) Annis I, Chen L, Barany G (1998) Novel solid-phase reagents for facile formation of intramolecular disulfide bridges in peptides under mild condition. *J Am Chem Soc* 120:7226-7 238.
(b) Yan B, Sun Q (1998) Crucial factors regulating site interactions in resin supports determined by single bead IR. *J Org Chem* 63:55-58.

63. Rijkers DTS, Kruijtzer JAW, Killian JA, Liskamp RMJ (2005) A convenient solid phase synthesis of S-palmitoyl transmembrane peptide. *Tetrahedron Lett* 46:3341-3345.

64. Thieriet N, Alsina J, Giralt E, Guibé F, Albericio F (1997) Use of alloc-amino acids in solid-phase peptide synthesis. Tandem deprotection-coupling reactions using neutral conditions. *Tetrahedron Lett* 38:7275-7278.

65. Mandal PK, McMurray JS (2007) Pd-C-Induced catalytic transfer hydrogenation with triethylsilane. *J Org Chem* 72:6599-6601.

66. Futaki S, Nakase I, Suzuki T, Zhang YJ, Sugiura Y (2002) Translocation of branched-chain arginine peptides through cell membranes: flexibility in the spatial disposition of positive charges in membrane-permeable peptides. *Biochemistry* 41:7925–7930.

67. (a) Barlos K, Gatos D, Eleftheriou S, Mourtas S, Tzavara C, Athanassopoulos P (1998) *Proceedings of the European Peptide Symposium.* Budapest, Aug. 30-Sept. 4.
(b) Li X, Kawakami T, Aimoto S (1998) Direct preparation of peptide thioesters using an Fmoc solid-phase method. *Tetrahedron Lett* 39:8669-8672.

68. Kaiser E, Colescott RL, Bossinger CD, Cook PI (1970) Color test for detection of free terminal amino groups in the solid-phase synthesis of peptides. *Anal Biochem* 34:595-598.

69. Ellman GL (1959) Tissue sulfhydryl groups. *Arch Biochem Biophys* 82:70-77.

70. Vázquez J, Albericio F (2001) A useful and sensitive color test to monitor aldehydes on solid-phase. *Tetrahedron Lett* 42:6691-6693.

Appendix Chapter 4

a)

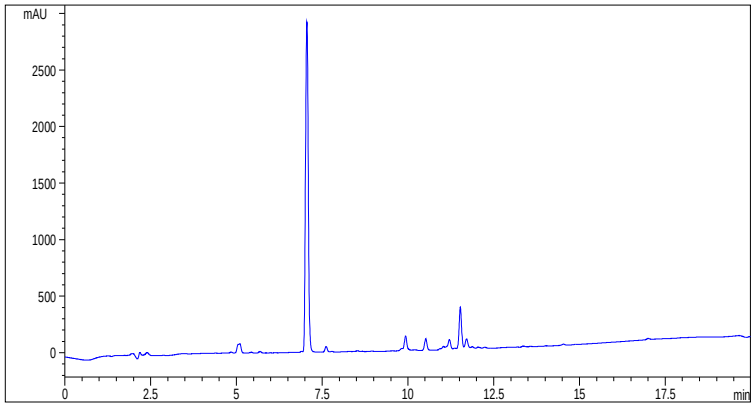

b)

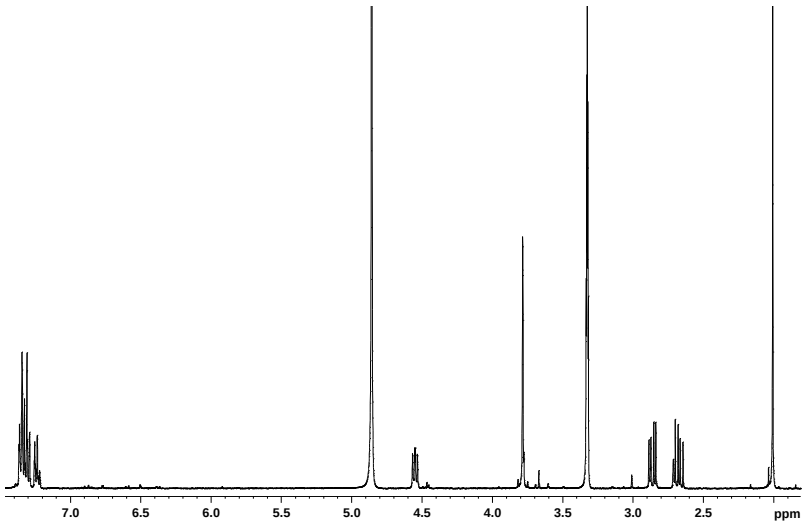

Fig. A4.1: a) HPLC profile of pure compound **75**: 5-95% CH_3CN in H_2O with 0,1% TFA in 17 min, UV_{220}, 5µL, 1 mL/min and b) ^{1}H-NMR spectrum in CH_3OD.

a)

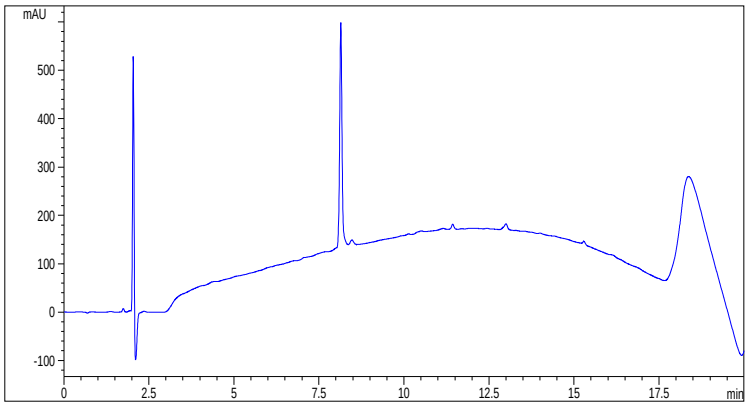

b)

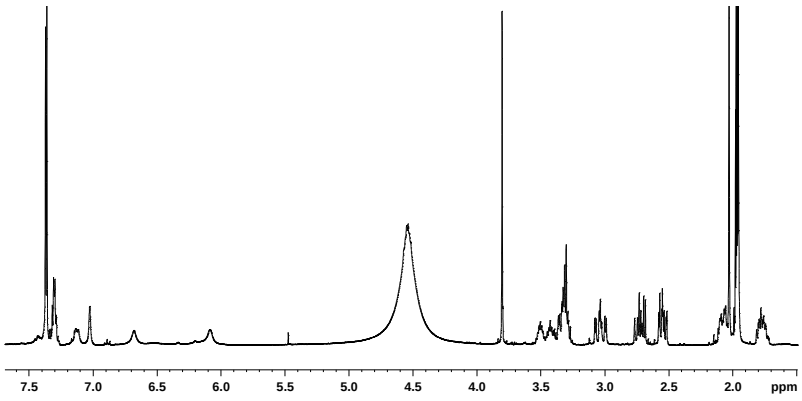

Fig. A4.2: a) HPLC profile of pure compound **81**: 5-95% CH_3CN in H_2O with 0,1% TFA in 15 min, UV_{210}, 5µL, 1 mL/min and b) ^{1}H-NMR spectrum in CD_3CN.

a)

a)

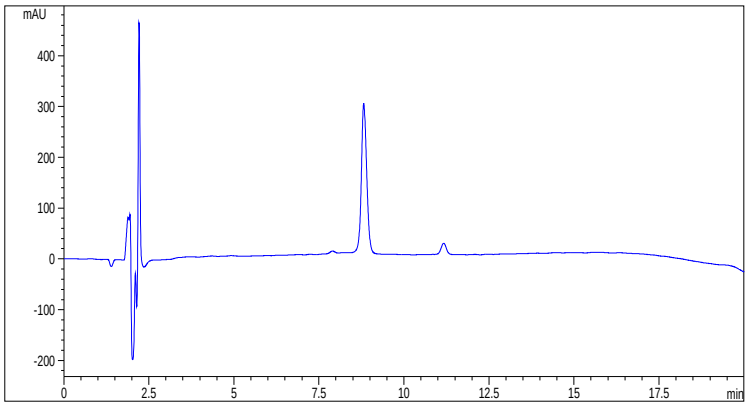

b)

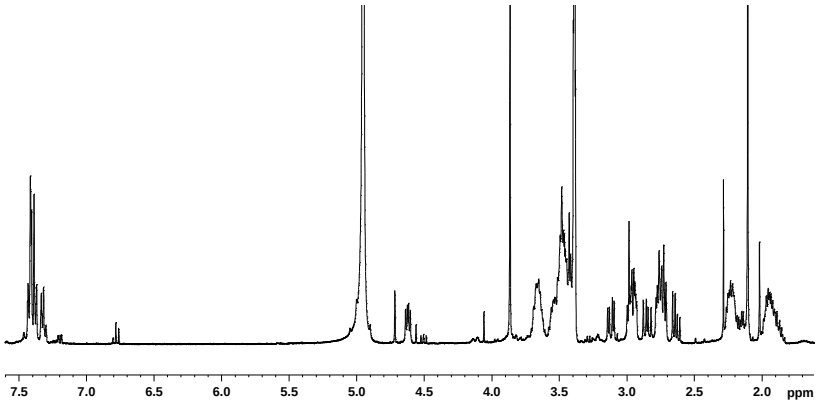

Fig. A4.3: a) HPLC profile of pure compound **82**: 20-60% CH_3CN in H_2O with 0,1% TFA in 15 min, UV_{210}, 5 µL, 1 ml/min; b) ^{1}H-NMR spectrum in CH_3OD.

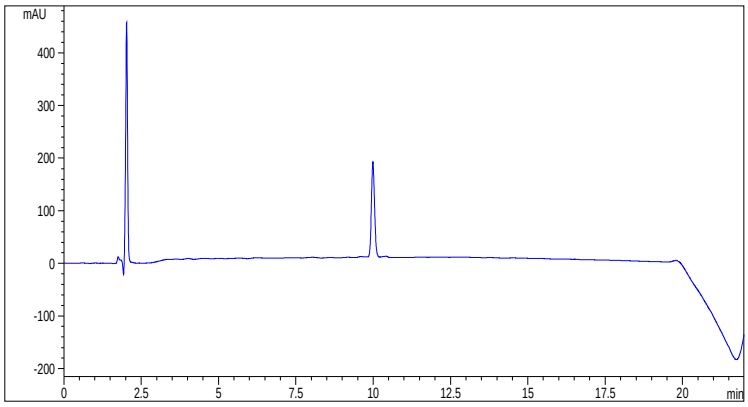

b)

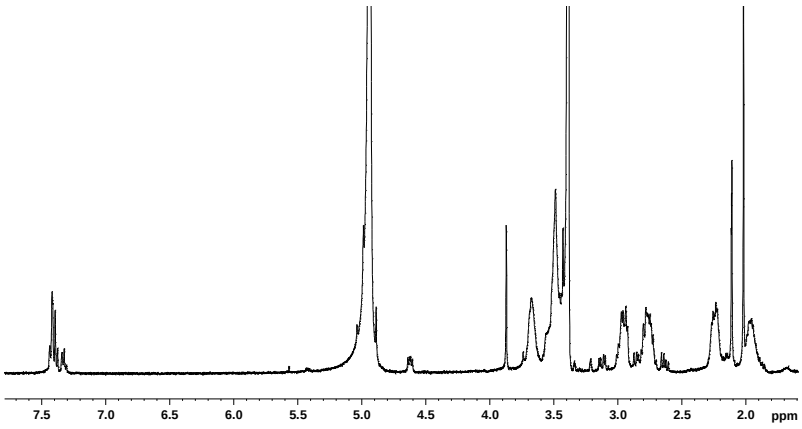

Fig. A4.4: a) HPLC profile of pure compound **83**: 20-50% CH_3CN in H_2O with 0,1% TFA in 17 min, UV_{210}, 5µL, 1 mL/min and b) ^{1}H-NMR spectrum in CH_3OD.

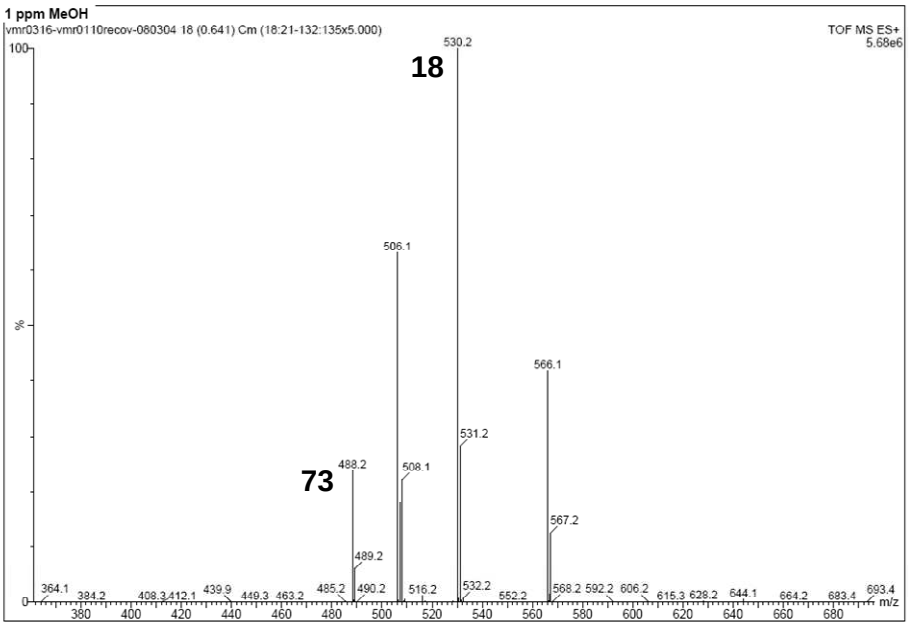

Fig. A4.5: ESI(+)-MS of crude compound **18** recovered by filtration from coupling reaction.

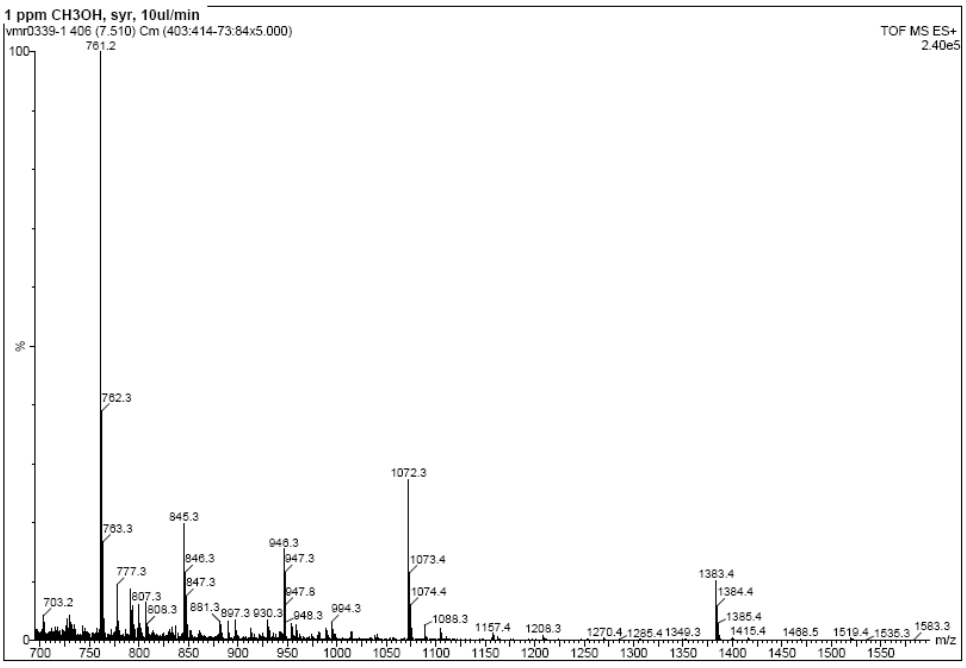

Fig. A4.6: ESI(+)-MS of crude compound **87**; 761.2 uma: [**82** + H - TFA]$^{+}$, 845.3 uma: [Triguanidinium oligomer + H - 3TFA]$^{+}$, 946.3: [**87** + 2H - 2TFA]$^{2+}$, 1072.3: [Triguanidinium oligomer + H - TFA]$^{+}$, 1383.4: [**83** + H - TFA]$^{+}$.

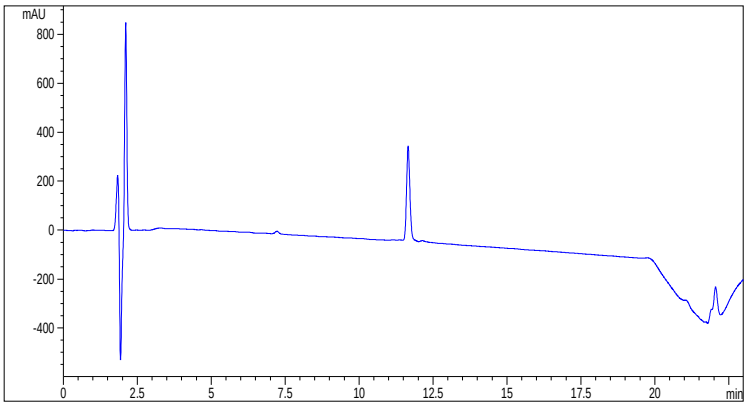

Fig. A4.7: HPLC profile of pure compound **88** (20-50% CH_3CN in H_2O with 0.1% TFA in 17 min, UV_{210}, 5 µL, 1 mL/min).

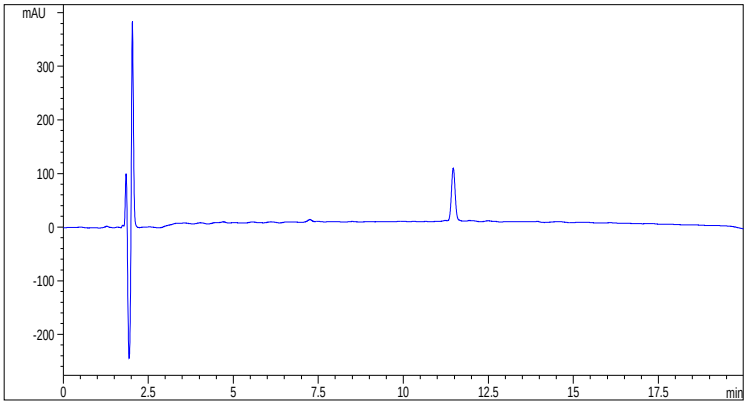

Fig. A4.8: HPLC profile of pure compound **92** (20-50% CH_3CN in H_2O with 0.1% TFA in 17 min, UV_{210}, 5µL, 1 mL/min)

Summary

This thesis deals with the combination of preorganized scaffolds and guanidnium-based recognition elements to give rise on one hand to specific protein surface ligands and on the other to transfection agents.

In *Chapter 1* we introduce the concepts of non covalent biomolecular recognition and multivalency, both at the basis of biological surface interactions. Supramolecular chemistry, which deals with the self-assembly and recognition of molecules *via* non covalent interactions, contributes to the understanding and mimicry of these biological events. Preorganized multivalent scaffolds, grafted with recognition elements, such as guanidine, are paving new ways for biomolecular recognition and drug discovery (1).

Moreover, we describe in this first Chapter the specific objectives of the thesis as well as the main compounds employed.

Chapter 2 deals with the recognition of the surface of protein p53. P53 is an oligomeric transcription factor, of crucial role for cell cycle and genomic integrity. Its activity is dependent on its tetrameric state, therefore association-deffective mutants of its tetramerization domain (p53TD) constitute valuable therapeutic targets. Designed calix[4]arene ligands **1a** and **1b,** described in *Chapter 2***,** both bind p53TD and stabilize its naturally occuring mutant p53R337H, as assessed by biophysical techniques. The association takes place, as predicted by molecular dynamics simulations, *via* hydrophobic and guanidinium-oxoanion interactions (2). Differences in the affinity constants between compounds **1a** and **1b** rely on their overall

distinct flexibility: Higher flexibility, both in the protein and in the ligand, afford in this case for enhanced association (3).

Chapter 3 provides a general introduction to the function, the structure as well as to the pharmacological interest of K^+ channels. Thereafter, the synthesis of a series of calix[4]arene ligands as potential blockers of the voltage dependent K_v1 family, is described. Binding according to a conical C_4 symmetry design is predicted by molecular modeling and the effects on channel function are assessed. Non toxic, reversible inhibition is observed for compounds **3**, **6** and **11**, tetraacylguanidinium or tetraarginine members of the series with small lower rim *O*-substituents. Moreover, electrophysiological evaluation of their binding mode is in keeping with expectations for docking in the central pore and interaction with the pore domain "turret" (4).

Molecular and drug transporters across cell membranes are most often functionalized with guanidinium groups as these polycations have shown to be crucial for interaction with phosphate and other anionic moieties on the liposomal cell surface. In *Chapter 4* we present a family of molecular transporters that internalize into mitochondria, based on thioether-bound bicyclic guanidinium subunits (5). For the purpose of preparing a series of these oligomers, several synthetic strategies on solid support are described. The best approach is based on Merrifield-like peptide synthesis: A difunctionalized bicyclic guanidinium synthon, compound **18**, bearing both electrophile (OMs) and protected nucleophile (SMmt) groups, is repeatedly grafted *via* nucleophilic substitution. The sequence requires removal of methoxytrityl, reduction with 1,4-dithiothreitol, as well as coupling and

capping with benzyl bromide. Moreover, a bicyclic guanidinium monomer containing an amino group and a carboxylic acid function is evaluated as an alternative building block for novel amide-bridged strands (6).

1. Martos V, Castreño P, Valero J, de Mendoza J (2008) Binding to protein surfaces by supramolecular multivalent scaffolds. *Curr Op Chem Biol* 12:698-706.

2. Gordo S, Martos V, Santos E, Menéndez M, Bo C, Giralt E, de Mendoza J (2008) Stability and structural recovery of the tetramerization domain of p53-R337H mutant induced by a designed templating ligand. *Proc Natl Acad Sci USA* 105:16426-16431.

3. Gordo S, Martos V, Vilaseca M, Menéndez M, de Mendoza J, Giralt E. On the role of flexibility in protein-ligand interactions: The example of p53 tetramerization domain. (2008) *J Am Chem Soc*, submitted.

4. Martos V, Bell S, Santos E, Trauner D, Isacoff E, de Mendoza J. Calix[4]arene-based conical-shaped ligands for voltage dependent potassium channels. (2008) *Proc Natl Acad Sci USA*, submitted.

5. Fernández-Carneado G, Van Gool M, Martos V, Castel S, Prados P, de Mendoza J, Giralt G (2005) Highly efficient, nonpeptidic oligoguanidinium vectors that selectively internalize into mitochondria. *J Am Chem Soc* 27:869-874.

6. Martos V, Castreño P, Royo M, Albericio F, de Mendoza J Solid phase synthesis of chiral bicyclic guanidinium oligomers. (2008) *J Comb Chem*, accepted.

Introducción general y conclusiones

Las interacciones no covalentes entre superficies de macromoléculas biológicas constituyen la base de numerosos mecanismos celulares esenciales, como el reconocimiento, la internalización y la señalización celular. El desarrollo de moléculas capaces de simular o inhibir dichas interacciones constituye un reto, dadas las características de las superficies de unión implicadas, que carecen de una topología característica, y por otra parte son extensas, planas y discontinuas, además de flexibles y dinámicas (1). Otra característica que dificulta el diseño de ligandos pequeños con fines terapéuticos, es la solvatación de las superficies, expuestas al medio acuoso, ya que las moléculas de agua compiten por muchas de las interacciones no covalentes de naturaleza polar (2).

La química supramolecular es la química de las interacciones débiles y estudia el reconocimiento entre moléculas mediante interacciones no covalentes generando sistemas de mayor estabilidad y complejidad. Por ello, con frecuencia los químicos supramoleculares se inspiran en la naturaleza para diseñar sistemas capaces de establecer asociaciones reversibles y al mismo tiempo fuertes y específicas, incluso en disolventes tan polares como el agua (3). En este sentido, el fenómeno de la multivalencia, ampliamente representado en la naturaleza, ha inspirado un gran número de sistemas basados en esqueletos preorganizados (como porfirinas, calix[4]arenos, dendrímeros, rotaxanos etc.), dotados de múltiples elementos de reconocimiento, cuyas interacciones son débiles consideradas de forma aislada pero que en su conjunto proporcionan afinidad y especificad de unión (4).

La naturaleza emplea frecuentemente el grupo funcional guanidina, como por ejemplo el presente en la cadena lateral del aminoácido arginina, porque permite establecer pares iónicos fuertes con grupos carboxilato, fosfato o sulfato presentes en los sistemas biológicos (5). De esa forma, la combinación de esqueletos semirígidos o preorganizados con elementos de reconocimiento con estructura de guanidina ha permitido el desarrollo de numerosos receptores de biomoléculas (6), así como de transportadores moleculares (7).

En esta memoria se describen, por un lado, el diseño, la síntesis y la evaluación de ligandos con estructura de calix[4]areno dotados de grupos funcionales guanidinio para el reconocimiento de superficies proteicas específicas y, por otro, el desarrollo de estrategias de síntesis en fase sólida para la obtención de vectores celulares basados en oligómeros de guanidina bicíclica.

La proteína p53 es un factor de transcripción, a veces denominado “guardián del genoma”, por su papel crucial en el ciclo celular y en la integridad genómica. Cuando el ADN se ve dañado, p53 interrumpe el ciclo celular y simultáneamente induce la expresión de la maquinaria de reparación del ADN. Si el daño es irreversible, la misma proteína desencadena el proceso de apoptosis. Estructuralmente, es un homotetrámero que da lugar a varios dominios de regulación, de unión a ADN y de tetramerización, y se encuentra mutado en aproximadamente un 50% de cánceres humanos (8). Aunque la mayoría de las mutaciones afectan al dominio de unión a ADN, unas pocas se producen en el dominio de tetramerización. Es el caso de la mutación p53R337H que desestabiliza

el tetrámero y en consecuencia aumenta la probabilidad de aparición de tumores en el organismo (9).

En el *capítulo 2* describimos el diseño racional, la síntesis y el estudio de dos ligandos **1a** y **1b** concebidos para mantener unidos los cuatro monómeros de la proteína mutada p53-R337H y recuperar así la integridad tetramérica de la proteína nativa.

Ambos ligandos están basados en un esqueleto de calix[4]areno cónico, dotado de cuatro grupos catiónicos metilguanidinio en el borde más ancho y de cadenas hidrofóbicas en el cerco inferior (propilos en el caso de **1a** y puentes de dietilenglicol en el caso de **1b**). Del estudio realizado se han extraido las siguientes conclusiones (10, 11):

- La estructura de los complejos formados por la asociación entre los ligandos **1a** y **1b** y los tetrámeros de la proteína p53 nativa y el mutante p53R337H se predijo correctamente por dinámica molecular y se confirmó mediante técnicas biofísicas (CD, DSC, NMR, MS-ESI(+)).
- Las interacciones hidrofóbicas juegan un papel esencial en dichos complejos, si bien las interacciones guanidino-carboxilato, contribuyen a fortalecerlos.
- Ambos ligandos **1a y 1b** estabilizan y se asocian de manera cooperativa al tetrámero mutado p53R337H, además de ser más afines a éste que al tetrámero nativo.
- El ligando **1a** establece asociaciones más fuertes con ambos tetrámeros que su análogo **1b**, además de causar una ligera distorsión en la estructura tetramérica original.
- La flexibilidad, tanto de la biomolécula como del ligando, contribuye en este caso a una mejor adaptación y en consecuencia a una

mayor fortaleza de la asociación.

- El estudio pone de relieve y demuestra que una deficiencia estructural que impide la oligomerización de determinadas proteínas, como p53R337H, puede corregirse mediante una pequeña molécula que, al fijarse sobre la superficie proteica, actúa a modo de molde (chaperón) molecular, restituyendo su estructura nativa.

Los canales de potasio constituyen los canales iónicos más difundidos y están presentes en prácticamente todas las células eucariotas y procariotas. Conducen cationes potasio de forma selectiva a través de la membrana celular y controlan procesos esenciales como la excitabilidad, la homeostasis y la secreción (12). La relación estructura atómica-función de dichos canales fue elucidada por R. McKinnon, que fue galardonado en el año 2003 con el premio Nobel de química por dicho descubrimiento. Dado que las deficiencias en los canales de K^+ causan múltiples patologías, éstos constituyen importantes objetivos farmacológicos, sobre todo los correspondientes a la familia de canales dependientes de voltaje K_v1 (13).

En el *capítulo 3* de la presente memoria describimos el diseño y la síntesis de una serie de ligandos de calix[4]areno (**3**-**14**), y su evaluación como bloqueantes de canales K_v1, a los que se unen sobre la entrada del poro. Las conclusiones de este estudio fueron (14):

- La estrategia sintética empleada permite una fácil variación de los sustituyentes del cerco superior y da acceso a una amplia gama de potenciales ligandos, con diversa funcionalización.

- El diseño de unión a los dominios del poro extracelulares, según una simetría cuaternaria cónica, se ha confirmado a nivel teórico mediante cálculos de dinámica molecular.
- La funcionalidad celular se valoró por métodos electrofisiológicos (*two electrode voltage clamp y voltage clamp fluorometry*) *in vitro* sobre oocitos de *Xenopus laevis*, lo que permitió demostrar una inhibición no tóxica y reversible para los compuestos **3**, **6** y **11**, funcionalizados con grupos tetraacilguanidinio o tetraarginina en su cerco superior y *O*-sustituyentes cortos en su cerco inferior.
- Las constantes de asociación aparentes para el ligando **6** se encuentran en un rango micromolar bajo y muestran coeficientes de Hill de 1, consistentes con un único sitio de unión.
- La disminución de corriente inducida por **6** se ve acompañada de un desplazamiento, dependiente del voltaje, hacia voltajes más positivos de la apertura de los canales.
- Asímismo se observa una ralentización tanto en el movimiento del dominio sensor de voltaje (S4), como en la velocidad de apertura de los canales, inducida por la unión de **6**.
- Ambas conclusiones indican que la unión de **6** con K_v1 implica una interacción con el dominio *turret* de K_v1, que se transmite al dominio S4, modificando así la cinética de apertura del canal, así como su respuesta a los cambios de voltaje.
- Los calix[4]arenos funcionalizados con grupos guanidinio constituyen por tanto un punto de partida para el desarrollo de ligandos reversibles, no tóxicos, específicos y afines a distintos canales de K_v1^+.

La eficacia terapéutica de un fármaco depende de su capacidad para llegar a su diana en tejidos, células u orgánulos. Sin embargo, una de las principales limitaciones actuales en el desarrollo de fármacos eficaces con estructuras químicas polares sigue siendo el traspasar la barrera constituída por las membranas celulares. Por ello, la unión de los fármacos a determinados compuestos que ayuden a franquear dichas barreras, y denominados por ello con frecuencia caballos de Troya, supone un importante avance al respecto. Los transportadores moleculares están dotados generalmente de grupos guanidinio porque dichas moléculas policatiónicas interaccionan fácilmente con los grupos fosfato y demás oxoaniones de la superficie celular (7).

En nuestro grupo de investigación se describió recientemente una nueva familia de transportadores guanidínicos basados en oligómeros de guanidina bicíclica unidos mediante enlaces de tipo tioéter (15, 16). La necesidad de establecer estudios sistemáticos de estructura-función ha motivado el desarrollo de estrategias sintéticas en fase sólida, es decir resinas de poliestireno convencionales.

Las estrategias sintéticas descritas a lo largo del *capítulo 4* parten de diferentes sintones de subunidades de guanidina bicíclica (**15**-**20**), los cuales condicionan el uso de resinas poliméricas y reacciones diferentes. El desarrollo de estas estrategias ha permitido llegar a las conclusiones siguientes (17):

- La formación de puentes disulfuro durante la reacción de acoplamiento, así como la baja reactividad del anión tiolato creado *in situ*, dificultan la síntesis de oligómeros sobre la resina NHR-BAL-MBHA a partir de los sintones **15** y **16**.

- El empleo de subunidades de guanidina bicíclica dotadas, en uno de sus brazos, de buenos grupos salientes y en el otro de un nucleófilo de tipo tiol, covenientemente enmascarado, como los compuestos **17**, **18** y **19**, constituyen el sintón ideal ya que reducen la secuencia sintética de cada ciclo de introducción de guanidina a dos reacciones acoplamiento y desprotección.
- La formación de puentes disulfuro durante la reacción de acoplamiento entre grupos tiol de la propia resina impide el acoplamiento eficaz de subunidades de guanidina bicíclica **17,** probablemente debido a la alta funcionalización inicial de la resina empleada (4-metoxitritiltiol).
- La combinación del sintón **18** y el soporte basado en la resina Cys-Rinkamide-MBHA, permite la introducción iterativa del sintón **18** con un rendimiento de aprox. 80% para cada acoplamiento.
- La neutralización de los grupos tiol sin reaccionar con bromuro de bencilo y los tratamientos reductores previos a las reacciones de acoplamiento, mejoran el rendimiento de los compuestos finales y facilitan la purificación final.
- El empleo del grupo alloc como protector semipermanente permite el anclaje en esta secuencia sintética de moléculas o fármacos en cualquier momento de la síntesis del oligómero.
- El sintón **20** puede emplearse como un sucedáneo de un amino ácido en una síntesis convencional de péptidos modificados y abre la puerta a nuevos oligómeros de guanidina bicíclica unidos por enlaces amida.

1. Arkin MR, Wells JA (2004) Small-molecule inhibitors of protein–protein interactions: progressing towards the dream. *Nature Rev* 3:301-317.

2. Stites WE (1997) Protein interactions: Interface structure, binding thermodynamics, and mutational analysis. *Chem Rev* 97:1233-1250.

3. Krishnamurthy VM, Semetey V, Paul JB, Shen N, Whitesides GB (2007) Polyvalent interactions in biological systems: implications for design and use of multivalent ligands and inhibitors. *J Am Chem Soc* 129:1312-1320.

4. Martos V, Castreño P, Valero J, de Mendoza J (2008) Binding to protein surfaces by supramolecular multivalent scaffolds. *Curr Op Chem Biol* 12:698-706.

5. Woods AS, Ferre SJ (2005) Amazing stability of the arginine-phosphate electrostatic interaction. *Proteome Res* 4:1397-1402.

6. Schmuck C (2006) How to improve guanidinium cations for oxoanion binding in aqueous solution? The design of artificial peptide receptors. *Coord Chem Rev* 250:3053-3067.

7. Wender PA, Galliher WC, Goun EA, Jones LR, Pillow TH (2008) The design of guanidinium-rich transporters and their internalization mechanisms. *Adv Drug Del Rev* 60:452-472.

8. Joerger AC, Fersht AL (2008) Structural Biology of the tumor suppressor p53. *Annu Rev Biochem* 77:557-582.

9. Di Giammarino EL, Lee AS, Cadwell C, Zhang W, Bothner B, Ribeiro RC, Zambetti G, Kriwacki RW (2002) A novel mechanism of tumorigenesis involving involving pH-dependent destabilization of a mutant p53 tetramer. *Nat Struct Biol* 9:12-16.

10. Gordo S, Martos V, Santos E, Menéndez M, Bo C, Giral E, de Mendoza J (2008) Stability and structural recovery of the tetramerization domain of p53-R337H mutant induced by a designed templating ligand.*Proc Natl Acad Sci USA* 105:16426-16431.

11. Gordo S, Martos V, Vilaseca M, Menéndez M, de Mendoza J On the role of flexibility in protein-ligand interactions: The example of p53 tetramerization domain. *J Am Chem Soc*, submitted.

12. Hille B (2001) Ion Channels of Excitable Membranas, 3ed., Sinauer (Sunderland)

13. Shieh CC, Coghlan M, Sullivan JP, Gopalakrishnan M (2000) Potassium channels: molecular defects, diseases, and therapeutic opportunities. *Pharma Rev* 52:557-593.

14. Martos, V.; Bell, S. C.; Santos, E.; Trauner, D.; Isacoff, E.Y.; de Mendoza, J. (2008) Calix[4]arene-based conical-shaped ligands for voltage dependent potassium channels. *Proc Natl Acad Sci USA*, submitted.

15. Fernández-Carneado G, Van Gool M, Martos V, Castel S, Prados P, de Mendoza J, Giralt G (2005) Highly efficient, nonpeptidic oligoguanidinium vectors that selectively internalize into mitochondria. *J Am Chem Soc* 27:869-874.

16. Kielar F Congreve A Law G-l, New EJ, Parker D, Wong K-L, Castreño P, de Mendoza J (2008) Two-photon microscopy study of the intracellular compartmentalisation of emissive terbium complexes and their oligo-arginine and oligo-guanidinium conjugates. *Chem Commun* 2435-2437.

17. Martos V, Castreño P, Royo M, Albericio F, de Mendoza J (2008) Solid phase synthesis of chiral bicyclic guanidinium oligomers. *J Comb Chem*, accepted.